University of Salerno

Department of Chemistry and Biology "Adolfo Zambelli"

PhD Thesis in Chemistry

New insights on the ecology of underground ecosystems toward a sustainable management strategy

Supervisor

Prof. Daniela Baldantoni

PhD Candidate

Dr. Rosangela Addesso

PhD Coordinator

Prof. Claudio Pellecchia

XXXIV Cycle

Academic year 2020/2021

To the heart and the strength of a great woman,

Grandma Rosa

Index

General introduction

Underground cavities represent some of the less explored places on the planet (Lee et al., 2012). In fact, excluding the known carbonate dissolution/precipitation processes, leading to the formation of holes in the host rock, as well as speleothems, little is known about the ecology of these fascinating and enigmatic ecosystems. In spite of this, caves are generally object of tourist adaptations, which can activate an irreversible impairment of the biogeochemical equilibria, whose load, until now, is not estimated accurately, due to the scanty information in this regard (Chiesi and Badino, 2008).

The anthropogenic effects on the air compartment represent the most indiscernible and not immediately recognizable alteration, just thinking to the heat or breathing produced by human body, influencing the natural temperature, relative humidity and CO_2 concentrations. Moreover, visitors can be carriers of inorganic and organic matter (dust, hair, bacteria, seeds…) constituting an important energy input, as well as a trophic source, in the cave oligotrophic ecosystem, affecting its natural energy regime (Russell and MacLean, 2008; Jurado et al., 2008; Smith et al., 2013; Bruno et al., 2014).

These factors are able to influence the reactions at the interface between the atmosphere and the other compartments (lithosphere, hydrosphere and biota), fundamental in controlling the ecosystem processes, that ensure the functioning of the whole underground ecosystem (Pulido-Bosch et al., 1997; Milanolo and Gabrovšek, 2009; de Freitas, 2010; Lang et al., 2015a; Lang et al., 2015b; Howarth, 2019). Hence, the necessity to develop new, sturdy and low-cost tools, including also sensors for data acquisition and modelling applications (Bugmann et al., 2000; Schmolke et al., 2010), to monitor and assess continuously cave atmosphere, providing to the authority valid and efficient devices helping them in the sustainable management.

Cave waters, in particular, besides having a key role in the origin processes of subterranean holes, are carrier of the principal, if not unique, organic source in the trophic-poor cave system, coming almost totally from surface. Crossing the topsoil and the vadose zone, allochthonous organic and inorganic resources, such as dissolved organic matter, sediments, microorganisms and small-sized fauna, represent a very important trophic supply for the hypogean biota sustenance (Fairchild and Treble, 2009; Lauritzen, 2018; Culver and Pipan, 2019). Exploring cave water chemical features sheds light on the natural biogeochemical processes occurring in all the profile, from the surface to the deeper zone, allowing assessing also potential anthropogenic impacts from their ecological quality (Motyka et al., 2005; Moldovan et al., 2007; Fairchild and Treble, 2009; Hartland et al., 2012; Fehér et al., 2016). But besides their ecological role, waters, as well as clastic sediments, can preserve considerable information about the current and past environmental, geomorphological, sedimentological, hydrological and paleoclimatological history of the subterranean system (White, 2007; Tremaine and Froelich, 2013; Rossi and Lozano, 2016; Arriolabengoa et al., 2015; Nava-Fernandez et al., 2020).

Nevertheless, the most worrying fact related to human frequentation of underground ecosystems is the development of photoautotrophic and mixotrophic communities on the surfaces, commonly called lampenflora, caused by the permanent artificial lighting (Mulec and Kosi, 2009). In fact, these green patinas implement aesthetical alterations of the natural surfaces and biodeterioration processes due to their mechanical destruction and chemical corrosion activated by the appendages and acid secretions of the organisms composing the community. Moreover, they are responsible for an ecological imbalance, due to a consistent “alien” organic input in the cave oligotrophic environment, due to the absence of surface photoautotrophic primary producers (Mulec,

2019). Lampenflora alters not only mineral substrates, with irreversible consequences on the speleothems, but also peculiar structures conservation, such as vermiculations (Hill and Forti, 1997), discontinuous deposits of incoherent particles, mainly calcite, occurring on the walls of natural and artificial cavities. They display several morphologies, colors and sizes, but their origin process has not actually elucidated yet (Parenzan, 1961, 1965; Bini et al., 1978).

Currently, no definitive solutions exist to remove and control lampenflora, but only several practices, mainly through chemico-physical methods, that the cave managers perform based on few scientific studies and without a real knowledge of their efficacy and their consequent effects on the ecosystem (Baquedano Estévez et al., 2019).

In light of all such considerations, European Member States in the Annex I of the European Directive 92/43/EEC (Habitat Directive), established the rocky habitats and caves among the natural systems of Community interest, whose protection and conservation require the designation of special areas of conservation. Moreover, the International Show Caves Association (ISCA) has drawn up a document for the definition of "ISCA Standards", quality criteria to be followed all the interventions in the hypogean environments, designed to optimize the tourist usability and to minimize the impacts, realizing a sustainable management of such precious natural assets (Cigna, 2019; Chiesi and Badino, 2008). Therefore, a comprehensive study of the cave ecosystem, considering all the environmental compartments (atmosphere, lithosphere, hydrosphere and biota), can reveal its natural dynamics and identify the potential sources of damages from tourism fruition, allowing the proposal of focused and efficient controlling actions in a sustainable management and conservation view of these fragile ecosystems.

References

Addesso, R., Bellino, A., D'Angeli, I.M., De Waele, J., Miller, A.Z., Carbone, C., Baldantoni, D., 2019. Vermiculations from karst caves: The case of Pertosa-Auletta system (Italy). CATENA 182, 104178. doi: 10.1016/j.catena.2019.104178

Arriolabengoa, M., Iriarte, E., Aranburu, A., Yusta, I., Arrizabalaga, A., 2015. Provenance study of endokarst fine sediments through mineralogical and geochemical data (Lezetxiki II cave, northern Iberia). Quaternary International 364, 231–243. doi: 10.1016/j.quaint.2014.09.072

Baquedano Estévez, C., Moreno Merino, L., de la LosaRomán, A., DuránValsero, J.J., 2019. The lampenflora in show caves and its treatment: an emerging ecological problem. International Journal of Speleology 48 (3), 249-277. doi: 10.5038/1827-806X.48.3.2263

Bini, A., Cavalli Gori, M., Gori, S., 1978. A critical review of hypotheses on the origin of vermiculations. International Journal of Speleolology 10, 11–33.

Bruno, L., Belleza, S., Urzì, C., De Leo, F., 2014. A study for monitoring and conservation in the Roman Catacombs of St. Callistus and Domitilla, Rome (Italy), in: Saiz-Jimenez, C. (Ed.), The Conservation of Subterranean Cultural Heritage. CRC Press, pp. 37–44. doi: 10.1201/b17570-6

Bugmann, H., Lindner, M., Lasch, P., Flechsig, M., Ebert, B., Cramer, W., 2000. Scaling issues in forest succession modelling. Climate Change 44: 265–289. doi: 10.1023/A:1005603011956

Chiesi, M., Badino, G., 2008. Turisticamente sostenibili. Note e riflessioni sugli adattamenti e la gestione delle grotte turistiche. Speleologia 59: 44-47

Cigna, A.A., 2019. Show caves, in: Encyclopedia of Caves. Elsevier, pp. 909–921. doi: 10.1016/B978-0-12-814124-3.00108-4

Culver, D.C., Pipan, T., 2019. The Biology of Caves and Other Subterranean Habitats, 2nd ed. Oxford University Press. doi: 10.1093/oso/9780198820765.001.0001

D'Angeli, I.M., Ghezzi, D., Leuko, S., Firrincieli, A., Parise, M., Fiorucci, A., Vigna, B., Addesso, R., Baldantoni, D., Carbone, C., Miller, A.Z., Jurado, V., Saiz-Jimenez, C., De Waele, J., Cappelletti, M., 2019. Geomicrobiology of a seawater-influenced active sulfuric acid cave. PLoS ONE 14, e0220706. doi: 10.1371/journal.pone.0220706

de Freitas, C.R., 2010. The role and the importance of cave microclimate in the sustainable use and management of show caves. Acta Carsologica 39: 477-489.

Fairchild, I. J., & Treble, P. C., 2009. Trace elements in speleothems as recorders of environmental change. Quaternary Science Reviews 28(5–6), 449–468. doi: 10.1016/j.quascirev.2008.11.007

Fairchild, I.J., Treble, P.C., 2009. Trace elements in speleothems as recorders of environmental change. Quaternary Science Reviews 28, 449–468. doi: 10.1016/j.quascirev.2008.11.007

Fehér, K., Kovács, J., Márkus, L., Borbás, E., Tanos, P., & Hatvani, I. G., 2016. Analysis of drip water in an urban karst cave beneath the Hungarian capital (Budapest). Acta Carsologica 45(3): 213-231. doi: 10.3986/ac.v45i3.3440

Hartland, A., Fairchild, I. J., Lead, J. R., Borsato, A., Baker, A., Frisia, S., & Baalousha, M., 2012. From soil to cave: Transport of trace metals by natural organic matter in karst dripwaters. Chemical Geology 304–305: 68–82. doi: 10.1016/j.chemgeo.2012.01.032

Hill, C.A., Forti P., 1997. Cave Minerals of the World. National Speleological Society, 2nd Ed, 463.

Howarth, F.G., 2019. Adaptive shifts, in: White, W.B., Culver, D.C., Pipan, T. (Eds.), Encyclopedia of Caves (3th Ed). Academic Press, pp. 47–55.

Jones, D.S., Lyon, E.H., Macalady, J.L., 2008. Geomicrobiology of biovermiculations from the Frasassi cave system, Italy. Journal of Caves and Karst Studies 70(2): 28-93.

Jurado, V., Sanchez-Moral, S., Saiz-Jimenez, C., 2008. Entomogenous fungi and the conservation of the cultural heritage: A review. International Biodeterioration & Biodegradation 62, 325–330. doi: 10.1016/j.ibiod.2008.05.002

Lang, M., Faimon, J., Ek, C., 2015a. The relationship between carbon dioxide concentration and visitor numbers in the homothermic zone of the Balcarka Cave (Moravian Karst) during a period of limited ventilation. International Journal of Speleology 44: 167–176.

Lang, M., Faimon, J., Ek, C., 2015b. A case study of anthropogenic impact on the CO_2 levels in low-volume profile of the Balcarka Cave (Moravian Karst, Czech Republic). Acta Carsologica 44.

Lauritzen, S.-E., 2018. Physiography of the Caves, in: Moldovan, O.T., Kováč, Ľ., Halse, S. (Eds.), Cave Ecology, Ecological Studies. Springer International Publishing, Cham, pp. 7–21. doi: 10.1007/978-3-319-98852-8_2

Lee, N.M., Meisinger, D.B., Aubrecht, R., Kovacik, L., Saiz-Jimenez, C., Baskar, S., Baskar, R., Liebl, W., Porter, M.L., Engel, A.S., 2012. Caves and karst environments, in: Bell, E.M. (Ed.), Life at Extremes: Environments, Organisms and Strategies for Survival. CABI, Wallingford, pp. 320–344. doi: 10.1079/9781845938147.0320

Milanolo, S., Gabrovšek, F., 2009. Analysis of Carbon Dioxide Variations in the Atmosphere of Srednja Bijambarska Cave, Bosnia and Herzegovina. Boundary-Layer Meteorology 131: 479–493.

Moldovan, O. T., Pipan, T., Iepure, S., Mihevc, A., & Mulec, J., 2007. Biodiversity and Ecology of Fauna in Percolating Water in Selected Slovenian and Romanian Caves. Acta Carsologica 36(3): 493-501. doi: 10.3986/ac.v36i3.183

Motyka, J., Gradziński, M., Bella, P., & Holúbek, P., 2005. Chemistry of waters from selected caves in Slovakia—A reconnaissance study. Environmental Geology 48(6): 682–692. doi: 10.1007/s00254-005-0006-2

Mulec, J., 2019. Lampenflora, in: Encyclopedia of Caves. Elsevier, pp. 635–641. doi: 10.1016/B978-0-12-814124-3.00075-3

Mulec, J., Kosi, G., 2009. Lampenflora algae and methods of growth control. Journal of Cave and Karst Studies 71(2): 109–115.

Nava-Fernandez, C., Hartland, A., Gázquez, F., Kwiecien, O., Marwan, N., Fox, B., Hellstrom, J., Pearson, A., Ward, B., French, A., Hodell, D.A., Immenhauser, A., Breitenbach, S.F.M., 2020. Pacific climate reflected in Waipuna Cave drip water hydrochemistry. Hydrol. Earth Syst. Sci. 24, 3361–3380. doi: 10.5194/hess-24-3361-2020

Parenzan, P., 1961. Sulle formazioni argillo-limose dette vermicolari. Atti del Symposium Internazionale di Speleologi, Varenna 1960 sui “Riempimenti naturali di grotta”. Memoria Rassegna Speleologica Italiana 5 (2), 120–125.

Parenzan, P., 1965. Le formazioni vermicolari della grotta di Sant'Angelo di Statte (Taranto). Atti IX Congresso Nazionale di Speleoleologia, Trieste, 1962. Memoria Rassegna

Pulido-Bosch, A., Martín-Rosales, W., López-Chicano, M., Rodríguez-Navarro C.M., Vallejos A., 1997. Human impact in a tourist karstic cave (Aracena, Spain). Environmental Geolology 31: 142–149.

Russell, M.J., MacLean, V.L., 2008. Management issues in a Tasmanian tourist cave: Potential microclimatic impacts of cave modifications. Journal of Environmental Management 87, 474–483. doi: 10.1016/j.jenvman.2007.01.012

Schmolke, A., Thorbek, P., DeAngelis, D.L., Grimm, V., 2010. Ecological models supporting environmental decision making: a strategy for the future. Trends in Ecology & Evolution 25: 479–486. doi: 10.1016/j.tree.2010.05.001

Smith, A., Wynn, P., Barker, P., 2013. Natural and anthropogenic factors which influence aerosol distribution in Ingleborough Show Cave, UK. IJS 42, 49–56. doi: 10.5038/1827-806X.42.1.6

Tremaine, D.M., Froelich, P.N., 2013. Speleothem trace element signatures: A hydrologic geochemical study of modern cave dripwaters and farmed calcite. Geochimica et Cosmochimica Acta 121, 522–545. doi: 10.1016/j.gca.2013.07.026

White, W.B., 2007. Cave sediments and paleoclimate. Journal of Cave and Karst Studies 69:76–93.

Project aim and experimental plan

The most of research activities were carried out in the karst system of the Pertosa-Auletta Cave (Southern Italy), located in the Cilento, Vallo di Diano and Alburni National Park, chosen as study model. This location is very interesting for scientific studies, representing a perfect laboratory, since it opens in the limestone Alburni Massif, with trails characterized by different natural characteristics (the fossil trail without flowing waters and the active trail crossed by a perennial subterranean river) and by different human fruition (tourist and closed to the public paths). Since 2010, it is included in the European Geoparks Network for its relevant geological heritage, why, every year, hosts more than 60.000 visitors.

The project aimed at shedding light on the abiotic and biotic compartments of this relatively unknown ecosystem and at the understanding of the effects of tourist adaptations in cave environment, with the definition of mitigation strategies of damages. To this end, a multidisciplinary approach (Figure 1) was adopted, allowing:

(i) the study of chemism at the interface among the abiotic and biotic environmental compartments of the cave ecosystem: substrate (clastic sediments and vermiculations), water (dripping and river) and atmosphere, as well as lampenflora characterization (Section I), in order to highlight their natural dynamics and consequently assess potential anthropogenic pressures on such abiotic and biotic characteristics in relation to the surface activities and tourism impact in caves;

(ii) the study of alteration processes implemented by the human presence over the natural dynamicscharacterizing the cave system, focusing on thedevelopment of new and high-resolution monitoring techniques, on the modelling of important processes and on the suggestionof innovative and

functional solutions to realize a sustainable management of cave tourism. In particular, investigations on the possible relationships between tourist load and cave atmospheric parameters alterations, with a wavelet analysis, clearly identifying the specific cross-correlation signatures (or absence of cause-effect relationship) between the number of visitors and each one of the key environmental parameters, simulations of the airflow and the particle dispersions and depositions of tourist sections of the Pertosa-Auletta Cave and tests on the efficacy and sustainability, in terms of lampenflora reduction and alterations activated on the surfaces, of the most used removal and control methods, have been carried out (Section II).

During the three years of the research activity, two main cave trails of Pertosa-Auletta Cave were investigated: the tourist one, lit and frequented by human, and the fossil one, closed to the public. The annual dynamics of several atmospheric parameters (temperature, relative humidity, CO_2, VOCs and particulate) were monitored, for two years, through novel low-cost monitoring stations, developed *ad hoc* using hardware platforms for physical computing (Chapter 8). These data allowed also to build a simulation of thenatural cave airflow and to predict the scattering and consequentdeposition of particles transported by tourists, employing COMSOL Multiphysic software, for the first time to simulate human impacts in caves (Chapter 9). In the same trails, drip and Negro river waters were seasonally analyzed, for one year, in order to determine pH, redox potential,conductivity, anions, cations and chemical elements (Chapter 2), obtaining detailed information about the hydrogeological features of the Alburni Massif characterized for its groundwater flow and spring functioning (Chapter 1). Simultaneously, by spectrometric and X-ray diffractometric techniques, sediments (on rock recesses and on the floor, above and underwater) (Chapter 3) and

vermiculations (Chapter 5) were characterized in various sections of the entire cave. Moreover, the microbiological features of vermiculations were also investigated through modern methods of molecular biology and microscopy, in order to highlight their microbial biodiversity and its role in their formation processes (Chapter 6). A geochemical and microbiological characterization of vermiculations, water filaments and moonmilk from an active sulfuric acid cave (Fetida Cave in Apulia region, Southern Italy) was also carried out, in order to widening the knowledge of these peculiar and few known deposits (Chapter 4).

After an accurate biological and eco-physiological characterization of green biofilms growing in the lighted tourist trail (Chapter 7), an experimental trial to test, over time, the efficacy and the effects on surfaces, bare and with vermiculations, of the most used chemical (NaClO and H_2O_2) and physical (UVC) removal and control lampenflora methods was fine-tuned in the final section of the cave, in order to avoid disturbance by visitors (Chapter 10).The responses to the different treatments, in terms of metabolism and visible cleaning of surfaces, were monitored over time through *in situ* and non-destructively chlorophyll fluorescence measurements and image capture, whereas, at the end, chemical, microscopy and microbiological surveys were performed to evaluate the potential alterations of biological community and of substrate integrity.

Due to the complexity of results obtained from the continuous and periodical monitoring, as well as by the chemical, mineralogical and microbiological analyses, the data were elaborated through uni- and multivariate analyses, with particular attention to the spatial and temporal dynamics and to the relationships among the investigated parameters.

The completion of the entire work was carried out in the period from November 2018 to November 2021 at the Department of Chemistry and Biology “Adolfo Zambelli” of the

University of Salerno, supervised by Prof. Daniela Baldantoni, with the cooperation of Prof. Jo De Waele from the Department of Biological, Geological and Environmental Sciences of Alma Mater Studiorum University of Bologna and of Prof. Mariana Amato, scientific director of MIdA Foundation, manager of Pertosa-Auletta Cave. During the study period, four months were spent working with Dr. Ana Miller and her group, at the Instituto de Recursos Naturales y Agrobiología de Sevilla (IRNAS-CSIC, Sevilla – Spain) and at HERCULES Laboratory, University of Évora (Portugal).Moreover, there were partnerships also with Prof. Giovanni Vigliotta, from the Department of Chemistry and Biology "Adolfo Zambelli" of the University of Salerno, Prof. Laura Tositti, from the Department of Chemistry "G. Ciamician" of the University of Bologna, Dr. Bruno Bisceglia, from the Department of Industrial Engineering ofthe University of Salerno, and Prof. Mario Parise, from the Department of Earth and Geo-environmental Sciences, of the Aldo MoroUniversity of Bari.

Special thanks go to Ana Teresa Caldeira from HERCULES Laboratory, University of Évora (Portugal) and to Angel Fernandez-Cortes from University of Almería (Spain)for the revision of the thesis.

This work was funded by several projects:

- ORSA197159 and ORSA205530 projects of the Università degli Studi di Salerno (Italy),
- PID2019-108672RJ-I00 project, funded by MCIN/AEI/10.13039/501100011033 and, as appropriate, by "ERDF A way of making Europe", the "European Union" or by the "European Union NextGenerationEU/PRTR",
- the Spanish project MINECO [CGL2016-75590-P] with European Regional Development Fund,
- the Europlanet 2020 15-EPN1-029 and 17-EPN3-021 projects.

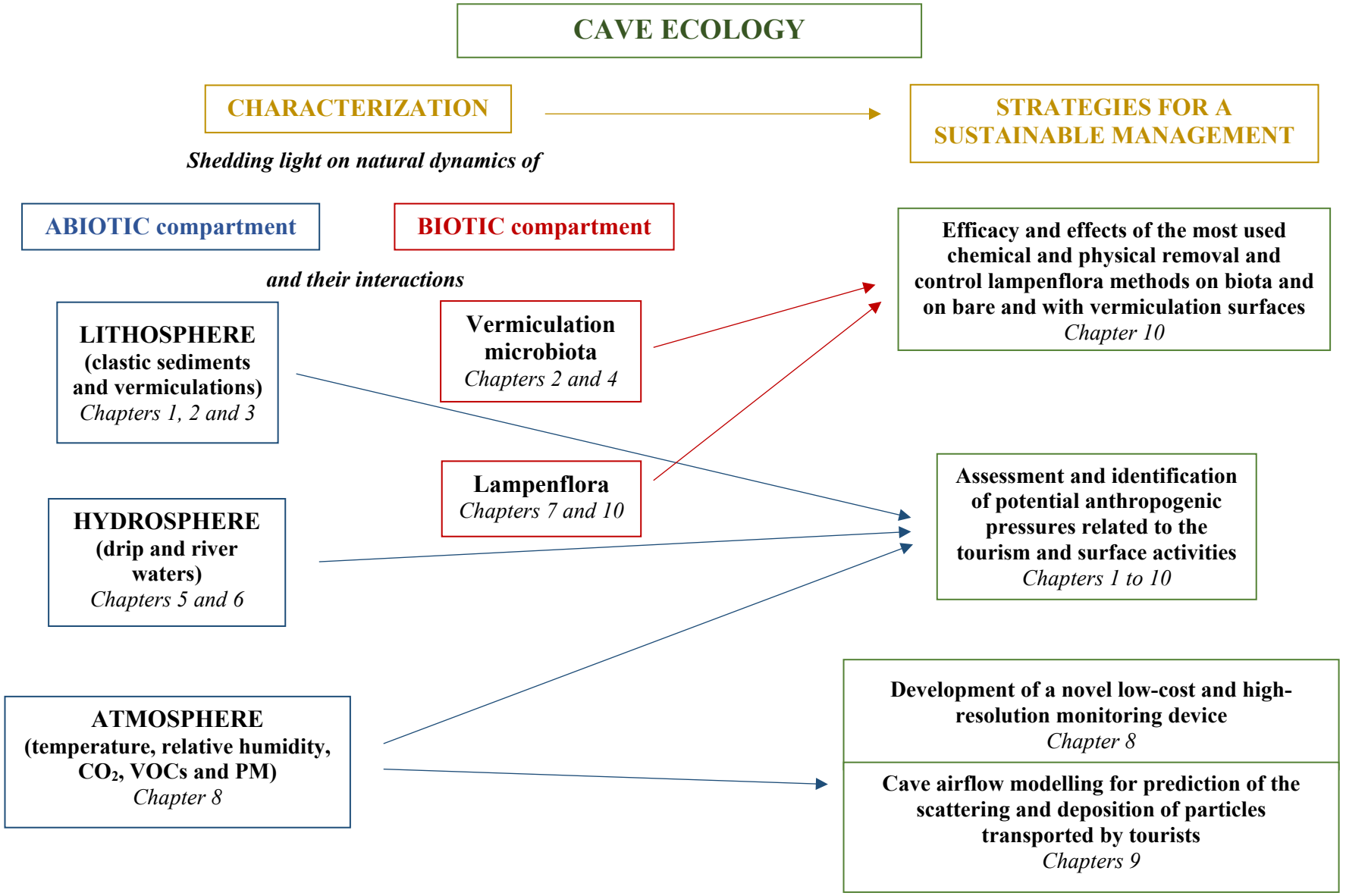

Figure 1 Conceptual framework of the PhD project

Section I

CAVE ABIOTIC AND BIOTIC COMPARTMENTS CHARACTERIZATION

In this section, a comprehensive characterization of the cave abiotic (lithosphere, hydrosphere and atmosphere) and biotic (vermiculation microbiota and lampenflora) compartments of Pertosa-Auletta Cave, taken as the main study model in the entire PhD project, were presented, shedding light on their natural dynamics and interactions.

In particular, clastic sediments were investigated, providing an overview about their mineralogical and elemental composition, as well as important information about the fluviokarst activity interesting the karst system of Pertosa-Auletta (Chapter 1).

A focus on the geochemical and microbiological nature of vermiculations sedimentary structures, both from the sulfuric acid Fetida Cave (Chapter 2) and from the tourist system of Pertosa-Auletta Cave (Chapters 3 and 4) were carried out, highlighting the biogenic processes involved in their formation.

Moreover, after studying the hydrogeological features of the Alburni Massif system (Chapter 5), to which Pertosa-Auletta Cave belongs, a chemical analysis of its drip and river waters was performed (Chapter 6), pointing out the ecohydrology of the hypogean ecosystem.

Chapter 7 is focused on the characterization of lampenflora and the destructive processes implemented on surfaces.

CHAPTER 1

Uncertainties in understanding groundwater flow and spring functioning in karst

Francesco Fiorillo, Mauro Pagnozzi Mauro, **Rosangela Addesso**, Simona Cafaro, Ilenia Maria D'angeli, Libera Esposito, Guido Leone, Isabella Serena Liso, Mario Parise*

Book chapter in **AGU Books**, **Wiley Black Well**

doi: 10.1002/essoar.10508452.1

**corresponding author*

The main hydrogeological features of the Alburni Massif, one of the most important karst areas of southern Italy (Campania, Italy), to which the Pertosa-Auletta Cave belongs, have been investigated, demonstrating its high degree of heterogeneity and anisotropy characterizing such underground model ecosystem.

Uncertainties in understanding groundwater flow and spring functioning in karst

FIORILLO Francesco [1], PAGNOZZI Mauro [1], ADDESSO Rosangela [2], CAFARO Simona [2], D'ANGELI Ilenia Maria [3], ESPOSITO Libera [1], LEONE Guido [1], LISO Isabella Serena [3], PARISE Mario [3*]

[1] Dipartimento di Scienze e Tecnologie, University of Sannio, Benevento, Italy

[2] MIDA Foundation, Pertosa, Italy

[3] Dipartimento di Scienze della Terra e Geoambientali, University Aldo Moro, Bari, Italy

[*] corresponding author (mario.parise@uniba.it)

Abstract

In karst environments, typically characterized by peculiar hydrogeological features and high heterogeneity and anisotropy, the connection between the recharge areas and the springs is often not straightforward. Rapid infiltration underground, and the resulting network of karst conduits, are frequently at the origin of a lack of correspondence among topographic divides and underground watersheds. As a consequence, in many karst areas there is still much work to do to fully understand the groundwater flow, with the only "underground truth" often being provided by cave data. In this contribution we start from general considerations about the difficulty in comprehending hydrogeology in karst, and use them to analyze one of the most important karst areas of southern Italy, the Alburni Massif in Campania (Italy). In detail, we present data about the main karst features at the surface (dolines, endorheic basins, etc.), the most important cave systems (reaching maximum depth of about 450 m below the surface), and the main basal springs coming out at the massif borders. Integration of the different sources of data allows to

hypothesize the main directions of groundwater flows, and to perform the first attempts in correlating recharge and discharge data, but such hypothesis then often prove to be wrong by data from cave and diving explorations.

Key words: karst, springs, dolines, hydrogeology, Alburni

Introduction: peculiarities of karst hydrogeology

Karst is an extremely peculiar setting, with unique landscapes characterized by a variety of landforms (such as dolines, swallets, shafts, karrenfields, poljes, etc.), which act as sites of concentrated recharge for the aquifers and, together with the main geological and hydrogeological features of soluble materials, are at the origin of the turbulent flow of water within the karst rock masses (Worthington et al. 2001; Brinkmann and Parise 2012). Such peculiarities cause the need to approach hydrogeological studies in karst with dedicated methods and techniques, since implementation of the classical hydrogeological laws and procedures is not significant (Goldscheider and Drew 2007; Jourde et al. 2007). Starting from the non-correspondence among hydrographic boundaries at the surface and hydrogeological boundaries underground (Gunn, 2007; Parise, 2016), the whole issue of infiltration, transfer, and discharge of water in karst is extremely complex (Stevanovic, 2015, and references therein). In such a context, mapping some of the most typical karst landforms such as dolines/sinkholes, endorheic basins and poljes (Angel et al. 2004; Dorsaz et al. 2013; Miao et al. 2013; Fragoso-Servòn et al. 2014; Wu et al. 2016; Pagnozzi et al. 2019; Zumpano et al. 2019), understanding their mechanisms of formation (Waltham et al. 2005; Del Prete et al. 2010; Gutierrez et al. 2014; Parise 2019), and their hydraulic role as well (Bonacci 1995, 2001; Fiorillo et al. 2015; Parise et al. 2015), is of crucial importance to gain insights into the actual hydrogeological regime in karst areas.

In this contribution, through illustration of the Alburni case study (S Italy), one of the most significant karst areas in the country, we intend to point out to the difficulties inherent in understanding karst hydrogeology, the crucial importance to co-operate with direct explorations by cavers, and the need to

approach the issue with specifically designated approaches. At this aim, we analyze the karst depressions at the summit plateau, estimate the related recharge, and compare it to the total amount coming from the main springs surrounding the massif. Then, through information derived from cave surveys, including diving explorations through some of the sumps within the cave systems, we point out to the still open problems regarding hydrogeology in the Alburni Massif.

Materials and methods

Mapping of dolines and endorheic areas on the Alburni Massif plateau was carried out through an integrated methodology, consisting of bounding their limits on 1:5000 scale topographic maps, supported by field survey, and uploading in GIS environment the geomorphological data together with those regarding strata attitude and presence of tectonic faults, as mapped from the official geological maps (Cestari 1971; Scandone 1971; De Riso and Santo, 1997).

The regional inventory of karst caves in Campania (managed by the Campanian Speleological Federation, available at http://www.fscampania.it/catasto-2/catasto/) was the starting point for the analysis of the main characters of the caves in the area: namely, through scrutiny of the individual cave surveys, in the forms of plan map and profiles, the presence of water within each inventoried cave was checked. Typically, this corresponds to stop in exploration of the cave, unless those few cases where it is possible to keep continuing through diving explorations. When the condition above (presence of water) was satisfied, its altitude within the cave system (corresponding to the maximum depth of the cave) was extracted as water level reference at the site. Collecting all these data, a preliminary attempt in reconstructing the Alburni water table was carried out. In addition, the outcomes of several tracing experiments, particularly cave-to-spring multitracer tests, carried out during the last 10 years in the area, were considered to prove some connections among caves and springs.

Data about the main springs in the area derive from detailed analysis of the existing scientific literature, but without any doubt they represent still a pitfall in the overall analysis, due to lack of continuity in recording

the spring discharges. Rainfall and temperature data were taken from the official reports by the Italian Hydrography Service during the last decades.

Eventually, the groundwater recharge at the long-term scale was estimated by applying the annual model proposed by Fiorillo et al. (2015), which can be implemented especially for wide areas with strong morphological irregularities, not entirely covered by hydrological monitoring. Based on long-term mean annual data, the total amount of meteoric precipitation, runoff, and recharge are computed in GIS environment in the model, estimating the recharge and the runoff coefficient for both open and endorheic areas. The annual model provides a mean long-term estimation of the recharge.

Based on a 20 x 20 m Digital Elevation Model, the spatial annual mean rainfall and annual mean temperature have been estimated by GIS tools; temperature and rainfall data were collected for the time period 1971-1999, then a reliable correlation was found using annual mean rainfall and annual mean temperature regression lines (Pagnozzi et al., 2019). The equations provided were implemented using raster data, and raster calculator tools in GIS environment. Then, using the Turc (1954) formula, the long-term annual mean of the actual evapotranspiration was estimated; this grid has been subtracted from the annual mean rainfall distribution grid, providing the long-term annual mean effective rainfall distribution grid.

In the endorheic area, A_E, as the runoff cannot escape, the recharge amount, R, can be considered equal to the effective afflux, F_{eff}:

$$(R)_{A_E} = (F_{eff})_{A_E}$$

In the open areas, A_O, the recharge amount R can be estimated assuming that all the groundwater flow feeds the spring discharges, Q_S, and no-flow boundaries occurs towards the argillaceous, terrigenous and flysch sequences (impervious terrains). Following this assumption, the total discharge, Q_s, from springs is:

$$Q_s = (R)_{A_E} + (R)_{A_o}$$

which allows to obtain the recharge in the open areas in the case of null groundwater abstraction:

$$(R)_{A_o} = Q_s - (F_{eff})_{A_E}$$

and the total recharge on the catchment area, A_C, is:

$$(R)_{A_c} = (R)_{A_o} + (R)_{A_E} = Q_s$$

valid if no groundwater occurs in the spring catchment, as for the Alburni karst massif.

The model assumes that all the amount of recharge reaches the basal water table, even though the vadose zone may present local saturated zones (i.e., sumps within karst systems, perched water tables, etc.).

The most common hydrologic parameter used to estimate aquifer recharge is the ratio between the volume of spring discharge and the rainfall. This is computed annually, assuming that cross boundary flow does not occur (Drogue 1971; Bonacci and Magdalenic 1993; Bonacci, 2001). Such a rough estimation can be improved considering the evapotranspiration processes and distinguishing the areas characterized by different recharge conditions. Among these latter, there are endorheic basins, that are closed depressions where the runoff is completely adsorbed (internal runoff; White, 2002; Sauro 2012), and are generally hydraulically connected to one or more springs.

The recharge coefficient used is expressed in term of fraction of the effective afflux, F_{eff}, providing the effective recharge coefficient, C_R; if water pumping does not occur, the following equation can be deducted (Fiorillo et al. 2015):

$$(C_R)_{A_E} = 1;\ (C_R)_{A_o} = \frac{(R)_{A_o}}{(F_{eff})_{A_o}};\quad (C_R)_{A_c} = \frac{(R)_{A_c}}{(F_{eff})_{A_c}}$$

The same coefficients can be expressed in function of total afflux, *F,* in a generic area, *A,* the recharge coefficient is:

$$(C'_R)_A = \frac{(R)_A}{(F)_A}$$

Finally, another evaluation is the contribution of endorheic areas to spring discharge. In this case, as all the recharge amounts inside endorheic areas (minus the pumping amount, Q_P) are assumed to reach basal springs, the effective contribution to spring discharge, C_S, can be expressed by

$$(C_S)_{A_E} = \frac{(F_{eff} - Q_P)_{A_E}}{Q_s}$$

As a consequence, the effective contribution to spring discharge of open areas, A_O, is:

$$(C_S)_{A_o} = 1 - (C_S)_{A_E}$$

In terms of total afflux, *F*, the total contribution to spring discharge in a generic area, *A*, could be estimated by the following equation:

$$(C'_s)_A = \frac{(F - Q_P)_A}{Q_s}$$

Further details of the method are described in Fiorillo et al. (2015).

The Alburni Massif

The Alburni Massif (Campania region of S Italy) extends over 270 Km^2, reaching a maximum altitude of 1742 m a.s.l. It is characterized by steep slopes bounding a mostly flat and undulating summit plateau. Two rivers bound the massif: namely, the Calore Lucano to the SW, and the Tanagro river to the NE, their valleys being filled by heterogeneous alluvial deposits, slope breccias, sand and conglomeratic deposits (Fig. 1).

The massif can be described as a monoclinal SW-dipping ridge marked by faults and composed of a Mesozoic carbonate sequence of Jurassic – Cretaceous age (Sartoni and Crescenti 1962); these soluble rocks are covered by a Miocene flysch sequence consisting of clays and sandstones (Scandone 1972; Ippolito et al. 1973; Patacca and Scandone 2007). During the Pliocene and Pleistocene, several faults caused the uplift of the massif (Gioia et al. 2011; Cafaro et al. 2016), and the development of deep karst processes (Santangelo and Santo 1997). The summit plateau shows a variety of sites of concentrated water infiltration, typical of karst settings, such as dolines and shafts (Klimchouk 2000; Ford and Williams, 2007; Palmer 2007; Williams 2008), which rapidly transfer the runoff into a complex network of caves and conduits (Del Vecchio et al., 2013; Cafaro et al., 2016), and then to the saturated zone of the aquifer. This concentrated recharge occurs mainly after intense rainstorms and snowmelt, whilst during normal rainfall events the recharge shows a diffuse modality, in function of the epikarst characters at the summit plateau.

144 The main springs (Basso Tanagro and Pertosa on the N side, Castelcivita and Auso to the S) drain the saturated
145 zone of the aquifer, and are distributed in the areas surrounding the massif; a systematic record of their
146 discharge is missing, with only sporadic measurements available (Brancaccio et al. 1973; Celico et al. 1994;
147 Ducci 2007). Overall, the total discharge can be estimated being in the order of 7-8 mc/sec (Table 1).
148 Other minor springs are present along the massif, and still others drain perched water tables in the
149 unsaturated zones.
150 In karst settings, due to scarcity or limited length of the surface runoff, endorheic areas play a prominent role
151 in the recharge processes (Denizman 2003; Palmer 2010; Heidari et al. 2011; Parise et al. 2015; Zumpano et
152 al. 2019). Their size and spatial distribution is typically linked to the structural control by faults and the main
153 discontinuity systems in the rock mass (Palmer 1991, 2007; Hauselmann et al. 1999; Parise 2011).
154 Mapping of dolines and endorheic areas on the Alburni Massif was carried out through an integrated
155 approach (Fig. 2), consisting of bounding their limits on 1:5000 scale topographic maps, supported by field
156 survey, and uploading in GIS environment the geomorphological data together with those regarding strata
157 attitude and presence of tectonic faults, as mapped from the official geological map.
158 The morphometric analysis proved that closed depressions (extending up to a few square kilometers)
159 developed on strata mostly characterized by horizontal or near-to-horizontal attitude; differently from other
160 karst areas in Campania (Matese and Picentini Mts.) the high density of sinkholes on the Alburni karst plateau
161 has therefore to be related to the mostly horizontal bedding.
162 Recharge can be defined as the downward flow of water reaching the water table (De Vries and Simmers,
163 2002). In order to assess the recharge on the karst system at the Alburni, the hydrological analysis was
164 preceded by a detailed geomorphological investigation of the karst landforms (dolines and depressions) on
165 the summit plateau; both hydrological and morphometric analyses allowed to depict a specific overview of
166 recharge processes in which such karst landforms play a predominant role, because the effective meteoric
167 water falling on it contributes to feed the springs.
168 About 400 caves, with several of them reaching depth around 450 m, and with development of some
169 kilometres, characterize the Alburni Massif (Bellucci et al. 1991, 1995). This remarkable karst is essentially
170 related to the presence of the wide high plateau, bounded by fault systems, and with a variety of infiltration

sites, mainly corresponding to blind valleys and small catchments on the flysch deposits, which surface hydrology feeds the many swallets at the contact with the limestones (Santangelo and Santo, 1997; Del Vecchio et al. 2013; Cafaro et al., 2016). Through scrutiny of the data about the Alburni caves, all those where water was found were selected (Fig. 1 and Table 2). It must be pointed out that in these caves generally the presence of water corresponds to the end of the explorations, given the impossibility (in some cases) and the difficulty (in others) to pass the flooded passages. Further, presence of water does not necessarily mean that the saturated zone has been reached; actually, some of the water could be related to perched groundwater, due to less permeable intercalations within the stratigraphy, or to local clogging by debris and breakdown deposits. Nevertheless, we used the elevations at which water was documented into caves to build the hydrogeological profile shown in ~~figure~~ Figure 3, by assuming water as representative of the base water table.

Results

The Alburni karst massif can be considered a wide karst system, where surficial and groundwater hydrology are strictly linked, but still unclear. Surficial hydrology appears controlled by the wide summit plateau, which has been assumed as a wide closed area, where the runoff infiltrates in sinking points, providing a concentrated recharge. Outside of it, along the steep slopes bounding the plateau, the runoff can escape from the catchment and feed directly the rivers.

All karst landforms mapped and digitalized in a GIS environment provided a total number of 539 dolines, with average density of 5~~,~~97 depressions per km^2 (Fig. 2); 62% of these close depressions has area less than 0,1 km^2 (Pagnozzi et al. 2019). Their pattern distribution highlights that the central plateau is mostly affected by dolines of small size, whilst only along the north-western, eastern and southern borders, endorheic areas are generally ≥ 1 km^2. The statistical approach adopted in the study area allowed to assess the pitting index (total karst area/plateau area) which represent a measure of superficial karst development, providing information about the extent of karstification (Denizman, 2003; Haryono et al., 2017). At Alburni the ratio between karst area and plateau is 2.96.

196 To estimate the recharge, a preliminary delimitation of the catchment spring area, A_c, has to be provided.
197 Definition of the spring catchment area is a challenge in karst settings (Gunn 2007; Parise 2016), especially if
198 a wide karst system is drained by several springs, as at the Alburni Massif. A useful approach is to associate
199 the whole mountain or karst system to a lumped system, and to consider the overall output from spring
200 outlets, without focusing the analysis on a single spring and its relative catchment. In the Alburni case, the
201 karst terrains are bounded by impervious terrains which make the delimitation of the lumped spring
202 catchment easier; only along the SE sector, the spring catchment cannot be accurately defined.
203 Figure 3 provides the hydrogeological cross-section along the Alburni Massif considering some of the main
204 springs (Auso, 277 m a.s.l., to the S, and Pertosa, 250 m a.s.l., to the NE); the different elevation between
205 these springs is coherent with fault systems affecting the carbonate hydrostructure. Dolines and endorheic
206 basins drain the meteoric water on the summit plateau through the below network of shafts and conduits.
207 Looking at figure 3, the cave profiles, redrawn from the Regional Inventory of Caves of Campania, and adding
208 bedding information, highlight that development of the karst systems is highly controlled by the prevailing
209 discontinuity systems in the rock mass, both as sub-horizontal passages (bedding) and as vertical pits
210 (fractures or faults).
211 However, it is very arduous to assess the groundwater flowpath in the shafts (Jouves et al., 2017), so that in
212 many cases scholars refer to indirect methods in order to gain insights about the karst flow system
213 (geophysics, geodesy, etc.; Martel et al., 2018). In our case, detailed studies were carried out on the Alburni
214 catchment area, based on a methodical collection of available data about hydrology, water geochemistry and
215 piezometric data of the aquifer with its main outflows. Being the karst environment interested by a complex
216 system of conduits, passages and shafts (only partly known), the most reliable approach to propose a valid
217 hydrological model is represented by tracing experiments, particularly the cave-to-spring multitracer tests
218 (Goldscheider and Drew 2007; Filippini et al., 2018).
219 At Alburni, looking at the karstified limestone outcrops and at the morphological features of the calcareous
220 area with an elevation higher than that of the springs, the estimated recharge area is 267 Km^2. This wide area
221 includes the karst plateau, considered as a unique closed area, A_E, extended 90.09 Km^2. The catchment zones
222 outside the internal runoff area constitute the open areas ($A_O=A_C-A_E$).

The main results are shown in Table 3; taking into account the effective rainfall distribution and the temperature values, the mean actual evapotranspiration at Alburni Massif can be estimated (**545 mm/year)**. This value is comparable to evapotranspiration rates for nearby karst massifs of Southern Italy (Fiorillo et al., 2015; Fiorillo and Pagnozzi, 2015), whilst the amount of recharge is higher in Alburni, due to concentrated recharge at the summit plateau and to runoff being limited along the steep slopes bounding the massif. Looking at the numbers listed in Table 3, the annual effective afflux (P_{eff}) of the whole catchment area is **246 x 10^6 m^3**, the annual spring discharge (Q) is **230.6 x 10^6 m^3**, and the ratio Q/P_{eff} provides the effective recharge coefficient of **0.94**. The difference between the effective recharge from precipitation (**7.8 m^3/s**) and the spring discharge (**7.4 m^3/s**), estimated in **0.4 m^3/s**, could be associated to runoff losses and/or to minor springs, for which discharge data are unavailable.

An high effective recharge coefficient (**C_R = 0.90**) has been found for the open area (zone outside the summit plateau), where the runoff amount is only **13.4 x 10^6 m^3**. Even if the runoff amount is believed to be a very limited component in the hydrological balance in karst areas, this value could be considered as underestimated if compared to other areas of the Southern Apennines (cf. Fiorillo et al., 2015), due to poor knowledge of the total discharge amount and spring catchment area boundaries of the Alburni massif.

Considering only the summit plateau (90 km^2), this area totally contributes to spring discharge, as all the recharge amounts inside endorheic areas are assumed to reach the basal springs; in particular it represents 34% of the total Alburni catchment, but provides about half of the effective contribution to spring discharge (C_S= 0.45), and is even higher in terms of total rainfall (C'_S=0.65).

The above estimations refer to a long-term scale (annual mean rainfall over a time span of several decades), though annual recharge changes yearly, typically concentrating in specific seasons. Kessler (1967) highlighted the role of the first four months of the year in controlling the recharge in a karst environment of Hungary, and its dependence on the amount of rainfall recorded in the previous year (during the last four months). These characteristics are even exacerbated in Mediterranean climate areas, especially within the framework of the climate changes we are experiencing. At the Alburni Massif, recharge occurs mainly during the winter

and spring seasons, and depends on the previous autumn rainfall and the snowmelt as well, which are needed to satisfy the retention water of the soil cover.

Discussion and Conclusions

As repeatedly demonstrated worldwide, anthropogenic activities may produce significant changes in the hydraulic and hydrogeological regimes of karst areas (Bakalowicz, 1995, 2005; Ozanić et al. 2003; Ravbar & Sebela 2015; Chen et al., 2017; Parise et al. 2018). This occurs through a variety of human actions, ranging from land use changes (Foley et al., 2005; Quine et al., 2017; Peng et al., 2020), to quarrying and mining (Gunn 1993, 2003; Hobbs and Gunn 1993; Formicola et al. 2010; Parise 2010, 2016), variations in the amount and distribution of the natural vegetative cover (Ravbar et al. 2011; Huebsch et al. 2014), and overexploitation of groundwater resources (Hartmann et al. 2012; Finger et al. 2013; Musgrove et al. 2016; Jia et al. 2017). All these actions often lead to severe disturbance to the natural karst environment (Calò and Parise 2009), as proved through the application of the Karst Disturbance Index (Van Beynen and Townsend, 2005; North et al., 2009) to many different karst settings in the globe (Calò and Parise 2006; Day 2011). In the Alburni case study, the rural character of the area, that is a mountain setting mostly dedicated to pasture, and with a limited human presence, essentially distributed at its borders, is not considered to have in the near future a possible role in changing the hydrological regime. Nevertheless, protection and safeguard of karst groundwater, and more in general, of karst ecosystems (Bonacci et al. 2009; Fleury 2009; Gabrovsek et al. 2018) needs to be continuously pursued. This is one of the main goals of this contribution, hopefully helping to emphasize this remarkable karst area, aimed at improving and spreading its knowledge among the local inhabitants and the scientific community, in the effort to increase the awareness of the natural resources it hosts. It is also worth to mention the fact that the area is included in a National Park (*Parco Nazionale del Cilento, Alburni e Vallo di Diano*, http://www.cilentoediano.it), that was also declared Geopark by UNESCO in 2010, thus becoming member of the UNESCO network of Global Geoparks (Aloia et al. 2012; Santangelo et al. 2015).

The analysis presented in this article, based upon computation of the recharge at the summit plateau of Alburni Massif and its comparison with the total spring discharge, in spite of the many assumptions, shows a general agreement of the outcomes. Nevertheless, this cannot be considered as a definitive result, since many issues still remain to be fully examined and understood. Tracer tests in Alburni have shown in the past how the expected outcomes, in terms of sites of emergence, flow directions and velocity, and discharge values as well, have often been quite different from those forecasted on the basis of previous knowledge.

In the history of Alburni cave explorations, many tracer tests were addressed to prove the links among the karst systems and the basal springs (Del Vecchio et al. 2013; Parise and Santo 2017). Among the first outcomes, it has been demonstrated since the 1950's the link between the Castelcivita Caves and the Auso spring, for a total development of more than 6 km (Santo 1994). These researches were also useful to develop a first conceptual hydrogeological model along the Calore River. During the 1990's, an automatic datalogger installed at Risorgenza del Mulino provided data which indicated a deep circuit for the water at this spring (T 16,5 °C), as also proved by later cave diving explorations. Further, the delay (24 to 48 hours) in temperature changes after intense rainstorms on the Alburni highplain testified the connection between the vertical systems and the basal water table (Santangelo and Santo 1997). More recently, other tracing tests demonstrated the hydrogeological connection among the active swallow holes in Piana dei Campitelli and at Grotta del Falco with the nearby spring at Grotta dell'Acqua (Bocchino et al. 2014; Cozzolino et al. 2015). At the same time, the fluorescein was detected also at the waterfall within the Pertosa Cave and at some springs in the Tanagro River, outlining a quite complex scenario, which still needs further data to be entirely understood (Pedrali et al. 2015; Pastore 2016). In particular, cave diving explorations at Grotta del Falco proved the development of the cave system through one of the main tectonic lines of the Massif, the Vallone Lontrano – Petina (Gueguen et al. 2012; Cafaro et al. 2016), which seems to transfer the water from this system to the central part of the Alburni Massif, toward Grava del Fumo and the S. Maria karst system, and, in turn, to the Auso spring on the SW foothills of the massif. This tectonic line acts certainly as an important draining structure, as actually previously hypothesized by Bellucci and co-workers (1991).

The so far available tracer test data still hold some doubts regarding the central sector of the summit plateau: whether this is in communication with the SW or the NE side of the massif, and if there actually is the possibility of some dispersion within the groundwater network, with different functioning during the dry seasons (when the karst conduits may act independently) and during floods.

In conclusion, notwithstanding the efforts and the many continuing explorations, hydrogeology of the Alburni Massif still has several dark points, which need further work. This was also favored by high dispersion of data in the past, due to lack of communication among cave grottos, and to unpublished materials. The few available data, especially those concerning the spring discharges around the Alburni Massif, make any conclusion quite uncertain, since more detailed surveys and monitoring actions are needed.

Nevertheless, through the example of the Alburni Massif we have pointed out to some of the difficulties inherent in carrying out karst hydrogeology research, and to the need of a continuous and updated exchange of information with the cavers exploring the cave systems, since they represent the main source of new data ("the underground truth") in such settings.

References

Aloia, A., Guida, D. & Valente, A. (2012) Geodiversity in the Geopark of Cilento and Vallo di Diano as heritage and resource development. *Rend. Online Soc. Geol. It.*, 21, 688–690.

Angel, J.C., Nelson, D.O., & Panno, S.V. (2004) Comparison of a new GIS-based technique and a manual method for determining sinkhole density: An example from Illinois' sinkhole plain. *Journal of Cave and Karst Studies*, 66, 9−17.

Bakalowicz, M. (1995) La zone d'infiltration des aquifers karstiques. Methodes d'etude. Structure et fonctionnement. *Hydrogeologie*, 4, 3–21.

Bakalowicz, M. (2005) Karst groundwater: a challenge for new resources. *Hydrogeology Journal*, 13, 148–160.

Bellucci, F., Giulivo, I., Pelella, L., & Santo, A., (1991) Carsismo ed idrogeologia del settore centrale dei Monti Alburni (Campania). *Geologia Tecnica*, 3, 5–12.

Bellucci, F., Giulivo, I., Pelella, L., & Santo, A., (1995) *Monti Alburni. Ricerche Speleologiche*. De Angelis, Avellino.

Bocchino B., Del Vecchio U., De Nitto L., Lo Mastro F., Marraffa M., Maurano F., Minieri G., Parise M. & Ruocco M. (2014) Increasing people's awareness about the importance of karst landscapes and aquifers: an experience from southern Italy. In N. Kukuric, Z. Stevanović & N. Kresic (Eds.), *Proceedings International Conference and Field Seminar "Karst without boundaries"* (pp. 398-405).

Bonacci, O. (1995) Ground water behaviour in karst: example of the Ombla Spring (Croatia). *Journal of Hydrology*, 165, 113–134. https://doi.org/10.1016/0022-1694(94)02577-X

Bonacci, O. (2001) Monthly and annual effective infiltration coefficient in Dinaric karst: example of the Gradole karst spring catchment. *Hydrological Sciences Journal*, 46(2), 287–300.

Bonacci, O., & Magdalenić~~Magdalenic~~, A. (1993) The catchment area of the Sv. Ivan Karst spring in Istria, Croatia. *Ground Water*, 31(5), 767–773.

Bonacci, O., Pipan, T. & Culver, D.C. (2009) A framework for karst ecohydrology. *Environmental Geology*, 56, 891–900.

Brancaccio, L., Civita, M., & Vallario, A. (1973) Prime osservazioni sui problemi idrogeologici dell'Alburno, Campania. *Boll. Soc. Naturalisti Napoli*, 82.

Brinkmann, R., & Parise, M. (2012) Karst Environments: Problems, Management, Human Impacts, and Sustainability. An introduction to the Special Issue. *Journal of Cave and Karst Studies*, 74 (2), 135-136.

Cafaro, S., Gueguen, E., Parise, M., & Schiattarella, M. (2016) Morphometric analysis of karst features of the Alburni mts, southern Apennines, Italy. *Geogr. Fis. Dinam. Quat.,* 39*,* 121-128.

Calò, F. & Parise, M. (2006) Evaluating the human disturbance to karst environments in southern Italy. *Acta Carsologica*, 35, 47–56.

Calò, F. & Parise, M. (2009) Waste management and problems of groundwater pollution in karst environments in the context of a post-conflict scenario: the case of Mostar (Bosnia Herzegovina). *Habitat International*, 33, 63–72.

Celico, P., Pelella, L., Stanzione, D., & Aquino, S., (1994) Sull'idrogeologia e l'idrogeochimica dei Monti Alburni. *Geologica Romana*, 30, 687–698.

Cestari, G., (1971) *Note illustrative della Carta Geologica d'Italia alla scala 1:100.000. Foglio 198 Eboli.* Nuova Tecnica Grafica, Roma.

Chen, Z., Auler, A.S., Bakalowicz, M., Drew, D., Griger, F., Hartmann, J., Jiang, G., Moosdorf, N., Richts, A., Stevanović, Z., Veni, G. & Goldscheider, N. (2017) The World Karst aquifer mapping project: concept, mapping procedure and map of Europe. *Hydrogeology Journal*, 25, 771-785, 10.1007/s10040-016-1519-3.

Cozzolino, L., Damiano, N., Del Vecchio, U., Minieri, G., Testa, L., & Trifone, P. (2015) Prove di colorazione e recenti esplorazioni nell'area della Grotta del Falco - Monti Alburni. In *Proc. XXII Nat. Congr. Speleol.*, 323-328.

Day, M., Halfen, A. & Chenoweth, S. (2011) The cockpit country, Jamaica: boundary issues in assessing disturbance and using a karst disturbance index in protected areas planning. In P.E. Van Beynen (Ed.), *Karst Management.* Springer, Dordrecht (pp. 399–414).

Del Prete, S., Iovine, G., Parise, M., & Santo, A. (2010) Origin and distribution of different types of sinkholes in the plain areas of Southern Italy. *Geodinamica Acta*, 23(1/3), 113−127. https://doi.org/10.3166/ga.23.113-127

Del Vecchio U., Lo Mastro F., Maurano F., Parise M. & Santo A. (2013) The Alburni Massif, the most important karst area of southern Italy: history of cave explorations and recent developments. In M. Filippi & P. Bosak (Eds.), Proceedings 16th International Congress of Speleology, Brno, 21-28 July 2013, 1, (pp. 41-46).

Denizman, C. (2003) Morphometric and spatial distribution parameters of karstic depressions, lower Suwannee river basin, Florida. *Journal of Cave and Karst Studies*, 65, 29−35.

De Riso, R., & Santo, A. (1997) Geologia, evoluzione geomorfologica e frane del Bacino del T. Pietra (Campania). *Quaderni di Geologia Applicata*, 4(2), 19–33.

De Vries, J.J., & Simmers, I. (2002) Groundwater recharge: an overview of processes and challenges. *Hydrogeology Journal* 10, 5–17.

Dorsaz, J.M., Gironás, J., Escauriaza, C., & Rinaldo, A. (2013) The geomorphometry of endorheic drainage basins: implications for interpreting and modelling their evolution. *Earth Surface Processes and Landforms*, 38, 1881–1896.

Drogue, C. (1971) Coefficient d'infiltration ou infiltration eficace, sur le roches calcaires. *Actes du Colloque d'Hydrologie en Pays Calcaire*, Besancon 15, 121–130.

Ducci, D. (2007) Intrinsic vulnerability of the Alburni Karst System southern Italy. In M. Parise, & J. Gunn (Eds.), *Natural and Anthropogenic Hazards in Karst Areas: Recognition, Analysis, and Mitigation.* Geological Society, London, sp. publ. 279 (pp. 137–152).

Filippini, M., Squarzoni, G., De Waele, J., Fiorucci, A., Vigna, B., Grillo, B., Riva, A., Rossetti, S., Zini, L., Casagrande, G., Stumpp, C., & Gargini, A. (2018) Differentiated spring behavior under changing hydrological conditions in an alpine karst aquifer. *Journal of Hydrology* 556, 572-584.

Finger, D., Hugentobler, A., Huss, M., Voinesco, A., Wernli, H., Fischer, D., Weber, E., Jeannin, P.Y., Kauzlaric, M., Wirz, A., Vennemann, T., Hüsler, F., Schädler, B. & Weingartner, R. (2013) Identification of glacial meltwater runoff in a karstic environment and its implication for present and future water availability. *Hydrology and Earth System Sciences*, 17, 3261–3277.

Fiorillo, F., & Pagnozzi, M. (2015) Recharge process of Matese karst massif southern Italy. *Environmental Earth Sciences*, 74, 7557–7570.

Fiorillo, F., Pagnozzi, M., & Ventafridda, G. (2015) A model to simulate recharge processes of karst massifs**.** *Hydrological Processes*, 29, 2301–2314.

Fiorillo, F., Pagnozzi, M., & Ventafridda, G. (2019) Analysis of annual mean recharge in main karst systems of southern Italy. *Rend. Online Soc. Geol. It.*, Vol. 47, pp. 36-40. https://doi.org/10.3301/ROL.2019.07

Fleury, S. (2009) *Land Use Policy and Practice on Karst Terrains. Living on Limestone*. Springer, Dordrecht.

Foley, J.A., DeFries, R., Asner, G.P., Barford, C., Bonan, G., Carpenter, S.R., Chapin, F.S., Coe, M.T., Daily, G.C., Gibbs, H.K., Helkowski, J.H., Holloway, T., Howard, E.A., Kucharik, C.J., Monfreda, C., Patz, J.A., Prentice, I.C., Ramankutty, N & Snyder, P.K. (2005) Global consequences of land use. *Science*, 309 (5734), 570-574, 10.1126/science.1111772.

Ford, D.C., & Williams, P.W. (2007) Karst geomorphology and hydrology. 2nd ed. John Wiley & Sons, Chichester, U.K. https://doi.org/10.1002/9781118684986

Formicola W., Gueguen E., Martimucci V., Parise M. & Ragone G. (2010) Caves below quarries and quarries above caves: problems, hazard and research. A case study from southern Italy. *Geol. Soc. America Abs. with Program*, 42 (5).

Fragoso-Servón, P., Bautista, F., Frausto, O., & Pereira, A. (2014) Caracterización de las depresiones kársticas (forma, tamaño y densidad) a escala 1:50000 y sus tipos de inundación en el Estado de Quintana Roo, México. *Revista Mexicana de Ciencias Geológicas*, 31(1), 127−137.

Gabrovsek, F., Peric, B. & Kaufmann, G. (2018) Hydraulics of epiphreatic flow of a karst aquifer. *Journal of Hydrology*, 560, 56–74.

Gioia, D., Schiattarella, M., Mattei, M., & Nico, G. (2011) Quantitative morphotectonics of the Pliocene to Quaternary Auletta basin, southern Italy. *Geomorphology*, 134, 326-343.

Goldscheider, N., & Drew, D. (2007) *Methods in Karst Hydrogeology.* International Association of Hydrogeologists 26, Taylor & Francis, London.

Gueguen, E., Cafaro, S., Schiattarella, M., & Parise, M., (2012) A new methodology for the analysis of morpho-structural data of karstic caves in the Alburni Mountains of southern Italy. *Rendiconti Online Società Geologica Italiana*, 21 (1), 614-616.

Gunn, J. (1993) The geomorphological impact of limestone quarrying. *Catena*, 25, 187-198.

Gunn, J. (2003) Quarrying of limestones. In J. Gunn (Ed.), *Encyclopedia of cave and karst science*. Routledge, London (pp. 608-611).

Gunn, J. (2007) Contributory area definition for groundwater source protection and hazard mitigation in carbonate aquifers. In M. Parise, & J. Gunn (Eds.), *Natural and Anthropogenic Hazards in Karst Areas: Recognition, Analysis, and Mitigation.* Geological Society, London, sp. publ. 279 (pp. 97–109). https://doi.org/10.1144/SP279.9

Gutiérrez, F., Parise, M., De Waele, J., & Jourde, H. (2014) A review on natural and human-induced geohazards and impacts in karst. *Earth-Science Reviews*, 138, 61–88. https://doi.org/10.1016/j.earscirev.2014.08.002

Hartmann, A., Lange, J., Vivo Aguado, A., Mizyed, N., Smiatek, G. & Kunstmann, H. (2012) A multi-model approach for improved simulations of future water availability at a large Eastern Mediterranean karst spring. *Journal of Hydrology*, 468–469, 130–138.

Haryono, E., Trijuni Putro, S., & Suratman, S. (2017) Polygonal karst morphology of Karangbolong area, Java-Indonesia. *Acta Carsologica* 46-1, 63–72.

Häuselmann, P., Jeannin, P.Y., & Bitterli, T. (1999) Relationships between karst and tectonics: case-study of the cave system Northof Lake Thun Bern, Switzerland. *Geodinamica Acta*, 12(6), 377-387.

Heidari, M., Khanlari, G.R., Taleb Beydokhti, A.R., & Momeni, A.A. (2011) The formation of cover collapse sinkholes in North of Hamedan, Iran. *Geomorphology*, 132, 76−86. https://doi.org/10.1016/j.geomorph.2011.04.025

Hobbs, S.L. & Gunn, J. (1998) The hydrogeological effect of quarrying karstified limestone: options for protection and mitigation. *Quart. J. Eng. Geol.*, 31, 147-157.

Huebsch, M., Horan, B., Blum, P., Richards, K.G., Grant, J. & Fenton, O. (2014) Statistical analysis correlating changing agronomic practices with nitrate concentrations in a karst aquifer in Ireland. *WIT Transactions on Ecology and the Environment*, 182, 99–109.

Ippolito, F., Ortolani, F., & Russo, M. (1973) Struttura marginale tirrenica dell'Appennino campano: Reinterpretazione di dati di antiche ricerche di idrocarburi. *Memorie della Società Geologica Italiana* 12**,** 227-250.

Jia, Z., Zang, H., Zheng, X. & Xu, Y. (2017) Climate change and its influence on the karst groundwater recharge in the Jinci Spring Region, Northern China. *Water*, 9, 267.

Jourde, H., Roesch, A., Guinot, V., & Bailly-Comte, V. (2007) Dynamics and contribution of karst groundwater to surface flow during Mediterranean flood. *Environmental Geology*, 51(5), 725–730. https://doi.org/10.1007/s00254-006-0386-y

Jouves, J., Viseur, S., Arfib, B., Baudement, C., Camus, H., Collon, P., & Guglielmi, Y. (2017) Speleogenesis, geometry, and topology of caves: A quantitative study of 3D karst conduits. *Geomorphology* 298, 86 –106.

Kessler, H. (1967) Water balance investigations in the karstic regions of Hungary. In *Proceedings of the Symposium "Hydrology of fractured rocks"*. Dubrovnik, October 1965, vol. 1, Int. Ass. Scientific Hydrology, UNESCO (pp. 91–105).

Klimchouk, A.B. (2000) The formation of epikarst and its role in vadose speleogenesis. In A.B. Klimchouk, D.C. Ford, A.N. Palmer, & W. Dreybrodt (Eds.), *Speleogenesis. Evolution of Karst Aquifers* (pp. 91–99). National Speleological Society, Huntsville, Alabama, USA.

Martel, R., Castellazzi, P., Gloaguen, E., Trépanier, L., & Garfias, J. (2018) ERT, GPR, InSAR, and tracer tests to characterize karst aquifer systems under urban areas: The case of Quebec City. *Geomorphology* 310, 45-56.

Miao, X., Qiu, X., Wu, S.-S., Luo, J., Gouzie, D.R., & Xie, H. (2013) Developing efficient procedures for automated sinkhole extraction from Lidar DEMs. *Photogrammetric Engineering Remote Sensing*, 79(6), 545–554. https://doi.org/10.14358/PERS.79.6.545

Musgrove, M., Opsahl, S.P., Mahler, B.J., Herrington, C., Sample, T.L. & Banta, J.R. (2016) Source, variability, and transformation of nitrate in a regional karst aquifer: Edwards aquifer, central Texas. *Science of the Total Environment,* 568, 457–469.

North, L.A., Van Beynen, P.E. & Parise, M. (2009) Interregional comparison of karst disturbance: west central Florida and southeast Italy. *Journal of Environmental Management*, 90, 1770–1781.

Ozanić, N. & Rubinić, J. (2003) The regime of inflow and runoff from Vrana Lake and the risk of permanent water pollution. *RMZ - Materials and Geoenvironment*, 50, 281–284.

Pagnozzi, M., Fiorillo, F., Esposito, L., Leone, G. (2019) Hydrological features of endorheic areas in Southern Italy. *Italian Journal of Engineering Geology and Environment*, Special Issue 1, 85-9. DOI: 10.4408/IJEGE.2019-01.S-14

Palmer, A.N., (1991) Origin and morphology of limestone caves. *Geological Society of America Bulletin*, 103, 1-25.

Palmer, A. N. (2007) *Cave Geology.* Cave Books.

Palmer, A.N. (2010) Understanding the hydrology of karst. *Geologia Croatica*, 63, 143−148. https://doi.org/10.4154/gc.2010.11

Parise, M. (2010) The impacts of quarrying in the Apulian karst. In F. Carrasco, J.W. La Moreaux, J.J. Duran Valsero & B. Andreo (Eds.), *Advances in research in karst media*. Springer (pp. 441-447).

Parise, M. (2011) Surface and subsurface karst geomorphology in the Murge (Apulia, southern Italy). *Acta Carsologica*, 40(1), 79-93.

Parise, M. (2016) Modern resource use and its impact in karst areas – mining and quarrying. *Zeitschrift fur Geomorphologie*, 60 (X), 199-216.

Parise, M. (2016) How confident are we about the definition of boundaries in karst? Difficulties in managing and planning in a typical transboundary environment. In Z. Stevanovic, N. Kresic, & N. Kukuric (Eds.), *Karst without boundaries* (pp. 27−38). IAH-Selected Papers on Hydrogeology, 23, ISBN 9781138029682, CRC Press. https://doi.org/10.1201/b21380-4

Parise, M. (2019) Sinkholes. In W.B. White, D.C. Culver & T. Pipan (Eds.), *Encyclopedia of Caves* (pp. 934-942). Academic Press, Elsevier, 3rd edition, ISBN ISBN 978-0-12-814124-3.

Parise, M. & Santo, A. (2017) Tracer tests history in the Alburni Massif (Southern Italy). *IOP Conference Series: Earth and Environmental Science*, 95, 062006, doi :10.1088/1755-1315/95/6/062006

Parise, M., Ravbar, N., Živanović, V., Mikszewski, A., Krešić, N., Mádl-Szőnyi, J., & Kukurić, N.~~Živanovic, V., Mikszewski, A., Kresic, N., Mádl-Szo´Nyi, J., & Kukuric, N.~~ (2015) Hazards in karst and managing water resources quality. In Z. Stevanović (Ed.), *Karst Aquifers – Characterization and Engineering* (pp. 601−687). Professional Practice in Earth Sciences, Springer. https://doi.org/10.1007/978-3-319-12850-4_17

Parise, M., Gabrovsek, F., Kaufmann, G. & Ravbar, N. (2018) Recent advances in karst research: from theory to fieldwork and applications. In M. Parise, F. Gabrovsek, G. Kaufmann & N. Ravbar (Eds.), *Advances in Karst Research: Theory, Fieldwork and Applications*. Geological Society, London, Special Publication 466 (pp. 1-24), https://doi.org/10.1144/SP466.26.

Pastore, C. (2016) *Analisi idrogeologica dell'area carsica dei Monti Alburni Salerno, Campania*. Master Thesis, Univ. Alma Mater, Bologna, Italy.

Patacca, E., & Scandone P. (2007) Geology of the southern Apennines. *Italian Journal of Geosciences*, Special Issue 7, 75-119.

Pedrali, L., Buongiorno, V., Antonini, G., Cafaro, S., & De Nitto, L. (2015) Convergenza di dati per l'esplorazione della Grotta del Falco sul Massiccio degli Alburni (Campania). In *Proc. XXII Nat. Congr. Speleol.*, 537-542.

Peng, J., Tian, L., Zhang, Z., Zhao, Y., Green, S.M., Quine, T.A., Liu, H. & Meersmans, J. (2020) Distinguishing the impacts of land use and climate change on ecosystem services in a karst landscape in China. *Ecosystem Services*, 46, 101199, https://doi.org/10.1016/j.ecoser.2020.101199.

Quine, T., Guo, D., Green, S.M., Tu, C., Hartley, I., Zhang, X., Dungait, J., Wen, X., Song, Z., Liu, H., Buss, H., Barrows, T., Evershed, R., Johnes, P. & Meersmans, J. (2017) Ecosystem service delivery in karst landscapes: Anthropogenic perturbation and recovery. *Acta Geochimica*, 36 (3), 416-420, 10.1007/s11631-017-0180-4

Ravbar, N. & Šebela, S. (2015) The effectiveness of protection policies and legislative framework with special regard to karst landscapes: insights from Slovenia. *Environmental Science Policy*, 51, 106–116.

Ravbar, N., Engelhardt, I. & Goldscheider, N. (2011) Anomalous behaviour of specific electrical conductivity at a karst spring induced by variable catchment boundaries: the case of the Podstenjšek spring, Slovenia. *Hydrological Processes*, 25, 2130–2140.

Santangelo, N., & Santo, A. (1997) Endokarst processes in the Alburni massif Campania, Southern Italy: Evolution of ponors and hydrogeological implications. *Zeitschrift fur Geomorphologie*, 41(2), 229-246.

Santangelo, N., Romano, P. & Santo, A. (2015) The Geo-itineraries in the Cilento Vallo di Diano Geopark: A Tool for Tourism Development in Southern Italy. *Geoheritage* 7, 319-335.

Santo, A. (1994) Idrogeologia dell'area carsica di Castelcivita (M. Alburni – SA). *Geologia Applicata e Idrogeologia*, 28, 663-673.

Sartoni, S., & Crescenti, U. (1962) Ricerche biostratigrafiche nel Mesozoico dell'Appennino meridionale. *Giornale di Geologia*, **2**, Bologna.

Sauro, U. (2005) Closed depressions. In D.C. Culver & W.B. White (Eds.), *Encyclopedia of Caves* (pp. 108-127). Elsevier, Amsterdam.

Scandone, P. (1971) *Note illustrative della Carta Geologica d'Italia alla scala 1:100.000. Fogli 199 e 210 Potenza e Lauria.* Nuova Tecnica Grafica, Roma.

Scandone, P. (1972) Studi di geologia lucana: carta dei terreni della serie calcareo-silico-marnosa e note illustrative. *Boll. Soc. Nat. Napoli*, 81, 225-300.

Stevanović, Z. (Ed.) (2015) *Karst Aquifers – Characterization and Engineering*. Professional Practice in Earth Sciences, Springer.

Turc, L. (1954) Le bilan d'eau des sols. Relations entre les precipitations, l'evaporation et l'ecoulement. *Ann. Agric.*, 5, 4-24.

Van Beynen, P.E. & Townsend, K. (2005) A disturbance index for karst environments. *Environmental Management*, 36, 101–116.

Waltham, T., Bell, F., & Culshaw, M. (2005) *Sinkholes and subsidence. Karst and cavernous rocks in engineering and construction*. Springer Praxis.

White, W.B. (2002) Karst hydrology: recent developments and open questions. *Engineering Geology*, 65, 85–105. https://doi.org/10.1016/S0013-7952(01)00116-8

Williams, P.W. (2008) The role of the epikarst in karst and cave hydrogeology: a review. *International Journal of Speleology*, 37, 1−10. https://doi.org/10.5038/1827-806X.37.1.1

Worthington, S., Ford, D., & Beddows, P. (2001) Characteristics of porosity and permeability enhancement in unconfined carbonate aquifers due to the development of dissolutional channel systems. In G. Gunay, D. Ford, P.

Williams, & K. Johnson (Eds.), *Present state and future trends of karst studies* (pp. 13–29). Technical Documents in Hydrology. UNESCO, Paris, 49.

Wu, Q., Deng, C., & Chen, Z., (2016) Automated delineation of karst sinkholes from LIDAR-derived digital elevation models. *Geomorphology*, 266, 1−10. https://doi.org/10.1016/j.geomorph.2016.05.006

Zumpano, V., Pisano, L., & Parise, M. (2019) An integrated framework to identify and analyze karst sinkholes. *Geomorphology*, 332, 213-225.

538

539

540 **Figures**

541 1) Geological map of the Alburni Massif.

542 2) Map showing dolines and endorheic basins on the summit plateau of the Alburni Massif.

543 3) Hydrogeological schematic cross-section across the Alburni Massif, based upon speleological
544 data from the Regional Inventory of Caves of Campania, managed by the Campanian
545 Speleological Federation. Trace of section in figure 1. Some profiles of selected caves are
546 also shown, after the surveys from Campanian Speleological Federation
547 (http://www.fscampania.it/catasto-2/catasto/), with addition of the strata attitude.

548 4) Karst features of the Alburni Massif: A) the sump at Grotta del Falco (photo: GSAVD); B)
549 view of the shafts in the Parchitiello system (photo: GSAVD); C) downhill sump in the Grave
550 del Minollo (photo: GSAVD); D) Auso spring, at the S foothills of the massif (photo: F.
551 Fiorillo).

552

553 **Tables**

554 1) Springs surrounding the Alburni Massif, and related discharge values (if available).

555 2) Caves (yellow stars in figure 1) where water has been found within the karst systems.
556 Labels as in figure 3.

557 3) Hydrological parameters obtained from the recharge analysis for the Alburni Massif
558 (modified after Fiorillo et al. 2019). Key: *F*, afflux (mean precipitation on the catchment); T,
559 temperature; AET, actual evapotranspiration; F_{eff}, effective afflux (mean effective
560 precipitation on the catchment); *RO*, runoff; Q_P, groundwater abstracted; R, recharge; C_R,

561 effective recharge coefficient; C'_R, total recharge coefficient; C_s, effective contribution to

562 spring discharge; C'_s, total contribution to spring discharge.

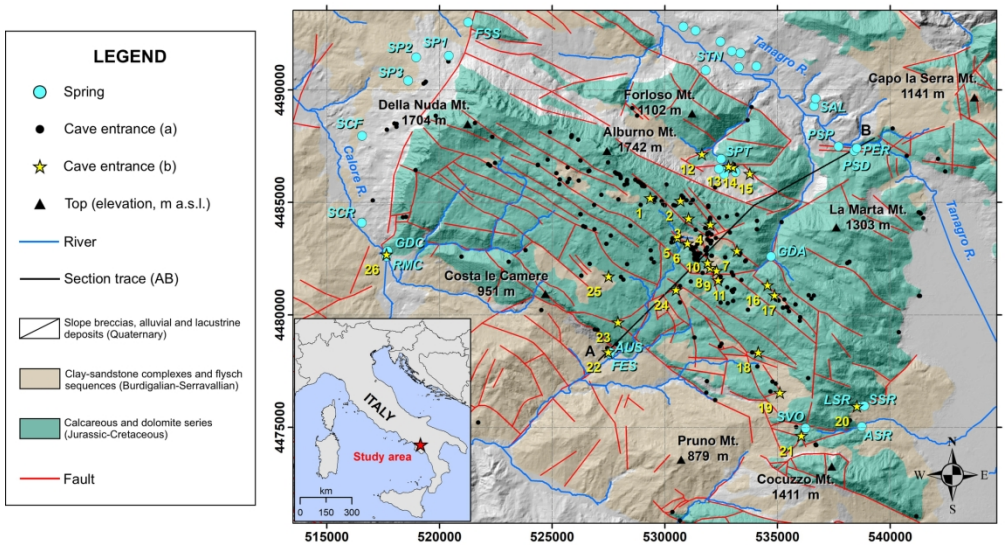

Geological map of the Alburni Massif.

200x108mm (300 x 300 DPI)

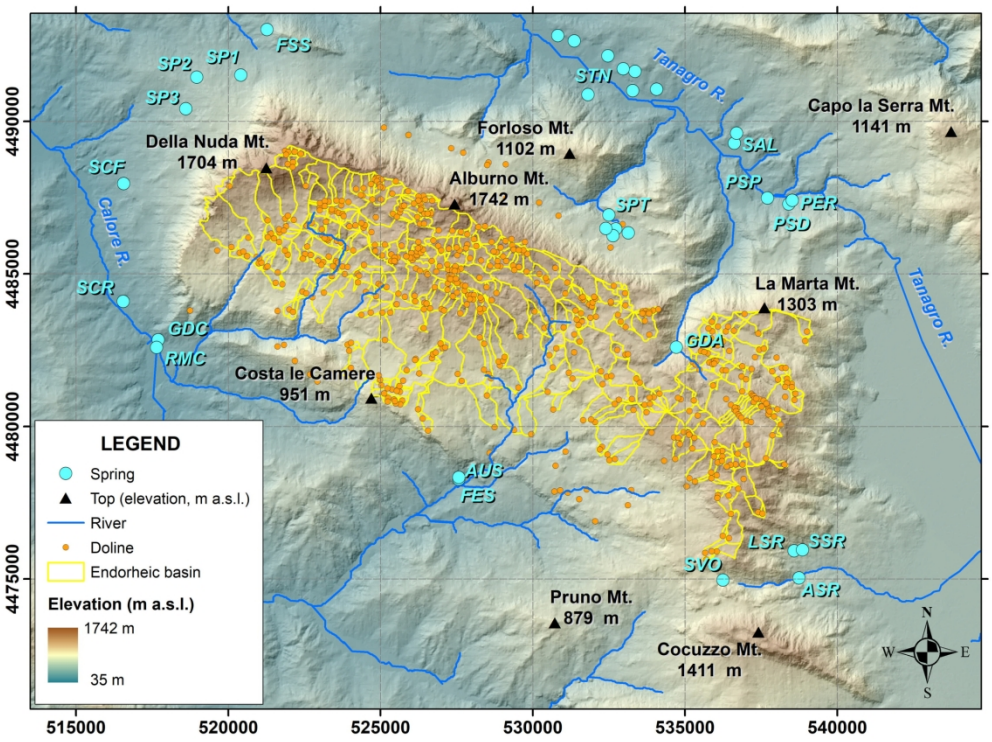

Map showing dolines and endorheic basins on the summit plateau of the Alburni Massif.

184x136mm (300 x 300 DPI)

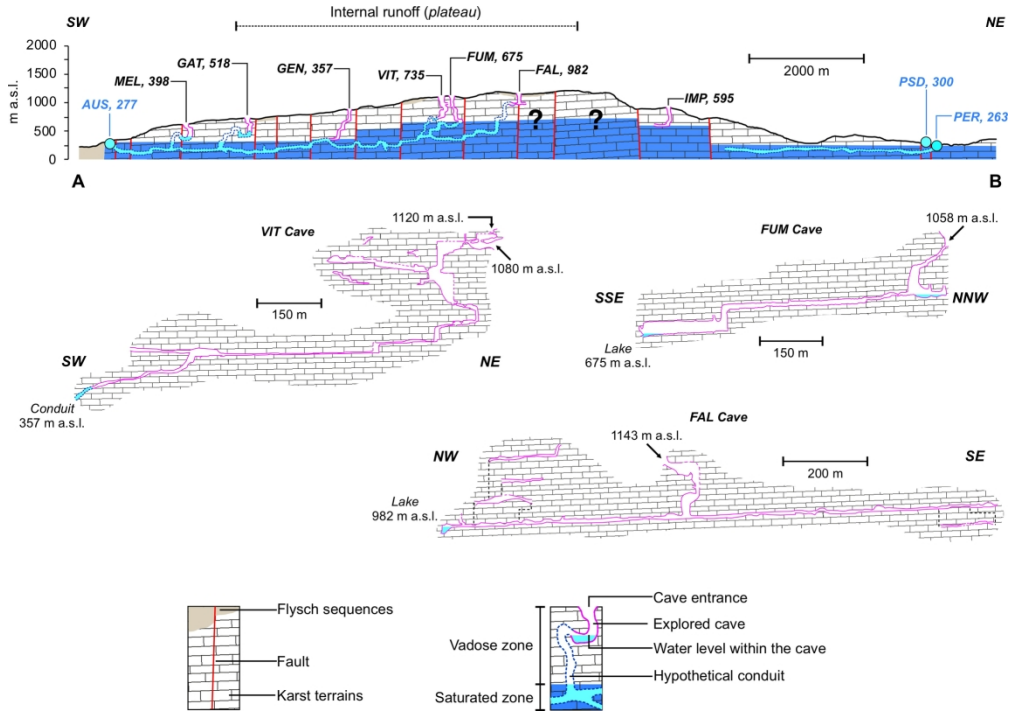

Hydrogeological schematic cross-section across the Alburni Massif, based upon speleological data from the Regional Inventory of Caves of Campania, managed by the Campanian Speleological Federation. Trace of section in figure 1. Some profiles of selected caves are also shown, after the surveys from Campanian Speleological Federation (http://www.fscampania.it/catasto-2/catasto/), with addition of the strata attitude.

193x136mm (300 x 300 DPI)

4) Karst features of the Alburni Massif: A) the sump at Grotta del Falco (photo: GSAVD); B) view of the shafts in the Parchitiello system (photo: GSAVD); C) downhill sump in the Grave del Minollo (photo: GSAVD); D) Auso spring, at the S foothills of the massif (photo: F. Fiorillo).

289x202mm (300 x 300 DPI)

Table 1

LABEL	*SPRING NAME*	*Elevation (m a.s.l.)*	*Mean annual discharge (m^3/s)*
RMC	Risorgenza del Mulino di Castelcivita	65	nd
GDC	Grotta di Castelcivita	94	1,.50
SCR	Controne	100	0,.10
SP1	Postiglione1	570	0,.10
SP2	Postiglione2	570	0,.10
SP3	Postiglione 3	570	0,.10
SCF	Sorgenti Cafaro	180	nd
FSS	Fontana Scorzo Sicignano	363	0,.01
STN	Sorgenti del Tanagro	204	3,.5
SAL	Sorgenti Auletta	235	nd
PSP	Polle sorgive Pertosa	195	nd
SPT	Sorgenti Petina	647	0,.10
PSD	Polle Santa Domenica	243	nd
PER	Grotta di Pertosa	263	1,.10
LSR	Lavatoio San Rufo	669	0,.01
SSR	Sorgente San Rufo	636	nd
ASR	Abbotituro San Rufo	672	0,.01
SVO	Sorgente Valetorno	848	nd
AUS	Risorgenza dell'Auso	280	1,.00
FES	Sorgente Festola	280	nd
GDA	Grotta dell'acqua	875	nd

Table 2

ID	*LABEL*	*CAVE NAME*	*Cave entrance ELEVATION (m a.s.l.)*	*WATER ELEVATION (m a.s.l.)*
1	MAR	Grava di Maria	1300	1097
2	VEN	Grava del Vento	1270	1231
3	ISC	Inghiottitoio sotto Serra Carpineto	1230	1076
4	INV	Grava d'Inverno	1150	949
5	VIT	Grotta dei Vitelli	1120	735
6	FUM	Grotta del Fumo	1058	615
7	PAR	Grava II del Parchitiello	1112	907
8	SM2	Inghiottitoio Piani di Santa Maria II	1096	1094
9	SM3	Inghiottitoio Piani di Santa Maria III	1076	656
10	SM1	Inghiottitoio Piani di Santa Maria I	1086	807
11	OSS	Grava delle Ossa	1060	769
12	LAU	Grotta del Lauro	550	532
13	POE	Grava del Poeta	635	590
14	MIL	Grotta Milano	640	600
15	IMP	Inghiottitoio di Mastro Peppe	680	595
16	FAL	Grotta del Falco	1105	944
17	CAM	Grotta II di Campitelli	1099	993
18	MIN	Grava del Minollo	888	577
19	SER	Grava del Serrone	970	754
20	GSR	Grotta di san Rufo	698	672
21	GPA	Grotte del Piano di Allaga	912	870
22	GAO	Grotta dell'Auso di Ottati	280	260
23	MEL	Grava di Melicupo	674	415
25	GEN	Grava dei Gentili	841	404
24	GAT	Grava dei Gatti	943	541
26	GAU	Grotta dell'Ausino	69	49

Table 3

Category	Mean elevation m a.s.l.	Area Km²	F		T °C	AET mm/y	F_{eff}		RO m^3X10^6	Q_p m^3X10^6/y	R m^3X10^6/y	C_R	C'_R	C_s	C'_s
			m^3x10^6/y	mm/y			m^3x10^6/y	mm/y							
Plateau area, A_E	1175	90	149	1658	7.9	500	104	1157	0,0	0.0	104	1,00	0.69	0.450	0.646
Open area, A_O	828	177	243	1375	10.5	569	142	805	13.4	0.0	128.6	**0.90**	0.53	0.550	0.354
Alburni, A_C	945	267	392	1470	9.6	545	246	923	13.4	0.0	232.6	0.94	0.59	1.000	1.000

CHAPTER 2

Dripping and river waters shed light on cave ecohydrology in a managed show cave

Rosangela Addesso*, Pietro Morozzi, Laura Tositti,

Jo De Waele, Daniela Baldantoni

Manuscript in preparation for submission to **Ecohydrology**

**corresponding author*

The chemical features of the Pertosa-Auletta Cave waters (dripping and Negro river) have been investigated, both in terms of space (in the three different trails with diverse natural characteristics and human fruition) and time (seasonally) scales, highlighting their important ecological role in the model cave ecosystem, and turning out to be a good indicator to assess the potential surface anthropogenic pressures.

Dripping and river waters shed light on cave ecohydrology in a managed show cave

Rosangela Addesso [1*], Pietro Morozzi [2], Laura Tositti [2], Jo De Waele [3], Daniela Baldantoni [1]

[1] Department of Chemistry and Biology "Adolfo Zambelli", University of Salerno, Via Giovanni Paolo II, 132, 84084 Fisciano (SA), Italy

[2] Department of Chemistry "G. Ciamician", Alma Mater Studiorum University of Bologna, Via Selmi, 2, 40126 Bologna, Italy

[3] Department of Biological, Geological and Environmental Sciences, Alma Mater Studiorum University of Bologna, Via Zamboni, 67, 40126 Bologna, Italy

*: Corresponding author (Name: Rosangela Addesso; Address: Department of Chemistry and Biology "Adolfo Zambelli", University of Salerno, Via Giovanni Paolo II, 132, 84084 Fisciano (SA), Italy; Tel.: +39 089 969542; Fax: +39 089 969603; email: raddesso@unisa.it)

Abstract

Caves are only apparently confined environments wherein water and air flow connect the surface airshed with the underground system, therefore influencing their chemistry and physical properties. The aim of this work was to investigate the chemical characteristics of Pertosa-Auletta Cave (Italy) waters, in particular from drip sites and from the underground Negro river, through time (seasonally) and through space (different trails). In particular, three different subterranean trails presenting distinct natural features and human fruition were investigated in order to highlight the different processes affecting the ecological equilibrium of the hypogean ecosystem. Dripping and flowing river waters, both rich in Ca because of their interaction with the same calcareous lithology, present significant chemical differences regarding K and Mg related to different water-rock interactions. The rainy or dry seasons also affected the chemical composition of the waters, increasing or decreasing the dilution effect respectively, and lead to a different atmospheric contribution to the water chemistry. Bat colonies, dwelling mainly along the fossil trail, have been found to contaminate dripping waters, enriching them in P and N, both probably also related to the agricultural activities on the lands above covered by farmed fields and woods, responsible of the relevant organic supply to the cave system.

Keywords: Cave hydrology, Karst, Water chemistry, Subterranean ecosystem, Pertosa-Auletta Cave

1 Introduction

Water has a key role in subterranean karst systems, creating and modifying them continuously. According to Williams (2008), surface rainfall percolates vertically through the soil driven by gravity, traversing the unsaturated vadose zone, and ultimately reaching the phreatic (or saturated) zone. The unsaturated vadose zone can be subdivided in the upper epikarst zone and the underlying transmission zone. The epikarst, or subcutaneous zone, is the uppermost part of the unsaturated vadose zone in karst areas. This particular zone acts as a water storage, slowly recharging the underlying less permeable transmission zone. Permeability in the epikarst zone is determined by the presence of fissures variously enlarged by dissolution, whose density rapidly diminishes downward with depth. Overall permeability in the underlying transmission zone is concentrated along a few enlarged major fissures, and is therefore much smaller than that in the overlying epikarst (Williams, 1983, 2008; Klimchouk, 2004; Poulain et al., 2015; Lauritzen, 2018). Before reaching the saturated zone, waters can pass through variable apertures in the rock (e.g., fractures, bedding planes, caves) and create drips, and eventually small underground streams, giving rise to dissolution/precipitation phenomena typical of karst. These incoming waters are the major energy and nutrient supply to these otherwise sheltered and oligotrophic habitats (Culver and Pipan, 2019; Addesso et al., 2022). In fact, water represents an important carrier of allochthonous trophic resources (dissolved organic matter, solutes, microorganisms, small-sized fauna…), connecting the nutrient-rich surface to the oligotrophic underground environment. These infiltrating waters also transfer external chemical signatures to the underground, where these environmental tracers can be trapped and stored into chemical precipitates and/or sedimentary records (Fairchild and Treble, 2009; Fairchild and Baker, 2012; Lauritzen, 2018).

Shedding light on underground water chemistry allows exploring not only hydrology, but also the ecology of caves. Indeed, the investigation of infiltrating waters permits to understand the natural biogeochemical processes occurring in the vadose zone ecosystem, and to assess their ecological features in relation to potential anthropogenic impacts (Motyka et al., 2005; Moldovan et al., 2007; Fairchild and Treble, 2009; Hartland et al., 2012; Fehér et al., 2016). In particular, dripping waters, and especially their chemical precipitates (speleothems), represent valuable proxies of changes over time, making cave systems important paleoenvironmental archives (Fairchild et al., 2000; Baldini et al., 2006; Wong et al., 2011; Fairchild and Baker, 2012; Riechelmann et al., 2013; Tremaine and Froelich, 2013; Rossi and Lozano, 2016; Columbu et al., 2018, 2019, 2020; Nava-Fernandez et al., 2020). In fact, to our knowledge, most researches concerning cave waters have been and still are primarily focused on dissolution/precipitation processes occurring in such environments (Fairchild and Baker, 2012), on the hydrology of the karst aquifer (Motyka et al., 2005; Nannoni et al., 2020) and on the surface contaminan sources affecting underground systems (Mahler and Massei, 2007; Jiménez-Sánchez et al., 2008; Ruggieri et al., 2017).

In this study, we provide an extensive characterization of the chemistry of seasonally collected dripping and cave river waters, during one year from the three main visitor paths (Tourist, Fossil, and Paradise) in the Pertosa-Auletta Cave, each characterized by distinct natural features and degree of anthropogenic disturbance (Addesso et al., 2019). The Pertosa-Auletta cave system is a 3-km-long natural cave, open to public since the 1930s, located in the south of Campania region (southern Italy). The cave is the terminal part of a large karst system carved in well-bedded and relatively pure limestones of Middle-Upper Jurassic age. These limestone beds are a few decimeters to several meters thick and generally separated by rather thin (cm to dm) layers of greenish

marls and clays, and locally by red-orange levels of bauxites, testifying to short periods of emersion (Cafaro et al., 2016).

The aim of this research was to shed light on the ecohydrology of this karst system, providing new insights (in both temporal and spatial dimensions) about relatively long-term compositional variations of the circulating water. We wanted to examine the factors influencing the ecological processes as well as the potential anthropogenic alterations of the natural ecological equilibrium in this model karst system open to the public.

2 Methods

Sampling of dripping waters and those flowing in the Negro subterranean river in the Pertosa-Auletta Cave (WGS84: 40°53′62″ N; 15°45′48″ E) was carried out along three main paths (Tourist, Fossil, and Paradise trails) of the cave, having different natural features and human fruition, and during the four seasons, from spring 2020 to winter 2021 (Figure 1a, Table 1).

The active part of the cave was not sampled due to logistical difficulties (being occupied by the river over its entire length), bur Negro River samples were taken near the start of Paradise trail. The geographical setting of the cave is characterized by a poorly human-affected landscape, with natural forests and a few olive tree groves; further up the hill,

there is the motorway, the abandoned rail network, and a water accumulation basin for a hydroelectric power plant (Figure 1b).

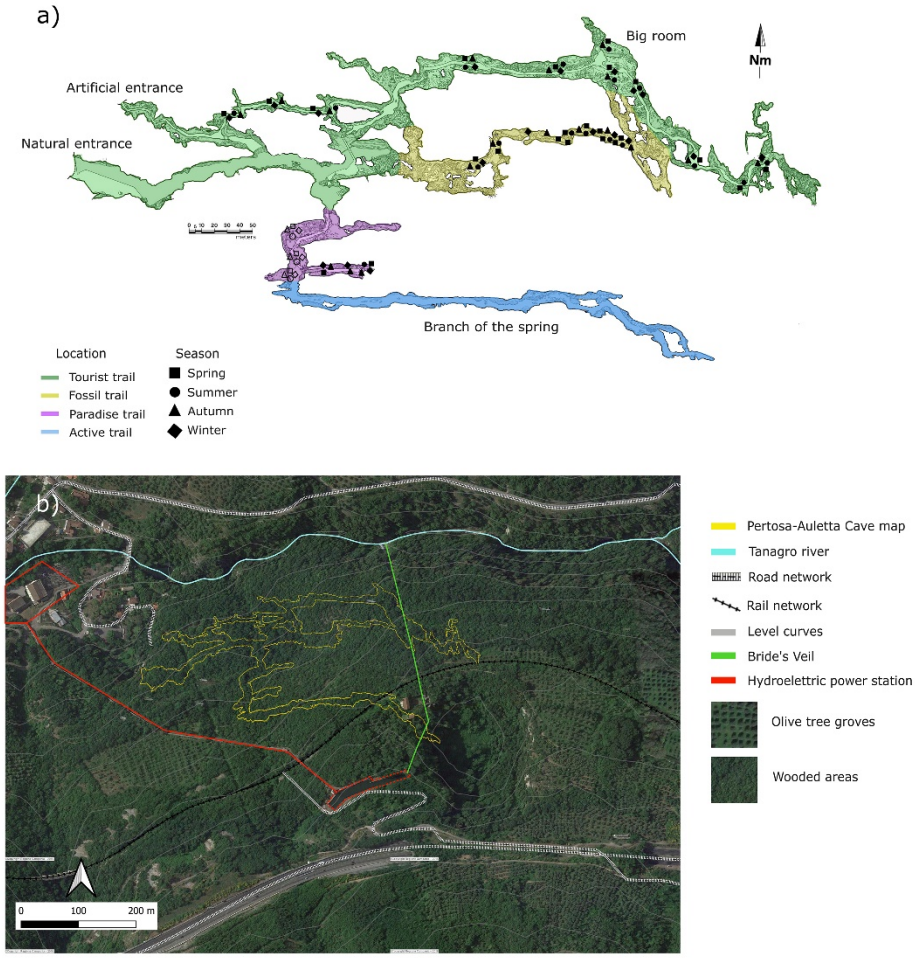

Figure 1 a. Map of the Pertosa-Auletta Cave, reporting the sampling sites organized according to their location in different trails (green, Tourist; yellow, Fossil; violet, Paradise), the season (circles, spring; triangles, summer; squares, autumn; rhombi, winter) and the water typology (dripping, full shapes; river, empty shapes) **b.** Pertosa-Auletta Cave geographical setting, reporting the cave map (yellow line), the Tanagro river (light blue line), the Bride's Veil (green line), the road and rail network (black and white lines, respectively), the hydroelettrical power station (red line) with the water storage tank (dotted red line) and the level curves (light grey lines).

Inside the cave, dripping water samples were collected leaving polyethylene bottles positioned at ground level below dripping speleothems for one week. Sampling sites were selected based on dripping activity, always in the same area over the four seasons.

Negro river water was manually sampled on the same day, after the drip water bottles were retrieved.

Table 1 Number (N) of water samples (dripping and river) collected in the three trails (Tourist, Fossil, Paradise) and in the Negro river of Pertosa-Auletta Cave along the four seasons (spring, summer, autumn, winter)

Season	Location	N
Spring (N = 26)	Tourist	11
	Fossil	10
	Paradise	2
	Negro	3
Summer (N = 20)	Tourist	10
	Fossil	6
	Paradise	1
	Negro	3
Autumn (N = 21)	Tourist	9
	Fossil	6
	Paradise	3
	Negro	3
Winter (N = 20)	Tourist	9
	Fossil	5
	Paradise	3
	Negro	3

Field water analyses were also performed during sampling using a probe Pioneer 65 Radiometer Analytical (HACH) for electric conductivity, and a waterproof portable logging multiparameter probe HI-98196 (Hanna Instrument) for pH and redox potential (ORP).

Total concentrations of Al, B, Ba, Ca, Cd, Co, Cr, Cu, Fe, K, Li, Mg, Mn, Mo, Na, Ni, P, Pb, S, Si, Sr, Ti, V, and Zn were obtained by inductively coupled plasma - optical emission spectroscopy (ICP-OES), Optima 7000 DV (PerkinElmer), quantifying the chemical elements using a multi-point calibration curve from standard multi-element

solutions. The precision of the method, calculated as relative standard deviation (n = 9), ranged from 2 to 6%, depending on each element. Total N, as well as total, organic (C org) and inorganic (C inorg) C were measured with a TOC-VCSH/CSN analyzer, containing a TN-unit (Shimadzu), through catalytic oxidation method with oxygen at 680 °C, and with non-dispersive infrared spectroscopy (NDIR) as detection method (injected volume: 50 µL; acid ratio (HCl): 2%; sparge time: 2 min). Anions (F^-, Cl^-, NO_3^-, SO_4^{2-}, CH_3COO^-) and cations (Na^+, K^+, Mg^{2+}, Ca^{2+}) were determined by ion chromatography, using respectively Ion Chromatography Systems ICS2000 and ICS90 (Thermo-Dionex). Certified Reference Material (ERM-CA408), containing the main ions in natural waters, was also analyzed to assess the analytical accuracy.

Dissimilarities in the chemical composition of samples, considering three fixed variables, the location (Tourist, Fossil, and Paradise trails), the type of sample (dripping or Negro river waters) and the season (spring, summer, autumn, and winter), were evaluated by a permutational multivariate analysis of variance (PERMANOVA), based on the Euclidean distance metric and $1 \cdot 10^6$ permutations. Nonmetric multidimensional scaling (NMDS) on 2 axes was subsequently applied, using the same distance metric, with the superimposition of confidence ellipses ($\alpha = 0.05$) for the seasons. Non-negative matrix factorization (NMF) was performed by Brunet algorithm (standard NMF; Brunet et al., 2004) and six new factors were calculated as a linear combination of the 36 original chemical variables of the analyzed waters. A network based on the Pearson's correlation coefficients was also executed. Data analyses were performed through R 4.0.0 software (R Core Team, 2020) with functions from the "vegan", "qgraph", "ggplot2", and "NMF" packages.

3 Results

The Pertosa-Auletta cave exhibits a hydrological activity variable in space, within and among the three considered paths (Tourist, Fossil, and Paradise), and in time, through the seasons (spring, summer, autumn, and winter). All the experimental data collected are summarized in Table 2, showing minimum and maximum values for each of them, organized by typology, location, and season. The complete dataset is displayed in the supplementary material: Table S1, spring; Table S2, summer; Table S3, autumn; Table S4, winter.

Overall, conductivity ranges from 76.2 to 660.0 μS/cm for dripping water and from 164.6 to 387.0 μS/cm for river water, whereas ORP shows values from 84.8 to 227.3 mV for dripping water and from 113.5 to 215.0 mV for river water. pH ranges from 5.9 to 8.4 for dripping and from 6.9 to 7.8 for river waters, respectively.

Total C varies from 12.5 to 65.3 mg/L for dripping water and from 24.4 to 43.3 mg/L for river water. Organic C concentration is more than twice as high as that of inorganic carbon for most of the samples, with mean values of 23.1 and 8.7 mg/L for dripping waters and of 25.3 and 10.9 mg/L for river water samples, respectively. N shows variable concentrations according to the sampling trails: a mean value of 0.9 mg/L for dripping and river waters from tourist trails, and a mean value of 8.7 mg/L for samples from the fossil trail. On average, Ca (53.8 mg/L), Cd (0.7 μg/L), Co (0.8 μg/L), Cr (0.4 μg/L), Cu (2.0 μg/L), K (1.9 mg/L), Mn (2.7 μg/L), Mo (2.0 μg/L), Na (7.1 mg/L), Ni (3.4 μg/L), Pb (6.6 μg/L), S (2.9 mg/L), Si (4.0 mg/L), Sr (60.6 μg/L), V (1.8 μg/L) and Zn (6.2 μg/L) show concentrations comparable between dripping and river waters, whereas Fe, Li, Mg, P, and Ti show differences among dripping (11.3, 11.8, 6000, 44.9, and 69.4 μg/L, respectively) and river (17.3, 24.4, 14800, 50.6, and 110.1 μg/L,

Table 2 Minimum and maximum values of water parameters from Pertosa-Auletta Cave, reported on the basis of the season (spring, summer, autumn, winter), location (Tourist, Fossil, Paradise trails) and typology (DW: dripping water; NR: Negro river); b.d.l: below detection limit

Season	Spring								Summer								Autumn								Winter							
Trail	Tourist		Fossil		Paradise				Tourist		Fossil		Paradise				Tourist		Fossil		Paradise				Tourist		Fossil		Paradise			
Type	DW		DW		DW		NR		DW		DW		DW		NR		DW		DW		DW		NR		DW		DW		DW		NR	
Value	min	max	min	max	min	max	min	max	min	max	min	max	min	max	min	max	min	max	min	max	min	max	min	max	min	max	min	max	min	max	min	max
Conductivity (µS/cm)	212.0	521.0	125.0	660.0	269.0	309.0	221.0	247.0	248.0	619.0	233.0	459.0	230.0	230.0	384.0	390.0	118.5	206.0	76.2	504.0	108.2	185.6	164.6	202.0	177.4	266.0	95.7	211.0	155.3	251.0	209.0	218.0
ORP (mV)	122.1	183.0	99.1	138.0	142.8	152.8	132.4	137.4	84.8	126.7	101.3	113.0	99.3	99.3	109.8	113.9	165.4	211.1	156.0	172.9	157.3	178.2	152.9	160.2	200.8	227.3	198.6	216.9	206.2	218.6	210.9	215.0
pH	6.5	7.8	6.9	8.4	5.9	6.5	6.9	7.0	7.1	8.2	7.7	8.0	8.1	8.1	7.7	7.8	6.6	7.5	7.2	7.5	6.9	7.5	7.5	7.6	7.0	7.6	7.1	7.6	7.1	7.4	7.2	7.3
C (mg/L)	20.8	52.8	17.5	38.1	36.7	36.9	33.9	38.1	25.8	65.3	23.5	39.9	21.4	21.4	42.3	46	20.2	41.8	12.5	38.5	19.4	47.5	24.4	33.0	21.9	47.8	13.1	26.7	20.3	42.5	33.1	36.1
C org (mg/L)	15.1	37.5	12.6	34.1	26.5	26.8	23.7	27.4	18.1	42.0	16.4	27.7	15.4	15.4	28.2	30.7	14.4	29.0	9.1	26.1	12.6	31.6	16.2	21.9	16.2	35.2	10.1	20.7	15.3	31.1	24.1	26.7
C inorg (mg/L)	5.7	15.2	2.2	5.9	9.9	10.4	10.2	10.7	7.7	23.3	7.1	12.2	6.0	6.0	13.9	15.3	5.8	12.8	3.4	12.4	6.8	15.9	8.2	11.4	5.7	12.6	3.0	6.0	5.0	11.4	7.9	9.6
N (mg/L)	0.3	1.6	0.4	47.7	0.4	0.4	0.8	1.1	0.3	1.6	0.9	11.7	0.4	0.4	1.1	1.2	0.3	3.8	0.5	66.9	0.3	0.8	0.7	1.1	0.3	1.0	0.4	22.2	0.4	0.5	1.5	2.0
Al (µg/L)	12.7	58.1	9.3	58.2	14.9	24.6	21.5	28.1	19.8	67.8	16.3	122.7	46.3	46.3	40.1	57.7	8.8	31.3	8.1	67.3	7.2	12.4	7.1	13.3	14.3	27.8	11.9	47.0	13.1	19.7	45.9	53.0
B (µg/L)	11.3	45.7	8.7	55.2	46.3	53.9	53.1	81.5	25.0	76.8	25.2	42.1	22.8	22.8	29.9	40.2	4.4	48.7	4.2	49.5	25.5	89.1	23.6	83.4	31.4	73.4	13.2	131.5	28.7	60.6	25.0	118.7
Ba (µg/L)	3.8	29.5	5.4	46.2	20.0	22.6	29.6	39.4	7.3	34.4	13.7	22.3	21.9	21.9	18.9	32.0	5.0	14.8	3.4	24.1	6.8	11.9	9.7	19.8	4.6	21.8	3.9	26.1	10.7	12.0	8.2	27.3
Ca (mg/L)	45.2	104.2	41.0	138.0	70.5	74.6	39.4	45.1	39.4	80.0	45.5	74.8	47.6	47.6	41.9	61.0	17.9	27.5	13.0	109.2	18.6	30.1	15.6	21.4	44.2	93.8	36.0	63.3	43.7	81.7	51.8	54.6
Cd (µg/L)	0.1	0.2	b.d.l.	0.2	0.0	0.1	0.1	0.2	2.2	2.5	2.3	2.6	2.4	2.4	2.4	2.6	0.1	0.3	0.1	0.4	0.1	0.3	0.1	0.2	0.1	0.3	b.d.l.	0.3	0.2	0.4	0.1	0.3
Co (µg/L)	0.2	0.9	b.d.l.	1.1	0.6	0.6	0.8	1.3	1.7	2.5	2.0	2.5	2.5	2.5	1.7	2.7	0.2	0.5	0.2	0.5	0.3	0.4	0.2	0.3	0.1	0.4	0.2	0.4	0.4	0.4	0.2	0.4
Cr (µg/L)	0.1	1.0	0.2	0.8	b.d.l.	0.1	0.4	0.6	b.d.l.	b.d.l.	b.d.l.	b.d.l.	b.d.l.	b.d.l.	b.d.l.	b.d.l.	0.2	0.6	0.2	0.8	0.3	0.5	0.2	0.8	0.2	1.0	b.d.l.	1.2	0.4	0.6	0.6	1.4
Cu (µg/L)	0.3	1.7	b.d.l.	1.2	1.2	2.5	0.7	1.7	3.3	11.3	3.7	7.3	5.4	5.4	4.2	4.4	0.2	2.3	0.4	2.2	0.3	1.2	0.8	1.6	0.7	2.2	0.3	1.4	0.7	1.8	0.7	1.6
Fe (µg/L)	0.8	11.7	0.4	47.3	10.0	11.3	13.7	15.2	7.5	52.5	10.0	68.5	30.2	30.2	16.3	35.3	2.0	25.6	1.3	34.6	1.6	6.9	1.9	7.3	0.6	11.1	3.9	17.5	1.3	2.4	16.7	28.6
K (mg/L)	0.7	2.7	0.7	22.3	1.4	1.5	1.6	2.2	1.3	13.9	1.0	2.7	1.0	1.0	2.3	2.5	0.5	1.9	0.6	1.8	0.6	0.8	1.5	1.8	0.9	3.1	0.7	2.7	1.2	2.0	1.8	2.7
Li (µg/L)	0.7	22.2	1.0	35.6	20.2	22.3	26.3	38.3	1.6	39.0	2.6	12.9	3.2	3.2	2.5	12.2	1.0	25.4	3.6	25.1	3.7	19.7	12.9	48.3	0.9	37.8	0.5	42.8	7.9	25.6	2.5	41.8
Mg (mg/L)	3.0	13.2	1.7	9.9	4.2	5.1	11.7	13.8	2.9	16.3	2.6	7.6	3.5	3.5	18.7	22.2	2.6	12.1	2.2	7.3	1.9	3.6	11.7	14.6	2.9	15.7	1.5	10.8	4.2	5.2	11.2	14.1
Mn (µg/L)	0.7	9.9	0.6	13.9	5.7	6.4	9.3	13.0	1.5	11.1	1.5	5.0	7.0	7.0	2.0	5.1	b.d.l.	1.0	b.d.l.	2.3	0.4	0.6	0.6	1.6	b.d.l.	1.0	b.d.l.	0.9	b.d.l.	0.2	1.0	1.9
Mo (µg/L)	b.d.l.	0.4	b.d.l.	0.8	b.d.l.	b.d.l.	b.d.l.	0.2	6.3	11.1	6.9	8.4	7.8	7.8	7.6	8.5	b.d.l.	0.8	b.d.l.	1.1	b.d.l.	0.5	b.d.l.	1.1	b.d.l.	1.9	b.d.l.	0.5	b.d.l.	b.d.l.	b.d.l.	1.5
Na (mg/L)	5.4	11.8	1.4	9.5	6.3	6.6	4.8	5.9	5.5	12.7	3.8	9.6	6.1	6.1	7.8	8.6	4.1	10.1	2.7	8.9	2.6	6.3	5.3	6.5	5.8	12.0	3.1	9.8	6.7	8.2	5.6	7.7
Ni (µg/L)	b.d.l.	1.7	b.d.l.	2.7	0.6	2.6	0.7	1.4	8.5	13.4	10.5	13.3	11.9	11.9	10.6	11.7	b.d.l.	1.7	b.d.l.	1.7	b.d.l.	2.0	b.d.l.	1.7	0.7	2.6	0.4	1.7	b.d.l.	1.0	0.6	1.6
P (µg/L)	6.5	42.4	7.1	932.3	7.6	11.7	30.4	33.7	36.1	92.1	43.0	96.3	63.1	63.1	87.5	109.0	9.6	33.5	2.1	89.9	12.3	16.9	30.8	32.8	3.3	46.4	12.2	21.9	2.4	9.6	33.4	47.6
Pb (µg/L)	b.d.l.	1.2	b.d.l.	b.d.l.	b.d.l.	1.0	b.d.l.	b.d.l.	22.7	29.9	22.6	27.3	25.2	25.2	24.4	25.1	b.d.l.	2.4	2.4	4.0	0.3	1.8	b.d.l.	2.5	b.d.l.	6.0	b.d.l.	6.0	b.d.l.	3.3	0.2	2.7
S (mg/L)	1.4	5.6	0.5	14.6	1.7	1.8	2.1	2.6	1.6	18.5	1.8	6.5	4.0	4.0	5.4	6.2	0.9	3.0	0.6	2.6	0.7	1.5	2.1	2.8	1.0	3.4	0.5	3.7	1.5	1.9	1.8	2.9
Si (mg/L)	2.7	7.0	1.7	6.6	2.6	3.8	3.4	4.1	3.4	8.0	3.9	7.7	4.1	4.1	4.7	5.4	2.2	9.7	0.6	5.6	1.9	3.7	1.7	3.2	0.9	9.9	0.8	3.0	0.7	6.3	1.9	2.8
Sr (µg/L)	49.0	82.7	28.8	93.3	47.6	52.7	62.3	63.6	0.1	129.3	45.6	86.7	75.7	75.7	74.8	85.5	34.6	119.5	32.5	124.5	46.4	48.0	42.1	55.3	44.5	129.6	32.0	63.1	49.6	73.5	59.2	66.5
Ti (µg/L)	b.d.l.	0.5	0.1	6.6	0.1	0.1	0.2	0.6	145.5	388.8	178.0	963.7	278.0	278.0	369.1	499.3	0.2	1.1	0.1	3.1	0.1	0.2	0.1	0.4	b.d.l.	2.6	0.3	1.4	0.2	0.2	1.4	4.0
V (µg/L)	0.6	1.7	b.d.l.	1.6	0.8	1.3	0.9	1.9	2.1	3.9	2.6	4.5	3.6	3.6	4.5	5.9	0.9	1.9	0.4	1.7	b.d.l.	1.5	1.4	2.8	0.1	1.7	0.6	1.4	1.0	1.2	1.6	2.7
Zn (µg/L)	2.9	35.4	0.3	19.0	4.7	7.0	8.7	30.0	12.4	27.7	12.9	17.2	16.4	16.4	14.0	16.3	b.d.l.	9.4	b.d.l.	b.d.l.	b.d.l.	b.d.l.	b.d.l.	b.d.l.	b.d.l.	b.d.l.	b.d.l.	b.d.l.	b.d.l.	b.d.l.	b.d.l.	b.d.l.
Na^+ (mg/L)	5.5	11.9	2.5	9.7	5.9	6.0	4.3	5.5	2.8	10.5	2.9	8.3	4.6	4.6	6.3	6.4	5.5	12.4	2.7	9.9	5.0	6.7	7.4	7.5	5.5	12.5	3.1	8.8	5.9	8.0	5.4	6.6
K^+ (mg/L)	0.3	2.5	0.6	2.5	0.6	0.6	1.2	1.5	0.2	1.8	0.6	2.3	0.5	0.5	2.1	2.1	0.3	2.8	0.7	2.3	0.7	1.6	2.1	2.2	0.4	2.6	0.7	1.7	0.6	2.1	1.7	2.3
Mg^{2+} (mg/L)	1.8	11.1	1.1	7.9	2.0	2.3	10.4	12.7	1.2	12.4	1.4	4.6	1.6	1.6	12.9	13.3	1.8	13.8	1.6	8.0	2.2	2.3	15.1	15.8	2.0	16.4	1.0	7.5	1.9	3.4	8.9	10.3
Ca^{2+} (mg/L)	23.8	52.4	20.4	41.8	33.0	34.2	26.4	34.7	30.8	58.8	33.6	54.6	37.7	37.7	44.1	55.8	44.4	112.6	40.8	171.1	36.0	111.6	36.5	64.7	14.3	37.0	14.0	40.6	19.7	37.7	26.0	28.7
F^- (mg/L)	0.05	0.16	0.06	0.17	0.08	0.09	0.10	0.10	0.05	0.13	0.05	0.15	0.12	0.12	0.12	0.12	0.04	0.12	0.01	0.15	0.06	0.12	0.06	0.08	0.05	0.19	0.06	0.15	0.05	0.14	0.10	0.25
Cl^- (mg/L)	6.2	15.3	3.5	14.9	14.2	14.4	6.8	8.8	4.8	12.9	4.1	14.7	9.8	9.8	9.9	10.1	7.7	16.7	3.1	13.9	9.9	12.1	9.4	9.5	9.0	20.5	4.4	18.9	14.9	17.9	9.4	9.8
NO_3^- (mg/L)	0.2	7.8	1.1	317.0	0.2	0.2	3.0	4.1	0.3	7.0	3.5	184.5	0.7	0.7	4.2	4.2	0.4	18.2	1.6	391.4	0.3	3.1	4.7	4.7	0.2	3.8	1.0	97.2	0.1	0.6	5.6	5.7
SO_4^{2-} (mg/L)	2.9	19.2	0.9	7.9	3.4	3.9	2.8	3.9	1.3	5.7	1.2	7.0	3.3	3.3	4.6	4.8	2.8	9.5	0.7	7.3	1.6	3.1	4.7	4.9	1.8	9.5	1.0	7.6	2.1	4.1	4.5	5.2
CH_3COO^- (µg/L)	3.5	22.1	3.5	14.8	9.8	11.6	5.5	12.4	3.5	20.9	4.9	17.5	6.3	6.3	14.8	18.7	29.4	168.8	11.4	47.9	b.d.l.	46.4	26.6	51.5	b.d.l.	93.0	b.d.l.	118.6	b.d.l.	107.8	b.d.l.	148.9

respectively) waters. Moreover, as reported in Tables S1-S4, Cd, Co, Cr, Cu, Mn, Mo, Ni, Pb, Ti, V, and Zn turn out to be below the detection limits for several analyzed samples.

Among the cations, Na^+ shows comparable concentrations between water types, with mean values of 7.2 mg/L in dripping water and 1.3 mg/L in river water. K^+ and Mg^{2+} present differences between the two water typologies, with mean values, respectively, of 1.2 and 4.6 mg/L for dripping water and 38.3 and 1.9 mg/L for river water. Among the anions, only SO_4^{2-} (on average 4.7 mg/L) shows comparable concentrations between dripping and river waters, whereas F^-, Cl^-, NO_3^-, and CH_3COO^- display, respectively, mean concentrations equal to 0.1, 11.4, 21.5 mg/L and 25.1 µg/L for dripping water, and 0.1, 9.1, 4.5 mg/L and 38.6 µg/L for river water.

PERMANOVA enabled the identification of significant differences in relation to both the seasons (P = 0.001) and locations (P = 0.007) fixed factors, but not between the

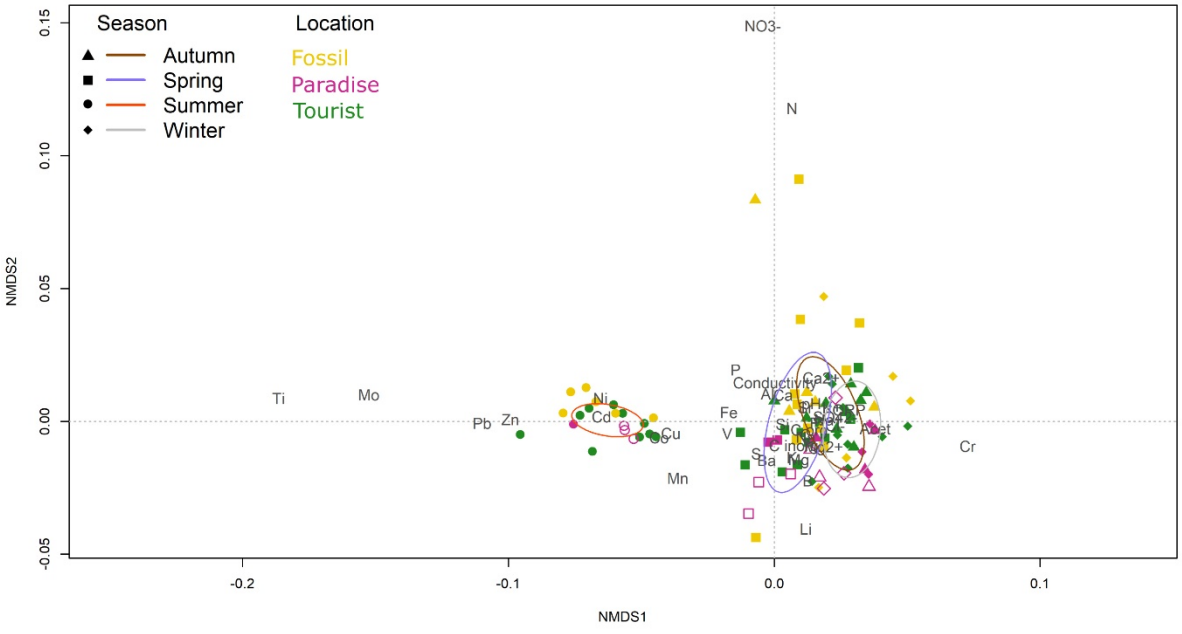

Figure 2 NMDS biplot based on the water characteristics, with the superimposition of confidence ellipses for α = 0.05, according to the seasons.

types of water (P = 0.337). The NMDS multivariate ordination with superimposition of confidence ellipses (Figure 2), shows differentiation among the water samples on a seasonal basis; in particular, summer samples are considerably different from those of the other seasons owing to their higher Cd, Co, Cu, Mn, Mo, Ni, Pb, Ti, and Zn concentrations. Finally, several samples from the Fossil trail show the highest concentration of NO_3^- as well as of total N.

Figure 3 shows the stacked bar chart of the percentage concentrations of each chemical species contributing to the six factors, representing each the source chemical profile identified in the NMF analysis. Factor 1 is mainly characterized by C org, C inorg, and Ca^{2+}; Factor 2 is mainly defined by Si, Cd, Fe, V, Co, Cr, and Cu; Factor 3 is characterized by K, Zn, and Mn; Factor 4 is defined by Mg^{2+}, Mg, and K; Factor 5 is mainly defined by SO_4^{2-}, Na^+, Cl^-; Factor 6 is characterized by N and NO_3^-. The interpretation of the six factors from a chemical and geological point of view is reported

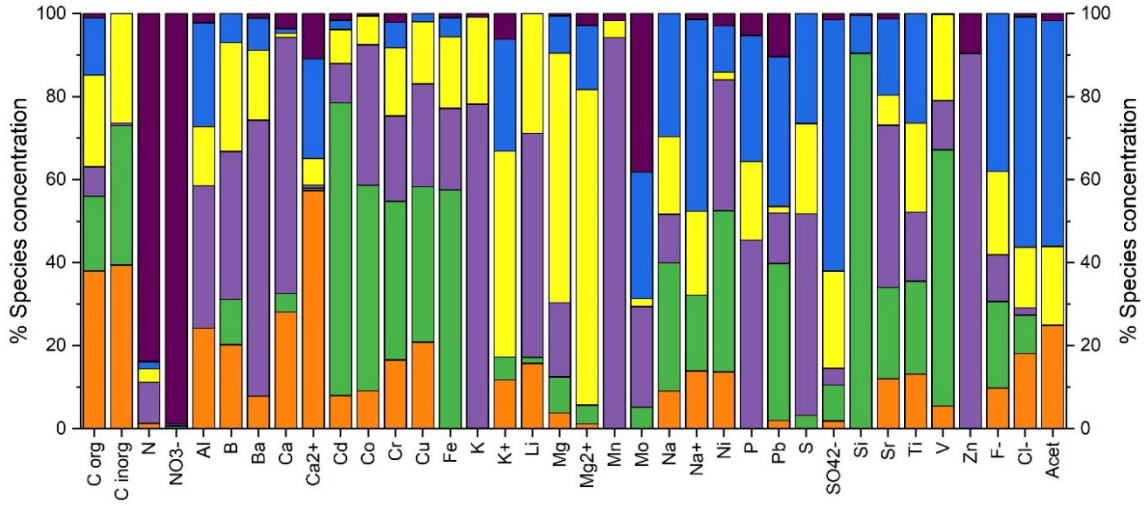

Figure 3 Factor fingerprint screen obtained through NMF analysis (orange, Factor 1; green, Factor 2; violet, Factor 3; yellow, Factor 4; blue, Factor 5; magenta, Factor 6).

in the discussion section. Figure 4 and Figure 5 display boxplots of the NMF factors and

chemical-physical parameters showing, respectively, significant seasonal and locational differences.

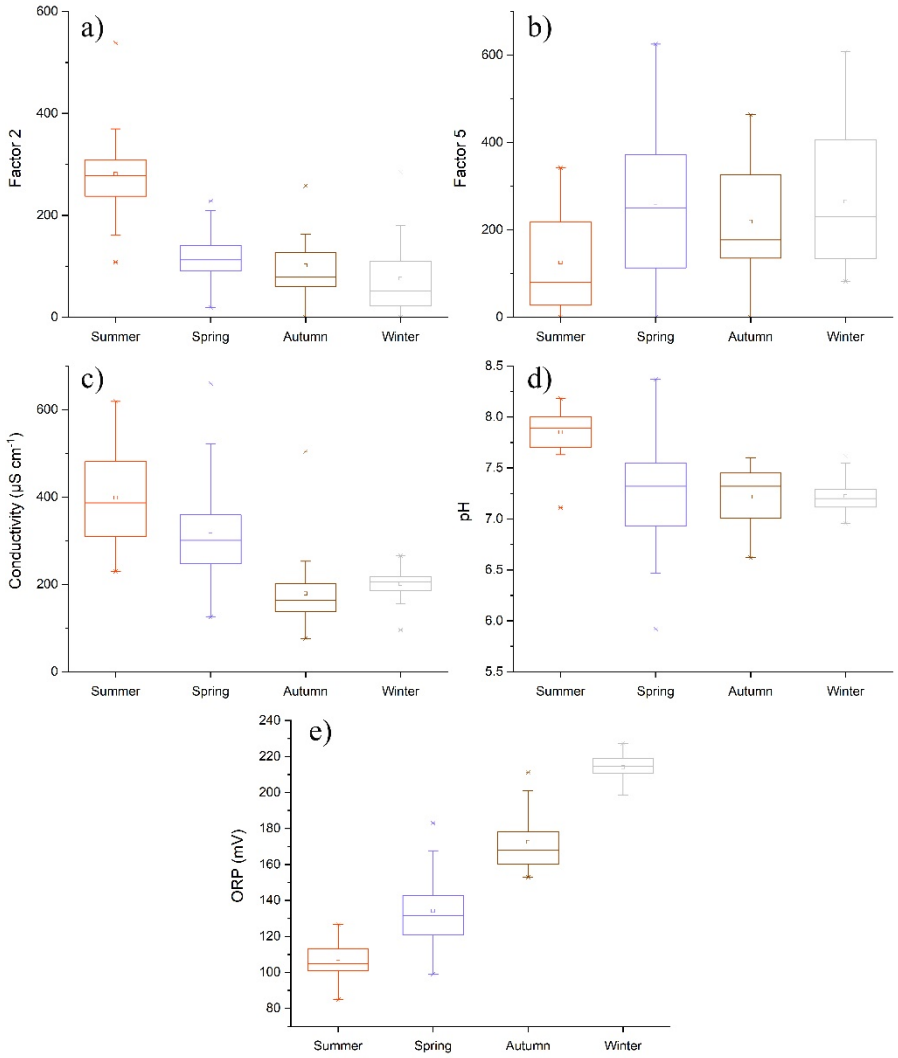

Figure 4 Boxplots of the NMF factors (**a** and **b**) and studied parameters (**c**, **d** and **e**) showing significant temporal differences ($\alpha = 0.05$ associated with ANOVA tests).

The relationships among the analyzed chemical parameters in all the samples (Figure 6) are displayed through a network based on Pearson's correlation coefficients (Table S5), showing several clusters of variables for which either positive or negative correlations ($0.001 < P < 0.05$) exist. The main group is characterized by a number of relationships:

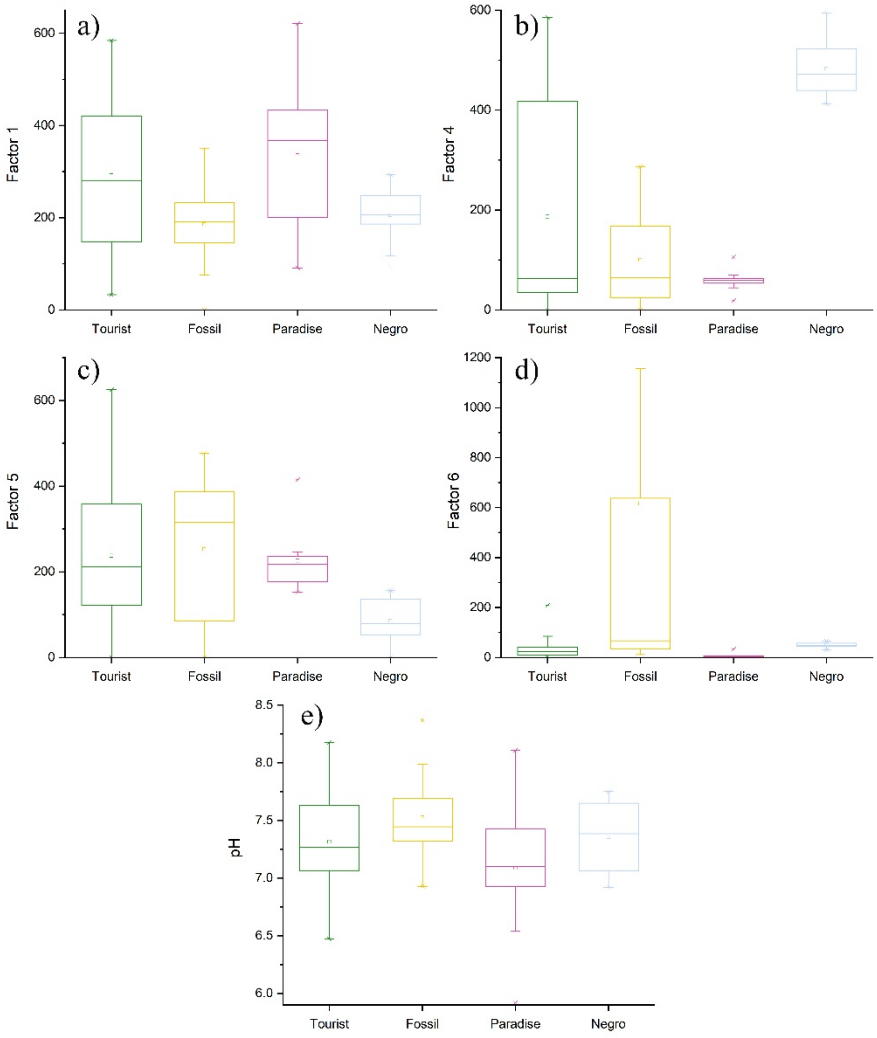

Figure 5 Boxplots of the NMF factors (**a**, **b**, **c** and **d**) and studied parameters (**e**) showing significant spatial differences (α = 0.05 associated with ANOVA tests).

conductivity is positively correlated with C org and total C, Ca, Cd, Mo, Ni, Pb ($0.50 < r < 0.61$; $P < 0.001$), and negatively correlated with ORP ($r = -0.52$; $P < 0.001$), which is in turn negatively correlated with pH, Cd, Co, Cu, Mn, Mo, Ni, Pb, Ti, V, Zn ($-0.67 < r < -0.52$; $P < 0.001$) and positively correlated with Cr ($r = 0.50$; $P < 0.001$); pH is positively correlated with Cd, Co, Cu, Mo, Ni, Pb, Ti, V ($0.52 < r < 0.63$; $P < 0.001$). Cr shows a negative correlation with Cu, Mo, Ni, Pb, Ti, Zn ($-0.62 < r < -0.52$; $P < 0.001$), whereas Co, Cu, Cd, Mo, Ni, Pb, Ti and Zn show positive correlations ($0.58 < r < 0.99$; $P < 0.001$). Moreover, Fe and Al are positively correlated with Mo, Ti, V ($0.50 < r < 0.68$; $P < 0.001$) and, Al also with Ni and Pb ($r = 0.50$; $P < 0.001$). B shows a positive

correlation with Li (r= 0.77; P < 0.001), whereas Ba with Li, Mn, Sr, Zn (0.50 < r < 0.77). Other small groups can be also detected, represented by the positive correlations between S and K (r= 0.80; P <0.001), N and Ca^{2+} (r=0.61; P < 0.001), N and NO_3^- (r=0.94; P < 0.001), Na with Na^+, F^-, Cl^-, SO_4^{2-}, S (0.50 < r < 0.78; P < 0.001), and Na^+ with F^-, Cl^-, SO_4^{2-} (0.51 < r < 0.79; P < 0.001). Moreover, Mg^{2+} displays positive correlations with Mg and with K^+ (r= 0.90 and r=0.68, respectively; P < 0.001), whereas total C with C org and C inorg (r=0.96 and r=0.88, respectively; P < 0.001).

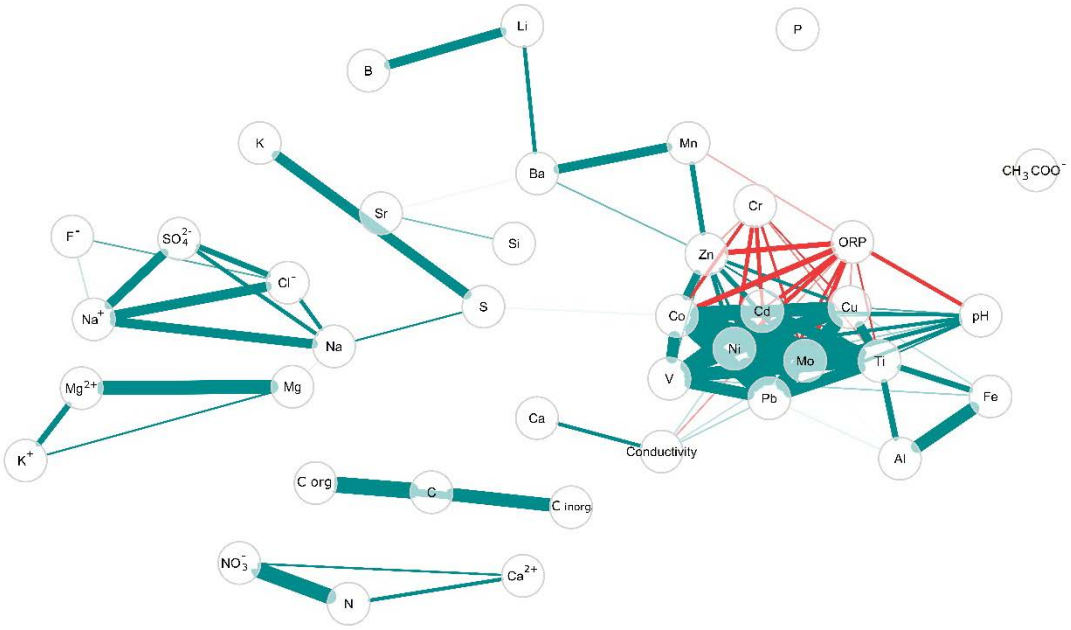

Figure 6 Network based on Pearson's correlation coefficients, reporting negative (red) and positive (green) correlations; line ticks indicate more or less strong correlations between the variables.

4 Discussion

The qualitative and quantitative characterization of cave waters in relation to the different seasons and trails in the Pertosa-Auletta system highlighted significant

differences both in time and space. The investigated Tourist, Fossil, and Paradise trails present distinct characteristics regarding their natural features and types of human fruition. The first one is characterized by abundant active speleothems (stalactites, stalagmites, columns…), with locally intense dripping. There is no flowing water, except for a small tributary in the Large Room, where water is periodically discharged artificially. This occasional flow, and most of the intense drippings, are fed by an above lying surface stream, known under the name "Velo della sposa" (Bride's Veil). This steep waterfall is generated by a derivation from the higher located hydroelectric dammed reservoir, returning to the Tanagro river crossing a surface channel partially cemented and on bare rock outcrops (shown in green in Figure 1b). The Fossil path develops along a set of fractures, is characterized by a succession of shallow lakes fed by infrequent as well as scarce dripping, and no running water. Differently from the Tourist trail, this branch lacks speleothems, but is rich in guano deposits due to the presence of bat colonies, that use this quieter trail (away from the tourist paths) in several phases of their life cycle. This can explain the higher concentration of nitrogen compounds, highlighted also by the NMDS and NMF (Factor 6, Figure 5d) analyses, in some samples collected from the Fossil trail, most likely contaminated by chiroptera droppings. The presence of bat guano is of great ecological importance, being part of the food chain in the usually oligotrophic cave environment, therefore sustaining a rich biological community (Venarsky and Huntsman, 2018; Misra et al., 2019; Sakoui et al., 2020). Another potential origin of NO_3^- may be linked to the natural N-cycling processes occurring at the soil surface above the cave, related to the biological activities of soil microbiota. Chemical fertilization in agriculture can also be taken into account, given the presence of olive tree groves above the cave (Katz, 2019), as also evidenced by a relevant presence of phosphorus in the fossil path, in respect to other trails. The

Paradise trail is the section adapted to the visits of the active branch, which is crossed by the underground Negro river and not investigated for dripping waters along its length due to the difficult access. However, this trail was sampled for river waters in the final part of the Negro river, immediately upstream of the underground waterfall. The exact provenance of these waters is still unknown, but it is assumed that they might partly originate from the surface (Tanagro river), and partly from the Alburni Massif, to which Pertosa-Auletta Cave belongs (Celico, 1994; Cozzolino et al., 2015; Pastore, 2016).

River waters display higher concentrations of Mg, Mg^{2+}, and K^{+} compared to the dripping waters, chemical species that mainly defined the Factor 4 obtained by NMF analysis (see Figure 3). This factor suggests that river waters are more influenced by the dissolution of potassium silicates that are contained in the typical continental sediments (flysch) overlying the Mesozoic carbonate rocks in the Alburni plateau, and the water-rock interaction with Cretaceous dolomitic limestones along the underground flow path. This does not happen in drip waters, that are mostly the result of the local interaction of infiltrating waters with the pure Jurassic limestone in which the cave opens (Fairchild et al., 2000; Cafaro et al., 2010). Furthermore, river water presents lower concentrations of SO_4^{2-}, Na^{+}, and Cl^{-} compared to the dripping water, revealing an atmospheric influence, as described by the Factor 5 in Figure 3. Indeed, drip waters derive from meteoric waters whose composition is closely linked to the hygroscopic atmospheric aerosol components acting as cloud condensation nuclei and triggering precipitation formation (Tremaine et al., 2016). These evidences are described in Figure 5, in which the river water samples are characterized by higher values of the Factor 4 (dissolution of limestone, dolostone, and silica rocks, Figure 5b) and lower values of the Factor 5 (atmospheric influence, Figure 5c). The long underground path of the Negro River and the relevant dissolution phenomena, can also explain the high concentration of Ca^{2+} in

all the samples, defined by the Factor 1 in NMF analysis, together with both organic and inorganic carbon, characterizing the karst process interesting such system (Fairchild and Baker, 2012). Moreover, such carbonate equilibrium factor presents lower values for the dripping water samples in the fossil section respect to the others, which could be related to faster flow through the more fractured overlying rocks, decreasing the water-rock interaction, with consequent decrease of water acidity (see Factor 1 and pH boxplots in Figures 5a and 5e). Overall, Ca and Mg concentrations in Pertosa-Auletta Cave waters are comparable to those found in several caves in Slovakia, as reported by Motyka et al. (2005). Moreover, the considerable Si concentration in the analyzed waters can be related to the weathering of silicates in the flysch-derived cave sediments, with the release of hydrated silica (H_4SiO_4) (Merlak, 2013).

Almost all the C detected in both water types is organic, with an evident differentiation in the Fossil trail (as previously described) and among the seasons. The organic C in water might originate from the leaching of top soil organic compounds deriving from plants and several microbial metabolic activities, and inherent pH and redox conditions. Higher concentrations are found during warmer and wetter climate conditions (spring and summer), according to the higher metabolic activity during these seasons. Organic matter input into the cave is also variable in composition and concentration depending on the infiltration velocity, which modulates the time of contact of the fluids with the organic matrices, and on the hydrological conditions, such as the rainfall duration and intensity (Venarsky and Huntsman, 2018). The same reasoning holds for the chemical elements and their ionic forms (Baldini et al., 2006; Hartland et al., 2012). Such mechanism explains the differentiation of summer samples, recording the highest concentrations of Cd, Co, Cu, Mn, Mo, Ni, Pb, Ti, and Zn as compared to the other seasons. This evidence is highlighted also by Factor 2 obtained by NMF analysis,

showing an increase of these chemical elements of lithogenic origin (Tadros et al., 2019) in summer (see Figure 4a). These observations are likely related to the scarcity of precipitations in the summer season, which reduces the dilution effect, increasing the duration of water-rock interaction with and subsequent leaching of the mineral background of the system. This also results in a higher calcite saturation index in the summer although all the analyzed drip waters are undersaturated (negative saturation index). In addition, the drier climate with reduced precipitation in the summer period is responsible not only of the deficit in dripping water, but also causes the decrease in SO_4^{2-}, Na^+, and Cl^- species in the drip waters, typically related to aerosol chemistry and its subsequent role in precipitation formation by cloud processing (see Factor 5 in Figure 4b). It is worth noting that, in the warm season, water samples are more acidic due to the higher soil microbial activity, which increases the dissolution processes and the consequent mobility of solutes. However, external supply due to anthropogenic activities is not ruled out, especially for Pb, showing the highest concentrations in summer season, with a mean value of 25.1 μg/L, exceeding the contamination threshold of 10 μg/L in underground waters, according to the Italian Legislative Decree 152/2006.

As from Figures 4c and d, the highest conductivity and pH values are observed in the summer period. The opposite trend occurs instead for ORP (Figure 4e), as it strongly depends on hydrogen ion concentration. This might be related to the greater water-rock interaction explained previously, that increases the concentration of dissolved salts and hence conductivity.

Rainwater dominates the water flow across a soil profile; it is always characterized by a chemical composition tightly linked to the aerosol particles on which the hydrometeor has been generated. It typically includes a series of highly soluble compounds such as

for example ammonium sulfates and nitrate, as well as NaCl, according to the history of air masses and their chemical processing in the troposphere (Tositti et al., 2018, 2020). These chemical fingerprints are therefore conserved during the downward penetration through soil down to depth, though in part modified by water/soil-rock interactions (Fairchild and Treble, 2009, Dredge et al., 2013; Tositti et al., 2020). SO_4^{2-}, Cl^-, and Na^+, which show positive correlations in the network analysis, as well as defined by Factor 5 in NMF analysis, can be attributed both to evapotranspiration processes related to exchange phenomena in the mineral compartment of the karst system and to the atmospheric aerosols, mainly of marine origin (sea spray), depending on atmospheric circulation and weather conditions (Raes et al., 2000; Tremaine and Froelich, 2013; Tremaine et al., 2016).

5 Conclusions

In the light of our results, cave waters reveal important information about the natural ecological dynamics, as well as the potential surface anthropogenic impacts, interesting these apparently confined underground ecosystems. Indeed, the characterization of Pertosa-Auletta cave waters compartment provided a clear description of its hydrology, highlighting the several natural and artificial drivers affecting the subterranean ecosystem. The different features of the three investigated paths emerge also in the chemical composition of the waters, in particular in the Fossil trail, where bat guano contaminates the drip waters with nitrogen compounds. A potential pollution source related to the agriculture practiced on the overlying soils is not excluded, as also indicated by a higher concentration of phosphorus in water from this trail. Furthermore, we observed a lower concentration of Ca^{2+} and total carbon in the Fossil trail in respect

to the others, likely in relation to the faster flow through the more fractured overlying rocks, decreasing the water-rock interaction.

The two water typologies (drip and Negro river) exhibited relevant differences as regards the higher concentrations of Mg^{2+} and K^{+} in the river, likely related to the fact that these waters, along their long underground path, also encounter Cretaceous dolomitic limestones. The organic C constitutes the almost totality of C detected, arriving in the cave through leaching from the vegetated top soil. Seasonal differences were also identified, especially for the summer sampling, showing highest concentrations of several elements (Cd, Co, Cu, Mn, Mo, Ni, Pb, Ti, Zn) and atmospheric-derived ions (SO_4^{2-}, Na^{+}, Cl^{-}), probably in relation to the dry weather, less dilution, and longer water-rock interaction, as well as to the increased anthropogenic activities.

Additional investigations on new samples from further sampling campaigns are required for a comprehensive long-scale evaluation. Future geochemical surveys will concern the top soil, the different lithologies in the cave (carbonate beds, the shaly interlayers, and the reddish bauxites), the flysch outcropping on the Alburni massif, and the upstream water characterization. More also needs to be known regarding the cave ventilation processes, which cause evaporation and condensation to occur in the cave in different areas and seasons, with a great impact also on the geochemistry of the hanging droplets.

Funding

This work was funded by Università degli Studi di Salerno (Italy) within the ORSA197159 project.

Conflicts of interest

None declared.

Acknowledgments

Thanks to MIdA Foundation (Italy), in particular, to the speleoguide, Mr. Vincenzo Manisera, for the field support.

References

Addesso, R., De Waele, J., Cafaro, S., & Baldantoni, D. (2022). Geochemical characterization of clastic sediments sheds light on energy sources and on alleged anthropogenic impacts in cave ecosystems. *International Journal of Earth Sciences*. doi: 10.1007/s00531-021-02158-x

Addesso, R., Bellino, A., D'Angeli, I. M., De Waele, J., Miller, A. Z., Carbone, C., & Baldantoni, D. (2019). Vermiculations from karst caves: The case of Pertosa-Auletta system (Italy). *Catena, 182*, 104178. doi: 10.1016/j.catena.2019.104178

Baldini, J. U. L., McDermott, F., & Fairchild, I. J. (2006). Spatial variability in cave drip water hydrochemistry: Implications for stalagmite paleoclimate records. *Chemical Geology*, *235*(3–4), 390–404. doi: 10.1016/j.chemgeo.2006.08.005

Brunet, J.-P., Tamayo, P., Golub, T. R., & Mesirov, J. P. (2004). Metagenes and molecular pattern discovery using matrix factorization. *Proceedings of the National Academy of Sciences, 101*(12), 4164–4169. doi: 10.1073/pnas.0308531101

Cafaro, S., Gueguen, E., Adurno, I., & Schiattarella M. (2010) Il controllo geologico nella speleogenesi della grotta dell'Angelo (Appennino campano-lucano). *Atti del II Convegno Regionale di Speleolologia*, 71-81.

Cafaro, S., Gueguen, E., Parise, M. & Schiattarella, M. (2016). Morphometric analysis of karst features of the Alburni Mts, Southern Apennines, Italy. *Geografia Fisica e Dinamica Quaternaria, 39*, 121–128. doi: 10.4461/GFDQ.2016.39.11

Celico, P., Pelella, L., Stanzione, D., & Aquino, S. (1994). Sull'idrogeologia e l'idrogeochimica dei monti Alburni (SA). *Geologica Romana, 30*, 687-697.

Columbu, A., Chiarini, V., Spötl, C., Benazzi, S., Hellstrom, J., Cheng, H., & De Waele, J. (2020). Speleothem record attests to stable environmental conditions

during Neanderthal–modern human turnover in southern Italy. *Nature Ecology & Evolution, 4*(9), 1188-1195. doi: 10.1038/s41559-020-1243-1

Columbu, A., Spötl, C., De Waele, J., Yu, T. L., Shen, C. C., & Gázquez, F. (2019). A long record of MIS 7 and MIS 5 climate and environment from a western Mediterranean speleothem (SW Sardinia, Italy). *Quaternary Science Reviews, 220*, 230-243. doi: 10.1016/j.quascirev.2019.07.023

Columbu, A., Sauro, F., Lundberg, J., Drysdale, R., & De Waele, J. (2018). Palaeoenvironmental changes recorded by speleothems of the southern Alps (Piani Eterni, Belluno, Italy) during four interglacial to glacial climate transitions. *Quaternary Science Reviews, 197*, 319-335. doi: 10.1016/j.quascirev.2018.08.006

Cozzolino, L., Damiano, N., Del Vecchio, U., Minieri, G., Testa, L., & Trifone, P. (2015) Prove di colorazione e recenti esplorazioni nell'area della Grotta del Falco - Monti Alburni (Campania). *Atti XXII Congresso Nazionale di Speleologia*, Auletta-Pertosa, 387-392.

Culver, D. C., & Pipan, T. (2019). *The Biology of Caves and Other Subterranean Habitats* (2nd ed.). New York: Oxford University Press. doi: 10.1093/oso/9780198820765.001.0001

Dredge, J., Fairchild, I. J., Harrison, R. M., Fernandez-Cortès, A., Sanchez-Moral, S., Jurado, V., ... & Grassineau, N. (2013). Cave aerosols: distribution and contribution to speleothem geochemistry. *Quaternary Science Reviews, 63*, 23-41. doi:10.1016/j.quascirev.2012.11.016

Fairchild, I. J., & Baker, A. (2012). *Speleothem Science: From Process to Past Environments*. Chichester, UK: John Wiley & Sons, Ltd. doi: 10.1002/9781444361094

Fairchild, I. J., & Treble, P. C. (2009). Trace elements in speleothems as recorders of environmental change. *Quaternary Science Reviews*, *28*(5–6), 449–468. doi: 10.1016/j.quascirev.2008.11.007

Fairchild, I. J., Borsato, A., Tooth, A. F., Frisia, S., Hawkesworth, C. J., Huang, Y., Spiro, B. (2000). Controls on trace element (Sr–Mg) compositions of carbonate cave waters: Implications for speleothem climatic records. *Chemical Geology*, 166, 255–26915.

Fehér, K., Kovács, J., Márkus, L., Borbás, E., Tanos, P., & Hatvani, I. G. (2016). Analysis of drip water in an urban karst cave beneath the Hungarian capital (Budapest). *Acta Carsologica*, *45*(3), 213-231. doi: 10.3986/ac.v45i3.3440

Hartland, A., Fairchild, I. J., Lead, J. R., Borsato, A., Baker, A., Frisia, S., & Baalousha, M. (2012). From soil to cave: Transport of trace metals by natural organic matter in karst dripwaters. *Chemical Geology*, *304–305*, 68–82. doi: 10.1016/j.chemgeo.2012.01.032

Jiménez-Sánchez, M., Stoll, H., Vadillo, I., López-Chicano, M., Domínguez-Cuesta, M., Martín-Rosales, W., & Meléndez-Asensio, M. (2008). Groundwater contamination in caves: four case studies in Spain. *International Journal of Speleology, 37*(1), 53-66.

Katz, B. G. (2019). Nitrate contamination in karst groundwater. In: D.C. Culver, W.B. White, T. Pipan (Eds.), *Encyclopedia of Caves* (pp. 756–760). Elsevier. doi: 10.1016/B978-0-12-814124-3.00091-1

Klimchouk A.B. (2004). Towards defining, delimiting and classifying epikarst: its origin, processes and variants of geomorphic evolution. In: W.K. Jones, D.C. Culver, & J.S. Herman (Eds.). Epikarst (pp. 23-25). Sheperdstown (West Virginia): Karst Water Institute, Special Publication 9.

Lauritzen, S.-E. (2018). Physiography of the Caves. In O.T. Moldovan, Ľ. Kováč, & S. Halse (Eds.), *Cave Ecology* (pp. 7–21). Cham: Springer International Publishing. doi: 10.1007/978-3-319-98852-8_2

Mahler, B., & Massei, N. (2007). Anthropogenic contaminants as tracers in an urbanizing karst aquifer. *Journal of Contaminant Hydrology, 91*(1-2), 81-106. doi: 10.1016/j.jconhyd.2006.08.010

Merlak, E. (2013). Solubilità della silice nell'interazione acqua-flysch del carso classico. *Atti e Memorie della Commissione Grotte "E. Boegan", 44*, 73-89.

Misra, P. K., Gautam, N. K., & Elangovan, V. (2019). Bat guano: a rich source of macro and microelements essential for plant growth. *Annals of Plant and Soil Research*, *21*(1), 82–86.

Moldovan, O. T., Pipan, T., Iepure, S., Mihevc, A., & Mulec, J. (2007). Biodiversity and Ecology of Fauna in Percolating Water in Selected Slovenian and Romanian Caves. *Acta Carsologica*, *36*(3), 493-501. doi: 10.3986/ac.v36i3.183

Motyka, J., Gradziński, M., Bella, P., & Holúbek, P. (2005). Chemistry of waters from selected caves in Slovakia - A reconnaissance study. *Environmental Geology*, *48*(6), 682–692. doi: 10.1007/s00254-005-0006-2

Nannoni, A., Vigna, B., Fiorucci, A., Antonellini, M., & De Waele, J. (2020). Effects of an extreme flood event on an alpine karst system. *Journal of Hydrology, 590*, 125493. doi: 10.1016/j.jhydrol.2020.125493

Nava-Fernandez, C., Hartland, A., Gázquez, F., Kwiecien, O., Marwan, N., Fox, B., Breitenbach, S. F. M. (2020). Pacific climate reflected in Waipuna Cave drip water hydrochemistry. *Hydrology and Earth System Sciences*, *24*(6), 3361–3380. doi: 10.5194/hess-24-3361-2020

Pastore, C. (2016). Analisi idrogeologica dell'area carsica dei Monti Alburni (Salerno, Campania). Master Thesis, University of Bologna.

Poulain, A., Rochez, G., Bonniver, I., & Hallet, V. (2015). Transmissive and Capacitive Behavior of the Unsaturated Zone in Devonian Limestones, Implications for the Functioning of the Epikarstic Aquifer: An Introduction. In B. Andreo, F. Carrasco, J. J. Durán, P. Jiménez, & J. W. LaMoreaux (Eds.), *Hydrogeological and Environmental Investigations in Karst Systems* (pp. 35–43). Berlin, Heidelberg: Springer Berlin Heidelberg. doi: 10.1007/978-3-642-17435-3_5

R Core Team (2020). R: a language and environment for statistical computing. Version 4.0. 2. Vienna, Austria.

Raes, F., Van Dingenen, R., Vignati, E., Wilson, J., Putaud, J. P., Seinfeld, J. H., & Adams, P. (2000). Formation and cycling of aerosols in the global troposphere. *Atmospheric environment*, 34(25), 4215-4240. doi:10.1016/S1352-2310(00)00239-9

Riechelmann, D. F. C., Deininger, M., Scholz, D., Riechelmann, S., Schröder-Ritzrau, A., Spötl, C.,, … Immenhauser, A. (2013). Disequilibrium carbon and oxygen isotope fractionation in recent cave calcite: Comparison of cave precipitates and model data. *Geochimica et Cosmochimica Acta*, *103*, 232–244. doi: 10.1016/j.gca.2012.11.002

Rossi, C., & Lozano, R. P. (2016). Hydrochemical controls on aragonite versus calcite precipitation in cave dripwaters. *Geochimica et Cosmochimica Acta*, *192*, 70–96. doi: 10.1016/j.gca.2016.07.021

Ruggieri, R., Forti, P., Antoci, M. L., & De Waele, J. (2017). Accidental contamination during hydrocarbon exploitation and the rapid transfer of heavy-mineral fines through an overlying highly karstified aquifer (Paradiso Spring, SE Sicily). *Journal of Hydrology*, *546*, 123-132. doi: 10.1016/j.jhydrol.2016.12.046

Sakoui, S., Derdak, R., Addoum, B., Serrano-Delgado, A., Soukri, A., & El Khalfi, B. (2020). The Life Hidden Inside Caves: Ecological and Economic Importance of Bat Guano. *International Journal of Ecology*, *2020*, 1–7. doi: 10.1155/2020/9872532

Tadros, C. V., Treble, P. C., Baker, A., Hankin, S., & Roach, R. (2019). Cave drip water solutes in south-eastern Australia: Constraining sources, sinks and processes. *Science of the Total Environment*, 651, 2175-2186.

Tositti, L., Moroni, B., Dinelli, E., Morozzi, P., Brattich, E., Sebastiani, B., … Cappelletti, D. (2020). Deposition processes over complex topographies: Experimental data meets atmospheric modeling. *Science of the Total Environment, 744*, 140974. doi: 10.1016/j.scitotenv.2020.140974

Tositti, L., Pieri, L., Brattich, E., Parmeggiani, S., & Ventura, F. (2018). Chemical characteristics of atmospheric bulk deposition in a semi-rural area of the Po Valley (Italy). *Journal of Atmospheric Chemistry*, *75*(1), 97–121. doi: 10.1007/s10874-017-9365-9

Tremaine, D. M., Sinclair, D. J., Stoll, H. M., Lagerström, M., Carvajal, C. P., & Sherrell, R. M. (2016). A two-year automated dripwater chemistry study in a remote cave in the tropical south Pacific: Using [Cl−] as a conservative tracer for seasalt contribution of major cations. *Geochimica et Cosmochimica Acta*, 184, 289–310. doi: 10.1016/j.gca.2016.03.029

Tremaine, D. M., & Froelich, P. N. (2013). Speleothem trace element signatures: A hydrologic geochemical study of modern cave dripwaters and farmed calcite. *Geochimica et Cosmochimica Acta, 121*, 522–545. doi: 10.1016/j.gca.2013.07.026

Venarsky, M. P., & Huntsman, B. M. (2018). Food Webs in Caves. In O.T. Moldovan, Ľ. Kováč, & S. Halse (Eds.), *Cave Ecology* (pp. 309–328). Cham: Springer International Publishing. doi: 10.1007/978-3-319-98852-8_14

Williams, P. W. (2008). The role of the epikarst in karst and cave hydrogeology: a review. International Journal of Speleology, 37(1), 1-10. doi: 10.5038/1827-806X.37.1.1

Williams, P. W. (1983). The role of the subcutaneous zone in karst hydrology. *Journal of Hydrology*, *61*(1–3), 45–67. doi: 10.1016/0022-1694(83)90234-2

Wong, C. I., Banner, J. L., & Musgrove, M. (2011). Seasonal dripwater Mg/Ca and Sr/Ca variations driven by cave ventilation: Implications for and modeling of speleothem paleoclimate records. *Geochimica et Cosmochimica Acta*, *75*(12), 3514–3529. doi: 10.1016/j.gca.2011.03.025

Table S1 Studied parameters in each water sample (green, Tourist trail; yellow, Fossil trail; violet, Paradise trail) collected in the Spring 2020 in Pertosa-Auletta Cave (DW: dripping waters; NR: Negro rivers; b.d.l: below detection limit).

Sample	pt1	pt2	pt3	pt4	pt5	pt6	pt7	pt8	pt9	pt10	pt11	pf1	pf2	pf3	pf4	pf5	pf6	pf7	pf8	pf9	pf10	pp1	pp2	pn1	pn2	pn3
Type	DW	DW	DW	DW	DW	DW	DW	DW	DW	DW	DW	DW	DW	DW	DW	DW	DW	DW	DW	DW	DW	DW	DW	NR	NR	NR
Conductivity (µS/cm)	270	359	333	228	366	295	212	317	521	377	419	125	151.8	660	268	269	514	312	330	247	307	269	309	241	247	221
ORP (mV)	138.9	167.7	183.0	145.0	134.3	122.1	129.8	144.7	178.2	128.8	131.0	118.0	114.7	120.9	119.6	118.3	99.1	138.0	124.8	121.1	110	152.8	142.8	132.4	137.4	135.3
pH	7.2	6.8	6.5	7.1	7.4	7.8	7.5	7.3	6.5	7.4	7.3	7.4	7.6	7.7	7.6	7.3	8.4	6.9	7.4	7.7	8.0	6.5	5.9	7.0	6.9	6.9
C (mg/L)	28.0	37.2	31.0	24.8	39.2	30.8	20.8	32.5	52.8	38.5	41.1	17.5	19.9	20.6	22.4	27.2	27.4	38.1	37.4	25.8	32.0	36.9	36.7	38.1	37.5	33.9
Corg (mg/L)	20.4	26.5	22.1	17.5	27.7	21.4	15.1	23.2	37.5	26.8	28.4	12.6	14.0	18.4	20.1	24.3	24.4	34.1	33.3	23.2	28.5	26.5	26.8	27.4	27.2	23.7
C inorg (mg/L)	7.6	10.7	8.9	7.3	11.5	9.4	5.7	9.3	15.2	11.8	12.7	4.9	5.9	2.2	2.3	2.9	2.9	4.0	4.1	2.6	3.5	10.4	9.9	10.7	10.2	10.2
N (mg/L)	1.3	0.4	0.5	0.3	0.3	0.9	1.6	1.0	0.8	0.4	0.5	0.5	0.4	47.7	6.0	5.5	28.3	1.4	0.9	1.5	1.4	0.4	0.4	1.1	0.9	0.8
Al (µg/L)	14.9	21.9	58.1	12.7	15.6	18.3	14.5	13.3	20.5	14.2	17.6	13.6	9.3	15.3	19.7	20	29.7	39.0	19.9	58.2	13.9	24.6	14.9	27.3	21.5	28.1
B (µg/L)	36.8	44.2	11.3	29.4	25.7	45.7	43.5	43.0	36.0	31.1	13.1	8.7	10.6	15.5	9.4	55.2	20.4	46.8	37.9	14.2	27.8	53.9	46.3	81.5	71.1	53.1
Ba (µg/L)	27.5	20	3.8	15.0	7.7	27.0	29.5	12.8	11.5	14.6	8.1	5.4	5.4	8.0	15.3	46.2	8.3	23.9	12.3	9.1	12.0	22.6	20	39.4	39.3	29.6
Ca (mg/L)	58.6	81.2	63.7	58.1	95.6	45.2	45.8	53.4	77.9	84.0	104.2	41.0	43.2	138.0	55.4	46.5	105.9	92.1	72.8	54.6	64.7	70.5	74.6	40.2	39.4	45.1
Cd (µg/L)	0.2	0.2	0.2	0.2	0.2	0.2	0.2	0.1	0.2	0.1	0.1	0.1	0.1	b.d.l.	0.1	b.d.l.	0.1	0.1	0.2	0.1	0.2	0.1	b.d.l.	0.2	0.2	0.1
Co (µg/L)	0.7	0.7	0.5	0.5	0.2	0.7	0.9	0.2	0.2	0.2	0.2	0.2	0.3	0.2	0.1	1.1	b.d.l.	0.3	0.3	0.5	0.3	0.6	0.6	1.1	1.3	0.8
Cr (µg/L)	0.1	0.2	0.8	0.5	0.4	0.3	1.0	0.4	0.5	0.4	0.8	0.2	0.2	0.5	0.3	0.4	0.4	0.4	0.8	0.7	0.4	b.d.l.	0.1	0.4	0.4	0.6
Cu (µg/L)	1.3	1.3	0.6	0.8	0.5	1.2	0.4	1.7	0.3	0.6	0.5	0.1	0.4	0.2	b.d.l.	1.2	0.7	1.1	0.1	b.d.l.	0.7	2.5	1.2	1.1	1.7	0.7
Fe (µg/L)	9.4	11.7	5.8	5.2	1.4	6.3	11.6	6.2	0.8	2.1	1.0	2.4	0.4	3.2	4.7	13.3	14.5	21.5	4.2	47.3	8.8	10	11.3	13.7	15.2	14.2
K (mg/L)	1.9	1.0	0.7	0.7	0.8	2.3	2.7	2.1	2.0	1.7	1.3	0.7	1.0	0.7	0.9	22.3	0.9	2.0	2.2	2.6	2.3	1.4	1.5	2.2	2.0	1.6
Li (µg/L)	12.6	22.2	0.7	11.9	7.2	20.4	22.0	18.4	12.1	12.5	2.5	2.0	1.6	3.5	1.0	35.6	4.7	24.5	15.8	2.2	10.3	22.3	20.2	38.3	38.1	26.3
Mg (mg/L)	4.0	3.9	3.6	3.2	3.3	13.2	3.9	12.3	11.8	6.2	3.0	1.7	2.5	1.7	5.1	7.8	2.4	8.4	9.9	5.5	9.3	4.2	5.1	11.9	13.8	11.7
Mn (µg/L)	6.0	8.3	2.1	3.4	1.8	9.9	8.4	3.2	2.8	3.7	0.7	1.6	0.8	1.6	0.6	13.9	2.0	7.0	3.1	2.5	2.9	6.4	5.7	11.8	13.0	9.3
Mo (µg/L)	0.2	b.d.l.	b.d.l.	0.4	b.d.l.	b.d.l.	0.4	b.d.l.	b.d.l.	b.d.l.	b.d.l.	0.1	0.2	0.8	b.d.l.	0.2	0.7	b.d.l.	0.6	b.d.l.	b.d.l.	b.d.l.	b.d.l.	0.2	0.2	b.d.l.
Na (mg/L)	7.4	6.3	11.8	5.6	6.0	9.4	6.3	9.5	9.5	5.7	5.4	2.5	3.8	1.4	9.5	9.0	2.3	9.1	8.9	7.8	8.6	6.3	6.6	5.4	5.9	4.8
Ni (µg/L)	1.3	1.0	0.5	1.7	1.3	b.d.l.	1.2	0.3	1.2	1.6	1.2	0.4	1.2	1.0	1.3	1.9	2.7	2.1	b.d.l.	0.5	1.2	2.6	0.6	1.1	1.4	0.7
P (µg/L)	15.0	8.5	10.4	7.9	6.5	23.5	42.4	23.8	19.2	15.5	10.9	14.7	7.4	7.1	932.3	107.4	149.2	39.7	20.0	24.6	22.4	11.7	7.6	33.7	33.0	30.4
Pb (µg/L)	b.d.l.	0.5	b.d.l.	b.d.l.	b.d.l.	b.d.l.	b.d.l.	1.2	b.d.l.	b.d.l.	b.d.l.	b.d.l.	b.d.l.	b.d.l.	b.d.l.	b.d.l.	b.d.l.	b.d.l.	b.d.l.	b.d.l.	b.d.l.	b.d.l.	1.0	b.d.l.	b.d.l.	b.d.l.
S (mg/L)	2.1	2.4	5.6	1.8	1.4	3.8	3.3	3.6	3.3	1.8	1.4	0.5	0.8	0.7	2.7	14.6	1.3	3.2	2.9	1.3	2.9	1.7	1.8	2.2	2.6	2.1
Si (mg/L)	6.7	7.0	6.6	5.1	3.8	3.7	5.6	3.6	2.7	5.0	4.3	3.1	4.7	1.7	4.5	5.1	2.2	4.5	4.5	6.6	4.8	2.6	3.8	3.4	4.1	4.0
Sr (µg/L)	73.9	82.7	70.8	67.0	49.1	69.9	61.8	51.0	60.1	60.7	49.0	34.4	48.6	28.8	85.0	93.3	33.6	65.3	57.4	52.0	47.8	52.7	47.6	62.3	63.6	62.7
Ti (µg/L)	0.5	0.1	0.4	0.1	0.1	0.3	0.1	0.2	0.1	0.1	0	0.3	0.2	0.1	0.3	0.2	0.9	1.6	0.3	6.6	0.4	0.1	0.1	0.6	0.2	0.5
V (µg/L)	1.5	1.4	0.6	0.7	0.8	1.4	1.5	1.2	1.5	1.7	0.7	1.4	1.6	0	0.7	1.1	0.7	0.7	1.6	1.3	1.1	0.8	1.3	0.9	1.9	1.4
Zn (µg/L)	35.4	27.7	4.5	3.0	3.4	6.7	7.1	3.3	3.1	6.9	2.9	4.3	4.0	19.0	2.3	16.3	6.0	3.3	1.8	0.3	1.5	7.0	4.7	30	8.7	9.0
Na^+ (mg/L)	8.0	6.1	11.9	5.5	5.6	9.3	6.0	9.8	9.9	6.1	6.3	2.5	4.1	5.2	8.9	9.1	8.5	9.7	8.4	7.9	8.7	6.0	5.9	4.3	4.8	5.5
K^+ (mg/L)	0.9	0.3	0.4	0.3	0.4	1.6	2.5	1.6	1.9	1.6	1.3	0.6	1.0	2.0	0.8	0.7	2.0	1.6	1.8	2.5	1.8	0.6	0.6	1.2	1.4	1.5
Mg^{2+} (mg/L)	2.9	2.1	2.8	1.8	1.9	11.0	2.5	11.1	10.4	5.4	2.6	1.1	2.0	3.2	4.9	5.2	4.1	6.4	7.1	4.7	7.9	2.3	2.0	10.4	10.9	12.7
Ca^{2+} (mg/L)	31.2	52.4	32.2	27.4	32.4	26.0	30.5	23.8	40.9	35.5	38.8	20.4	21.6	21.7	36.5	41.8	21.7	41.7	37.0	27.2	29.6	34.2	33.0	26.4	34.7	32.1
F^- (mg/L)	0.12	0.09	0.10	0.08	0.07	0.16	0.05	0.12	0.12	0.09	0.06	0.06	0.07	0.06	0.17	0.16	0.09	0.08	0.08	0.06	0.08	0.09	0.08	0.10	0.10	0.10
Cl^- (mg/L)	13.7	8.2	13.4	9.9	9.7	15.3	13.0	15.3	14.8	8.1	6.2	3.5	5.6	7.6	14.7	14.9	13.9	14.7	13.8	12.4	14.2	14.2	14.4	6.8	7.1	8.8
NO_3^- (mg/L)	5.7	0.2	1.8	0.4	0.5	4.1	7.8	4.1	3.2	1.0	1.0	1.7	1.1	317.0	32.5	29.0	165.3	5.2	3.7	6.9	6.6	0.2	0.2	3.2	3.0	4.1
SO_4^{2-} (mg/L)	5.1	2.9	19.2	3.7	4.1	9.3	7.0	8.9	8.2	4.6	2.9	0.9	1.7	2.4	7.2	7.2	7.7	7.9	6.8	3.7	6.9	3.9	3.4	3.2	2.8	3.9
CH_3COO^- (µg/L)	14.2	5.9	12.6	6.9	17.5	16.4	3.5	12.6	22.1	18.3	8.3	6.3	6.7	3.5	13.0	12.6	3.7	12.8	14.8	4.7	13.4	9.8	11.6	5.5	8.1	12.4

Table S2 Studied parameters in each water sample (green, Tourist trail; yellow, Fossil trail; violet, Paradise trail) collected in the Summer 2020 in Pertosa-Auletta Cave (DW: dripping waters; NR: Negro rivers; b.d.l: below detection limit).

Sample	et1	et2	et3	et4	et5	et6	et7	et8	et9	et10	ef1	ef2	ef3	ef4	ef5	ef6	ep1	en1	en2	en3
Type	DW	DW	DW	DW	DW	DW	DW	DW	DW	DW	DW	DW	DW	DW	DW	DW	DW	NR	NR	NR
Conductivity (µS/cm)	340	248	481	310	509	473	474	619	493	557	233	289	355	318	374	459	230	390	384	387
ORP (mV)	104.8	84.8	103.8	101.1	109.8	94.5	98.5	126.7	113.0	114.1	101.3	102.2	106.7	105.2	101.7	113.0	99.3	109.8	113.5	113.9
pH	8.1	8.2	7.8	7.9	7.8	8.1	8.0	7.1	7.8	7.6	7.9	8.0	7.9	7.9	8.0	7.7	8.1	7.8	7.7	7.7
C (mg/L)	35.7	25.8	35.7	28.2	52.0	45.1	45.3	65.3	48.4	50.1	27.8	28.4	23.5	32.2	27.9	39.9	21.4	46.0	42.3	43.3
C org (mg/L)	25.0	18.1	23.8	20.1	36.0	30.7	30.1	42.0	32.4	34.3	19.3	19.6	16.4	22.6	19.5	27.7	15.4	30.7	28.2	29.4
C inorg (mg/L)	10.7	7.7	11.9	8.1	16.0	14.4	15.2	23.3	16.0	15.8	8.5	8.8	7.1	9.6	8.4	12.2	6.0	15.3	14.1	13.9
N (mg/L)	1.4	1.6	0.3	0.5	1.1	1.0	1.1	0.9	0.6	0.7	1.7	1.1	11.4	1.0	11.7	0.9	0.4	1.1	1.2	1.1
Al (µg/L)	19.8	25.8	47.2	67.8	28.7	33.9	24.3	33.3	40.4	43.8	21.1	16.3	71.3	50.3	122.7	46.6	46.3	48.7	57.7	40.1
B (µg/L)	44.5	70.1	29.9	76.8	50	52.7	44.9	36.4	27.6	25.0	25.2	25.3	33.3	27.3	27.9	42.1	22.8	40.2	33.7	29.9
Ba (µg/L)	20.5	34.4	13.6	7.3	24.2	20.2	20.8	19.3	14.5	15.0	13.7	15.3	21.5	22.1	22.3	20.7	21.9	32.0	19.1	18.9
Ca (mg/L)	59.5	42.6	65.1	39.4	61.2	51.9	61.7	80.0	71.1	67.4	49.9	45.5	60.9	56.8	66.9	74.8	47.6	61.0	57.5	41.9
Cd (µg/L)	2.3	2.5	2.2	2.4	2.3	2.3	2.2	2.4	2.4	2.3	2.4	2.4	2.6	2.5	2.3	2.5	2.4	2.6	2.6	2.4
Co (µg/L)	2.0	2.4	1.7	2.5	2.3	2.3	2.5	2.0	2.2	2.2	2.5	2.2	2.5	2.3	2.2	2.0	2.5	2.7	2.2	1.7
Cr (µg/L)	b.d.l.	b.d.l.	b.d.l.	b.d.l.	b.d.l.	b.d.l.	b.d.l.	b.d.l.	b.d.l.	b.d.l.	b.d.l.	b.d.l.	b.d.l.	b.d.l.	b.d.l.	b.d.l.	b.d.l.	b.d.l.	b.d.l.	b.d.l.
Cu (µg/L)	8.0	7.0	5.5	11.3	4.8	6.2	4.2	3.3	4.3	4.1	4.8	3.7	7.3	4.0	5.5	4.3	5.4	4.1	4.4	4.2
Fe (µg/L)	7.5	13.0	16.0	52.5	15.7	14.0	7.9	14.3	21.8	13.9	10	10.4	31.0	32.2	68.5	10.5	30.2	32.7	35.3	16.3
K (mg/L)	1.3	1.4	1.3	1.4	2.2	2.8	1.9	13.9	1.8	1.4	1.0	1.4	2.7	1.2	1.7	2.4	1.0	2.5	2.3	2.3
Li (µg/L)	11.8	31.5	4.2	39.0	16.8	17.0	12.6	6.6	1.6	1.7	4.2	2.6	7.3	4.2	3.1	12.9	3.2	12.2	7.0	2.5
Mg (mg/L)	3.7	5.2	2.9	5.9	14.8	16.3	15.2	13.8	7.5	4.2	2.6	4.0	5.5	7.1	5.2	7.6	3.5	22.2	18.7	20.6
Mn (µg/L)	3.9	9.2	2.7	11.1	5.2	3.6	3.1	2.2	1.6	1.5	3.6	1.5	4.4	2.4	5.0	1.8	7.0	5.1	4.7	2.0
Mo (µg/L)	6.7	8.1	7.6	11.1	7.1	7.9	7.9	6.3	8.2	7.5	7.4	8.4	8.0	8.1	7.7	6.9	7.8	7.6	8.1	8.5
Na (mg/L)	11.2	9.3	5.5	6.5	11.1	12.7	11.3	10.5	6.7	6.8	3.8	5.6	8.0	9.3	8.6	9.6	6.1	8.6	7.8	8.2
Ni (µg/L)	13.4	11.7	12.3	12.5	11.2	10.9	8.5	9.6	10.9	10.4	10.5	11.8	13.3	11.2	12.1	11.0	11.9	11.4	11.7	10.6
P (µg/L)	36.1	76.6	77.7	92.1	64.3	80.5	70.1	77.3	58.9	46.4	82.9	43.0	83.1	59.1	96.3	74.6	63.1	109.0	90.5	87.5
Pb (µg/L)	25.7	22.7	25.0	24.8	25.0	29.9	25.3	25.5	25.2	26.6	24.9	22.6	27.3	24.0	25.6	23.4	25.2	25.1	24.4	24.7
S (mg/L)	2.6	5.0	1.6	3.5	5.8	7.2	6.3	18.5	3.3	3.3	1.8	2.3	3.5	6.5	5.9	4.3	4.0	6.2	5.4	5.5
Si (mg/L)	6.3	8.0	4.5	3.8	4.5	4.0	3.4	3.5	5.6	4.7	3.9	5.9	7.7	4.9	5.6	6.8	4.1	5.4	4.9	4.7
Sr (µg/L)	58.1	129.3	46.7	0.1	73.3	67.3	64.4	72.4	57.3	55.1	45.6	70.9	85.4	81.8	86.7	75.3	75.7	85.5	74.8	82.8
Ti (µg/L)	173.4	313.8	241.5	388.8	175.5	323.4	184.1	145.5	233.9	256.2	248.7	299.0	352.1	416.4	963.7	178.0	278.0	369.1	499.3	443.3
V (µg/L)	2.1	3.4	2.9	3.9	3.4	2.5	3.8	2.8	3.3	3.3	2.6	3.7	3.7	4.5	3.7	4.4	3.6	5.9	4.5	5.2
Zn (µg/L)	14.5	20	15.0	27.7	14.9	12.6	12.5	12.4	12.7	15.8	14.5	14.6	17.2	14.9	16.3	12.9	16.4	16.3	14.0	15.9
Na^+ (mg/L)	10.4	8.3	4.3	3.9	10.5	8.4	10.3	8.3	6.4	2.8	2.9	4.2	6.1	8.1	7.2	8.3	4.6	6.4	6.3	6.3
K^+ (mg/L)	0.7	0.3	0.3	0.2	1.8	1.2	1.5	1.0	1.7	0.7	0.6	1.0	1.9	0.7	0.9	2.3	0.5	2.1	2.1	2.1
Mg^{2+} (mg/L)	2.2	3.2	1.7	1.6	12.4	9.6	11.5	7.2	5.8	1.2	1.4	2.1	2.9	4.4	3.0	4.6	1.6	13.1	12.9	13.3
Ca^{2+} (mg/L)	30.8	30.8	35.9	34.9	39.8	36.0	37.2	56.8	39.6	58.8	33.6	34.5	49.7	43.1	54.6	44.7	37.7	55.8	44.1	47.1
F^- (mg/L)	0.12	0.13	0.06	0.05	0.12	0.12	0.13	0.10	0.07	0.06	0.06	0.05	0.09	0.15	0.15	0.08	0.12	0.12	0.12	0.12
Cl^- (mg/L)	12.9	6.4	6.4	4.8	9.2	11.8	9.5	11.1	6.8	8.3	4.1	4.8	10.2	14.7	12.8	13.3	9.8	9.9	10	10.1
NO_3^- (mg/L)	7.0	3.6	0.3	0.4	2.3	2.6	2.2	1.7	1.1	1.6	5.5	184.5	56.6	3.8	54.7	3.5	0.7	4.2	4.2	4.2
SO_4^{2-} (mg/L)	4.0	2.9	1.5	1.3	4.0	5.7	3.7	4.9	2.5	3.2	1.2	1.7	3.0	7.0	6.0	4.1	3.3	4.8	4.7	4.6
CH_3COO^- (µg/L)	20.9	5.5	8.3	3.5	7.7	16.6	11.0	13.8	4.3	9.0	5.5	4.9	6.9	17.5	11.6	10.6	6.3	15.0	18.7	14.8

Table S3 Studied parameters in each water sample (green, Tourist trail; yellow, Fossil trail; violet, Paradise trail) collected in the Autumn 2020 in Pertosa-Auletta Cave (DW: dripping waters; NR: Negro rivers; b.d.l: below detection limit).

Sample	at1	at2	at3	at4	at5	at6	at7	at8	at9	af1	af2	af3	af4	af5	af6	ap1	ap2	ap3	an1	an2	an3
Type	DW	DW	DW	DW	DW	DW	DW	DW	DW	DW	DW	DW	DW	DW	DW	DW	DW	DW	NR	NR	NR
Conductivity (µS/cm)	138.5	206	202	155.4	125.6	156.2	163.8	118.5	185.2	76.2	100.4	504	253	172.4	206	108.2	185.6	140.4	164.6	201	202
ORP (mV)	201.0	195.1	192.2	175.1	168.2	178.2	165.4	177.3	211.1	156.0	165.1	172.9	165.8	161.0	159.4	157.3	178.2	172.5	152.9	160.2	156.1
pH	6.7	6.8	6.8	7.3	7.4	7.2	7.5	7.3	6.6	7.4	7.3	7.2	7.3	7.3	7.5	7.5	6.9	7.0	7.6	7.5	7.6
C (mg/L)	35.0	41.8	39.3	23.9	21.5	36.0	20.2	23.6	30.2	15.4	19.3	12.5	20.2	28.3	38.5	19.4	47.5	39.3	24.4	32.3	33.0
C org (mg/L)	23.9	29.0	26.8	16.7	15.1	24.6	14.4	16.4	21.2	10.8	13.4	9.1	13.9	19.1	26.1	12.6	31.6	27.2	16.2	21.9	21.6
C inorg (mg/L)	11.1	12.8	12.5	7.1	6.4	11.3	5.8	7.2	9.0	4.6	6.0	3.4	6.3	9.3	12.4	6.8	15.9	12.2	8.2	10.4	11.4
N (mg/L)	0.4	0.5	1.4	1.6	0.4	0.3	2.1	0.7	3.8	0.9	0.5	66.9	17.4	1.1	1.8	0.4	0.3	0.8	0.7	0.9	1.1
Al (µg/L)	12.9	14.0	28.7	8.8	31.3	16.6	19.1	18.4	17.4	8.6	8.1	34.2	17.2	67.3	48.3	7.2	11.1	12.4	7.1	11.8	13.3
B (µg/L)	18.8	48.7	11.0	4.4	27.2	21.3	19.0	7.5	5.1	19.0	4.2	31.3	37.9	49.5	8.9	34.5	89.1	25.5	56.2	83.4	23.6
Ba (µg/L)	5.7	14.8	6.2	5.0	9.1	7.2	13.4	5.7	10.6	7.4	3.4	18.9	24.1	8.3	9.1	6.8	11.9	8.5	18.3	19.8	9.7
Ca (mg/L)	24.9	26.6	17.9	20.6	21.7	26.0	23.0	20.9	27.5	15.1	13.0	109.2	38.3	20.5	23.1	18.6	30.1	25.9	15.6	17.0	21.4
Cd (µg/L)	0.2	0.1	0.3	0.3	0.1	0.3	0.3	0.2	0.2	0.1	0.2	0.4	0.1	0.3	0.3	0.1	0.3	0.3	0.2	0.1	0.1
Co (µg/L)	0.3	0.2	0.4	0.3	0.2	0.3	0.4	0.2	0.5	0.3	0.5	0.4	0.3	0.5	0.2	0.3	0.3	0.4	0.2	0.3	0.3
Cr (µg/L)	0.2	0.6	0.3	0.3	0.6	0.4	0.2	0.2	0.3	0.2	0.5	0.8	0.2	0.5	0.2	0.5	0.5	0.3	0.8	0.8	0.2
Cu (µg/L)	1.0	0.9	2.3	0.2	1.3	2.3	1.3	0.9	1.5	2.2	0.4	1.6	0.6	1.1	1.2	0.3	1.2	1.1	1.0	1.6	0.8
Fe (µg/L)	2.0	2.6	25.6	3.5	15.0	4.7	7.5	7.9	9.4	8.4	9.6	1.3	5.0	28.8	34.6	1.6	1.6	6.9	1.9	7.3	2.6
K (mg/L)	1.0	1.5	1.9	1.7	0.8	0.7	0.6	0.5	1.4	0.7	0.6	1.2	0.9	1.8	1.4	0.6	0.8	0.6	1.5	1.8	1.7
Li (µg/L)	6.5	25.4	3.6	1.0	13.3	14.1	10	5.2	2.2	11.5	3.6	23.3	25.1	7.6	3.6	3.7	19.7	14.5	33.3	48.3	12.9
Mg (mg/L)	2.8	9.6	12.1	5.9	4.0	4.2	5.3	2.6	3.7	2.2	2.3	5.8	4.8	7.2	7.3	1.9	3.6	3.0	11.7	12.8	14.6
Mn (µg/L)	b.d.l.	0.1	0.1	0.4	0.4	0.1	1.0	b.d.l.	1.0	0.1	b.d.l.	1.9	2.3	1.9	1.0	0.6	0.4	0.5	0.6	1.6	0.6
Mo (µg/L)	b.d.l.	0.7	b.d.l.	b.d.l.	b.d.l.	0.2	0.8	b.d.l.	b.d.l.	b.d.l.	0.2	1.1	0.6	b.d.l.	b.d.l.	b.d.l.	b.d.l.	0.5	b.d.l.	1.1	0.3
Na (mg/L)	4.1	7.1	10.1	8.1	6.2	6.1	9.6	4.6	8.2	2.7	3.4	2.9	6.8	8.9	8.0	2.6	6.3	4.7	5.3	6.4	6.5
Ni (µg/L)	1.6	0.4	1.5	1.0	1.1	1.7	b.d.l.	1.2	0.9	1.7	b.d.l.	0.9	0.2	b.d.l.	0.2	b.d.l.	2.0	b.d.l.	b.d.l.	1.7	1.2
P (µg/L)	9.6	18.8	33.5	12.3	16.8	12.7	19.7	12.9	14.4	18.4	2.1	44.8	16.8	20.4	89.9	16.9	14.3	12.3	32.8	30.8	32.2
Pb (µg/L)	1.3	b.d.l.	2.4	1.1	b.d.l.	1.0	1.5	0.4	0.4	3.6	2.7	3.8	2.4	2.9	4.0	0.3	1.8	1.8	b.d.l.	1.0	2.5
S (mg/L)	0.9	2.4	3.0	2.2	1.7	1.3	2.8	1.1	2.3	0.7	0.6	1.5	2.6	2.0	2.3	0.7	1.5	1.1	2.3	2.8	2.1
Si (mg/L)	4.7	3.1	2.2	3.3	4.1	5.2	9.7	4.1	8.2	1.9	5.2	0.6	1.8	5.6	4.2	3.7	1.9	2.1	2.7	3.2	1.7
Sr (µg/L)	34.6	50.9	44.2	53.4	50.3	46.6	119.5	54.6	72.1	32.5	37.4	124.5	66.9	53.1	49.9	46.8	48.0	46.4	42.1	48.8	55.3
Ti (µg/L)	0.2	0.2	1.1	0.3	1.0	0.4	0.3	0.5	0.4	0.5	1.0	0.2	0.1	3.1	1.5	0.1	0.1	0.2	0.1	0.4	0.1
V (µg/L)	0.9	1.2	1.0	1.6	1.9	1.5	1.5	1.1	1.3	1.7	0.4	1.5	1.0	1.2	0.9	0.8	b.d.l.	1.5	1.4	2.8	2.3
Zn (µg/L)	b.d.l.	b.d.l.	b.d.l.	b.d.l.	b.d.l.	b.d.l.	9.4	b.d.l.	b.d.l.	b.d.l.	b.d.l.	b.d.l.	b.d.l.	b.d.l.	b.d.l.	b.d.l.	b.d.l.	b.d.l.	b.d.l.	b.d.l.	b.d.l.
Na^+ (mg/L)	6.6	11.3	12.4	9.5	6.2	5.5	10.4	5.6	9.0	3.2	4.9	2.7	9.2	9.9	9.8	5.0	6.7	6.3	7.4	7.5	7.4
K^+ (mg/L)	1.4	2.0	2.0	2.8	0.3	0.3	0.4	0.3	1.6	0.7	1.2	1.3	1.0	2.3	2.2	1.6	0.7	0.7	2.2	2.1	2.2
Mg^{2+} (mg/L)	3.0	11.8	13.8	6.2	2.4	2.3	4.0	1.8	2.9	1.6	2.4	4.6	4.1	6.8	8.0	2.3	2.2	2.2	15.8	15.1	15.7
Ca^{2+} (mg/L)	88.9	97.2	44.4	54.1	59.4	112.6	48.5	64.3	68.9	40.8	48.8	171.1	79.3	57.2	71.5	36.0	111.6	78.5	36.5	64.7	36.5
F^- (mg/L)	0.07	0.09	0.09	0.09	0.06	0.04	0.12	0.08	0.12	0.04	0.06	0.01	0.15	0.05	0.06	0.12	0.06	0.06	0.06	0.07	0.08
Cl^- (mg/L)	8.4	15.4	16.7	13.8	9.0	7.7	15.2	9.9	13.4	3.7	5.8	3.1	13.9	13.3	13.9	9.9	11.9	12.1	9.5	9.4	9.4
NO_3^- (mg/L)	1.6	2.7	5.1	6.5	1.3	0.4	8.4	2.5	18.2	4.1	1.6	391.4	99.5	4.6	6.0	2.1	0.3	3.1	4.7	4.7	4.7
SO_4^{2-} (mg/L)	3.6	7.4	9.5	7.4	2.9	3.1	7.5	2.8	6.4	0.7	1.6	2.6	7.3	4.9	6.6	1.6	3.1	1.9	4.9	4.7	4.8
CH_3COO^- (µg/L)	57.4	69.1	30.6	42.0	29.4	33.1	120.6	118.1	168.8	12.4	21.1	11.4	47.9	24.5	27.8	b.d.l.	46.4	b.d.l.	26.6	51.5	34.5

Table S4 Studied parameters in each water sample (green, Tourist trail; yellow, Fossil trail; violet, Paradise trail) collected in the Winter 2021 in Pertosa-Auletta Cave (DW: dripping waters; NR: Negro rivers; b.d.l: below detection limit).

Sample	it1	it2	it3	it4	it5	it6	it7	it8	it9	if1	if2	if3	if4	if5	ip1	ip2	ip3	in1	in2	in3
Type	DW	DW	DW	DW	DW	DW	DW	DW	DW	DW	DW	DW	DW	DW	DW	DW	DW	NR	NR	NR
Conductivity (µS/cm)	188.5	231	177.4	195.7	204	219	204	266	210	95.7	211	171.4	192.4	183.2	155.3	226	251	209	218	213
ORP (mV)	214.3	227.3	212.3	219.5	220	212.0	200.8	222.3	223.9	208.4	216.9	210.6	216.2	198.6	206.2	216.1	218.6	215.0	212.0	210.9
pH	7.2	7.0	7.2	7.1	7.2	7.3	7.6	7.1	7.0	7.3	7.1	7.3	7.2	7.6	7.4	7.2	7.1	7.2	7.2	7.3
C (mg/L)	28.8	46.8	21.9	38.6	37.7	34.8	29.4	47.8	37.0	16.2	13.1	23.5	26.7	24.0	20.3	37.9	42.5	36.1	34.7	33.1
C org (mg/L)	22.2	34.9	16.2	28.4	28.1	27.0	22.3	35.2	28.6	13.1	10.1	17.9	20.7	18.6	15.3	27.6	31.1	26.5	26.7	24.1
C inorg (mg/L)	6.6	11.9	5.7	10.2	9.6	7.7	7.1	12.6	8.4	3.1	3.0	5.6	6.0	5.4	5.0	10.4	11.4	9.6	7.9	9.0
N (mg/L)	1.0	0.4	0.6	0.3	0.3	0.8	1.0	0.8	0.9	0.4	22.2	0.5	0.9	1.3	0.4	0.5	0.5	1.5	2.0	1.7
Al (µg/L)	17.0	19.0	22.0	27.8	25.6	20.2	14.3	18.9	19.9	34.7	32.9	11.9	28.3	47.0	13.1	19.7	19.3	53.0	48.0	45.9
B (µg/L)	72.2	56.7	73.4	67.4	31.4	34.7	32.6	53.7	47.6	55.0	22.0	13.2	102.5	131.5	28.7	51.1	60.6	25.0	114.5	118.7
Ba (µg/L)	21.8	6.0	11.3	8.9	4.6	7.3	6.8	6.6	12.7	3.9	5.3	4.9	17.4	26.1	12.0	10.7	10.7	8.2	27.3	17.2
Ca (mg/L)	46.0	93.8	47.4	80.8	72.5	76.3	44.2	75.8	55.9	36.0	63.3	57.4	62.6	47.7	43.7	81.7	61.4	54.6	51.8	53.4
Cd (µg/L)	0.3	0.3	0.2	0.3	0.2	0.2	0.2	0.1	0.1	b.d.l.	0.3	0.2	0.1	0.3	0.4	0.2	0.3	0.2	0.1	0.3
Co (µg/L)	0.4	0.4	0.3	0.2	0.4	0.4	0.1	0.3	0.1	0.3	0.2	0.2	0.4	0.2	0.4	0.4	0.4	0.2	0.4	0.4
Cr (µg/L)	1.0	0.7	0.3	0.5	0.2	0.3	0.2	0.4	1.0	0.4	0	0.1	0.6	1.2	0.4	0.6	0.6	0.6	1.4	1.0
Cu (µg/L)	2.2	0.7	1.7	1.1	1.5	1.8	1.1	0.7	1.0	0.8	1.4	0.3	0.5	1.4	0.7	0.8	1.8	0.7	1.6	1.0
Fe (µg/L)	1.0	0.6	5.3	11.1	7.5	4.8	4.4	3.7	2.1	13.0	9.4	3.9	8.8	17.5	2.4	1.8	1.3	28.6	16.7	23.1
K (mg/L)	3.1	0.9	1.5	1.2	1.0	2.0	2.2	1.7	1.6	0.9	2.7	0.7	2.3	2.5	2.0	1.2	1.6	1.8	2.7	2.4
Li (µg/L)	37.8	13.3	1.6	8.8	0.9	3.4	1.1	3.9	27.3	0.5	1.4	1.0	26.8	42.8	7.9	20.2	25.6	2.5	41.8	29.7
Mg (mg/L)	5.8	3.7	4.8	3.8	2.9	14.1	15.7	11.6	5.9	1.5	2.5	4.0	6.1	10.8	4.6	4.2	5.2	11.2	13.7	14.1
Mn (µg/L)	1.0	0.2	0.6	1.0	b.d.l.	0.1	b.d.l.	b.d.l.	0.4	0.4	0.6	b.d.l.	0.2	0.9	b.d.l.	0.2	b.d.l.	1.6	1.9	1.0
Mo (µg/L)	1.9	b.d.l.	0.3	b.d.l.	b.d.l.	b.d.l.	b.d.l.	b.d.l.	b.d.l.	b.d.l.	b.d.l.	b.d.l.	0.3	0.5	b.d.l.	b.d.l.	b.d.l.	b.d.l.	1.5	b.d.l.
Na (mg/L)	8.6	6.5	12.0	5.8	6.2	9.4	10.1	8.8	6.6	3.1	3.3	5.5	8.3	9.8	8.2	6.7	7.7	5.6	7.7	7.2
Ni (µg/L)	2.6	1.8	2.2	1.0	1.9	2.3	1.4	1.8	0.7	1.1	1.7	0.4	0.5	1.0	1.0	b.d.l.	0.9	0.6	1.6	0.7
P (µg/L)	15.9	18.0	18.8	11.7	15.6	27.1	46.4	17.0	3.3	21.4	12.7	14.1	12.2	21.9	5.6	2.4	9.6	46.5	47.6	33.4
Pb (µg/L)	1.6	3.3	1.2	0.7	0.1	6.0	b.d.l.	b.d.l.	5.0	b.d.l.	b.d.l.	0.6	1.3	6.0	b.d.l.	3.0	3.3	2.3	2.7	0.2
S (mg/L)	2.5	2.1	3.4	1.1	1.0	2.7	3.2	2.1	1.8	0.5	0.6	1.3	2.4	3.7	1.5	1.6	1.9	1.8	2.9	2.6
Si (mg/L)	5.1	3.8	9.9	4.3	2.3	1.8	1.4	0.9	2.3	1.0	0.8	0.8	2.1	3.0	6.3	1.7	0.7	1.9	2.8	2.0
Sr (µg/L)	61.3	65.6	129.6	52.6	44.5	50	58.5	50.1	45.4	32.0	59.1	40.9	60.2	63.1	73.5	49.6	49.8	59.2	66.5	64.0
Ti (µg/L)	0.1	b.d.l.	0.4	0.9	2.6	0.5	1.0	0.2	0.3	1.4	0.7	0.3	1.2	1.3	0.2	0.2	0.2	4.0	1.4	1.7
V (µg/L)	0.1	1.0	1.0	0.4	1.5	0.4	0.9	0.9	1.7	1.2	0.6	0.9	0.8	1.4	1.2	1.2	1.0	2.7	1.6	1.7
Zn (µg/L)	b.d.l.	b.d.l.	b.d.l.	b.d.l.	b.d.l.	b.d.l.	b.d.l.	b.d.l.	b.d.l.	b.d.l.	b.d.l.	b.d.l.	b.d.l.	b.d.l.	b.d.l.	b.d.l.	b.d.l.	b.d.l.	b.d.l.	b.d.l.
Na^+ (mg/L)	10.1	6.6	12.5	5.5	6.5	10.9	11.4	9.8	5.8	3.1	3.1	8.5	7.7	8.8	8.0	6.4	5.9	6.6	5.4	5.9
K^+ (mg/L)	1.1	0.4	0.5	0.4	0.5	2.0	2.6	2.0	1.3	0.7	0.8	0.7	0.8	1.7	2.1	0.8	0.6	2.3	1.7	2.0
Mg^{2+} (mg/L)	2.8	2.0	3.8	2.2	2.5	13.5	16.4	10.5	2.4	1.0	1.7	4.9	3.6	7.5	3.4	2.1	1.9	10.3	8.9	10.2
Ca^{2+} (mg/L)	28.4	35.2	28.7	37.0	36.7	23.3	14.3	33.5	36.1	17.6	40.6	14.0	25.3	20.2	19.7	34.1	37.7	27.2	28.7	26.0
F^- (mg/L)	0.11	0.10	0.19	0.05	0.09	0.18	0.11	0.11	0.07	0.06	0.07	0.15	0.14	0.13	0.14	0.10	0.05	0.25	0.10	0.10
Cl^- (mg/L)	14.4	11.5	20.5	9.0	11.0	16.2	14.8	15.9	9.4	4.4	4.7	18.9	16.9	14.7	17.9	15.9	14.9	9.8	9.4	9.5
NO_3^- (mg/L)	2.8	0.2	2.3	0.4	0.7	3.0	3.8	2.8	1.3	1.0	97.2	1.6	2.2	3.2	0.6	0.2	0.1	5.6	5.6	5.7
SO_4^{2-} (mg/L)	3.4	4.8	9.0	1.8	2.4	8.7	9.5	6.3	2.1	1.0	1.7	6.4	5.3	7.6	4.1	2.4	2.1	5.2	4.5	4.9
CH_3COO^- (µg/L)	b.d.l.	b.d.l.	b.d.l.	42.4	b.d.l.	b.d.l.	93.0	b.d.l.	b.d.l.	b.d.l.	59.6	118.6	93.0	b.d.l.	b.d.l.	90.0	107.8	b.d.l.	148.9	127.3

Table S5 Positive (green) and negative (red) Pearson's correlation coefficients for water parameters from Pertosa-Auletta Cave.

	Cond	ORP	pH	C	C org	C inorg	N	Al	B	Ba	Ca	Cd	Co	Cr	Cu	Fe	K	Li	Mg	Mn	Mo	Na	Ni	P	Pb	S	Si	Sr	Ti	V	Zn	Na^+	K^+	Mg^{2+}	Ca^{2+}	F^-	Cl^-	NO^{3-}	SO_4^{2-}	CH_3COO^-
Cond	1.00																																							
ORP	-0.52	1.00																																						
pH	0.27	-0.62	1.00																																					
C	0.50	-0.06	-0.16	1.00																																				
C org	0.50	-0.03	-0.17	0.96	1.00																																			
C inorg	0.41	-0.10	-0.11	0.88	0.71	1.00																																		
N	0.38	-0.06	0.10	-0.35	-0.31	-0.35	1.00																																	
Al	0.29	-0.24	0.27	0.08	0.07	0.09	0.09	1.00																																
B	-0.08	0.23	-0.08	0.16	0.19	0.09	-0.14	0.11	1.00																															
Ba	0.23	-0.40	0.13	0.13	0.14	0.09	0.00	0.16	0.47	1.00																														
Ca	0.61	-0.25	0.04	0.27	0.25	0.25	0.47	0.38	-0.01	0.33	1.00																													
Cd	0.51	-0.62	0.60	0.31	0.21	0.44	-0.07	0.49	-0.04	0.27	0.43	1.00																												
Co	0.48	-0.67	0.55	0.28	0.19	0.40	-0.09	0.47	0.02	0.45	0.43	0.95	1.00																											
Cr	-0.28	0.50	-0.33	-0.12	-0.03	-0.26	0.06	-0.14	0.44	-0.01	-0.18	-0.62	-0.60	1.00																										
Cu	0.36	-0.52	0.53	0.19	0.10	0.31	-0.06	0.49	0.11	0.27	0.33	0.87	0.86	-0.55	1.00																									
Fe	0.15	-0.36	0.34	0.03	0.03	0.04	-0.03	0.87	0.04	0.21	0.20	0.48	0.50	-0.24	0.51	1.00																								
K	0.19	-0.13	-0.01	0.18	0.22	0.08	-0.02	0.05	0.14	0.44	0.20	0.08	0.16	-0.01	0.04	0.08	1.00																							
Li	-0.09	0.07	-0.14	0.06	0.09	-0.01	-0.02	-0.07	0.77	0.62	0.03	-0.16	-0.03	0.48	0.06	-0.04	0.21	1.00																						
Mg	0.26	-0.11	0.12	0.48	0.46	0.43	-0.15	0.17	0.31	0.39	0.13	0.24	0.26	0.01	0.15	0.20	0.24	0.27	1.00																					
Mn	0.22	-0.52	0.08	0.06	0.09	0.01	-0.03	0.19	0.24	0.77	0.25	0.21	0.43	-0.18	0.33	0.34	0.36	0.45	0.20	1.00																				
Mo	0.51	-0.64	0.63	0.26	0.17	0.38	-0.04	0.50	0.00	0.29	0.42	0.98	0.95	-0.58	0.90	0.50	0.07	-0.08	0.24	0.25	1.00																			
Na	0.22	-0.05	0.08	0.41	0.42	0.31	-0.34	0.25	0.23	0.28	0.11	0.30	0.28	-0.08	0.28	0.17	0.27	0.09	0.51	0.11	0.26	1.00																		
Ni	0.51	-0.63	0.61	0.28	0.19	0.39	-0.06	0.50	-0.02	0.29	0.42	0.98	0.94	-0.62	0.90	0.48	0.09	-0.14	0.20	0.25	0.97	0.27	1.00																	
P	0.14	-0.27	0.23	-0.04	0.01	-0.12	0.07	0.12	-0.12	0.12	0.14	0.14	0.11	-0.14	0.09	0.11	0.07	-0.11	0.07	0.04	0.15	0.16	0.16	1.00																
Pb	0.52	-0.59	0.61	0.32	0.22	0.45	-0.06	0.50	-0.02	0.26	0.43	0.99	0.94	-0.59	0.88	0.48	0.09	-0.13	0.26	0.18	0.98	0.30	0.97	0.14	1.00															
S	0.44	-0.34	0.17	0.40	0.37	0.38	-0.09	0.27	0.12	0.49	0.36	0.46	0.50	-0.22	0.34	0.26	0.80	0.12	0.46	0.36	0.44	0.56	0.43	0.15	0.47	1.00														
Si	0.06	-0.36	0.17	-0.06	-0.08	0.01	-0.25	0.19	-0.14	0.24	0.07	0.32	0.35	-0.21	0.28	0.22	0.05	-0.12	-0.12	0.26	0.30	0.37	0.31	0.07	0.26	0.19	1.00													
Sr	0.17	-0.13	0.10	-0.05	-0.07	-0.01	0.18	0.19	0.10	0.50	0.49	0.26	0.28	-0.11	0.14	0.07	0.22	0.05	0.20	0.23	0.22	0.45	0.23	0.19	0.22	0.40	0.53	1.00												
Ti	0.39	-0.56	0.55	0.17	0.09	0.28	-0.01	0.68	-0.05	0.26	0.41	0.85	0.81	-0.53	0.76	0.67	0.02	-0.15	0.22	0.23	0.86	0.22	0.85	0.15	0.84	0.38	0.28	0.25	1.00											
V	0.38	-0.55	0.52	0.27	0.16	0.40	-0.13	0.50	-0.02	0.33	0.41	0.86	0.83	-0.49	0.71	0.52	0.06	-0.05	0.42	0.24	0.86	0.23	0.82	0.11	0.84	0.41	0.27	0.28	0.79	1.00										
Zn	0.49	-0.66	0.36	0.16	0.12	0.20	0.03	0.30	0.03	0.53	0.34	0.61	0.71	-0.52	0.61	0.37	0.18	0.08	0.10	0.65	0.63	0.10	0.63	0.10	0.58	0.36	0.38	0.24	0.55	0.54	1.00									
Na^+	0.05	0.15	-0.06	0.22	0.27	0.10	-0.18	-0.02	0.03	0.04	-0.21	-0.10	-0.13	0.06	-0.09	-0.04	0.16	-0.02	0.34	-0.09	-0.13	0.78	-0.11	0.08	-0.10	0.31	0.22	0.26	-0.12	-0.15	-0.17	1.00								
K^+	0.12	-0.01	0.14	0.12	0.14	0.05	0.10	0.06	-0.01	0.05	-0.12	-0.06	-0.09	0.23	-0.19	0.12	0.05	0.01	0.56	-0.09	-0.08	0.16	-0.09	-0.01	-0.06	0.03	-0.11	-0.06	-0.06	0.10	-0.18	0.34	1.00							
Mg^{2+}	0.12	-0.01	0.06	0.34	0.32	0.31	-0.10	0.01	0.20	0.25	-0.09	0.01	0.02	0.09	-0.05	0.07	0.13	0.22	0.90	0.09	0.01	0.37	-0.02	0.05	0.02	0.26	-0.22	0.07	0.01	0.20	-0.06	0.44	0.68	1.00						
Ca^{2+}	0.44	0.10	-0.21	0.21	0.25	0.11	0.61	-0.05	-0.13	-0.19	0.46	-0.14	-0.21	0.12	-0.17	-0.21	-0.10	-0.08	-0.22	-0.21	-0.15	-0.21	-0.13	-0.07	-0.13	-0.12	-0.20	0.01	-0.14	-0.23	-0.12	-0.04	-0.04	-0.19	1.00					
F^-	0.00	0.08	0.07	0.04	0.07	-0.01	-0.17	0.11	0.13	0.29	-0.08	0.06	0.09	-0.12	0.03	0.10	0.20	-0.03	0.33	0.15	0.05	0.50	0.07	0.24	0.07	0.33	0.14	0.43	0.14	0.11	0.08	0.51	0.08	0.30	-0.28	1.00				
Cl^-	-0.08	0.30	-0.19	0.13	0.22	-0.04	-0.20	-0.04	0.11	0.04	-0.19	-0.23	-0.25	0.12	-0.24	-0.06	0.14	0.00	0.16	-0.12	-0.27	0.62	-0.24	0.07	-0.23	0.18	0.09	0.20	-0.17	-0.26	-0.25	0.79	0.21	0.21	-0.04	0.54	1.00			
NO_3^-	0.38	-0.11	0.15	-0.34	-0.30	-0.33	0.94	0.03	-0.16	-0.01	0.42	-0.02	-0.04	0.03	-0.04	-0.06	-0.03	-0.06	-0.17	-0.05	0.02	-0.36	0.01	0.06	-0.02	-0.10	-0.21	0.17	0.02	-0.08	0.07	-0.21	0.09	-0.12	0.57	-0.21	-0.24	1.00		
SO_4^{2-}	0.08	0.12	-0.15	0.08	0.14	-0.04	-0.06	0.10	-0.03	0.04	-0.10	-0.18	-0.19	0.18	-0.22	-0.01	0.13	-0.05	0.31	0.01	-0.21	0.62	-0.20	0.11	-0.19	0.30	0.14	0.26	-0.11	-0.17	-0.15	0.77	0.27	0.39	-0.02	0.47	0.67	-0.09	1.00	
CH_3COO^-	-0.28	0.44	-0.21	-0.06	-0.07	-0.03	-0.05	-0.10	0.13	-0.13	-0.21	-0.23	-0.26	0.19	-0.19	-0.13	-0.06	0.11	0.04	-0.29	-0.23	0.05	-0.26	-0.10	-0.23	-0.11	-0.11	0.02	-0.20	-0.18	-0.31	0.11	0.01	0.07	0.01	0.02	0.21	-0.08	0.10	1.00

CHAPTER 3

Geochemical characterization of clastic sediments sheds light on energy sources and on alleged anthropogenic impacts in cave ecosystems

Rosangela Addesso*, Jo De Waele, Simona Cafaro, Daniela Baldantoni

International Journal of Earth Sciences

doi: 10.1007/s00531-021-02158-x

**corresponding author*

A geochemical characterization of clastic sediments from the Pertosa-Auletta Cave has been performed, contributing to the comprehension of the fluviokarst activity in caves, as well as the sediment energy contribution in ecological terms and the potential impacts of natural and anthropogenic pressures on cave equilibria.

InternationalJournalofEarthSciences
https://doi.org/10.1007/s00531-021-02158-x

ORIGINAL PAPER

Geochemical characterization of clastic sediments sheds light on energy sources and on alleged anthropogenic impacts in cave ecosystems

Rosangela Addesso[1] · Jo De Waele[2] · Simona Cafaro[3] · Daniela Baldantoni[1]

Received:4October2021/Accepted:27December2021

Abstract
Caves are usually oligotrophic ecosystems, where the organic matter represents a limiting factor to the hypogeal community and sediments are often a signi cant energy source. With a view to identifying the energy input in uencing the ecological processes occurring in caves, as well as the potential alteration sources of the natural equilibriums, geochemical features of several typologies of clastic sediments from the Pertosa-Auletta Cave (Italy) were investigated. The collected sediments, analyzed for a number of chemical (organic matter, Al, B, Ba, Ca, Cd, Co, Cr, Cu, Fe, K, Li, Mg, Mn, Mo, Na, Ni, P, Pb, S, Si, Sr, Ti, V, Zn concentrations) and mineralogical (quartz, calcite, dolomite, clay minerals) characteristics, showed a di erent composition. Overall, their origin is supposed to be allochthonous, related to the important uviokarst activities interesting the cave in the past, whereas the abundance of calcitic and dolomitic compounds can be autochthonous, being the carbonate the main host rock. The highest concentrations of organic matter, together with C, Cu, Mo, N, P, Pb, S and Zn, highlighted in one sample composed mainly of bats guano, revealed an important bioavailable energy input as well as a pollutant accumulation, mainly of anthropogenic origin.

Keywords Cave sediments · Geochemistry · Mineralogy · Karst ecosystem · Pertosa-Auletta Cave

Introduction

Sediments represent a signi cant energy source in caves, being these ecosystems generally poor in nutrients, mainly due to the absence of organic matter deriving from the photoautotrophic primary producers, limited only to the lighted entrance areas (Gillieson 1996; Mammola and Isaia 2018) or to the lit trails of tourist caves (Mulec and Kosi 2009). In some cases, also cave con nement restricts the organic supplies from the external environment, but if a substantial degree of connectivity and interaction with the surface environment exist, cavities can be considered a perfect snare for detrital and organic matter, which accumulate in underground environments due to gravity fall or carried inside by water (Gillieson 1996; Arriolabengoa et al. 2015; Ková 2018). Such deposits, commonly called clastic sediments, can be autochthonous, originating from inner cave local inputs (guano, phosphate minerals, speleothem fragments, clays…), or allochthonous, carried from outside by surface water, which represents the main matter carrier in underground environments, hauled inside the cave by shafts or overlying soils through the epikarst and vadose zone (Gillieson 1996; White 2007; Ková 2018).

External pollutants from surface anthropogenic activities or visitors in show caves may represent further energy sources altering the natural nutrient-poor ecological equilibrium of underground ecosystems (Chelius et al. 2009; Dredge et al. 2013; Smith et al. 2013). Allochthonous particles, such as dust, bers, hair, but also bacteria, spores and seeds can constitute organic and inorganic inputs emanated in the cave (Russell and MacLean 2008) and depositing on the oor and wall surfaces.

✉ Rosangela Addesso
raddesso@unisa.it

[1] Department of Chemistry and Biology "Adolfo Zambelli", University of Salerno, Via Giovanni Paolo II, 132, 84084 Fisciano, SA, Italy

[2] Department of Biological, Geological and Environmental Sciences, University of Bologna, Via Zamboni, 67, 40126 Bologna, Italy

[3] MIdA Foundation, Integrated Environmental Museum, Via Muraglione, 18/20, 84030 Pertosa, SA, Italy

Published online: 10 January 2022

Besides their ecological importance in the cave food chain, sediments may preserve valuable information about the environmental, geomorphological, sedimentological, hydrological and paleo-climatological history of the underground spaces in which they originated or deposited (White 2007; Arriolabengoa et al. 2015).

The goal of this study was to investigate the geochemical nature of clastic sediments collected in the Pertosa-Auletta Cave (Campania Region, southern Italy), which represents an excellent model of a heterogeneous cave system (Addesso et al. 2019, 2021). Indeed it presents a di erent fruition between the trails (tourist and closed to the public paths), as well as a diversi cation of the environmental conditions in the same system (fossil areas where water is present only as dripping, and active trails where dripping is active and water pools seasonally change in extent, or cave branches with a large river owing through). Throughout an extensive geochemical sediment characterization, from pristine to disturbed states, this research aims to shed light on the energy sources in caves, helping also to identify potential anthropogenic impacts in the karst ecosystem.

Materials and methods

Sedimentsampling

Samples were manually collected in May 2020, using plastic tools to avoid metal contamination, in several places along the three principal paths (Fig. 1) of the Pertosa-Auletta Cave (WGS84: 40°53′62″ N; 15°45 ′ 48″ E), extensively described in Addesso et al. (2019). In particular, 6 samples were taken from the tourist trail (Ts), 5 from the fossil trail (Fs) and 5 from the active trail (As), collecting them from accumulations found on rock recesses (triangles in Figs. 1 and 2a) or those deposited on the oor (circles in the Figs. 1 and 2b), left there by intense water currents when the cave passages were still active. In the actual active trail, crossed by a perennial underground stream, called Negro, samples were collected on both above the water (lled symbols in Fig. 1) and underwater (empty symbols in Fig. 1).

Sedimentgeochemicalcharacterization

Fine sediments (< 2 mm) were dried in a stove at 75 °C to constant weight and then turned to dust using a pulverizing mill endowed with jars and agate balls (PM4, Retsch, Germany). Organic matter (OM) was determined (in triplicate) by calcination in a mu e furnace (B150, Nabertherm, Germany), at 550 °C for 4 h, and expressed as percentage of dry weight.

For elemental analysis, total C and N were determined (in triplicate) by a CHSN-O Analyzer Flash EA 1112 (Thermo Fisher Scienti c Inc., MA, USA), weighing ~ 3 mg in little tin capsules, with the blank and standards (holm oak leaves with a known concentration of C and N) used in the calibration curve. In addition, samples (125 mg) were mineralized (in triplicate) by a microwave oven (mls 1200, Milestone

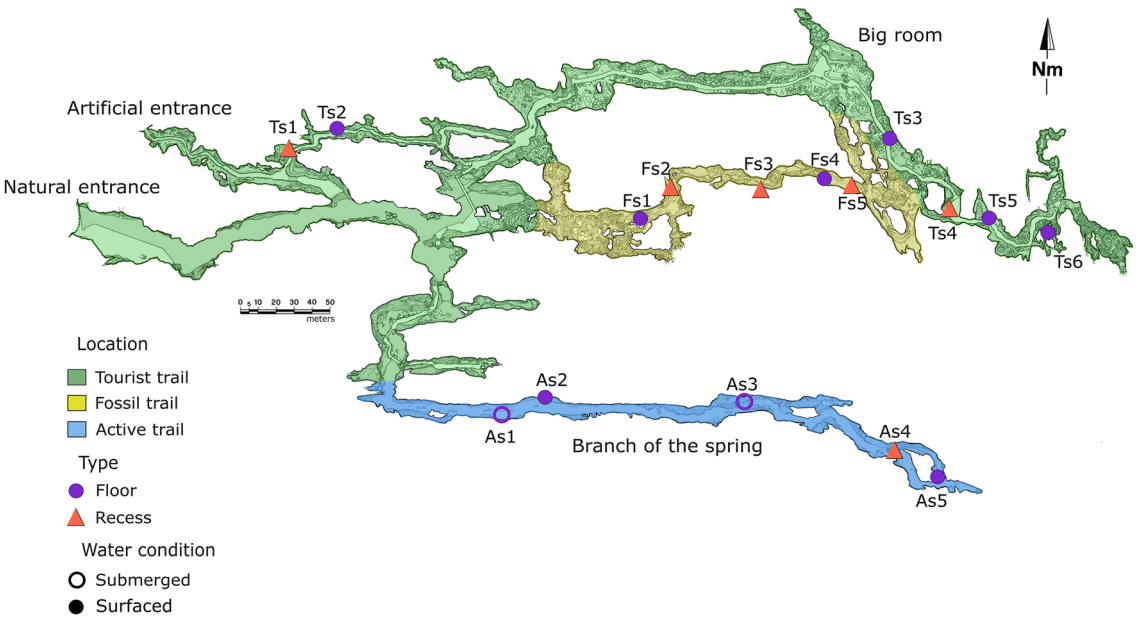

Fig. 1 Pertosa-Auletta Cave (Campania, southern Italy) map, with the three main paths: active (A, blue), tourist (T, green) and fossil (F, yellow). Sediments sampling sites are also reported, distinguishable in deposits collected to the oor (circles) and accumulated in the rock recesses (triangles). Empty circles in the active trail indicate submerged sediments collected underwater

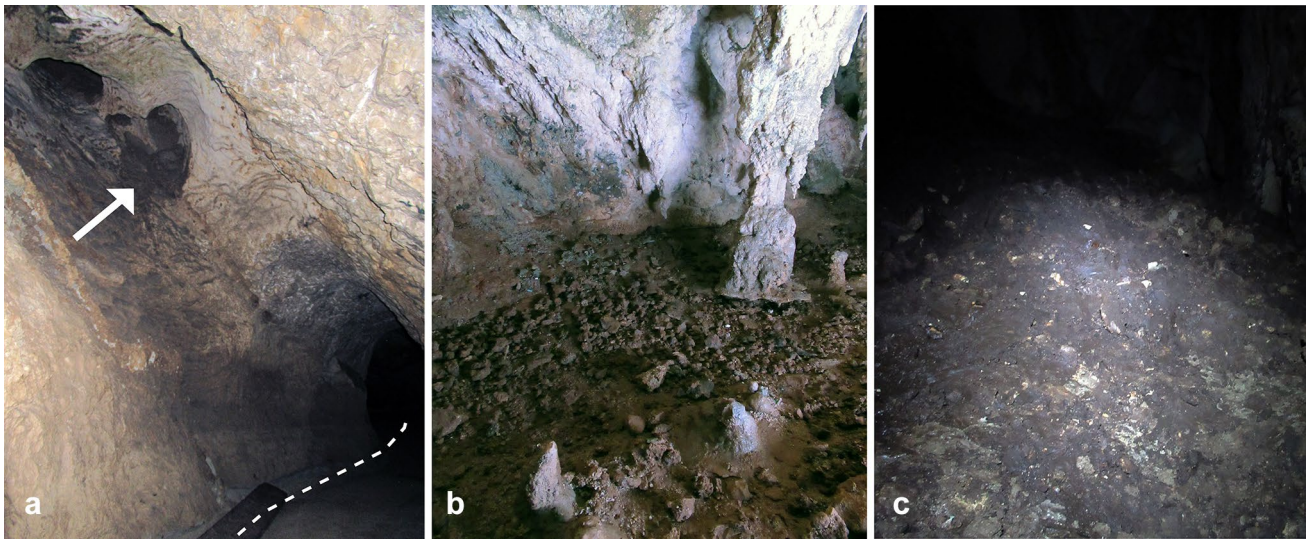

Fig. 2 Photographs of sediments from the Pertosa-Auletta Cave. **a** Ts4 sample: sediments deposited in the rock recess (white arrow; dotted line indicates the tourist pathway). **b** Ts2 sample: sediments to the oor. **c** Ts3 sample: sediments visibly constituted by bats guano

Microwave Laboratory Systems, Shelton, CT, USA), using a mixture of hydro uoric acid and nitric acid (50% HF: 65% HNO_3 = 1:2 = v: v). After digestion, deionized water was used to dilute the solution up to a nal volume of 25 mL. Al, B, Ba, Ca, Cd, Co, Cr, Cu, Fe, K, Li, Mg, Mn, Mo, Na, Ni, P, Pb, S, Si, Sr, Ti, V and Zn concentrations were analyzed using an Optima 7000 DV ICP-OES (PerkinElmer, Krakow, Poland). To estimate the analytical accuracy and possibly correct the analyzed element concentrations in the single samples, the Standard Reference Material NCS soil DC 73321 was also analyzed with the same procedure.

Sediment mineralogy was determined by X-ray di raction, using a D2 PHASER di ractometer (Bruker, Massachusetts, USA), equipped with a Cu tube (λ = 1.54184 Å, 10 mA, 30 kV, 5°–45° 2 with a step angle of 0.02°, analysis time = 1.5 s per step, variable rotation = 10/min). The open-source software Profex 4.0.2 using the BGMN database (Doebelin and Kleeberg 2015), through Rietveld re nement, according with Taylor and Rui (1992) method, was used for the identi cation and abundance estimation of the main minerals.

Dataanalysis

Differences among samples based on their overall geochemical characteristics, considering three xed variables, location (tourist, fossil and active trails), type of sampling (from the ground or from recesses), water conditions (at the surface or underwater), were evaluated using permutational multivariate analysis of variance (PERMANOVA), based on the Manhattan distance metric and 999 permutations. Non-metric multi-dimensional scaling (NMDS), based on the same distance metric and on 2 axes, with the superimposition of con dence ellipses (α = 0.05), was also performed. Subsequently, di erences according to the single analyzed parameters, considering the same xed variables as in PERMANOVA, were evaluated by three-way analyses of variance (three-way ANOVAs), followed by Tukey's *post hoc* tests. Finally, for the di erent sediment characteristics, a network based on the Pearson's correlation coe cients was obtained.

All the analyses were carried out in the R 4.0.0 programming environment (R Core Team 2020), with functions from the "vegan", "agricolae", "ggplot2" and "q graph" packages.

Results and discussion

The Pertosa-Auletta Cave presents several sediment accumulations along the three main trails, individuated based on their di erent fruition and environmental conditions (Addesso et al. 2019), evidence of its hydrological history, characterized by intense past oods. These di erent types of debris, carried in from outside (allochthonous) or deriving from near the sampling site (autochthonous), deposited on the ground or on the rock wall recesses depending on their dimensional and physical features (Dykes 2007). Parts of these sediments were altered, moved and reused to build the path for tourists, such as in the long passage before the "Great Room" (Fig. 1), where the sediments solidi ed, making the sampling di cult. In the other sectors, they resulted in a pristine state, object of collection for this study. All the 16 collected sediments (Fig. 1) had a ne-grained texture and a brown coloring with di erent gradations, in one case

(Ts3, Fig. 2c) tending to black, probably because of the presence of bats guano.

Chemical composition of the analyzed sediments (Table 1) highlighted a broad variability among the samples, with di erences in element concentrations of one, and, in some cases, of two orders of magnitude. The observed mean values of Ba, C, Co, Cu, Ni, Pb, Sr and V are however comparable with the average concentrations of the same elements measured in sediments from the Modri Cave (Croatia), reported by Miko et al. (2002); conversely, Cd and Zn showed lower concentrations in sediments from the Pertosa-Auletta Cave. Ts3 sample, visibly composed for the most part by guano (Fig. 2c), diverged from the others for the higher concentrations of several elements, in particular Cu (4269 g/g d.w.), Mo (87 g/g d.w.), P (40 mg/g d.w.), Pb (41 g/g d.w.), S (5.8 mg/g d.w.) and Zn (428 g/g d.w.). Also for C, N and organic matter, presenting average values of 0.1, 2.9 and 5.0% d.w., respectively, Ts3 sample displayed the highest concentrations, equal to 3.0, 16.9 and 46.0% d.w., respectively (Table 1), con rming its organic origin (Miko et al. 2001).

Guano deposits can be classi ed as autochthonous clastic sediments (White 2007), representing an important energy source for several cave species, therefore called guanobites and guanophiles (Deharveng and Bedos 2018). These deposits are primarily constituted of organic matter, such as chitin from insects and other not digested compounds, combined over time with autochthonous inorganic materials, such as quartz, calcite and clay (Putra et al. 2019). Anyway, not only the high concentrations of organic matter and chemical elements (C, N, P, S) associated to its composition may be related to bat guano, but also elements of abiotic origin (Miko et al. 2001), similarly found in the Ts3 sample in high concentrations (particularly Pb). In this case, a bioaccumulation of persistent contaminants from the predation habitats may be expected, being bats excellent environmental biomonitors (Zukal et al. 2015; Wurster et al. 2015).

Mineralogical features of sediments from the Pertosa-Auletta Cave are reported in Table 2 and in Fig. 3, showing the estimated relative abundances of minerals composing the sediments and the di ractograms for each sample, respectively. As1, As2, As3, As5, Ts5, Ts6, Fs1 and Fs4 showed a similar mineralogical composition, with average values of -quartz, calcite and dolomite equal to 61.4, 17.6 and 21.0%, respectively. As4 displayed only -quartz and calcite minerals (81.3 and 18.7%, respectively). Ts1, Ts3, Ts4 and Fs3 were composed, in their entirety, of -quartz. Also Fs2 showed the main percentage of -quartz (96.3%), associated to lime (3.7%), not contained in any of the other samples, certainly related to unreacted residual of calcium carbide, used for acetylene burners by speleologist illuminating caves (Abdyzhaparova et al. 2021). Ts5 and Ts6 presented different amounts of -quartz (65.5 and 83.4%, respectively), calcite (18.2 and 6.1%, respectively) and dolomite (16.3 and 10.5%, respectively). Ts2 and Fs5, unlike the others, were mainly composed of calcite (88.1 and 97.3%, respectively) with a low amount of -quartz (11.9 and 6.3%, respectively). It was not possible to quantify clay minerals due to the limits of the protocol chosen for this investigation, but they were also detected in traces (Table 2). Especially, smectite, muscovite and kaolinite, indicated by di raction peaks around 6°, 8.8° and 12.5° 2 , respectively, according to Moore and Reynolds (1997), were identi ed in most samples (As1, As1, As3, As5, Ts2, Ts3, Ts5, Fs1 and Fs4). As4, Ts1, Fs2 and Fs3 sediments showed traces of kaolinite and muscovite; while Ts6 and Fs5 presented traces of kaolinite and muscovite, Ts4 of kaolinite and smectite, and Ts6 and Fs5 only of muscovite.

The presence of quartz, calcite and clay minerals in cave sediments is worldwide reported (Miko et al. 2002; Zupan Hajna et al. 2008; Arriolabengoa et al. 2015); anyway, the analyses carried out on the Pertosa-Auletta Cave sediments show a mineralogical variability among the samples. Calcite and dolomite are the most abundant and important carbonate minerals, deriving from the host rock. The Pertosa-Auletta Cave is one of the most important basal springs of the Alburni karst system, extending for a total length of 3000 m. It is divided into three main branches (Fig. 1), which mark the border fault of the carbonate massif with NW–SE orientation. Previous stratigraphic and sedimentological studies allowed identifying di erent bauxite horizons marking episodes of continental emersion of the Cretaceous limestone (Cafaro et al. 2010). The underground water ow inside the Alburni karst system, instead, is still poorly known, but part of the waters coming from the NW portion of the plateau have the Pertosa-Auletta Cave as their nal destination (Celico et al. 1994; Cozzolino et al. 2015a, b; Pedrali et al. 2015; Pastore et al. 2017). In particular, the Pertosa-Auletta Cave is crossed by an underground river, named “Negro”, which is currently present only in the southern branch. Nevertheless, there are several morphological evidences, such as residual uvial sediments placed at di erent elevations in all the branches, which suggest the presence of water ow all along the cave in the past.

Quartz found in sediment samples from the Pertosa-Auletta Cave might be attributed to both allogenic material or to impurities in the carbonate series, being silica, as well as clay minerals, the most common insoluble impurities in carbonate rocks. Together with silt, they represent the most widespread clastic deposits in caves. Because they are transported in suspension, these deposits may coat walls and even the ceiling, although most accumulation is on the oor. Their sources are diversi ed: allogenic material including uvial and lacustrine sediments, in ltrates from soils overhead and windborne dust are the most common. There is often a signi cant autogenic component from the weathering of walls

Table 1 Chemical composition (mean values ± standard deviations) of each sediment sample from the Pertosa-Auletta Cave

Samples	As1	As2	As3	As4	As5	Ts1	Ts2	Ts3	Ts4	Ts5	Ts6	Fs1	Fs2	Fs3	Fs4	Fs5
Type	Soil	Soil	Soil	Recess	Soil	Recess	Soil	Soil	Recess	Soil	Soil	Soil	Recess	Recess	Soil	Recess
Water condition	Submerged	Surfaced	Submerged	Surfaced	Surfaced	Surfaced	Surfaced	Surfaced	Surfaced	Surfaced	Surfaced	Surfaced	Surfaced	Surfaced	Surfaced	Surfaced
Al (mg/g d.w.)	35.8 ± 2.9	44.2 ± 6.4	42.7 ± 3.4	81.9 ± 1.6	33.0 ± 2.2	66.6 ± 2.3	20.3 ± 2.2	35.3 ± 1.6	93.4 ± 5.4	52.8 ± 2.5	29.8 ± 2.7	25.8 ± 2.8	67.2 ± 2.3	57.2 ± 2.4	36.6 ± 2.6	1.5 ± 0.1
B (µg/g d.w.)	58.5 ± 3.2	74.1 ± 6.9	62.3 ± 7.0	99.7 ± 1.4	61.2 ± 0.3	76.9 ± 4.8	81.3 ± 4.5	53.3 ± 2.2	108.6 ± 4.0	89.5 ± 5.0	35.0 ± 2.0	65.2 ± 6.7	77.0 ± 2.4	47.7 ± 2.7	61.3 ± 1.8	15.5 ± 1.4
Ba (mg/g d.w.)	0.142 ± 0.001	0.359 ± 0.045	0.502 ± 0.014	0.274 ± 0.037	0.002 ± 0.023	0.369 ± 0.051	0.040 ± 0.008	0.478 ± 0.030	0.298 ± 0.020	0.296 ± 0.025	0.362 ± 0.040	0.375 ± 0.050	0.397 ± 0.025	0.331 ± 0.024	0.388 ± 0.006	0.240 ± 0.001
C (% d.w.)	0.090 ± 0.005	0.104 ± 0.006	0.093 ± 0.002	0.113 ± 0.001	–	–	0.126 ± 0.004	3.054 ± 0.036	0.090 ± 0.001	0.147 ± 0.001	–	0.112 ± 0.009	0.044 ± 0.002	0.051 ± 0.002	0.071 ± 0.002	0.109 ± 0.003
Ca (mg/g d.w.)	63.9 ± 3.0	52.8 ± 6.3	45.6 ± 8.4	20.4 ± 1.5	39.1 ± 3.3	10.6 ± 1.3	84.7 ± 15.1	13.9 ± 0.9	8.1 ± 0.8	44.4 ± 1.6	49.8 ± 3.7	17.6 ± 1.5	5.3 ± 0.3	9.8 ± 0.1	26.7 ± 7.7	11.6 ± 0.8
Cd (µg/g d.w.)	0.064 ± 0.002	0.067 ± 0.008	0.059 ± 0.008	0.070 ± 0.006	0.057 ± 0.001	0.079 ± 0.006	0.112 ± 0.001	0.355 ± 0.010	0.074 ± 0.002	0.070 ± 0.002	0.061 ± 0.007	0.053 ± 0.005	0.050 ± 0.002	0.062 ± 0.003	0.050 ± 0.004	0.043 ± 0.003
Co (µg/g d.w.)	13.6 ± 1.0	15.0 ± 0.4	13.3 ± 0.7	20.7 ± 1.5	11.8 ± 0.6	20.2 ± 1.1	13.6 ± 0.2	15.9 ± 0.3	23.8 ± 0.8	18.0 ± 0.7	9.4 ± 0.4	11.9 ± 0.8	18.4 ± 0.7	16.7 ± 0.7	11.2 ± 0.3	2.0 ± 0.1
Cr (µg/g d.w.)	91.7 ± 4.5	120.0 ± 9.6	100.9 ± 8.3	170.3 ± 8.3	83.7 ± 4.5	125.8 ± 7.3	78.5 ± 1.9	94.6 ± 2.5	147.4 ± 5.2	156.4 ± 8.5	41.5 ± 3.1	76.4 ± 8.1	95.9 ± 3.4	70.9 ± 0.5	80.5 ± 1.2	12.9 ± 0.5
Cu (µg/g d.w.)	38.6 ± 2.1	46.0 ± 3.8	37.3 ± 2.9	68.1 ± 2.4	27.2 ± 0.7	35.0 ± 1.2	121.6 ± 4.5	4268.6 ± 110.6	133.0 ± 4.3	74.5 ± 2.7	15.5 ± 0.4	71.5 ± 5.1	40.7 ± 2.0	28.8 ± 1.2	26.1 ± 1.6	73.9 ± 4.5
Fe (mg/g d.w.)	25.0 ± 1.6	28.5 ± 3.2	26.6 ± 2.0	46.8 ± 1.2	19.7 ± 0.6	35.9 ± 0.3	18.4 ± 0.5	28.5 ± 0.9	58.9 ± 2.9	35.1 ± 1.7	14.7 ± 1.1	25.1 ± 1.2	39.8 ± 1.5	38.5 ± 1.8	27.4 ± 1.1	2.8 ± 0.3
K (mg/g d.w.)	11.1 ± 1.2	11.7 ± 1.2	12.0 ± 1.8	15.8 ± 0.3	11.6 ± 0.5	13.6 ± 0.2	7.0 ± 0.2	11.7 ± 0.6	16.7 ± 0.8	12.0 ± 0.6	13.9 ± 0.7	9.9 ± 0.4	15.9 ± 1.3	15.4 ± 1.3	12.6 ± 0.9	2.4 ± 0.2
Li (µg/g d.w.)	31.1 ± 1.8	37.5 ± 4.0	33.4 ± 3.6	72.3 ± 2.2	32.3 ± 3.5	57.4 ± 3.7	33.4 ± 0.6	13.5 ± 0.8	75.0 ± 3.2	48.8 ± 3.0	23.3 ± 3.3	30.7 ± 3.2	58.4 ± 2.3	45.2 ± 2.4	30.2 ± 1.6	2.5 ± 0.1
Mg (mg/g d.w.)	9.5 ± 0.6	13.1 ± 1.0	10.0 ± 0.1	10.5 ± 0.8	11.1 ± 1.1	6.8 ± 0.5	5.6 ± 0.7	2.9 ± 0.1	9.4 ± 0.9	10.1 ± 0.9	7.1 ± 1.1	13.0 ± 0.8	7.2 ± 0.2	5.9 ± 0.2	14.1 ± 0.6	1.0 ± 0.1
Mn (mg/g d.w.)	1.58 ± 0.05	1.00 ± 0.06	0.87 ± 0.04	1.68 ± 0.09	0.99 ± 0.04	1.87 ± 0.11	6.67 ± 0.06	0.08 ± 0.00	1.22 ± 0.09	1.31 ± 0.03	0.55 ± 0.02	1.17 ± 0.08	0.77 ± 0.01	5.51 ± 0.27	0.81 ± 0.02	1.15 ± 0.03
Mo (µg/g d.w.)	0.39 ± 0.18	0.93 ± 0.09	0.39 ± 0.11	0.67 ± 0.14	0.29 ± 0.06	-	3.13 ± 0.32	87.12 ± 4.07	1.00 ± 0.04	0.65 ± 0.20	-	0.46 ± 0.26	0.31 ± 0.18	0.35 ± 0.17	0.45 ± 0.25	0.11 ± 0.05
N (% d.w.)	3.25 ± 0.10	2.72 ± 0.02	2.60 ± 0.03	1.17 ± 0.02	2.70 ± 0.15	0.23 ± 0.02	6.90 ± 0.09	16.90 ± 0.28	0.76 ± 0.05	2.36 ± 0.06	1.48 ± 0.30	3.92 ± 0.12	0.45 ± 0.03	0.73 ± 0.03	3.15 ± 0.03	10.53 ± 0.16
Na (mg/g d.w.)	3.84 ± 0.06	2.79 ± 0.10	3.24 ± 0.27	1.80 ± 0.08	5.32 ± 0.20	7.88 ± 0.39	0.78 ± 0.08	2.76 ± 0.11	1.53 ± 0.15	2.21 ± 0.03	9.36 ± 0.64	4.21 ± 0.23	5.21 ± 0.21	4.80 ± 0.67	3.54 ± 0.24	0.07 ± 0.01
Ni (µg/g d.w.)	22.8 ± 2.3	23.2 ± 1.7	20.3 ± 4.1	48.3 ± 1.9	18.4 ± 0.8	13.6 ± 3.9	52.3 ± 5.5	19.3 ± 0.8	47.2 ± 1.5	40.8 ± 2.0	-	28.1 ± 2.6	33.7 ± 1.3	27.1 ± 0.8	26.6 ± 0.5	8.4 ± 0.8
P (mg/g d.w.)	1.55 ± 0.05	1.29 ± 0.05	1.39 ± 0.10	2.43 ± 0.18	1.98 ± 0.09	1.55 ± 0.10	10.97 ± 0.52	40.25 ± 1.03	1.75 ± 0.10	2.01 ± 0.07	0.70 ± 0.05	7.70 ± 0.44	0.76 ± 0.03	1.92 ± 0.19	1.29 ± 0.03	10.74 ± 0.61
Pb (µg/g d.w.)	14.2 ± 4.0	7.6 ± 5.2	9.2 ± 2.4	12.1 ± 0.4	11.4 ± 6.2	0.1 ± 0.1	2.1 ± 3.2	40.8 ± 3.9	24.1 ± 0.6	35.1 ± 5.0	9.9 ± 5.4	16.0 ± 1.4	20.7 ± 1.5	17.2 ± 1.2	13.2 ± 2.2	0.2 ± 0.1
S (mg/g d.w.)	0.30 ± 0.03	0.25 ± 0.01	0.23 ± 0.06	0.34 ± 0.01	0.23 ± 0.01	0.12 ± 0.02	1.23 ± 0.05	5.79 ± 0.12	0.33 ± 0.01	0.48 ± 0.02	0.08 ± 0.01	0.45 ± 0.03	0.14 ± 0.01	0.26 ± 0.04	0.22 ± 0.01	0.62 ± 0.04
Si (mg/g d.w.)	259.3 ± 13.7	300.5 ± 25.6	278.4 ± 17.3	281.2 ± 21.5	325.8 ± 13.7	518.2 ± 32.0	171.7 ± 7.7	198.8 ± 7.5	185.6 ± 7.2	315.8 ± 6.5	446.8 ± 36.6	189.6 ± 12.5	263.5 ± 12.4	394.0 ± 101.5	377.8 ± 8.6	53.4 ± 3.0
Sr (µg/g d.w.)	133.1 ± 6.3	138.5 ± 8.4	123.9 ± 6.9	102.3 ± 5.8	120.3 ± 7.6	104.6 ± 13.3	36.0 ± 1.9	92.6 ± 6.1	86.6 ± 5.5	107.5 ± 9.2	135.1 ± 24.3	63.9 ± 7.1	106.5 ± 17.8	144.1 ± 20.7	105.3 ± 6.1	10.4 ± 2.3
Ti (mg/g d.w.)	4.4 ± 0.3	6.1 ± 0.7	4.7 ± 0.8	6.3 ± 0.0	4.5 ± 0.2	8.7 ± 0.6	4.1 ± 0.3	4.2 ± 0.2	4.5 ± 0.2	6.1 ± 0.2	1.8 ± 0.1	4.1 ± 0.3	4.8 ± 0.1	3.4 ± 0.2	4.1 ± 0.1	1.1 ± 0.1
V (µg/g d.w.)	115.4 ± 1.2	142.3 ± 11.1	125.6 ± 12.2	204.8 ± 7.8	115.7 ± 7.5	174.6 ± 8.9	118.4 ± 5.9	93.4 ± 4.5	207.1 ± 6.6	187.9 ± 10.7	54.0 ± 3.6	100.4 ± 9.1	149.5 ± 4.2	102.0 ± 4.2	95.5 ± 1.7	30.0 ± 2.3
Zn (µg/g d.w.)	90.9 ± 4.9	99.2 ± 4.8	90.4 ± 5.2	153.3 ± 9.9	81.1 ± 2.2	163.0 ± 3.7	292.3 ± 10.6	427.7 ± 9.8	180.3 ± 7.0	140.9 ± 5.0	55.5 ± 1.4	151.8 ± 8.5	115.2 ± 2.5	114.0 ± 4.2	82.2 ± 3.1	211.3 ± 9.1
OM (% d.w.)	4.56 ± 0.12	5.74 ± 0.01	5.24 ± 0.20	7.88 ± 0.19	3.74 ± 0.04	3.82 ± 0.03	6.66 ± 0.20	45.99 ± 0.05	7.68 ± 0.12	9.20 ± 0.05	1.61 ± 0.08	4.39 ± 0.06	4.29 ± 0.07	3.92 ± 0.13	3.45 ± 0.04	2.90 ± 0.08

or the winnowing or decomposition of older deposits (Ford and Williams 2007).

Few studies have emphasized clay minerals and their ratios (Foos et al. 2000; Sasowsky, 2007) in cave sediments: although there is much variation, abundant kaolinite tends to indicate warm conditions either in the source rocks or during their weathering. Illite and chlorite are usually the most prominent clay minerals in glaciated regions, while the presence of smectite or montmorillonite suggests a drier climate. Based on the knowledge of the geology and the geomorphological evolution of this portion of the southern Italian Apennines, we have assumed various hypotheses that can explain the presence of clay sediments inside the cave. Considering the geomorphological evolution of the area, the sediments might have been transported by the water flows that over time have invaded the cavity. The sediments may derive from:

the erosion of the Miocene terrigenous deposits that once covered the inner plateau, and which are now only preserved in small depressions;

sediments of the Pleistocene lake that once existed in the Vallo di Diano basin, which could have had as its outflow the Polla cave, after the last ice age;

the residue of the clay-intercalations present within the carbonate succession.

Overall, PERMANOVA did not highlight significant differences among samples on the basis of their geochemical characteristics, considering the three fixed variables: location (tourist, fossil and active trail; $P=0.727$), type of sampling (to the ground or in the recesses; $P=0.178$), water conditions (in the surface or underwater; $P=0.965$). According to these results, the NMDS multivariate ordination, with the superimposition of confidence ellipses, did not show differentiations among the locations nor between the typology and environmental (water) conditions of the sampled deposits (Fig. 4). Only Ts3 and Fs5 samples were separated from the others for the higher concentrations of C, Cu, Mo, N, P and S. In the univariate domain, the three-way ANOVAs highlighted significant differences for Al ($P<0.05$) and Ca ($P<0.001$) in relation to the type of sampling, as well as for dolomite mineral in relation to the three fixed variables: $P<0.05$ for the location and water conditions, $P<0.001$ for the type of sampling.

The relationships between the studied parameters in the 16 analyzed samples are shown in Fig. 5, displaying a network based on Pearson's correlation coefficients (Online Resource 1). Positive and negative correlations ($0.001<P<0.05$) among several parameters were observed, highlighting two big clusters of variables that can have a similar origin, including roughly elements of abiotic or biotic origin. Investigating the characteristics of cave clastic sediments pointed out several evidences about the inorganic and organic available energy, basics for the organization of ecological communities (influencing their structure and function), and highlighted modifications due to the human presence (introducing exogenous materials), potentially altering the natural chemico-physical energy balance of the underground system (Chelius et al. 2009). In this context, bat colonies play a fundamental role in the enrichment in manures of the cave ecosystem, representing not only an important organic input, but also a key factor revealing environmental alterations and anthropogenic impacts (Putra et al. 2019). Future efforts will focus on the endokarst and top soil characterization, to understand

Table 2 α–quartz, calcite, dolomite and lime estimated relative abundances (mean values ± estimated standard deviations) of each sediment sample from the Pertosa-Auletta Cave

Sample	α – quartz (%)	Calcite (%)	Dolomite (%)	Lime (%)	Kaolinite	Smectite	Muscovite
As1	59.6 ± 2.0	20.4 ± 1.0	20.0 ± 1.0	–	*	*	*
As2	57.3 ± 2.0	12.4 ± 0.9	30.3 ± 1.0	–	*	*	*
As3	59.2 ± 1.0	19.5 ± 0.9	21.3 ± 0.9	–	*	*	*
As4	81.3 ± 9.0	18.7 ± 9.0	–	–	*	–	*
As5	55.8 ± 2.0	25.0 ± 1.0	19.2 ± 0.9	–	*	*	*
Ts1	100.0	–	–	–	*	–	*
Ts2	11.9 ± 4.0	88.1 ± 4.0	–	–	*	*	*
Ts3	100.0	–	–	–	*	*	*
Ts4	100.0	–	–	–	*	*	–
Ts5	65.5 ± 4.0	18.2 ± 2.0	16.3 ± 2.0	–	*	*	*
Ts6	83.4 ± 1.0	6.1 ± 0.6	10.5 ± 1.0	–	–	–	*
Fs1	44.7 ± 1.0	27.8 ± 0.9	27.4 ± 0.9	–	*	*	*
Fs2	96.3 ± 0.7	–	–	3.7 ± 0.7	*	–	*
Fs3	100.0	–	–	–	*	–	*
Fs4	65.6 ± 1.0	11.5 ± 0.6	22.9 ± 0.9	–	*	*	*
Fs5	6.3 ± 0.2	93.7 ± 0.2	–	–	–	–	*

Presence of clay minerals is also reported (*)

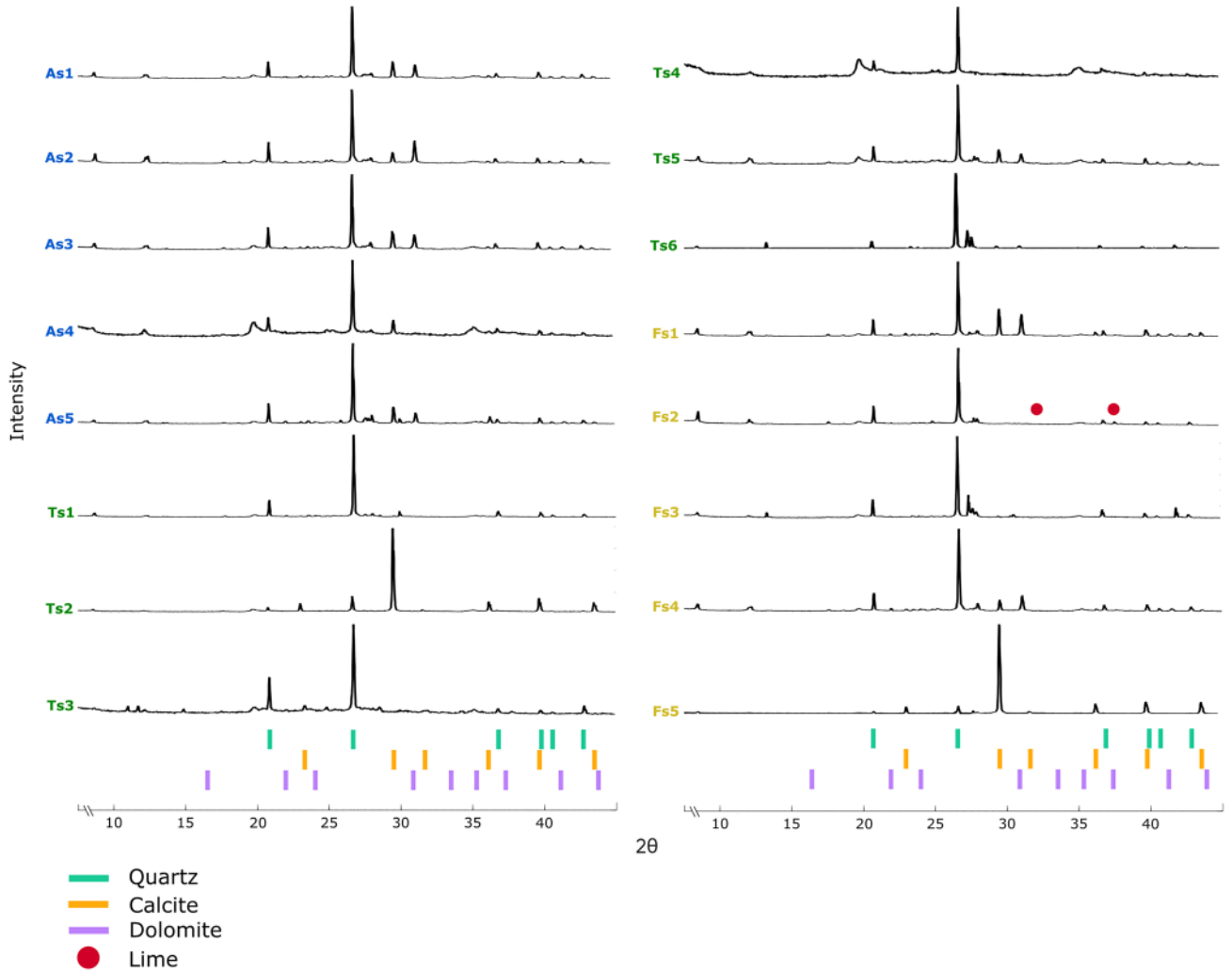

Fig. 3 Stacked diffractograms of cave sediments from the active (A, blue), tourist (T, green) and fossil (F, yellow) trails. α- quartz (teal), calcite (orange), dolomite (violet) diffraction lines are also reported. Lime phase occurring in F sample is indicated by red points

the genesis process of cave sediments, clarifying their provenance, such as their autochthonous or allochthonous origin, due to the past fluviokarst activity interesting the karst system.

Conclusion

The extensive geochemical characterization of clastic sediments from the Pertosa-Auletta Cave, in Italy, provided a whole knowledge of their chemico-physical features, describing one of the most important cave compartments, which influence the fragile ecological equilibrium, taking place in underground ecosystems. The clastic sediments, belonging to different typologies, showed variable compositions, with a clear differentiation of one sample, in particular, contaminated by bat guano. It revealed the highest concentration of organic matter and of several chemical elements (C, Cu, Mo, N, P, Pb, S, Zn), proving not only the important support of guano in terms of energy source for cave communities, but also an accumulation of pollutants from the external environments, likely related to the bat food chain.

Three main pathways about sediment provenances were drawn: (i) the autochthonous origin likely related to the cave host rock constituted by carbonate, dolomite and limestone, justifying the presence of calcitic and dolomitic minerals; (ii) the allochthonous origin related to the past cave hydrological activity, where water flow carried underground quartz compounds; (iii) the accumulation of guano, from bat colonies inhabiting the cave.

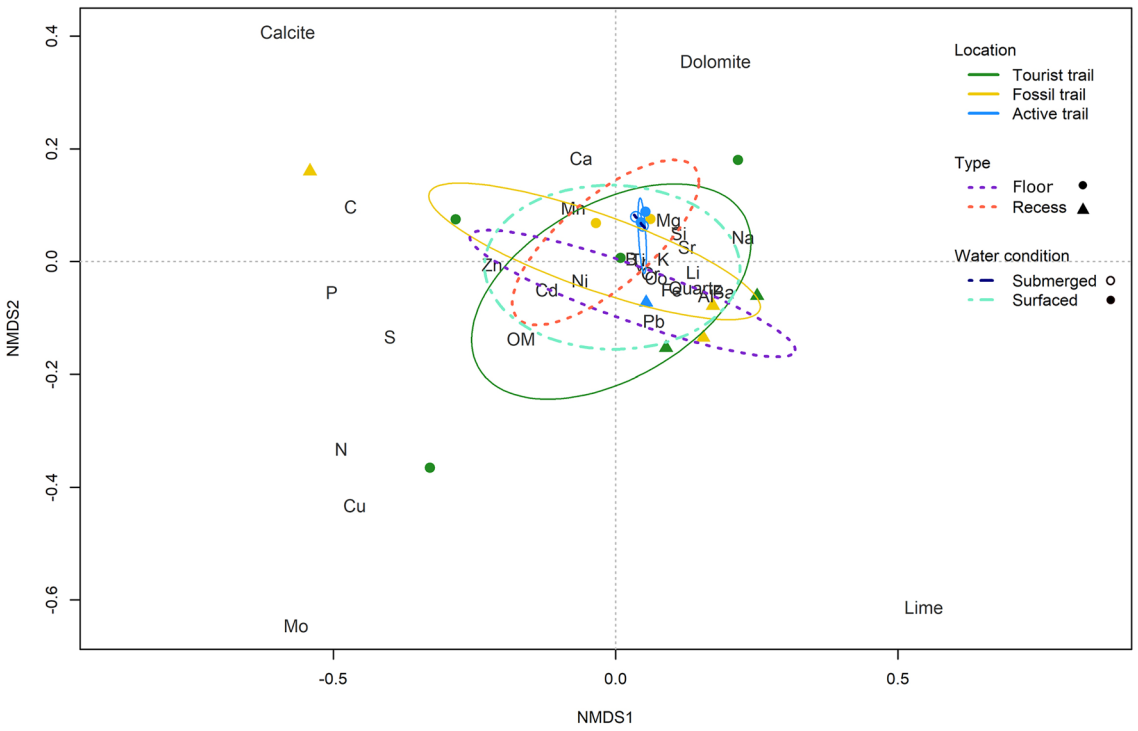

Fig. 4 NMDS bi-plot, with the superimposition of con dence ellipses for α = 0.05, based on chemical element, organic matter and mineral concentrations in cave sediments from the active (A, blue), tourist (T, green) and fossil (F, yellow) trails of the Pertosa-Auletta Cave

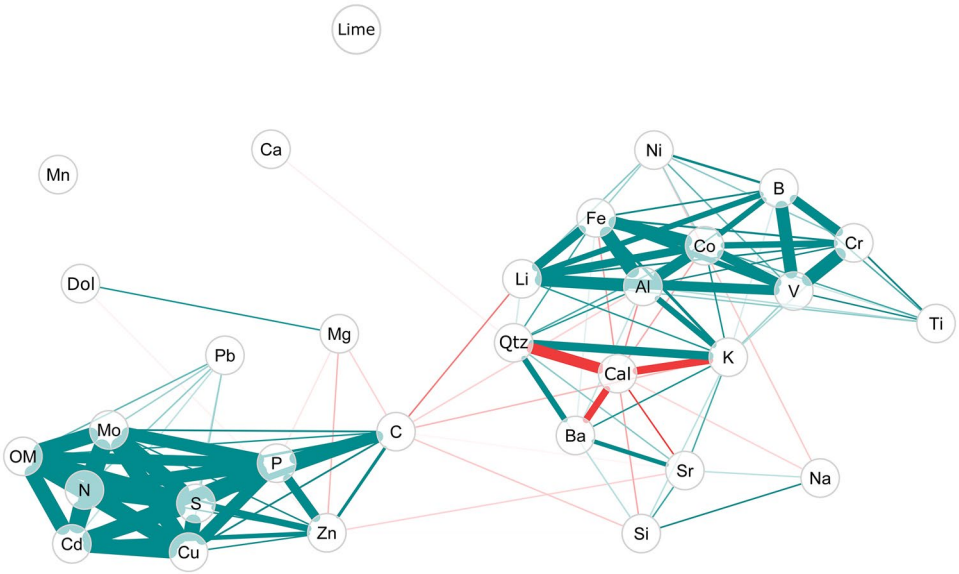

Fig. 5 Network based on Pearson's correlation coef- cients. Negative (red) and positive (green) correlations are reported; lines more or less thick indicate correlations more or less strong between the variables. For minerals, the following abbreviations (according to Kretz 1983) have been employed: *Cal* calcite, *Qtz* –quartz, *Dol* dolomite

Supplementary Information The online version contains supplementary material available at https://doi.org/10.1007/s00531-021-02158-x.

Acknowledgements We are obliged to MIdA Foundation, in particular, to the president, Dr. Francescantonio D'Orilia, the scienti c director, Prof. Mariana Amato, and the speleoguide, Mr. Vincenzo Manisera, for the precious support.

Funding This work, supported by Musei Integrati dell'Ambiente Foundation, was funded by Università degli Studi di Salerno (Italy) within the ORSA197159 project.

Declarations

Conflicts of interest None declared.

References

Abdyzhaparova A, Spasenov A, Mazina S (2021) Decomposition of organic waste in caves. Proced Environ Sci Eng Manag 8:381–387

Addesso R, Bellino A, D'Angeli IM et al (2019) Vermiculations from karst caves: the case of Pertosa-Auletta system (Italy). CATENA 182:104178. https://doi.org/10.1016/j.catena.2019.104178

Addesso R, Gonzalez-Pimentel JL, D'Angeli IM et al (2021) Microbial community characterizing vermiculations from karst caves and its role in their formation. Microb Ecol 81:884–896. https://doi.org/10.1007/s00248-020-01623-5

Arriolabengoa M, Iriarte E, Aranburu A et al (2015) Provenance study of endokarst fine sediments through mineralogical and geochemical data (Lezetxiki II cave, northern Iberia). Quatern Int 364:231–243. https://doi.org/10.1016/j.quaint.2014.09.072

Cafaro S, Gueguen E, Adurno I et al (2010) Il controllo geologico nella speleogenesi della grotta dell'Angelo (Appennino campano-lucano). In: Proceedings of Atti del II Conv Reg Speleol, Caselle in Pittari, Italy, 3–4 June 2010, pp 71–81

Celico P, Pelella L, Stanzione D et al (1994) Sull'idrogeologia e l'idrogeochimica dei Monti Alburni (SA). Geol Rom 30:687–698

Chelius M, Beresford G, Horton H et al (2009) Impacts of alterations of organic inputs on the bacterial community within the sediments of Wind Cave, South Dakota, USA. Int J Speleol 38:1–10. https://doi.org/10.5038/1827-806X.38.1.1

Cozzolino L, Damiano N, Del Vecchio U et al (2015a) Prove di colorazione e recenti esplorazioni nell'area della Grotta del Falco - Monti Alburni. In: Proceedings of XXII Nat Congr Speleol "Condividere i dati", Pertosa-Auletta, Italy, 30–31 May 2015, pp 323–328

Cozzolino L, Damiano N, Del Vecchio U et al (2015b) Recenti prove di colorazione nell'area di Petina (Sa) - Monti Alburni. In: Proceedings of XXII Nat Congr Speleol "Condividere i dati", Pertosa-Auletta, Italy, 30–31 May 2015, pp 353–358

Deharveng L, Bedos A (2018) Diversity of terrestrial invertebrates in subterranean habitats. In: Moldovan OT, Kováč L, Halse S (eds) Cave ecology. Springer Int Pub, Cham, pp 107–172. https://doi.org/10.1107/S1600576715014685

Doebelin N, Kleeberg R (2015) Profex: a graphical user interface for the Rietveld refinement program BGMN. J Appl Crystallogr 48:1573–1580

Dredge J, Fairchild IJ, Harrison RM et al (2013) Cave aerosols: distribution and contribution to speleothem geochemistry. Quat Sci Rev 63:23–41. https://doi.org/10.1016/j.quascirev.2012.11.016

Dykes AP (2007) Mass movements in cave sediments: investigation of a ~40,000-year-old guano mudflow inside the entrance of the Great Cave of Niah, Sarawak, Borneo. Landslides 4:279–290. https://doi.org/10.1007/s10346-006-0077-5

Foos AM, Sasowsky ID, LaRock EJ et al (2000) Detrital origin of a sedimentary fill, Lechuguilla cave, Guadalupe Mountains, New Mexico. Clays Clay Miner 48:693–698. https://doi.org/10.1346/CCMN.2000.0480610

Ford D, Williams P (2007) Karst hydrogeology and geomorphology. John Wiley & Sons Ltd, West Sussex, England. https://doi.org/10.1002/9781118684986

Gillieson D (1996) Caves. Blackwell Publishing Ltd., Oxford, UK

Kováč Ľ (2018) Caves as Oligotrophic Ecosystems. In: Moldovan OT, Kováč L, Halse S (eds) Cave ecology. Springer International Publications, Cham, pp 297–307

Kretz R (1983) Symbols for rock-forming minerals. Am Miner 68:277–279

Mammola S, Isaia M (2018) Cave communities and species interactions. In: Moldovan OT, Kováč L, Halse S (eds) Cave ecology. Springer International Publications, Cham, pp 255–267

Miko S, Kuhta M, Kapelj S (2001) Bat Guano Influence on the Geochemistry of Cave Sediments from Modrič Cave, Croatia. Int Congr Speleol. https://doi.org/10.13140/2.1.4853.2483

Miko S, Kuhta M, Kapelj S (2002) Environmental baseline geochemistry of sediments and percolating waters in the Modrič, Cave Croatia. Acta Carsologica 5:5. https://doi.org/10.3986/ac.v31i1.409

Moore DM, Reynolds RC (1997) X-ray diffraction and the identification and analysis of clay minerals. Oxford University Press, Oxford

Mulec J, Kosi G (2009) Lampenflora algae and methods of growth control. J Cave Karst Stud 71:109–115

Pastore C, De Waele J, Vigna B et al (2017) Nuovi contributi idrogeologici sull'area carsica dei Monti Alburni. In: Proceedings of Atti del III Conv Reg Speleol "Campania Speleologica", Napoli, Italy, 2–4 giugno 2017, Napoli, pp 15–32

Pedrali L, Buongiorno V, Antonini G et al (2015) Convergenza di dati per l'esplorazione della Grotta del Falco sul Massiccio degli Alburni (Campania). In: Proceedings of XXII Nat Congr Speleol "Condividere i dati", Pertosa-Auletta, Italy, 30–31 May 2015, pp 537–542

Putra R, Rifai H, Wurster CM (2019) Relationship between magnetic susceptibility and elemental composition of Guano from Solek Cave, West Sumatera. J Phys Conf Ser 1185:012011. https://doi.org/10.1088/1742-6596/1185/1/012011

R Core Team (2020) R Core Team R: a language and environment for statistical computing.

Russell MJ, MacLean VL (2008) Management issues in a Tasmanian tourist cave: Potential microclimatic impacts of cave modifications. J Environ Manag 87:474–483. https://doi.org/10.1016/j.jenvman.2007.01.012

Sasowsky ID (2007) Clastic sediments in caves - imperfect recorders of processes in karst. Acta Carsologica 36:143–149

Smith A, Wynn P, Barker P (2013) Natural and anthropogenic factors which influence aerosol distribution in Ingleborough Show Cave, UK. Int J Speleol 42:49–56. https://doi.org/10.5038/1827-806X.42.1.6

Taylor J, Rui Z (1992) Simultaneous use of observed and calculated standard profiles in quantitative XRD analysis of minerals by the multiphase Rietveld method: the determination of pseudorutile in mineral sands products. Powder Diff 7(3):152–161

White WB (2007) Cave sediments and paleoclimate. J Cave Karst Stud 69:76–93

Wurster CM, Munksgaard N, Zwart C et al (2015) The biogeochemistry of insectivorous cave guano: a case study from insular Southeast Asia. Biogeochem 124:163–175. https://doi.org/10.1007/s10533-015-0089-0

Zukal J, Pikula J, Bandouchova H (2015) Bats as bioindicators of heavy metal pollution: history and prospect. Mamm Biol 80:220–227. https://doi.org/10.1016/j.mambio.2015.01.001

Zupan Hajna N, Pruner P, Mihevc A et al (2008) Cave sediments from the Postojnska-Planinska cave system (Slovenia): evidence of multi-phase evolution in epiphreatic zone. Acta Carsologica 37:63–86. https://doi.org/10.3986/ac.v37i1.160

CHAPTER 4

Geomicrobiology of a seawater-influenced active sulfuric acid cave

Ilenia M. D'Angeli, Daniele Ghezzi, Stefan Leuko, Andrea Firrincieli, Mario Parise, Adriano Fiorucci, Bartolomeo Vigna, **Rosangela Addesso**, Daniela Baldantoni, Cristina Carbone, Ana Zelia Miller, Valme Jurado, Cesareo Saiz-Jimenez, Jo De Waele, Martina Cappelletti*

PLoS ONE (2019), 14(8): e0220706

doi: 10.1371/journal.pone.0220706

**corresponding author*

The geomicrobiology of several cave structures (water filaments, vermiculations and gypsum moonmilk) has been investigated in the Fetida Cave (Apulia, Italy), a seawater-influenced sulfuric acid cave, highlighting the biogeochemical processes implemented by the interaction between the microbiota and the abiotic compartment of such peculiar cave environment.

RESEARCH ARTICLE

*

Department of Biological, Geological and Environmental Sciences, University of Bologna, Bologna, Italy, Department of Pharmacy and Biotechnology, University of Bologna, Bologna, Italy, DLR Institute of Aerospace Medicine, Radiation Biology, Köln, Germany, School of Environmental and Forest Science, University of Washington, Seattle, WA, United States of America, Department of Geological and Environmental Sciences, University of Bari "Aldo Moro", Bari, Italy, Department of Environment, Land and Infrastructure Engineering, Polytechnic University of Turin, Torino, Italy, Department of Chemistry and Biology "Adolfo Zambelli", University of Salerno, Fisciano (SA), Italy, DISTAV, Department of Geological, Environmental and Biological Sciences, University of Genoa, Genoa, Italy, HERCULES Laboratory, University of Évora, Évora, Portugal, Instituto de Recursos Naturales y Agrobiologia, IRNAS-CSIC, Sevilla, Spain

These authors contributed equally to this work.
martina.cappelletti2@unibo.it

Fetida Cave is an active sulfuric acid cave influenced by seawater, showing abundant microbial communities that organize themselves under three main different morphologies: water filaments, vermiculations and moonmilk deposits. These biofilms/deposits have different cave distribution, pH, macro- and microelement and mineralogical composition, carbon and nitrogen content. In particular, water filaments and vermiculations had circumneutral and slightly acidic pH, respectively, both had abundant organic carbon and high microbial diversity. They were rich in macro- and microelements, deriving from mineral dissolution, and, in the case of water filaments, from seawater composition. Vermiculations had different color, partly associated with their mineralogy, and unusual minerals probably due to trapping capacities. Moonmilk was composed of gypsum, poor in organic matter, had an extremely low pH (0–1) and low microbial diversity. Based on 16S rRNA gene analysis, the microbial composition of the biofilms/deposits included autotrophic taxa associated with sulfur and nitrogen cycles and biomineralization processes. In particular, water filaments communities were characterized by bacterial taxa involved in sulfur oxidation and reduction in aquatic, aphotic, microaerophilic/anoxic environments (Campylobacterales, Thiotrichales, Arenicellales, Desulfobacterales, Desulforomonadales) and in chemolithotrophy in marine habitats (Oceanospirillales, Chromatiales). Their biodiversity was linked to the morphology of the water filaments and their collection site. Microbial communities within vermiculations were partly related to their color and showed high abundance of unclassified Betaproteobacteria and sulfur-oxidizing Hydrogenophilales (including), and Acidiferrobacterales (including), sulfur-reducing Desulfurellales, and ammonia-oxidizing Planctomycetes and Nitrospirae. The microbial community associated with gypsum moonmilk showed

the strong dominance (>60%) of the archaeal genus and lower abundance of chemolithotrophic , metal-oxidizing , , and .

This study describes the geomicrobiology of water filaments, vermiculations and gypsum moonmilk from Fetida Cave, providing insights into the microbial taxa that characterize each morphology and contribute to biogeochemical cycles and speleogenesis of this peculiar seawater-influenced sulfuric acid cave.

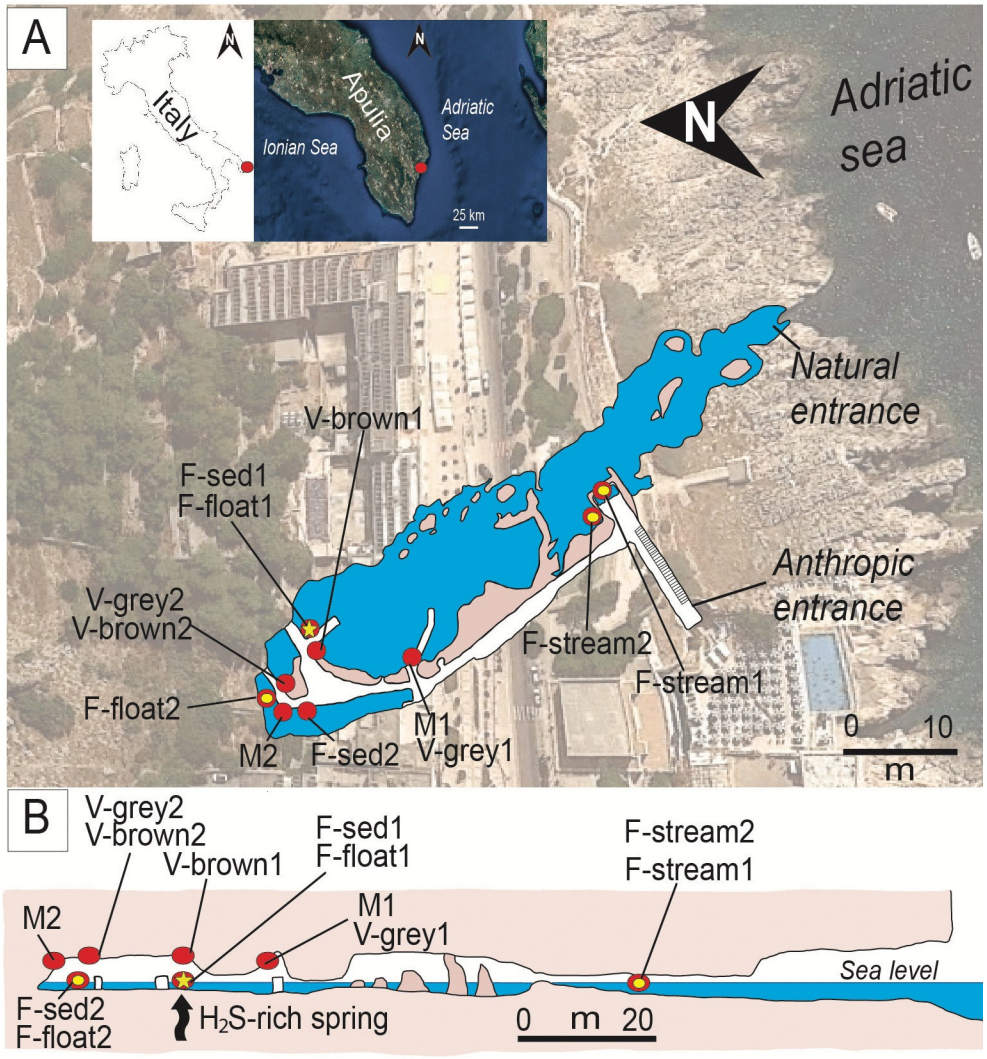
A
Italy
Ionian Sea
Apulia
Adriatic Sea
25 km
N
Adriatic sea
Natural entrance
Anthropic entrance
V-brown1
F-sed1
F-float1
V-grey2
V-brown2
F-float2
M2
F-sed2
M1
V-grey1
F-stream2
F-stream1
0 10
m
B
V-grey2
V-brown2
V-brown1
F-sed1
F-float1
M2
M1
V-grey1
F-stream2
F-stream1
Sea level
F-sed2
F-float2
H2S-rich spring
0 m 20

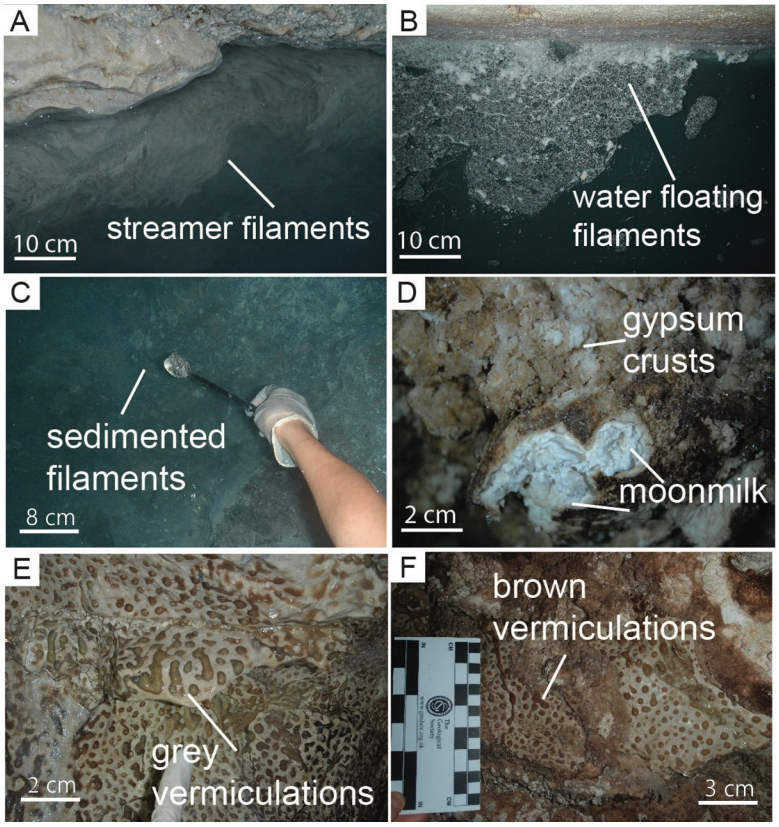
A
streamer filaments
10 cm
B
water floating
filaments
10 cm
C
sedimented
filaments
8 cm
D
gypsum
crusts
moonmilk
2 cm
E
grey
vermiculations
2 cm
F
brown
vermiculations
3 cm

5′GTGCCAGCMG-CCGCGGTAA′3 5′ GGACTACHVGGGTWTCTAAT′3

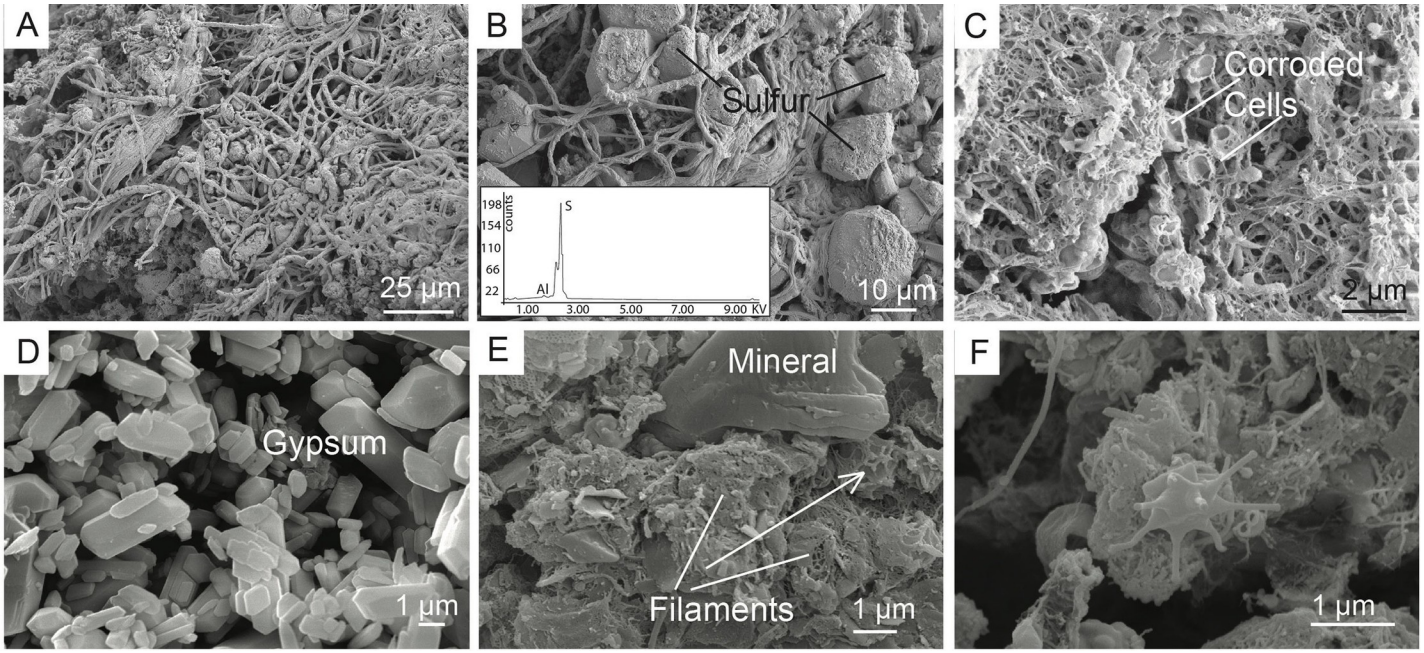
A
25 µm
B
Sulfur
198
154
110
66
22
counts
S
Al
1.00
3.00
5.00
7.00
9.00 KV
10 µm
C
Corroded
Cells
2 µm
D
Gypsum
1 µm
E
Mineral
Filaments
1 µm
F
1 µm

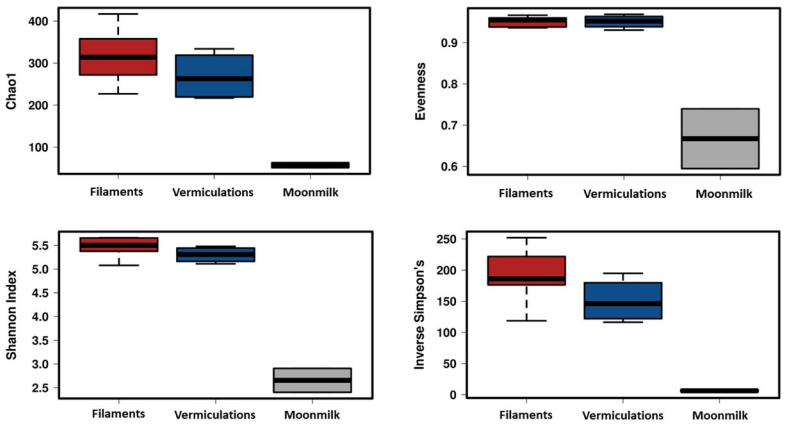
Chao1
Evenness
Shannon Index
Inverse Simpson's
Filaments
Vermiculations
Moonmilk

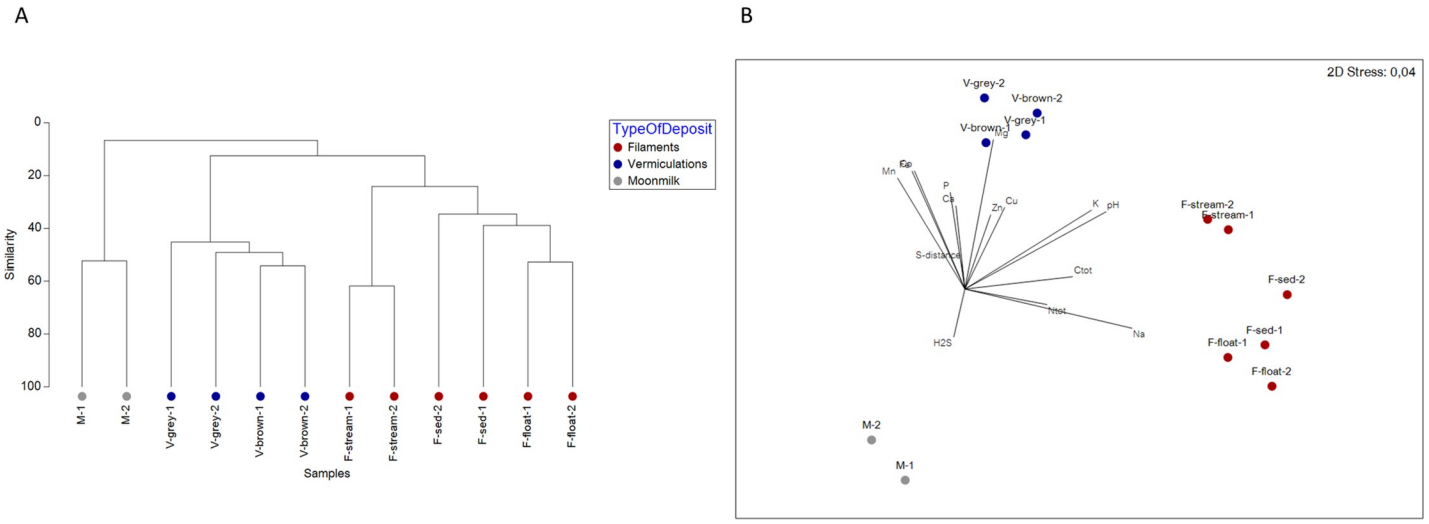
A
B
Similarity
Samples
TypeOfDeposit
Filaments
Vermiculations
Moonmilk
M-1
M-2
V-grey-1
V-grey-2
V-brown-1
V-brown-2
F-stream-1
F-stream-2
F-sed-2
F-sed-1
F-float-1
F-float-2
2D Stress: 0,04
S-distance
Ctot
Ntot
H2S
Na
K
pH
Cu
Zn
P
Mn
Mg

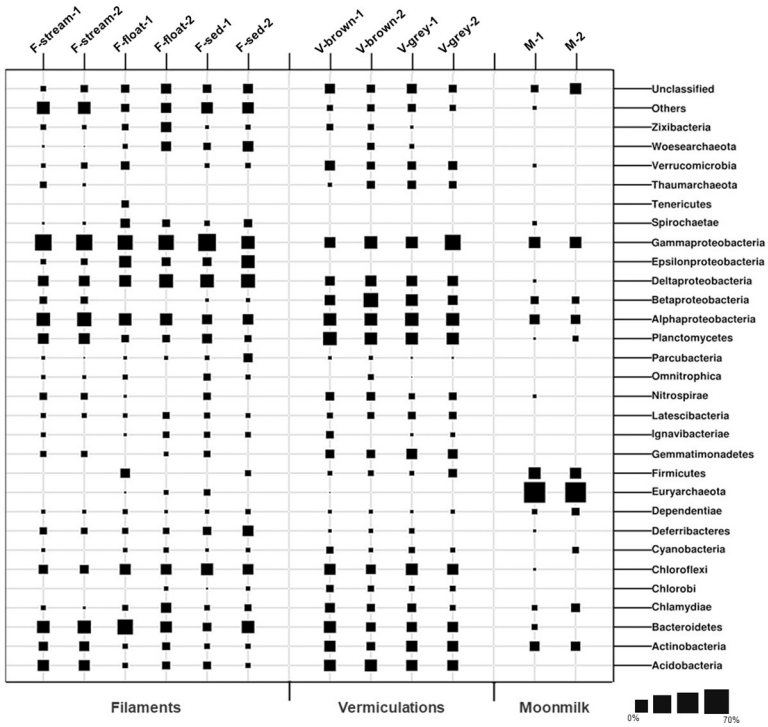
F-stream-1
F-stream-2
F-float-1
F-float-2
F-sed-1
F-sed-2
V-brown-1
V-brown-2
V-grey-1
V-grey-2
M-1
M-2
Unclassified
Others
Zixibacteria
Woesearchaeota
Verrucomicrobia
Thaumarchaeota
Tenericutes
Spirochaetae
Gammaproteobacteria
Epsilonproteobacteria
Deltaproteobacteria
Betaproteobacteria
Alphaproteobacteria
Planctomycetes
Parcubacteria
Omnitrophica
Nitrospirae
Latescibacteria
Ignavibacteriae
Gemmatimonadetes
Firmicutes
Euryarchaeota
Dependentiae
Deferribacteres
Cyanobacteria
Chloroflexi
Chlorobi
Chlamydiae
Bacteroidetes
Actinobacteria
Acidobacteria
Filaments
Vermiculations
Moonmilk
0%
70%

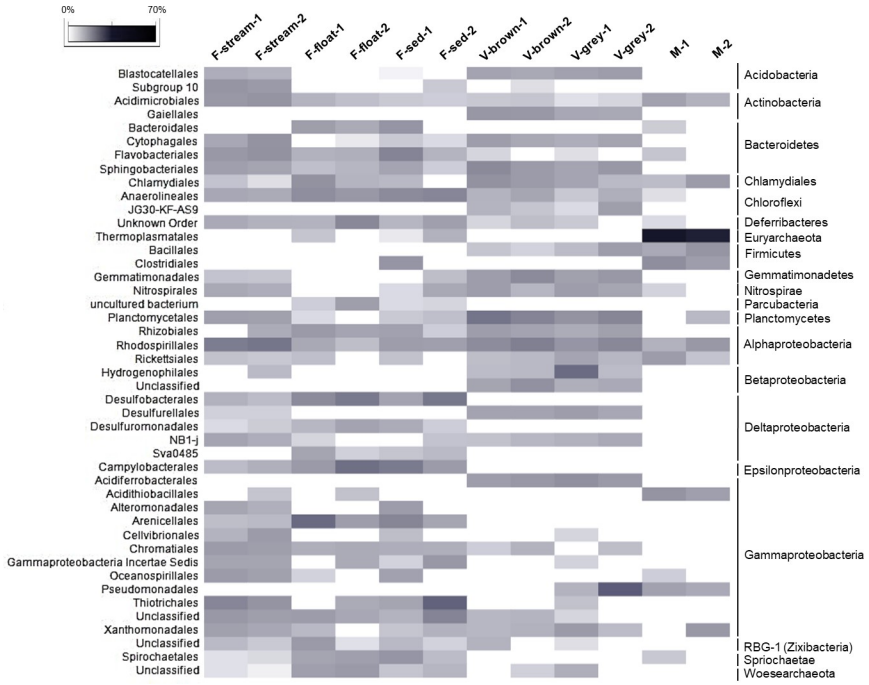
0%
70%
F-stream-1
F-stream-2
F-float-1
F-float-2
F-sed-1
F-sed-2
V-brown-1
V-brown-2
V-grey-1
V-grey-2
M-1
M-2
Blastocatellales
Subgroup 10
Acidimicrobiales
Gaiellales
Bacteroidales
Cytophagales
Flavobacteriales
Sphingobacteriales
Chlamydiales
Anaerolineales
JG30-KF-AS9
Unknown Order
Thermoplasmatales
Bacillales
Clostridiales
Gemmatimonadales
Nitrospirales
uncultured bacterium
Planctomycetales
Rhizobiales
Rhodospirillales
Rickettsiales
Hydrogenophilales
Unclassified
Desulfobacterales
Desulfurellales
Desulfuromonadales
NB1-j
Sva0485
Campylobacterales
Acidiferrobacterales
Acidithiobacillales
Alteromonadales
Arenicellales
Cellvibrionales
Chromatiales
Gammaproteobacteria Incertae Sedis
Oceanospirillales
Pseudomonadales
Thiotrichales
Unclassified
Xanthomonadales
Unclassified
Spirochaetales
Unclassified
Acidobacteria
Actinobacteria
Bacteroidetes
Chlamydiales
Chloroflexi
Deferribacteres
Euryarchaeota
Firmicutes
Gemmatimonadetes
Nitrospirae
Parcubacteria
Planctomycetes
Alphaproteobacteria
Betaproteobacteria
Deltaproteobacteria
Epsilonproteobacteria
Gammaproteobacteria
RBG-1 (Zixibacteria)
Spriochaetae
Woesearchaeota

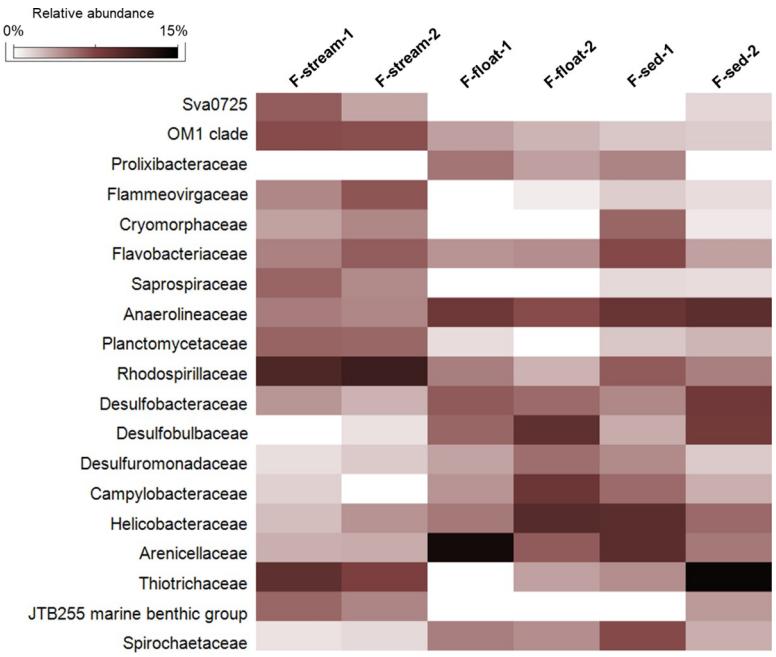
Relative abundance
0%
15%
F-stream-1
F-stream-2
F-float-1
F-float-2
F-sed-1
F-sed-2
Sva0725
OM1 clade
Prolixibacteraceae
Flammeovirgaceae
Cryomorphaceae
Flavobacteriaceae
Saprospiraceae
Anaerolineaceae
Planctomycetaceae
Rhodospirillaceae
Desulfobacteraceae
Desulfobulbaceae
Desulfuromonadaceae
Campylobacteraceae
Helicobacteraceae
Arenicellaceae
Thiotrichaceae
JTB255 marine benthic group
Spirochaetaceae

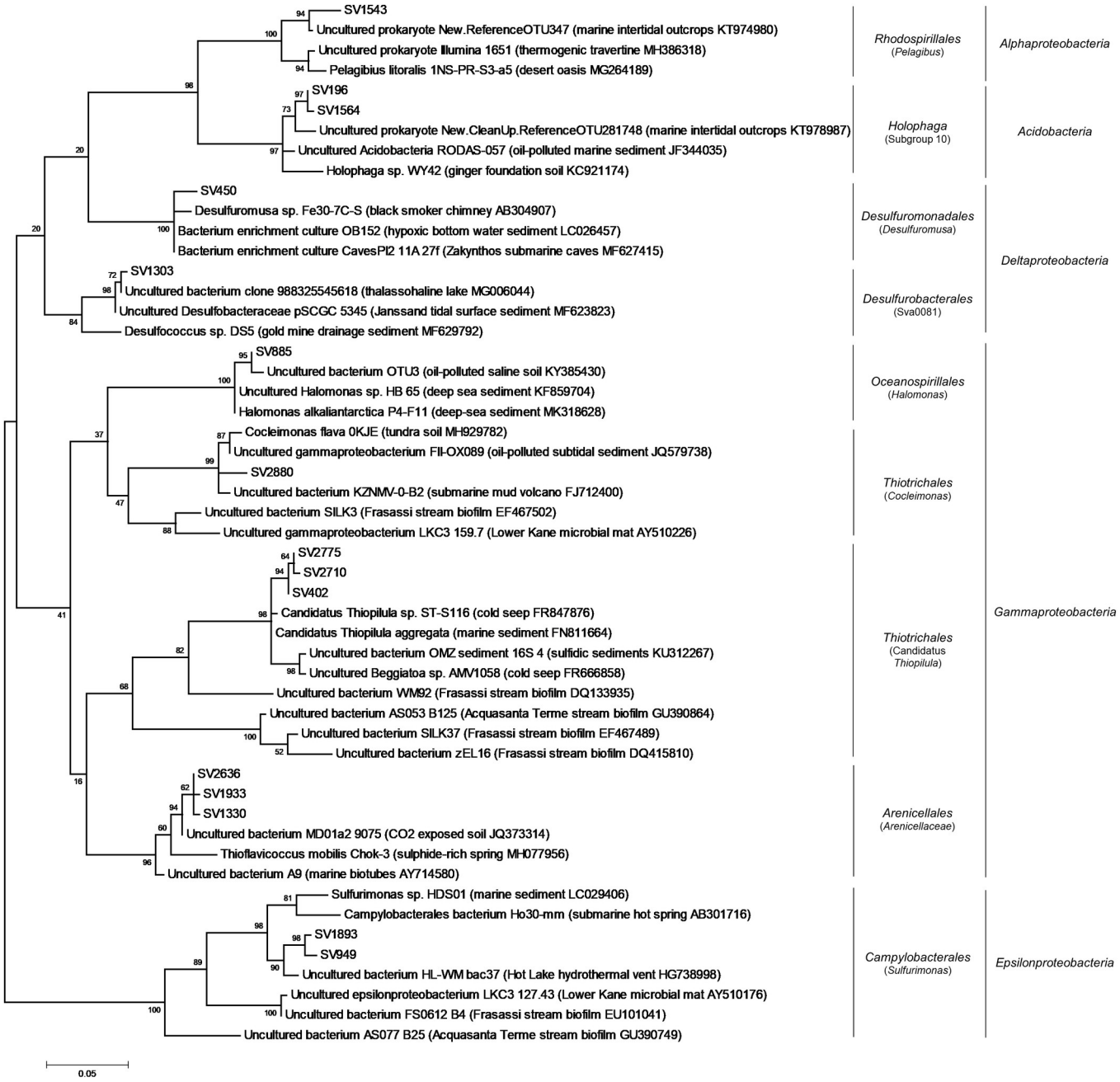
SV1543
Uncultured prokaryote New.ReferenceOTU347 (marine intertidal outcrops KT974980)
Uncultured prokaryote Illumina 1651 (thermogenic travertine MH386318)
Pelagibius litoralis 1NS-PR-S3-a5 (desert oasis MG264189)
SV196
SV1564
Uncultured prokaryote New.CleanUp.ReferenceOTU281748 (marine intertidal outcrops KT978987)
Uncultured Acidobacteria RODAS-057 (oil-polluted marine sediment JF344035)
Holophaga sp. WY42 (ginger foundation soil KC921174)
SV450
Desulfuromusa sp. Fe30-7C-S (black smoker chimney AB304907)
Bacterium enrichment culture OB152 (hypoxic bottom water sediment LC026457)
Bacterium enrichment culture CavesPl2 11A 27f (Zakynthos submarine caves MF627415)
SV1303
Uncultured bacterium clone 988325545618 (thalassohaline lake MG006044)
Uncultured Desulfobacteraceae pSCGC 5345 (Janssand tidal surface sediment MF623823)
Desulfococcus sp. DS5 (gold mine drainage sediment MF629792)
SV885
Uncultured bacterium OTU3 (oil-polluted saline soil KY385430)
Uncultured Halomonas sp. HB 65 (deep sea sediment KF859704)
Halomonas alkaliantarctica P4-F11 (deep-sea sediment MK318628)
Cocleimonas flava 0KJE (tundra soil MH929782)
Uncultured gammaproteobacterium FII-OX089 (oil-polluted subtidal sediment JQ579738)
SV2880
Uncultured bacterium KZNMV-0-B2 (submarine mud volcano FJ712400)
Uncultured bacterium SILK3 (Frasassi stream biofilm EF467502)
Uncultured gammaproteobacterium LKC3 159.7 (Lower Kane microbial mat AY510226)
SV2775
SV2710
SV402
Candidatus Thiopilula sp. ST-S116 (cold seep FR847876)
Candidatus Thiopilula aggregata (marine sediment FN811664)
Uncultured bacterium OMZ sediment 16S 4 (sulfidic sediments KU312267)
Uncultured Beggiatoa sp. AMV1058 (cold seep FR666858)
Uncultured bacterium WM92 (Frasassi stream biofilm DQ133935)
Uncultured bacterium AS053 B125 (Acquasanta Terme stream biofilm GU390864)
Uncultured bacterium SILK37 (Frasassi stream biofilm EF467489)
Uncultured bacterium zEL16 (Frasassi stream biofilm DQ415810)
SV2636
SV1933
SV1330
Uncultured bacterium MD01a2 9075 (CO2 exposed soil JQ373314)
Thioflavicoccus mobilis Chok-3 (sulphide-rich spring MH077956)
Uncultured bacterium A9 (marine biotubes AY714580)
Sulfurimonas sp. HDS01 (marine sediment LC029406)
Campylobacterales bacterium Ho30-mm (submarine hot spring AB301716)
SV1893
SV949
Uncultured bacterium HL-WM bac37 (Hot Lake hydrothermal vent HG738998)
Uncultured epsilonproteobacterium LKC3 127.43 (Lower Kane microbial mat AY510176)
Uncultured bacterium FS0612 B4 (Frasassi stream biofilm EU101041)
Uncultured bacterium AS077 B25 (Acquasanta Terme stream biofilm GU390749)
0.05
Rhodospirillales (Pelagibus)
Holophaga (Subgroup 10)
Desulfuromonadales (Desulfuromusa)
Desulfurobacterales (Sva0081)
Oceanospirillales (Halomonas)
Thiotrichales (Cocleimonas)
Thiotrichales (Candidatus Thiopilula)
Arenicellales (Arenicellaceae)
Campylobacterales (Sulfurimonas)
Alphaproteobacteria
Acidobacteria
Deltaproteobacteria
Gammaproteobacteria
Epsilonproteobacteria

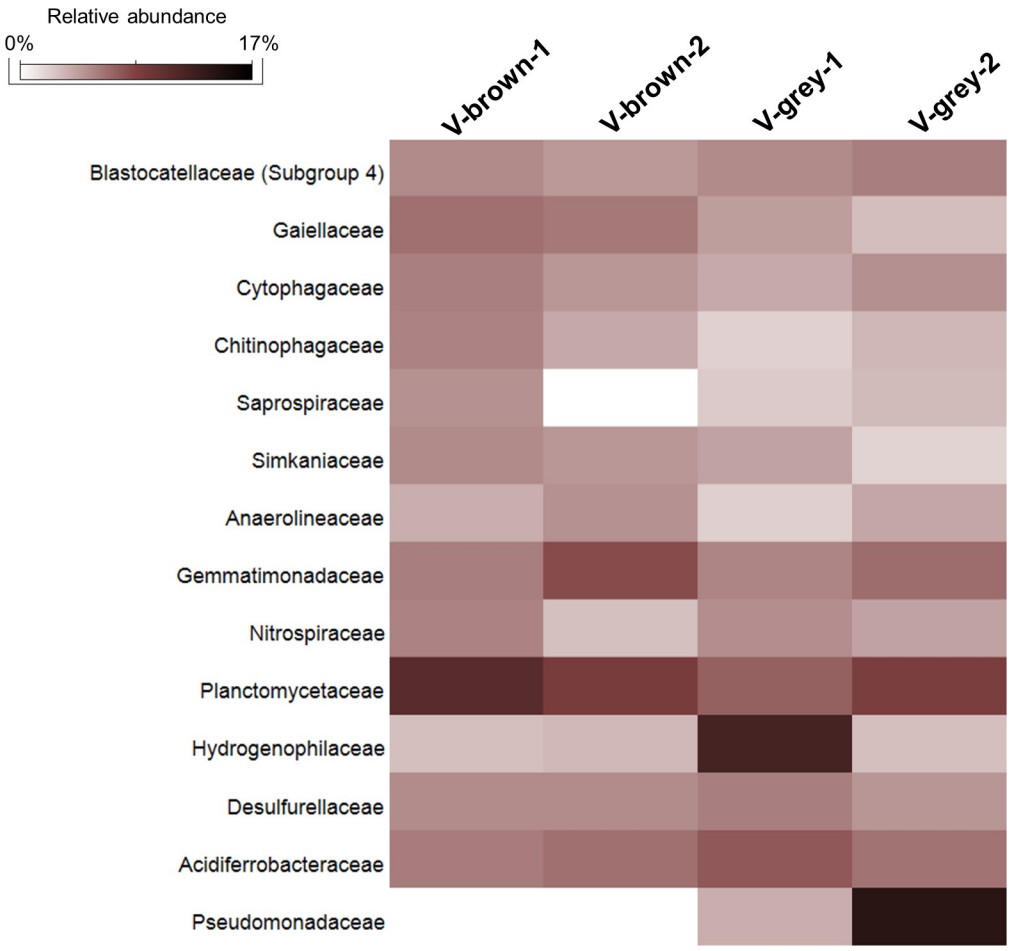
Relative abundance
0%
17%
V-brown-1
V-brown-2
V-grey-1
V-grey-2
Blastocatellaceae (Subgroup 4)
Gaiellaceae
Cytophagaceae
Chitinophagaceae
Saprospiraceae
Simkaniaceae
Anaerolineaceae
Gemmatimonadaceae
Nitrospiraceae
Planctomycetaceae
Hydrogenophilaceae
Desulfurellaceae
Acidiferrobacteraceae
Pseudomonadaceae

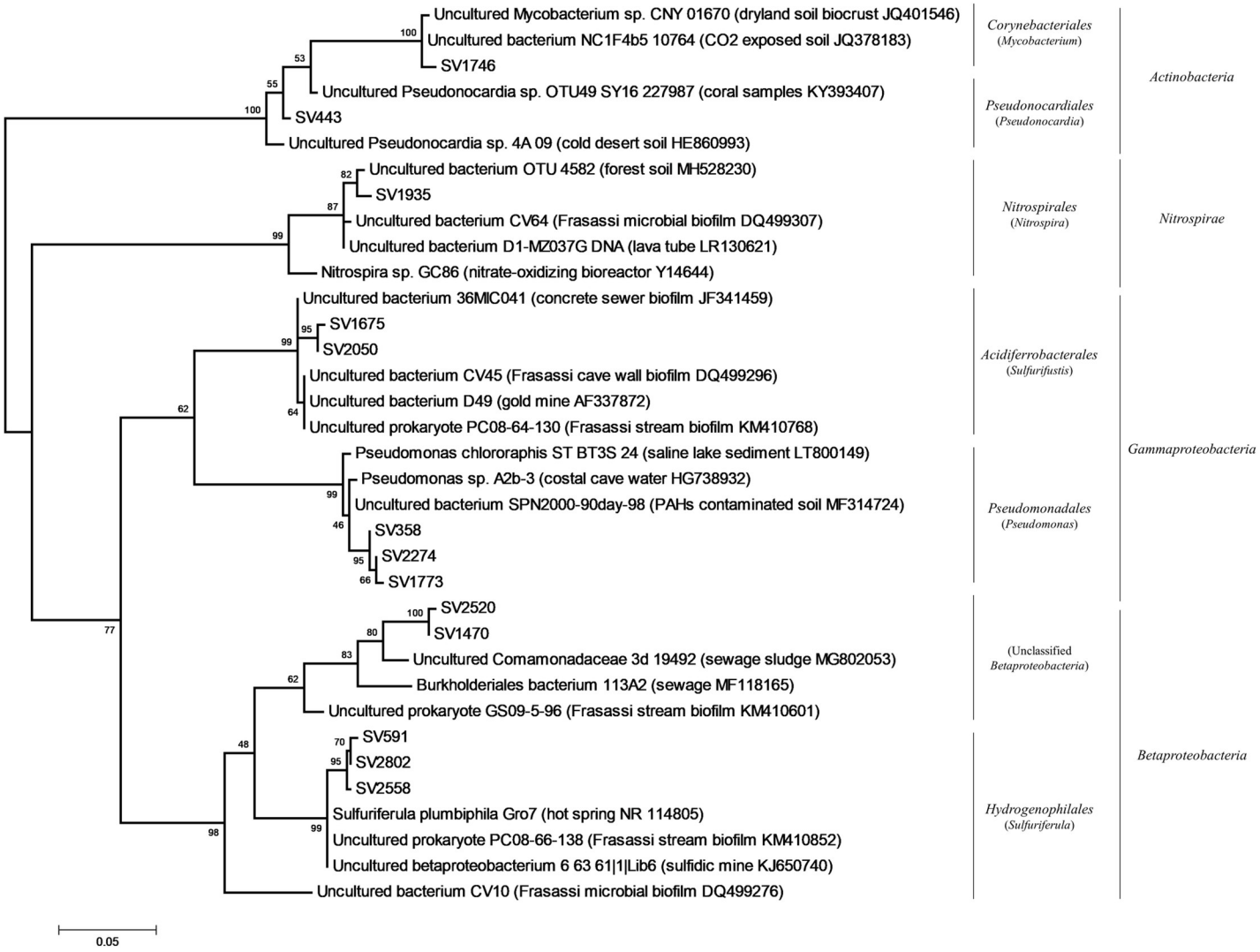
Uncultured Mycobacterium sp. CNY 01670 (dryland soil biocrust JQ401546)
Uncultured bacterium NC1F4b5 10764 (CO2 exposed soil JQ378183)
SV1746
Uncultured Pseudonocardia sp. OTU49 SY16 227987 (coral samples KY393407)
SV443
Uncultured Pseudonocardia sp. 4A 09 (cold desert soil HE860993)
Uncultured bacterium OTU 4582 (forest soil MH528230)
SV1935
Uncultured bacterium CV64 (Frasassi microbial biofilm DQ499307)
Uncultured bacterium D1-MZ037G DNA (lava tube LR130621)
Nitrospira sp. GC86 (nitrate-oxidizing bioreactor Y14644)
Uncultured bacterium 36MIC041 (concrete sewer biofilm JF341459)
SV1675
SV2050
Uncultured bacterium CV45 (Frasassi cave wall biofilm DQ499296)
Uncultured bacterium D49 (gold mine AF337872)
Uncultured prokaryote PC08-64-130 (Frasassi stream biofilm KM410768)
Pseudomonas chlororaphis ST BT3S 24 (saline lake sediment LT800149)
Pseudomonas sp. A2b-3 (costal cave water HG738932)
Uncultured bacterium SPN2000-90day-98 (PAHs contaminated soil MF314724)
SV358
SV2274
SV1773
SV2520
SV1470
Uncultured Comamonadaceae 3d 19492 (sewage sludge MG802053)
Burkholderiales bacterium 113A2 (sewage MF118165)
Uncultured prokaryote GS09-5-96 (Frasassi stream biofilm KM410601)
SV591
SV2802
SV2558
Sulfuriferula plumbiphila Gro7 (hot spring NR 114805)
Uncultured prokaryote PC08-66-138 (Frasassi stream biofilm KM410852)
Uncultured betaproteobacterium 6 63 61|1|Lib6 (sulfidic mine KJ650740)
Uncultured bacterium CV10 (Frasassi microbial biofilm DQ499276)
0.05
Corynebacteriales (Mycobacterium)
Pseudonocardiales (Pseudonocardia)
Actinobacteria
Nitrospirales (Nitrospira)
Nitrospirae
Acidiferrobacterales (Sulfurifustis)
Pseudomonadales (Pseudomonas)
Gammaproteobacteria
(Unclassified Betaproteobacteria)
Hydrogenophilales (Sulfuriferula)
Betaproteobacteria

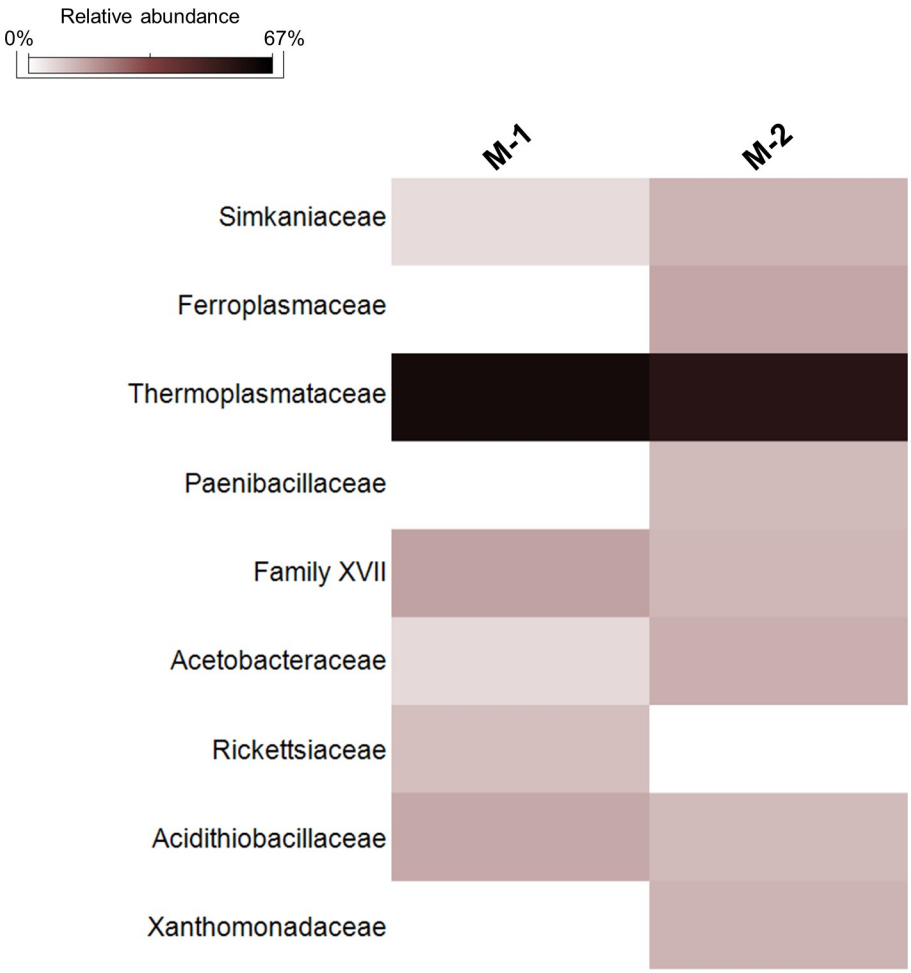
Relative abundance
0%
67%
M-1
M-2
Simkaniaceae
Ferroplasmaceae
Thermoplasmataceae
Paenibacillaceae
Family XVII
Acetobacteraceae
Rickettsiaceae
Acidithiobacillaceae
Xanthomonadaceae

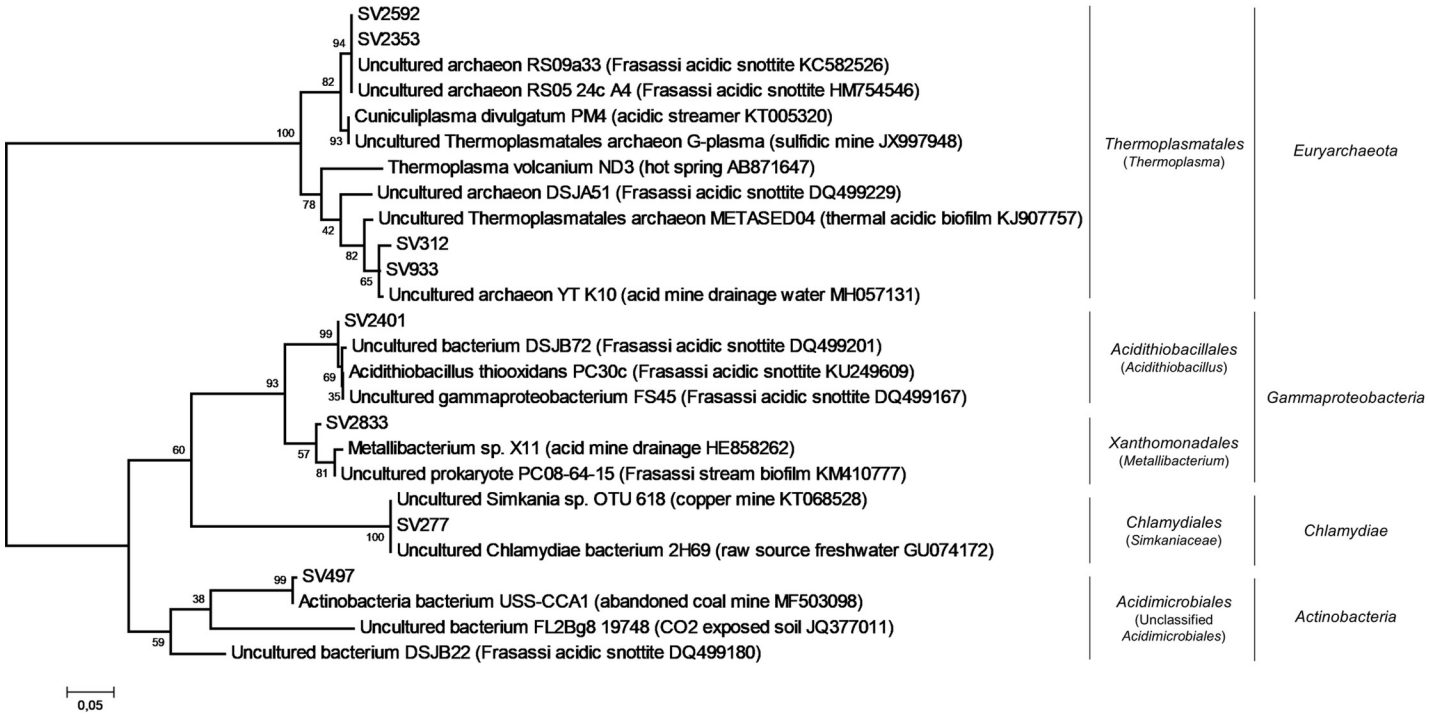
SV2592
SV2353
Uncultured archaeon RS09a33 (Frasassi acidic snottite KC582526)
Uncultured archaeon RS05 24c A4 (Frasassi acidic snottite HM754546)
Cuniculiplasma divulgatum PM4 (acidic streamer KT005320)
Uncultured Thermoplasmatales archaeon G-plasma (sulfidic mine JX997948)
Thermoplasma volcanium ND3 (hot spring AB871647)
Uncultured archaeon DSJA51 (Frasassi acidic snottite DQ499229)
Uncultured Thermoplasmatales archaeon METASED04 (thermal acidic biofilm KJ907757)
SV312
SV933
Uncultured archaeon YT K10 (acid mine drainage water MH057131)
SV2401
Uncultured bacterium DSJB72 (Frasassi acidic snottite DQ499201)
Acidithiobacillus thiooxidans PC30c (Frasassi acidic snottite KU249609)
Uncultured gammaproteobacterium FS45 (Frasassi acidic snottite DQ499167)
SV2833
Metallibacterium sp. X11 (acid mine drainage HE858262)
Uncultured prokaryote PC08-64-15 (Frasassi stream biofilm KM410777)
Uncultured Simkania sp. OTU 618 (copper mine KT068528)
SV277
Uncultured Chlamydiae bacterium 2H69 (raw source freshwater GU074172)
SV497
Actinobacteria bacterium USS-CCA1 (abandoned coal mine MF503098)
Uncultured bacterium FL2Bg8 19748 (CO2 exposed soil JQ377011)
Uncultured bacterium DSJB22 (Frasassi acidic snottite DQ499180)
94
82
100
93
78
42
82
65
99
69
35
93
60
57
81
100
99
38
59
0,05
Thermoplasmatales
(Thermoplasma)
Acidithiobacillales
(Acidithiobacillus)
Xanthomonadales
(Metallibacterium)
Chlamydiales
(Simkaniaceae)
Acidimicrobiales
(Unclassified
Acidimicrobiales)
Euryarchaeota
Gammaproteobacteria
Chlamydiae
Actinobacteria

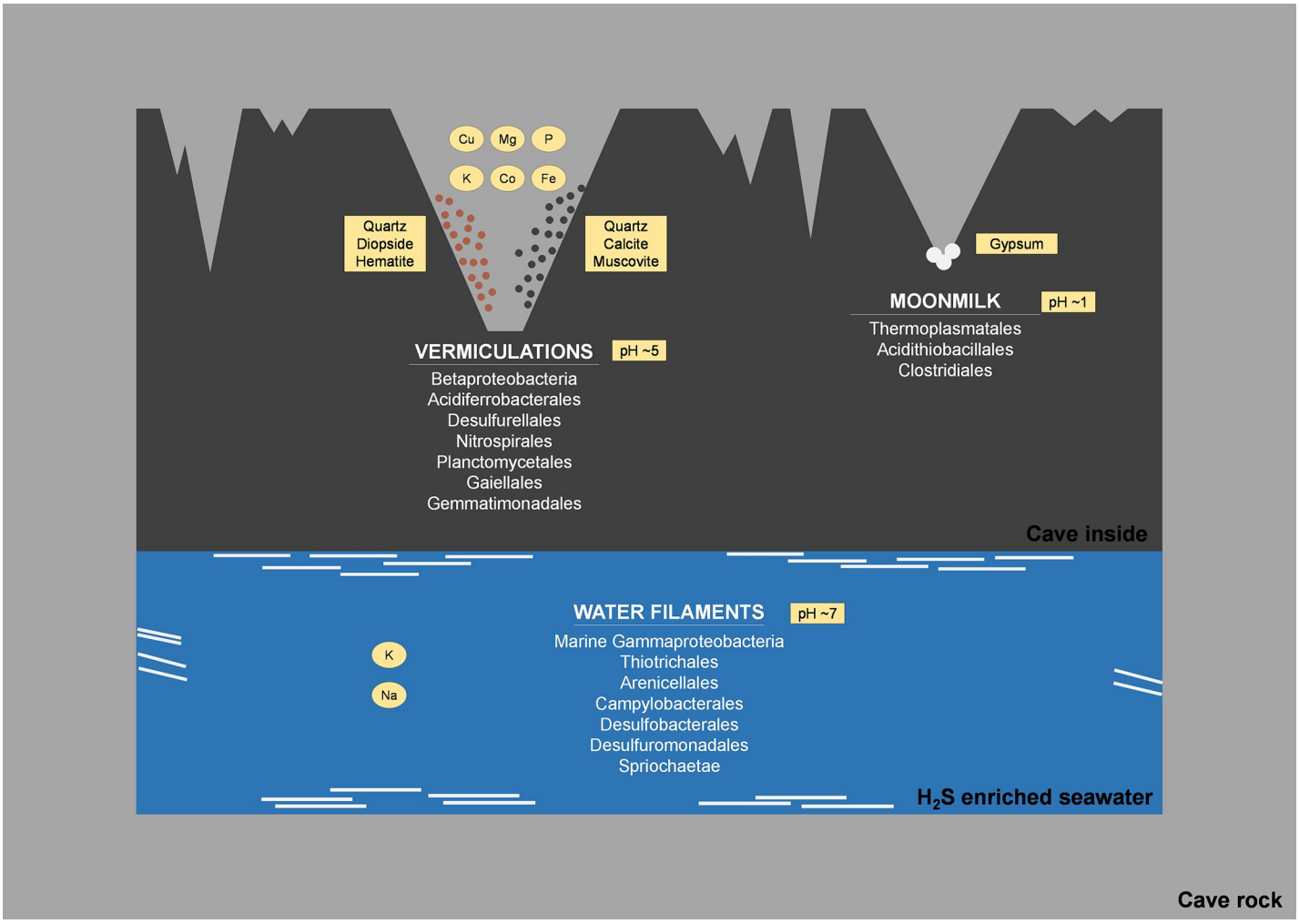
Cu
Mg
P
K
Co
Fe
Quartz
Diopside
Hematite
Quartz
Calcite
Muscovite
Gypsum
MOONMILK
pH ~1
Thermoplasmatales
Acidithiobacillales
Clostridiales
VERMICULATIONS
pH ~5
Betaproteobacteria
Acidiferrobacterales
Desulfurellales
Nitrospirales
Planctomycetales
Gaiellales
Gemmatimonadales
Cave inside
WATER FILAMENTS
pH ~7
K
Na
Marine Gammaproteobacteria
Thiotrichales
Arenicellales
Campylobacterales
Desulfobacterales
Desulfuromonadales
Spriochaetae
H2S enriched seawater
Cave rock

Tomczyk-Żak K, Zielenkiewicz U. Microbial diversity in caves. Geomicrobiol J. 2015; 33(1): 20–38.

Lavoie KH, Northup DE, Barton HA. Microbe-Mineral interactions: cave geomicrobiology. In: Jain SK, Khan AA, Rai MK, editors. Geomicrobiology. CRC Press, New York; 2010. pp. 1–45.

Northup DE, Lavoie KH. Geomicrobiology of caves: a review. Geomicrobiol J. 2001; 18: 199–222.

Jones DS, Macalady JL. The snotty and stringy: energy for subsurface life in caves. In: Hurst C.J., editor. Their World: A diversity of Microbial Environments. Advances in Environmental Microbiology 1. Springer; 2016. pp. 203–224.

Sauro F, Cappelletti M, Ghezzi D, Columbu A, Hong P, Zowawi HM, et al. Microbial diversity and biosignatures of amorphous silica deposits in orthoquartzite caves. Sci Rep. 2018; 8: 17569. https://doi.org/10.1038/s41598-018-35532-y PMID: 30514906

Boston PJ, Spilde MN, Northup DE, Melim LA, Soroka DG, Kleina LG, et al. Cave Biosignature Suites: Microbes, minerals, and Mars. Astrobiology. 2001; 1(1): 25–55. https://doi.org/10.1089/153110701750137413 PMID: 12448994

Riquelme C, Hathaway JJM, Dapkevicius MDLE, Miller AZ, Kooser A, Northup DE, et al. Actinobacterial diversity in volcanic caves and associated geomicrobiological interactions. Front Micrbiol. 2015; 6: 1342.

Rüffel V, Maar M, Dammbrück MN, Hauröder B, Neu TR, Meier J. Thermodesulfobium sp. strain 3baa, an acidophilic sulfate reducing bacterium forming biofilms triggered by mineral precipitation. Environ Microbiol. 2018; 20(10): 3717–3731. https://doi.org/10.1111/1462-2920.14374 PMID: 30105784

Tisato N, Torriani S, Monteaux S, Sauro F, De Waele J, Tavagna ML, et al. Microbial mediation of complex subterranean mineral structures. Sci Rep. 2015; 5: 15525. https://doi.org/10.1038/srep15525 PMID: 26510667

Engel AS, Stern LA, Bennett PC. Microbial contributions to cave formation: new insights into sulphuric acid speleogenesis. Geology. 2004; 32(5): 369–372.

Miller AZ, Dionísio A, Sequeira Braga MA, Hernández-Mariné M, Afonso MJ, Muralha VSF, et al. Biogenic Mn oxide minerals coating in a subsurface granite environment. Chem Geol. 2012; 322–323: 181–191.

Hose LD, Palmer AN, Palmer MV, Northup DE, Boston PJ, DuChene HR. Microbiology and geochemistry in a hydrogen-sulphide-rich karst environment. Chem Geol. 2000; 169: 399–423.

De Waele J, Audra P, Madonia G, Vattano M, Plan L, D'Ange li IM, et al. Sulfuric acid speleogenesis (SAS) close to the water table: examples from southern France, Austria and Sicily. Geomorphology. 2016; 253: 452–467.

Klimchouk AB. Types and settings of hypogene karst. In: Klimchouk AB, Palmer AN, De Waele J, Auler A, Audra P, editors. Hypogene karst regions and caves of the world. Springer; 2017. pp. 1–39.

Jones DS, Tobler DJ, Schaperdoth I, Maniero M, Macalady JL. Community structure of subsurface biofilms in the thermal sulfidic caves of Acquasanta Terme, Italy. Appl Environ Microbiol. 2010; 76(17): 5902–5910. https://doi.org/10.1128/AEM.00647-10 PMID: 20639361

Jones DS, Lyon EH, Macalady JL. Geomicrobiology of biovemiculations from the Frasassi cave systems, Italy. J Caves Karst Stud. 2008; 70(2): 78–93.

D'Angeli IM, Carbone C, Nagostinis M, Parise M, Vattano M, Madonia G, et al. New insights on secondary minerals from Italian sulfuric acid caves. Int J Speleol. 2018; 47(3): 271–291.

Galdenzi S, Menichetti M. Occurrence of hypogene caves in a karst region: examples from central Italy. Environ Geol. 1995; 26: 39–47.

Galdenzi S, Cocchioni F, Filipponi G, Morichetti L, Scuri S, Selvaggio R, et al. The sulfidic thermal caves of Acquasanta terme (Central Italy). J Caves Karst Stud. 2000; 72(1): 43–58.

Hose LD, Pisarowicz JA. Cueva de Villa Luz, Tabasco, Mexico: reconnaissance study of an active sulphuric spring cave and ecosystem. J Caves Karst Stud. 1999; 61(1): 13–21.

Engel AS, Meisinger DB, Porter ML, Payn RA, Schmid M, Stern LA, et al. Linking phylogenetic and functional diversity to nutrient spiraling in microbial mats from Lower Kane Cave (USA). ISME J. 2010; 4(1): 98–110. https://doi.org/10.1038/ismej.2009.91 PMID: 19675595

Macalady JL, Dattagupta S, Schaperdoth I, Jones DS, Druschel GK, Eastman D. Niche differentiation among sulfur-oxidizing bacterial populations in cave waters. ISME J. 2008; 2(6): 590–601. https://doi.org/10.1038/ismej.2008.25 PMID: 18356823

Macalady JL, Jones DS, Lyon EH. Extremely acidic, pendulous cave wall biofilms from the Frasassi cave system, Italy. Environ Microbiol. 2007; 9(6): 1402–1414. https://doi.org/10.1111/j.1462-2920.2007.01256.x PMID: 17504478

Jones DS, Albrecht HL, Dawson KS, Schaperdoth I, Freeman KH, Pi Y, et al. Community genomic analysis of an extremely acidophilic sulfur-oxidizing biofilm. ISME J. 2012; 6(1): 158–70. https://doi.org/10.1038/ismej.2011.75 PMID: 21716305

Jones DS, Schaperdoth I, Macalady JL. Biogeography of sulfur-oxidizing populations in extremely acidic cave biofilms. ISME J. 2016; 10(12): 2879–2891. https://doi.org/10.1038/ismej.2016.74 PMID: 27187796

Hill CA, Forti P. Cave minerals of the world. Huntsville, AL. National Speleological Society; 1997. pp. 221–223.

Bini DA, Cavalli Gori M, Gori S. A critical review of hypotheses on the origin of vermiculations. Int J Speleol. 1978; 10: 11–33.

Hose LD, Northup DE. Biovermiculations: Living vermiculation-like deposits in Cueva de Villa Luz, Mexico. Proceedings of the Society: selected abstract, National Speleological Society Convention. J Caves Karst Stud. 2004; 66: 112.

Galdenzi S, Maruoka T. Gypsum deposits in the Frasassi caves, central Italy. J Caves Karst Stud. 2003; 65(2): 111–125.

Onac BP, Ghergari L. Moonmilch mineralogy in some Romanian and Norwegian Caves. Cave Science. 1993; 20: 107–111.

Miller AZ, Garcia-Sanchez AM, Martin-Sanchez PM, Costa Pereira MF, Spangenberg JE, Jurado V, et al. Origin of abundant moonmilk deposits in a subsurface granitic environment. Sedimentology. 2018; 65(5): 1482–1503.

Portillo MC, Gonzalez JM. Moonmilk deposits originate from specific bacterial communities in Altamira Cave (Spain). Microb Ecol. 2011; 61(1): 182–9. https://doi.org/10.1007/s00248-010-9731-5 PMID: 20717660

D'Angeli IM, Vattano M, Parise M, De Waele J. The coastal sulfuric acid cave system of Santa Cesarea Terme (southern Italy). In: Klimchouk AB, Audra P, Palmer AN, De Waele J, Auler A, editors. Hypogene Karst Regions and Caves of the World. Springer; 2017. pp. 161–168.

Mattison RG, Abbiati M, Dando PR, Fitzsimons MF, Pratt SM, Southward AJ, et al. Chemoautotrophic Microbial Mats in Submarine Caves with Hydrothermal Sulphidic Springs at Cape Palinuro, Italy. Microb Ecol. 1998; 35(1): 58–71. PMID: 9459659

Amato A, Bianchi I, Piana Agostinetti N. Apulian crust: Top to bottom. J Geodyn. 2014; 82: 125–137.

Velaj T. New ideas on the tectonic of the Kurveleshi anticlinal belt in Albania, and the perspective for exploration in its subthrust. Petroleum 2015; 1: 269–288.

Calò GC, Tinelli R. Systematic hydrogeological study of a hypothermal spring (S. Cesarea Terme Apulia), Italy. J Hydrol. 1995; 165: 185–205.

Banerjee S, Joshi SR. Insights into Cave Architecture and the Role of Bacterial Biofilm. Proceedings of the National Academy of Sciences, India Section B: Biological Sciences. 2013; 83(3): 277–290.

Burlet C, Vanbrabant Y, Piessens K, Welkenhuysen K, Verheyden S. Niphargus: A silicon band-gap sensor temperature logger for high-precision environmental monitoring. Comput Geosci. 2015; 74: 50–59.

Da Cunha AR. Evaluation of measurement errors of temperature and relative humidity from HOBO data logger under different conditions of exposure to solar radiation. Environ Monit Assess. 2015; 187(5): 236. https://doi.org/10.1007/s10661-015-4458-x PMID: 25855203

Mackey EA, Becker DA, Spatz RO, Paul RL, Greenberg RR, Lindstrom RM, et al. Certification of NIST Standard Reference Material 1575a pine needles and results of an international laboratory comparison. NIST Special Publication. 2004;260–156.

Cappelletti M, Ghezzi D, Zannoni D, Capaccioni B, Fedi S. Diversity of Methane-Oxidizing Bacteria in Soils from "Hot Lands of Medolla" (Italy) Featured by Anomalous High-Temperatures and Biogenic CO_2 Emission. Microbes Environ. 2016; 31(4): 369–377. https://doi.org/10.1264/jsme2.ME16087 PMID: 27645100

Caporaso JG, Lauber CL, Walters WA, Berg-Lyons D, Lozupone CA, Turnbaugh PJ, et al. Global patterns of 16S rRNA diversity at a depth of millions of sequences per sample. Proceedings of the National Academy of Sciences. 2010; 108: 4516–4522.

Callahan BJ, McMurdie PJ, Rosen MJ, Han AW, Johnson AJ, Holmes SP. DADA2: High-resolution sample inference from Illumina amplicon data. Nat Methods. 2016; 13(7): 581–583. https://doi.org/10.1038/nmeth.3869 PMID: 27214047

Quast C, Pruesse E, Yilmaz P, Gerken J, Schweer T, Yarza P, et al. The SILVA ribosomal RNA gene database project: improved data processing and web-based tools. Nucleic Acids Research. 2013; 41 (D1): D590–D596.

Bolyen E, Rideout JR, Dillon MR, Bokulich NA, Abnet C, Al-Ghalith GA, et al. QIIME 2: Reproducible, interactive, scalable, and extensible microbiome data science. PeerJ. 2018.

Clarke KR, Gorley RN. "PRIMER v7: User Manual/Tutorial". PRIMER-E. 2015.

Kumar S, Stecher G, Li M, Knyaz C, Tamura K. MEGA X: Molecular Evolutionary Genetics Analysis across computing platforms. Mol Biol Evol. 2018; 35: 1547–1549. https://doi.org/10.1093/molbev/msy096 PMID: 29722887

Canganella F, Bianconi G, Kato C, Gonzalez J. Microbial ecology of submerged marine caves and holes characterized by high levels of hydrogen sulphide. Rev Environ Sci Biotechnol. 2006; 6: 61–70.

Barton HA, Taylor MR, Pace NR. Molecular Phylogenetic Analysis of a Bacterial Community in an Oligotrophic Cave Environment. Geomicrobiol J. 2004; 21: 11–20.

Callahan BJ, McMurdie PJ, Holmes SP. Exact sequence variants should replace operational taxonomic units in marker-gene data analysis. ISME J. 2017; 11: 2639–2643. https://doi.org/10.1038/ismej.2017.119 PMID: 28731476

Macalady JL, Lyon EH, Koffman B, Albertson LK, Meyer K, Galdenzi S, et al. Dominant microbial population in limestone-corroding stream biofilms, Frasassi cave system, Italy. Appl Environ Microbiol. 2006; 72(8): 5596–5609. https://doi.org/10.1128/AEM.00715-06 PMID: 16885314

Kumaresan D, Wischer D, Stephenson J, Hillebrand-Voiculescu A, Murrell JC. Microbiology of Movile cave—a chemolithoautotrophic ecosystem. Geomicrobiol J. 2014; 31: 186–93.

Engel AS, Lee N, Porter ML, Stern LA, Bennett PC, Wagner M. Filamentous "Epsilonproteobacteria" Dominate Microbial Mats from Sulfidic Cave Springs. Appl Environ Microbiol. 2003; 69(9): 5503–5511. https://doi.org/10.1128/AEM.69.9.5503-5511.2003 PMID: 12957939

Teramoto M, Yagyu K, Nishijima M. Perspicuibacter marinus gen. nov., sp. nov., a semi-transparent bacterium isolated from surface seawater, and description of Arenicellaceae fam. nov. and Arenicellales ord. nov. Int J Syst Evol Microbiol. 2015; 65: 353–358. https://doi.org/10.1099/ijs.0.064683-0 PMID: 25355707

Jones DS, Flood BE, Bailey JV. Metatranscriptomic analysis of diminutive Thiomargarita-like bacteria ("Candidatus Thiopilula" spp.) from abyssal cold seeps of the Barbados Accretionary Prism. Appl Environ Microbiol. 2015; 81(9): 3142–56. https://doi.org/10.1128/AEM.00039-15 PMID: 25724961

Hirano H, Yoshida T, Fuse H, Endo T, Habe H, Nojiri H, et al. Marinobacterium sp. strain DMS-S1 uses dimethyl sulphide as a sulphur source after light-dependent transformation by excreted flavins. Environ Microbiol. 2003; 5(6): 503–509. PMID: 12755717

Delmont TO, Quince C, Shaiber A, Esen ÖC, Lee ST, Rappé MS, et al. Nitrogen-fixing populations of Planctomycetes and Proteobacteria are abundant in surface ocean metagenomes. Nat Microbiol. 2018; 3(7): 804–813. https://doi.org/10.1038/s41564-018-0176-9 PMID: 29891866

Kang I, Lim Y, Cho JC. Complete genome sequence of Granulosicoccus antarcticus type strain IMCC3135T, a marine gammaproteobacterium with a putative dimethylsulfoniopropionate demethylase gene. Mar Genomics. 2018; 37: 176–181. https://doi.org/10.1016/j.margen.2017.11.005 PMID: 29175002

Marques ELS, Dias JCT, Gross E, Silva ABCE, de Moura SR, Rezende RP. Purple Sulfur Bacteria Dominate Microbial Community in Brazilian Limestone Cave. Microorganisms. 2019; 7(2): 29.

Mugge RL, Brock ML, Salerno JL, Damour M, Church RA, Lee JS, et al. Deep-Sea Biofilms, Historic Shipwreck Preservation and the Spill. Front Mar Sci. 2019; 6: 48.

Li Y, Tang K, Zhang L, Zhao Z, Xie X, Chen CA. Coupled Carbon, Sulfur, and Nitrogen Cycles Mediated by Microorganisms in the Water Column of a Shallow-Water Hydrothermal Ecosystem. Front Microbiol. 2018; 9: 2718. https://doi.org/10.3389/fmicb.2018.02718 PMID: 30555427

Wright KE, Williamson C, Grasby SE, Spear JR, Templeton AS. Metagenomic evidence for sulfur lithotrophy by Epsilonproteobacteria as the major energy source for primary productivity in a sub-aerial arctic glacial deposit. Borup Fiord Pass. Front Microbiol. 2013; 4: 63. https://doi.org/10.3389/fmicb.2013.00063 PMID: 23626586

Hamilton TL, Jones DS, Schaperdoth I, Macalady JL. Metagenomic insights into S^0 precipitation in a terrestrial subsurface lithoautotrophic ecosystem. Front Microbiol. 2015; 5: 756. https://doi.org/10.3389/fmicb.2014.00756 PMID: 25620962

Wirsen CO, Sievert SM, Cavanaugh CM, Molyneaux SJ, Ahmad A, Taylor LT, et al. Characterization of an autotrophic sulfide-oxidizing marine Arcobacter sp. that produces filamentous sulfur. Appl Environ Microbiol. 2002; 68(1): 316–25. https://doi.org/10.1128/AEM.68.1.316-325.2002 PMID: 11772641

Han Y, Perner M. The globally widespread genus Sulfurimonas: versatile energy metabolisms and adaptations to redox clines. Front Microbiol. 2015; 6: 989. https://doi.org/10.3389/fmicb.2015.00989 PMID: 26441918

Keller AH, Schleinitz KM, Starke R, Bertilsson S, Vogt C, Kleinsteuber S. Metagenome-Based Metabolic Reconstruction Reveals the Ecophysiological Function of Epsilonproteobacteria in a Hydrocarbon-Contaminated Sulfidic Aquifer. Front Microbiol. 2015; 6: 1396. https://doi.org/10.3389/fmicb.2015.01396 PMID: 26696999

Martín-Cuadrado AB, López-García P, Alba JC, Moreira D, Monticelli L, Strittmatter A, et al. Metagenomics of the deep Mediterranean, a warm bathypelagic habitat. PLoS One. 2007; 2(9): 914.

Engel AS. Observation on the biodiversity of sulfidic karst habitats. J Cave Karst Stud. 2007; 69: 187–206.

Rohwerder T, Sand W, Lascu C. Preliminary evidence for a sulfur cycle in Movile Cave, Romania. Acta Biotechnol. 2003; 23: 101–107.

Trembath-Reichert E, Case DH, Orphan VJ. Characterization of microbial associations with methanotrophic archaea and sulfate-reducing bacteria through statistical comparison of nested Magneto-FISH enrichments. PeerJ. 2016; 4: 1913.

Ionescu D, Siebert C, Polerecky L, Munwes YY, Lott C, Häusler S, et al. Microbial and chemical characterization of underwater fresh water springs in the Dead Sea. PLoS One. 2012; 7(6): 38319.

Addesso R, Bellino A, D'Angeli IM, De Waele J, Miller AZ, Carbone C, et al. Vermiculations from karst caves: The case of Pertosa-Auletta system (Italy). Catena. 2019;182. https://doi.org/10.1016/j.catena.2019.104178

Ye RW, Thomas SM. Microbial nitrogen cycles: physiology, genomics and applications. Curr Opin Microbiol. 2001; 4(3): 307–312. PMID: 11378484

Kojima H, Shinohara A, Fukui M. Sulfurifustis variabilis gen. nov., sp. nov., a sulfur oxidizer isolated from a lake, and proposal of Acidiferrobacteraceae fam. nov. and Acidiferrobacterales ord. nov. Int J Syst Evol Microbiol. 2015; 65(10): 3709–3713. https://doi.org/10.1099/ijsem.0.000479 PMID: 26220671

Issotta F, Moya-Beltrán A, Mena C, Covarrubias PC, Thyssen C, Bellenberg S, et al. Insights into the biology of acidophilic members of the Acidiferrobacteraceae family derived from comparative genomic analyses. Res Microbiol. 2018; 169(10): 608–617. https://doi.org/10.1016/j.resmic.2018.08.001 PMID: 30142431

Florentino AP, Stams AJ, Sánchez-Andrea I. Genome Sequence of Desulfurella amilsii Strain TR1 and Comparative Genomics of Desulfurellaceae Family. Front Microbiol. 2017; 8: 222. https://doi.org/10.3389/fmicb.2017.00222 PMID: 28265263

Wei H, Wang J, Hassan M, Han L, Xie B. Anaerobic ammonium oxidation-denitrification synergistic interaction of mature landfill leachate in aged refuse bioreactor: Variations and effects of microbial community structures. Bioresour Technol. 2017; 243: 1149–1158. https://doi.org/10.1016/j.biortech.2017.07.077 PMID: 28764129

Baker BJ, Lazar CS, Teske AP, Dick GJ. Genomic resolution of linkages in carbon, nitrogen, and sulfur cycling among widespread estuary sediment bacteria. Microbiome. 2015; 3: 14. https://doi.org/10.1186/s40168-015-0077-6 PMID: 25922666

Koch H, van Kessel MAHJ, Lücker S. Complete nitrification: insights into the ecophysiology of comammox Nitrospira. Appl Microbiol Biotechnol. 2019; 103(1): 177–189. https://doi.org/10.1007/s00253-018-9486-3 PMID: 30415428

Camejo PY, Santo J, Domingo D, McMahon KD, Noguera R. Genome-enabled insights into the ecophysiology of the comammox bacterium Nitrospira nitrosa. mSystems 2017; 2: e00059–17. https://doi.org/10.1128/mSystems.00059-17 PMID: 28905001

Umezawa K, Watanabe T, Miura A, Kojima H, Fukui M. The complete genome sequences of sulfur-oxidizing Gammaproteobacteria Sulfurifustis variabilis skN76(T) and Sulfuricaulis limicola HA5(T). Stand Genomic Sci. 2016; 11: 71. https://doi.org/10.1186/s40793-016-0196-0 PMID: 27651857

Pascual J, Wüst PK, Geppert A, Foesel BU, Huber KJ, Overmann J. Novel isolates double the number of chemotrophic species and allow the first description of higher taxa in Acidobacteria subdivision 4. Syst Appl Microbiol. 2015; 38(8): 534–544. https://doi.org/10.1016/j.syapm.2015.08.001 PMID: 26460220

McIlroy SJ, Kirkegaard RH, Dueholm MS, Fernando E, Karst SM, Albertsen M, et al. Culture-Independent Analyses Reveal Novel Anaerolineaceae as Abundant Primary Fermenters in Anaerobic Digesters Treating Waste Activated Sludge. Front Microbiol. 2017; 8: 1134. https://doi.org/10.3389/fmicb.2017.01134 PMID: 28690595

Marshall Hathaway JJ, Garcia MG, Balasch MM, Spilde MN, Stone FD, Dapkevicius ML, et al. Comparison of Bacterial Diversity in Azorean and Hawai'ian Lava Cave Microbial Mats. Geomicrobiol J. 2014; 31(3): 205–220. https://doi.org/10.1080/01490451.2013.777491 PMID: 26924866

Ghosh S, Paine E, Wall R, Kam G, Lauriente T, Sa-ngarmangkang PC, et al. In Situ Cultured Bacterial Diversity from Iron Curtain Cave, Chilliwack, British Columbia, Canada. Diversity. 2017; 9: 36.

Hester ER, Harpenslager SF, van Diggelen JMH, Lamers LL, Jetten MSM, Lüke C, et al. Linking Nitrogen Load to the Structure and Function of Wetland Soil and Rhizosphere Microbial Communities. mSystems. 2018; 3(1): e00214–17. https://doi.org/10.1128/mSystems.00214-17 PMID: 29404427

Jones DS, Roepke EW, An Hua A, Flood BE, Bailey JV. Complete Genome Sequence of Sulfuriferula sp. Strain AH1, a Sulfur-Oxidizing Autotroph Isolated from Weathered Mine Tailings from the Duluth Complex in Minnesota. Genome Announc. 2017; 5(32): e00673–17. https://doi.org/10.1128/genomeA.00673-17 PMID: 28798167

Liu JL, Yao J, Wang F, Min N, Gu JH, Li ZF, et al. Bacterial diversity in typical abandoned multi-contaminated nonferrous metal(loid) tailings during natural attenuation. Environ Pollut. 2019; 247: 98–107. https://doi.org/10.1016/j.envpol.2018.12.045 PMID: 30669085

Borsato A, Frisia S, Jones B, Van der Borg K. Calcite moonmilk: crystal morphology and environment of formation in caves in the Italian Alps. J Sediment Res. 2010; 70(5): 1179–1190.

Chirienco M. The crystalline phase of the carbonate moonmilk: a terminology approach. Acta Carsologica. 2004; 17: 257–264.

Ruepp A, Graml W, Santos-Martinez ML, Koretke KK, Volker C, Mewes HW, et al. The genome sequence of the thermoacidophilic scavenger Thermoplasma acidophilum. Nature. 2000; 407: 508–513. https://doi.org/10.1038/35035069 PMID: 11029001

Golyshina OV, Timmis KN. Ferroplasma and relatives, recently discovered cell wall-lacking archaea making a living in extremely acid, heavy metal-rich environments. Environ Microbiol. 2005; 7(9): 1277–88. https://doi.org/10.1111/j.1462-2920.2005.00861.x PMID: 16104851

Golyshina OV, Tran H, Reva ON, Lemak S, Yakunin AF, Goesmann A, et al. Metabolic and evolutionary patterns in the extremely acidophilic archaeon Ferroplasma acidiphilum YT. Sci Rep. 2017; 7(1): 997–12. https://doi.org/10.1038/s41598-017-00810-8

Justice NB, Norman A, Brown CT, Singh A, Thomas BC, Banfield JF. Comparison of environmental and isolate Sulfobacillus genomes reveals diverse carbon, sulfur, nitrogen, and hydrogen metabolisms. BMC Genomics. 2014; 15: 1107. https://doi.org/10.1186/1471-2164-15-1107 PMID: 25511286

Engel AS, Paoletti MG, Beggio M, Dorigo L, Pamio A, Gomiero T, et al. Comparative microbial community composition from secondary 1 carbonate (moonmilk) deposits: implications for the Cansiliella servadeii cave hygropetric food web. Int J Speleol. 2013; 42(3): 181–192.

Cirigliano A, Tomassetti MC, Di Pietro M, Mura F, Maneschi ML, Gentili MD, et al. Calcite moonmilk of microbial origin in the Etruscan Tomba degli Scudi in Tarquinia, Italy. Sci Rep. 2018; 8: 15839. https://doi.org/10.1038/s41598-018-34134-y PMID: 30367083

CHAPTER 5

Vermiculations from karst caves: The case of Pertosa-Auletta system (Italy)

Rosangela Addesso, Alessandro Bellino*, Ilenia Maria D'Angeli, Jo De Waele, Ana Zélia Miller, Cristina Carbone, Daniela Baldantoni

Catena 182 (2019): 104178

doi: 10.1016/j.catena.2019.104178

*corresponding author

A multiapproach geochemical characterization of cave vermiculations from the Pertosa-Auletta Cave has been carried out through elemental, mineralogical and microscopy analyses, clarifying their unknown nature and genesis processes.

Catena 182 (2019) 104178

ELSEVIER

CATENA

Available online 19 July 2019

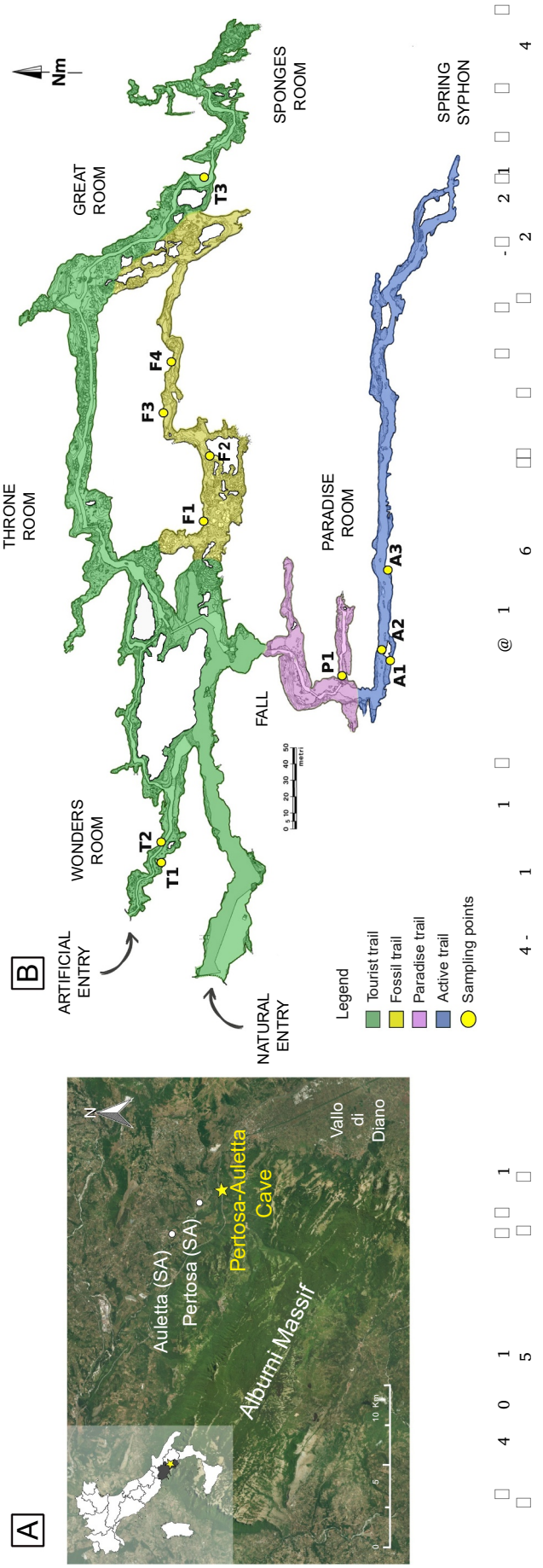
B
Nm
SPONGES ROOM
SPRING SYPHON
GREAT ROOM
T3
F4
F3
F2
F1
THRONE ROOM
PARADISE ROOM
A3
A2
A1
P1
FALL
WONDERS ROOM
T2
T1
ARTIFICIAL ENTRY
NATURAL ENTRY
Legend
Tourist trail
Fossil trail
Paradise trail
Active trail
Sampling points
A
N
Vallo di Diano
Pertosa-Auletta Cave
Auletta (SA)
Pertosa (SA)
Alburni Massif

T1
T2
T3
P1
F1
F2
F3
F4
A1
A2
A3
0 2 cm

□ 1 X □ □□ 4 C □ □ □ 6 □C YS B4BA □ □ 3 □
4

	:	H	G	-:	-H	-G	-K	:	:	H	G
L □42 4	: D=4G X : G4K	; 4K X B4K	: =4<X H4D	; 4 X : 4H	H4=X B4K	<4A X : 4	=4G X B4G	<4B X B4<	D4A X B4D	G4 X B4G	: B<4 X : K4
L □42 4	H; 4<B X : 4=D	B4KB X B4 <	B4=H X B4 H	B4H X B4BK	B4B=X B4BD	B4 G X B4B:	B4HG X B4B:	B4HB X B4B<	B4 H X B4B:	B4 B X B4B:	: A4KG X : 4K:
L □42 4	AK4D X : 4<	<4=X B4= □	: B4H X B4A	A4 X B4=□	K4B X B4K	<4 X B4D □	=4<X H4D □	A4G X : 4	A4D X B4D □	G4D X B4K	K<4K X : 4
, L □42 4	B4<G X B4 G	B4B=X B4BD	B4 G X B4 B	B4 D X B4HK	B4 B X B4 =	B4B<X B4 :	B4 : X B4B;	B4B: X B4B:	B4BA X B4BG	B4 H X B4 A	B4KK X B4BA
- L □42 4	: : 4A<X B4 B	B4HK X B4B:	B4A=X B4 B	B4 <X B4BH	B4BK X B4B:	B4 ; X B4BG	B4HD X B4BH	B4 D X B4BK	B4B<X B4B:	B4 B X B4BG	; 4AA X B4D:
□ L □42 4	G4=K X B4GK	B4AG X B4BG	B4AD X B4BD	B4KD X B4BK	B4GA X B4BD	B4<K X B4B;	B4A<X B4B:	B4G=X B4B;	B4KD X B4BK	B4 D X B4BG	K4 B X B4GK
R L □42 4	: G4==X K4=G	: 4BA X B4B<	G4H=X B4 <	: 4=; X B4B;	: 4B=X B4BA	G4DA X B4BD	H4<A X B4 =	G4A: X B4BK	G4BB X B4BG	B4=; X B4B=	HK4A; X : 4<D
L □42 4	H4GG X B4HA	B4H: X B4B:	B4KG X B4BD	B4HB X B4B:	B4B=X B4B:	B4H; X B4B:	B4H=X B4B:	B4H; X B4B:	B4 ; X B4B:	B4B; X B4B:	H4GG X B4HG
L □42 4	D4B<X B4HH	H4HG X B4BD □	<4<; X B4B=	B4 K X B4HD	B4D; X B4 ;	: 4KA X B4 H	K4GG X B4 K	B4GG X B4BK	B4KK X B4BK	: 4 ; X B4 A	: 4 B X B4 =□
□ L □42 4	K4KK X B4HH	B4BA X B4B:	B4=<X B4 B	B4B: X B4B:	B4B: X B4B:	B4H<X B4BK	B4BD X B4B:	B4BK X B4B:	B4B: X B4B:	B4B: X B4B:	HK4AD X : 4 :
P □42 4	K4DH X B4B=	: H4 K X B4 B □	: : 4KD X B4GH	: H4<H X B4B<	: H4=G X B4B:	: H4H<X B4 : □	: H4 D X B4BG □	: G4BH X B4 K	: H4DA X B4B<	: G4 D X B4 =	D4<G X B4B<
P □42 4	B4==X B4BA	B4KA X B4 G	B4 =X B4KH	G4B: X H4 =	G4 D X : 4 <	: 4AG X : 4 K	: 4=B X : 4 A	H4AD X : 4DA	A4 D X B4=D	<4BD X B4 <	H4 D X B4A;
L □42 4	B4G: X B4BK □	B4 ; X B4B: □	B4G=X B4 B	B4 ; X B4B: □	B4B; X B4B:	B4 : X B4B:	B4H<X B4B: □	B4GG X B4B<	B4 A X B4B:	B4A<X B4BH	B4K<X B4BK
Q L □42 4	KB4<H X K4HA	: : 4=<X : 4 : □	: K4=G X H4G;	: H4GD X H4DG □	=4H<X : 4 H□	: B4 =X B4 B □	=4GG X K4HA □	<4 H X B4 ; □	: : 4<A X B4 G □	G4<=X B4H<	H<4A=X : 4HB
□ Q L □42 4	: KA4HB X H<4HB	H4H: X B4KK	; 4K=X B4 ;	: 4 G X B4KG	: 4HG X B4<K	G4 G X B4A:	=4GG X H<4HB	B4 K X B4 D	: 4H=X B4BK	G4HA X B4BD	DK4H<X : : 4KD
□ Q L □42 4	A: 4=X <4	: 4A X B4	G4B X B4K	: 4 X B4G	B4A X B4	: 4H X B4	=4G X <4	: 4G X B4	: 4G X B4	B4<X B4	GD4 X A4D
Q L □42 4	<=4B X <4G	<4G X B4G □	: A4A X : 4H	A4 X B4K □	: 4A X B4 □	D4G X B4K □	D4K X B4H □	D4 X B4K □	G4G X B4 □	: 4=X B4H□	DA4B X ; 4A
Q L □42 4	G; 4 X G4	H4 X B4H	K4K X B4G	H4G X B4H	: 4<X B4	H4A X B4H	H4=X B4H	=4K X <4	: 4A X B4	: 4H X B4	G: 4B X G4H
, L □42 4	: 4BD X B4B;	B4HD X B4BA	B4D: X B4B=□	: 4 ; X B4BK	B4KA X B4BK □	B4HH X B4 ;	B4D: X B4BK □	: 4DG X B4BK	B4K=X B4HK □	G4==X B4H:	: 4G; X B4BG
, Q L □42 4	; ; 4==X : B4AK	A4 A X B4AG	: A4==X G4H:	<4B<X B4G<	: 4DK X B4D;	; 4GG X K4GB	<4 =X B4=<	H<4K: X : <4B:	D4 <X H4HA	=4 B X G4KH	: : ; 4<; X : K4G:
(Q L □42 4	H: ; 4<K X : 4<K	: H4HG X G4 D	A<4G; X : 4 =□	: <4=D X B4 ;	K4H; X B4GG	HB4H; X B4<B	<K4HK X : 4DH	; 4< X : 4 H	: H4H=X H4 ;	HD4 K X G4GG	: ; : 4=<X : D4BB
Q L □42 4	D; 4H X : 4D	G4A X B4A □	: H4B X B4H	D4K X B4A □	: 4 X B4	G4 X B4<□	: A4K X B4=	G4D X B4H □	G4D X B4A □	: H4=X : 4=	AD4 X K4H
Q L □42 4	<4BA X B4BD	B4H: X B4BG	B4=; X B4BA	B4G: X B4B:	B4 G X B4B:	B4GG X B4BG	B4BK X B4BK	B4HK X B4BK	B4 H X B4B:	B4 : X B4B:	: K4<G X B4 D
□ Q L □42 4	B4K; X B4 A	B4B<X B4BD □	B4G<X B4B; □	B4 A X B4BA □	B4BA X B4BA □	B4G: X B4B: □	=4GG X B4 A □	B4=B X B4GK	B4 K X B4B= □	B4B; X B4B=□	B4AK X B4B;

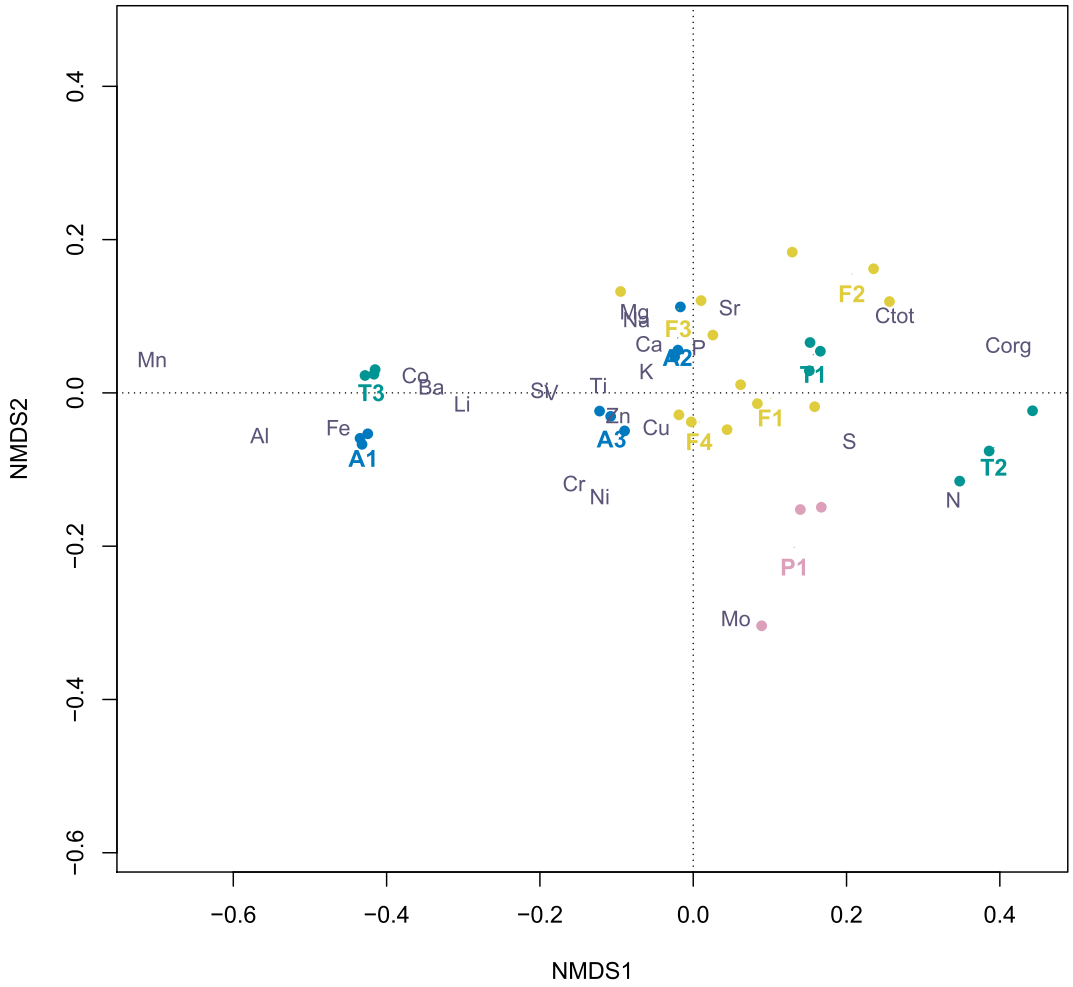
NMDS1
NMDS2
−0.6
−0.4
−0.2
0.0
0.2
0.4
Mn
Co
Ba
Li
Sr
Ti
V
Al
Fe
Mg
Na
Ca
P
K
Zn
Cu
Cr
Ni
S
N
Corg
Ctot
Mo
T1
T2
T3
A1
A2
A3
F1
F2
F3
F4
P1

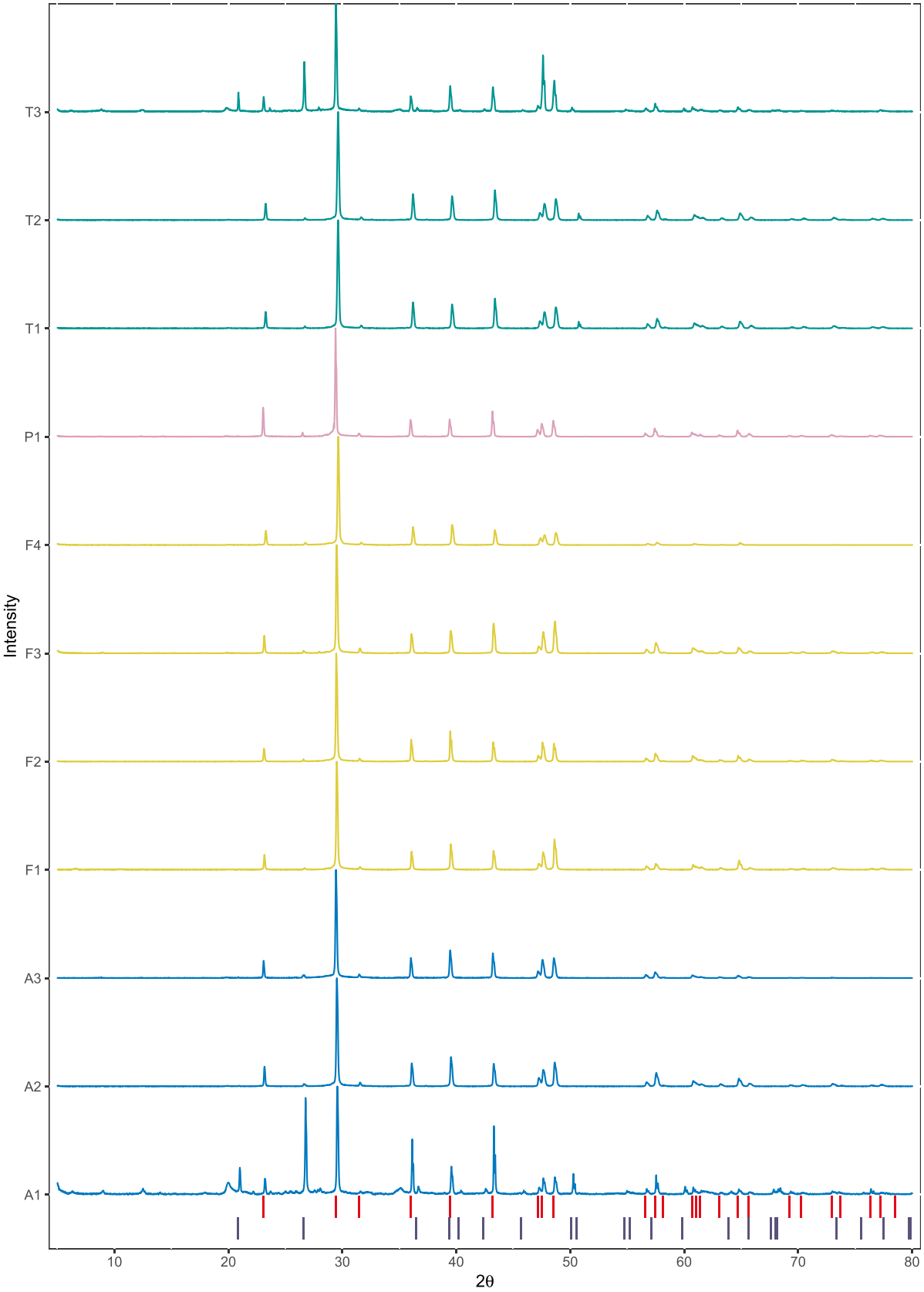

□□C □2 □ □ □ -□ 2 □1 □ □ □ □ □
4 C □ □Y 5 8 □ 2 4 - 1 6 □□ □
□ 2 4

X 5 8 Y 5 8 4
1 4

:	H	G	-:	-H	-G	-K	:	:	H	G
P	D<4 X B4=	; =4K X B4H	; <4 X B4H	; ; 4G X B4	; =4G X B4H	; ; 4G X B4	; <4A X B4K	; =4A X B4	; ; 4G X B4	; ; 4K X B4	=H4<X B4D
8 P	GH4 X B4=	: 4D X B4H	H4 X B4H	B4<X B4	: 4<X B4H	B4<X B4	H4A X B4K	: 4A X B4	B4<X B4	B4D X B4	: <4K X B4D
	•		•			•	•				•
- 1	•					•					•
	•	•	•	•	•	•	•	•	•	•	•
	•	•	•	•	•	•	•	•	•	•	•
R	•	•	•			•	•	•	•		•

1 4 1 1
1 2
1 2
1 1 1 4
1 C 2
1 1 4. C 2 2
5 1
4 6
1 1
2 4
7 1
9 1
C 4F 2
1 1 1 4
C 1
> B4BB: > B4BB:
, . 4 1 2 1 2
1 H4
7 2 1 , 1
- 4G
1 2 1
4 - H C 4
. 2 , 2
2 7 1 G 1
1 4 8 1
1 1 9 4 7
: 1 1
1 1 : @
- 4H 8 4
HB: A 4 : G 1
C
2 2
- 4
1 8
1 6 4
H 2
1
4 H
K4D : K4BP 2 42 4
2 2 F) 4 HB: :
7 - 2
2 K : <P 42 4' > HAP
1
: LG : LH
4 1

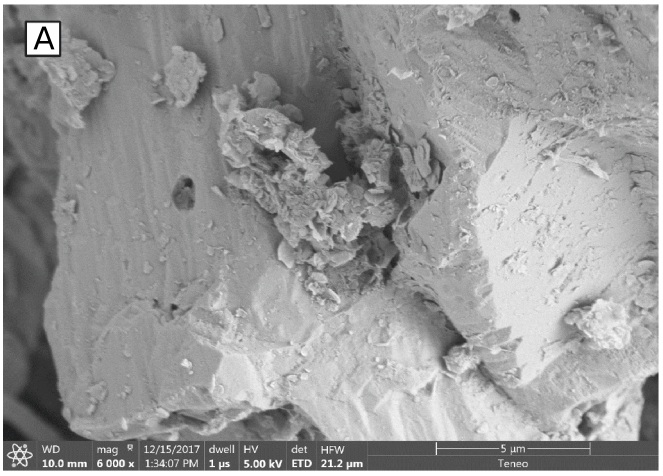

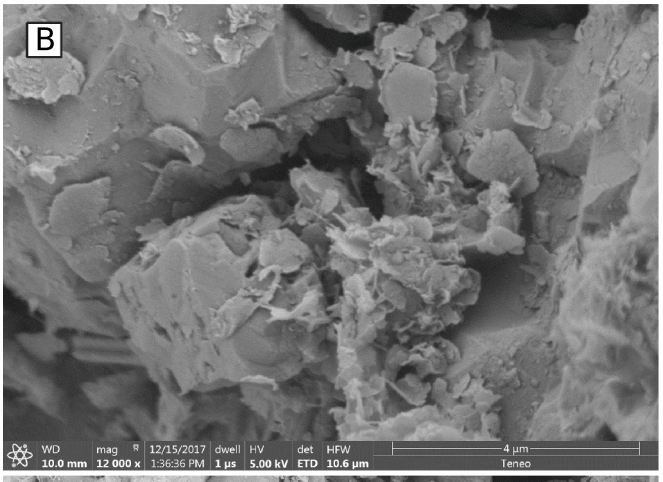

-: 4
74

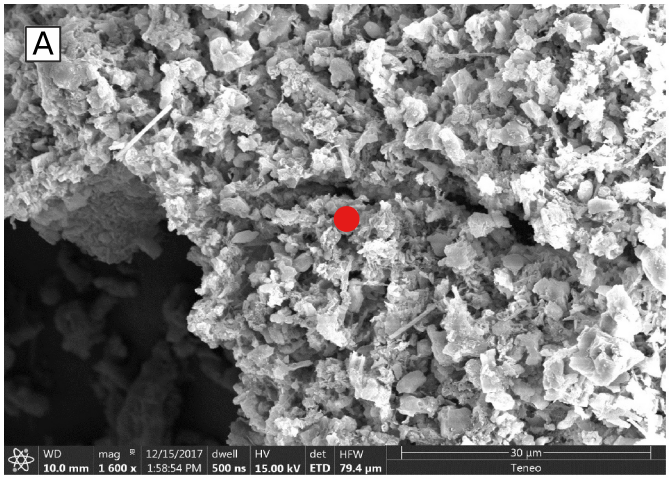
A
WD 10.0 mm
mag 1 600 x
12/15/2017 1:58:54 PM
dwell 500 ns
HV 15.00 kV
det ETD
HFW 79.4 µm
30 µm
Teneo

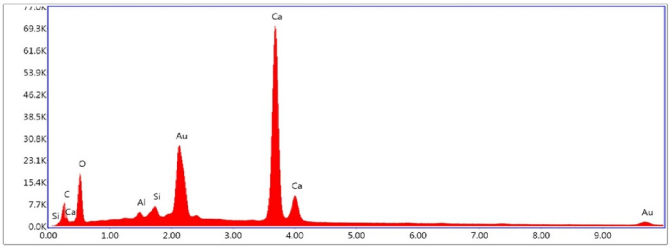
Ca
O
Au
C
Al
Si
Ca
Au

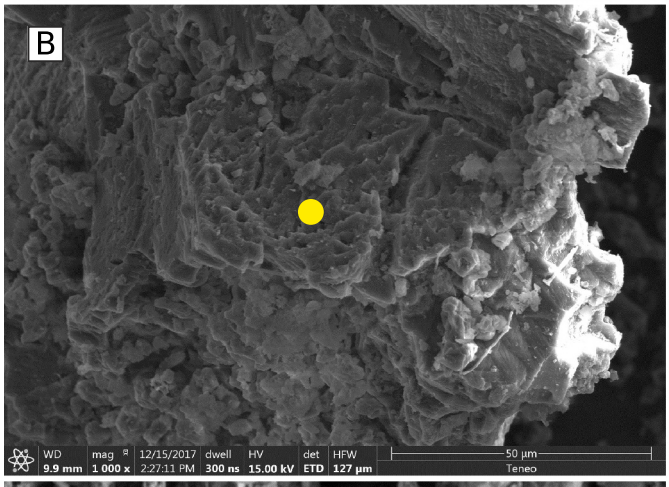
B
WD 9.9 mm
mag 1 000 x
12/15/2017 2:27:11 PM
dwell 300 ns
HV 15.00 kV
det ETD
HFW 127 µm
50 µm
Teneo

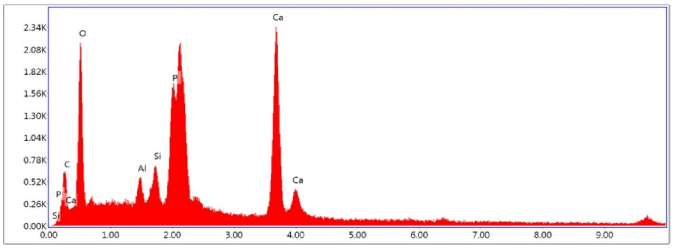
Ca
O
P
C
Al
Si
Ca

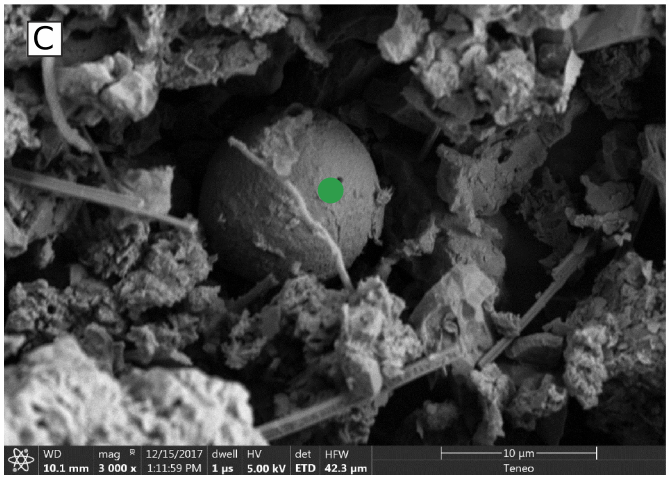
C
WD 10.1 mm
mag 3 000 x
12/15/2017 1:11:59 PM
dwell 1 µs
HV 5.00 kV
det ETD
HFW 42.3 µm
10 µm
Teneo

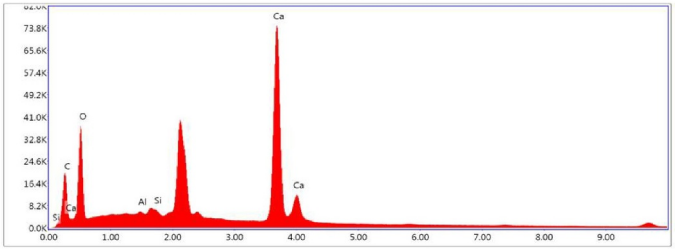
Ca
O
C
Al
Si
Ca

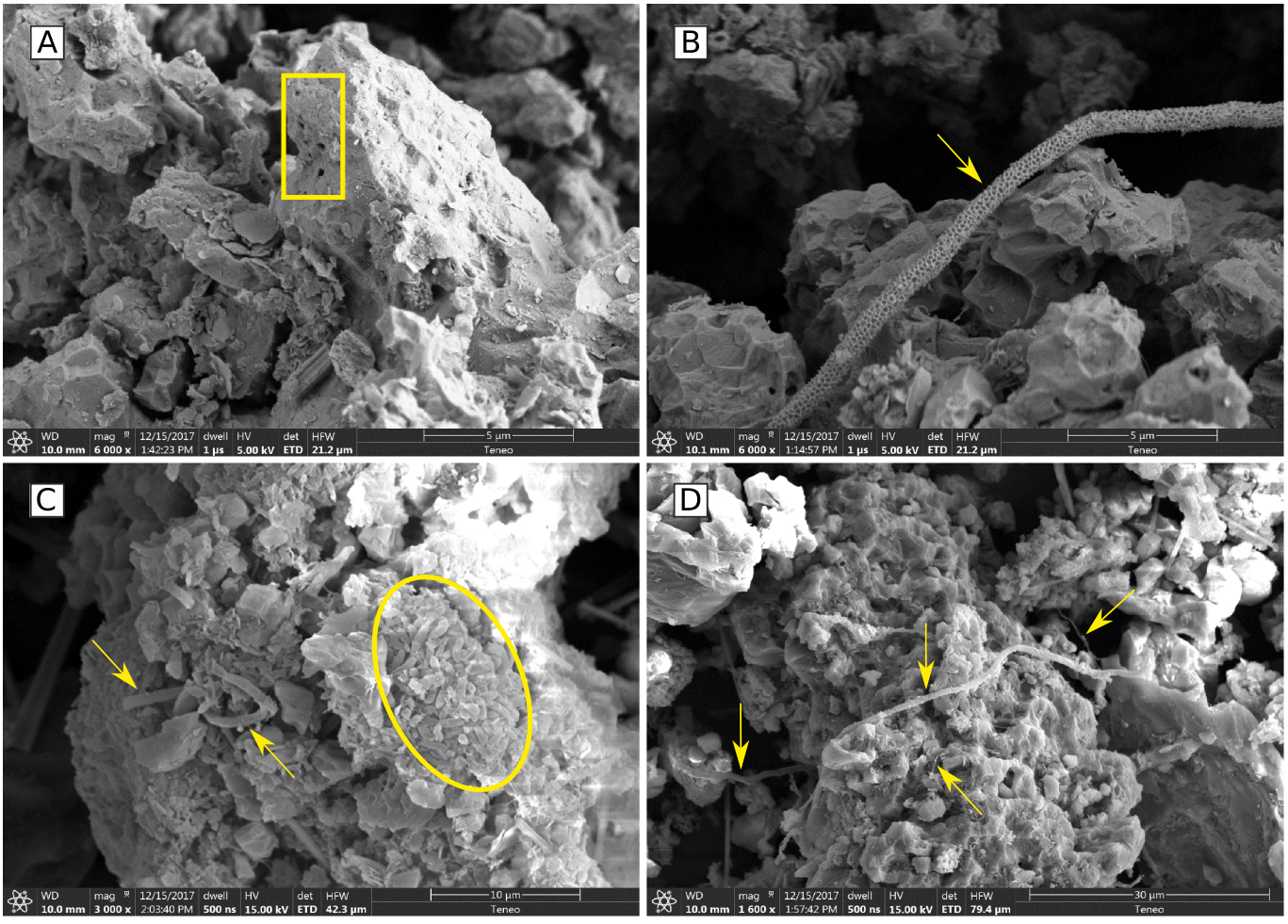
A
B
C
D

Catena 185 (2020) 104339

Contents lists available at ScienceDirect

Catena

journal homepage: www.elsevier.com/locate/catena

Corrigendum

Corrigendum to 'Vermiculations from karst caves: The case of Pertosa-Auletta system (Italy)'. [Catena 182 (2019) 104178]

Rosangela Addesso[a], Alessandro Bellino[a,*], Ilenia Maria D'Angeli[b], Jo De Waele[b], Ana Zelia Miller[c,d], Cristina Carbone[e], Daniela Baldantoni[a]

[a] Department of Chemistry and Biology "Adolfo Zambelli", University of Salerno, Via Giovanni Paolo II, 132, 84084 Fisciano, SA, Italy
[b] Department of Biological, Geological and Environmental Sciences, University of Bologna, Via Zamboni, 67, 40126 Bologna, Italy
[c] HERCULES Laboratory, University of Évora, Largo Marques de Marialva, 8, 7000-809 Évora, Portugal[1]
[d] Instituto de Recursos Naturales y Agrobiología de Sevilla, Consejo Superior de Investigaciones Científicas, Av. Reina Mercedes 10, 41012 Sevilla, Spain
[e] Department for the Earth, Environment and Life Sciences, University of Genoa, Corso Europa, 26, 16126 Genova, Italy

The authors regret the presence of incomplete information in the author affiliations (reported correctly above) and in the acknowledgments of the original article (provided in the amended version below).

The authors are obliged to Mr. Vincenzo Manisera, speleologist of the MIdA Foundation, for sharing his experiences and for his invaluable help in all the field activities, to Dr. Sacha A. Berardo (University of Salerno, Italy) for the language editing, and to the two anonymous reviewers, who provided helpful comments and suggestions. Funding was provided by the Spanish project MINECO CGL2016-75590-P with ERDF funds, by the MIdA Foundation, which generously supported the whole project, and by the University of Salerno, which provided facilities for carrying out the research.

The authors would like to apologise for any inconvenience caused.

DOI of original article: https://doi.org/10.1016/j.catena.2019.104178
* Corresponding author.
E-mail address: abellino@unisa.it (A. Bellino).
[1] Present address.

https://doi.org/10.1016/j.catena.2019.104339

Available online 16 November 2019
0341-8162/

CHAPTER 6

Microbial community characterizing vermiculations from karst caves and its role in their formation

Rosangela Addesso*, Jose L. Gonzalez-Pimentel, Ilenia M. D'Angeli, Jo De Waele, Cesareo Saiz-Jimenez, Valme Jurado, Ana Z. Miller Beatriz Cubero, Giovanni Vigliotta, Daniela Baldantoni

Microbial Ecology 81(2021): 884–896

doi: 10.1007/s00248-020-01623-5

**corresponding author*

An in-depth microbiological characterization of cave vermiculations from the Pertosa-Auletta Cave allowed highlighting the microbial community involved in biogeochemical cycles contributing to their formation processes.

Microbial Ecology
https://doi.org/10.1007/s00248-020-01623-5

ENVIRONMENTAL MICROBIOLOGY

Microbial Community Characterizing Vermiculations from Karst Caves and Its Role in Their Formation

Rosangela Addesso[1] · Jose L. Gonzalez-Pimentel[2] · Ilenia M. D'Angeli[3] · Jo De Waele[3] · Cesareo Saiz-Jimenez[4] · Valme Jurado[4] · Ana Z. Miller[2] · Beatriz Cubero[4] · Giovanni Vigliotta[1] · Daniela Baldantoni[1]

Received: 9 September 2020 / Accepted: 12 October 2020

Abstract

The microbiota associated with vermiculations from karst caves is largely unknown. Vermiculations are enigmatic deposits forming worm-like patterns on cave walls all over the world. They represent a precious focus for geomicrobiological studies aimed at exploring both the microbial life of these ecosystems and the vermiculation genesis. This study comprises the first approach on the microbial communities thriving in Pertosa-Auletta Cave (southern Italy) vermiculations by next-generation sequencing. The most abundant phylum in vermiculations was *Proteobacteria*, followed by *Acidobacteria* > *Actinobacteria* > *Nitrospirae* > *Firmicutes* > *Planctomycetes* > *Chloroflexi* > *Gemmatimonadetes* > *Bacteroidetes* > *Latescibacteria*. Numerous less-represented taxonomic groups (< 1%), as well as unclassified ones, were also detected. From an ecological point of view, all the groups co-participate in the biogeochemical cycles in these underground environments, mediating oxidation-reduction reactions, promoting host rock dissolution and secondary mineral precipitation, and enriching the matrix in organic matter. Confocal laser scanning microscopy and field emission scanning electron microscopy brought evidence of a strong interaction between the biotic community and the abiotic matrix, supporting the role of microbial communities in the formation process of vermiculations.

Keywords Vermicular deposits · Underground ecosystem · Geomicrobiology · Cave ecology · Next-generation sequencing · Pertosa-Auletta Cave

Introduction

The hypogean environments are the least known and studied on Earth [1]. Despite the prohibitive abiotic factors (e.g., oligotrophy, total darkness, and high mineral concentrations) for life development, they represent interesting ecological niches, hosting extremophile microorganisms, highly specialized and perfectly adapted to this peculiar ecosystem, showing an unexpected biodiversity within the *Bacteria* domain and countless novel species [2]. To overcome the limiting factors, microorganisms create mutualistic networks, cooperating in communities and favoring each other's survival. The autotrophic microorganisms generally draw energy by chemosynthesis, using chemical elements (such as Ca, Mg, Fe, Mn, and S) and organic and inorganic compounds abundant in the host rocks, cave sediments, groundwater, and atmosphere. Concurrently, several microbial groups rely on mixed metabolic pathways (mixotrophy) [3]. In any case, such microbial communities may contribute to the formation of caves, influencing several biogeochemical processes [1, 4–7]. In particular, they act inducing the precipitation [8, 9] or dissolution of minerals of speleothems and other structures occurring in underground environments, like moonmilk and vermiculation deposits [10, 11]. The genesis of all these examples is, indeed,

Supplementary Information The online version contains supplementary material available at https://doi.org/10.1007/s00248-020-01623-5.

✉ Rosangela Addesso
raddesso@unisa.it

[1] Department of Chemistry and Biology "Adolfo Zambelli", University of Salerno, Via Giovanni Paolo II, 132, 84084 Fisciano, SA, Italy

[2] HERCULES Laboratory, University of Évora, Largo Marques de Marialva 8, 7000-809 Évora, Portugal

[3] Department of Biological, Geological and Environmental Sciences, University of Bologna, Via Zamboni, 67, 40126 Bologna, Italy

[4] Instituto de Recursos Naturales y Agrobiología de Sevilla, IRNAS-CSIC, Av. Reina Mercedes, 10, 41012 Sevilla, Spain

difficult to be explained only by pure abiotic physicochemical processes [2].

Among cave structures, vermiculations are enigmatic deposits recurring on rock surfaces in caves all over the world [12–14], characterized by variable morphologies, colors, and dimensions [15, 16], and generally composed of calcite, associated with quartz, and traces of clay minerals [17]. Recent studies highlighted microbial evidences supporting their biological origin [10, 17–19]. Vermiculations can be indeed considered "life hotspots" and a precious support for the studies on cave geomicrobiology. To our knowledge, there are still few studies on their microbial characterization and most of these concern vermiculations from sulfuric acid speleogenetic systems [10, 20, 21].

Aimed at shedding light on the microbial community of vermiculations from the Pertosa-Auletta Cave (Campania, southern Italy) and on its role in their formation, this work represents one of the first microbiological studies of vermicular deposits from a normal epigenic karst system. To this end, molecular biology approaches have been employed. In addition, giving an important contribution to the knowledge of the hidden biological aspects of vermiculations, it represents a key step toward the protection and conservation of these peculiar biosignatures and of the whole cave ecosystem.

Methods

Vermiculation Samplings

Eleven different points were sampled in the four main branches of the Pertosa-Auletta Cave (Fig. 1), a limestone show cave in southern Italy. Approximately, 2 g of vermiculation deposits was collected. The four branches of the studied karst cave are characterized by various degrees of frequentation, namely (i) Active (A), (ii) Fossil (F), (iii) Paradise (P), and (iv) Tourist (T), where Active indicates the branch still influenced by an active water flow, Fossil identifies inactive conditions of water flow, Paradise is a short piece of the active branch, lit and frequented by humans, and Tourist is the illuminated trail opened to the public for regular visits.

An accurate description of the study area, as well as on the geochemistry of the vermiculations, is reported in Addesso et al. [17]. In particular, the 11 samples of vermicular deposits, described in detail for their morphology, color, chemical and mineralogical composition [17], showed several shapes as described by Parenzan [15, 22] classification and can be divided into hieroglyphic (A1, A2, A3, F2, T2), dendritic (F1, P1, T1), bubble-like spots (F3), large-leopard spots (F4), and tiger skin (T3). Colors ranged from whitish (A2, F1, T2) to grey (P1, T2) or brown (A1, A3, F1, F3, F4, T3), greenish in P1, probably due to the presence of photoautotrophs [17].

The sampling was performed using disposable and sterile scalpel blades and Eppendorf tubes, carefully avoiding damage to the walls. Stored at 4 °C, the samples were immediately sent to the Instituto de Recursos Naturales y Agrobiologia of Sevilla (IRNAS-CSIC, Spain) and maintained at − 80 °C, until processing.

Molecular Analyses

Total DNA was extracted using FastDNA™ Spin Kit for Soil, according to the producer's protocol (MP Biomedical). The DNA quality was determined by a Nanodrop ND-1000 Spectrophotometer, whereas the amount by a Qubit 2.0 Fluorometer (Invitrogen).

Prokaryotic 16S and eukaryotic 18S rRNA genes were amplified by polymerase chain reaction (PCR), using specific primers: 616F [23] and 1510R [24] for *Bacteria*, 109F and 915R [25] for *Archaea*, EukA and EukB [26] for *Eukarya*, ITS1 and ITS4 [27] for *Fungi*. PCR reactions were carried out using 0.2-mL PCR tubes with a minimal amount of extracted DNA (from 0.5 to 2.0 μL), pure and diluted to 2 and 5 ng/μL, and 50 μL of Mastermix solution [1 mL = 775 μL $H_2O(\sigma)$, 200 μL of PCR Buffer (BIOLINE) and 5 μL Taq Polymerase (BIOLINE), 10 μL specific primers (Reverse and Forward), 4 μL BSA 10%], employing a FlexCycler (Analytik Jena) and a T100 Thermal Cycler (Bio-Rad). The PCR thermal programs are given in Table S1. The amplified PCR products underwent 1% agarose gel electrophoresis (0.5 M TAE Buffer) for a qualitative analysis. Fingerprints of *Archaea* and *Bacteria* communities were obtained by denaturing gradient gel electrophoresis (DGGE) of samples, according to Muyzer et al. [28], using a DCODE™ System (Bio-Rad).

The extracted DNA (with a minimum concentration of ~ 5 ng/μL), after purification by Genomed and Genomic DNA Clean & Concentrator™-10 (Zymo Research), was analyzed by via next-generation sequencing (NGS) targeting the V3–V4 hypervariable region of Prokaryotes 16S rRNA, using Illumina MiSeq 2 × 250 paired end, according to Macrogen (Seoul, Korea) library preparation protocol. Chimeras were identified and removed by means of USEARCH [29]. Resulting reads were processed in Qiime [30], whereas UCLUST [29] was used for the similar sequences assignment to operational taxonomic units (OTUs) by clustering with a 97% similarity threshold. Paired-end reads were merged using FLASH [31]. RDP Release 11 was used as against reference database for taxonomic identification of query sequences. Alpha diversity analysis, including estimation of Chao1, Shannon, Simpson, and Good's Coverage indices, and rarefaction curves, based on the observed species metric, were performed through Qiime.

The graphs relative to molecular analysis data were elaborated in the R 3.6.0 programming environment [32]. The barplots, showing the relative abundances at phylum, class,

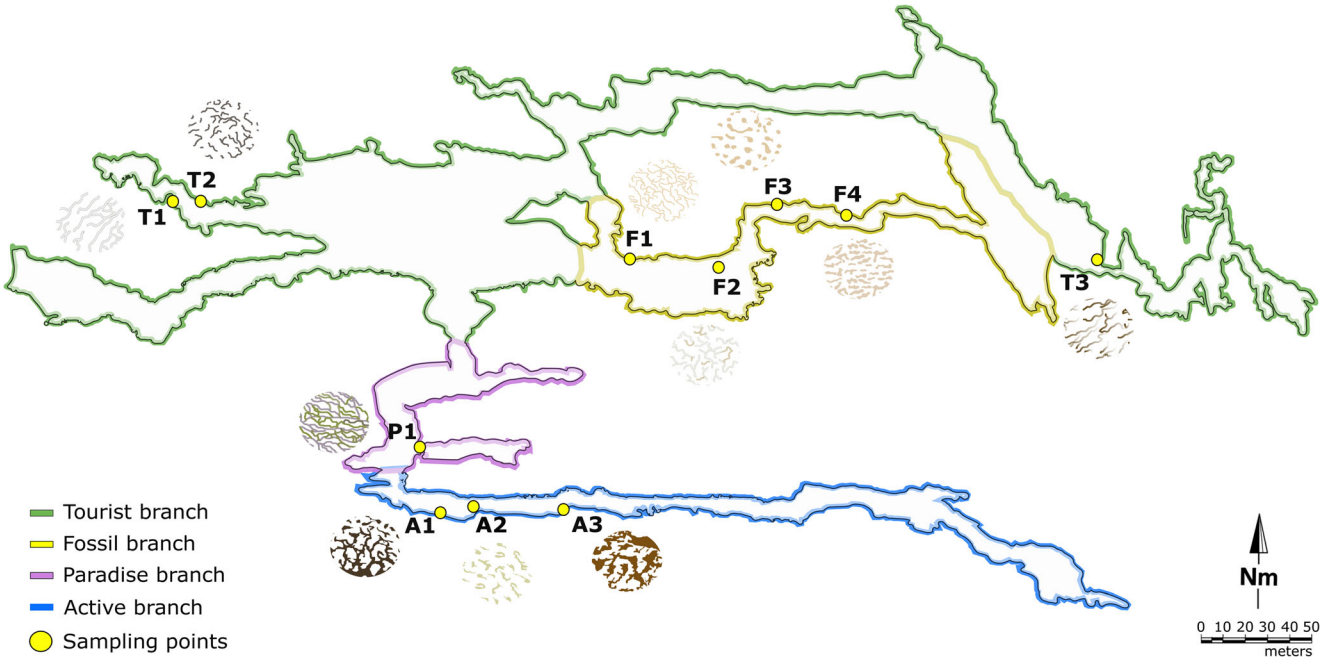

Fig. 1 Pertosa-Auletta Cave (Campania, southern Italy) karst system; yellow points indicate the collected vermiculations, with the corresponding texture model, in the Active (A, blue), Fossil (F, yellow), Paradise (P, violet), and Tourist (T, green) trails

and order levels for each sample, with associated dendrograms explaining the similarities among the samples, were created using "ggplots2", "dendextend", and "RColorBrewer" packages. Pearson's correlation coefficients (*r* values) were obtained using cor function to evaluate associations (for $\alpha = 0.05$) between geochemical characteristics and microbial phyla as well as among biological properties of the analyzed vermiculations. Non-metric multidimensional scaling (NMDS) analysis, with superimposition of confidence ellipses for branches ($\alpha = 0.05$), and principal component analysis (PCA) were performed using meta.mds function, based on Euclidean distance metric, and prcomp function, respectively, both from "vegan" package.

Microscopy

The nucleic acids of the whole cells were visualized using the specific SYBR Green fluorescent dye (1:100 dilution), on samples not handled further, under an Olympus FluoView FV1000 confocal laser scanning microscope, and the 488-nm excitation laser line with emission signal being collected at 510–530 nm. Images were analyzed with the FluoView 2.1 software (Olympus). FESEM images were acquired using FEI Teneo (Thermo Fisher, MA, USA). To this end, samples were prepared as reported in Addesso et al. [17]. In particular, they were fixed with 2.5% glutaraldehyde in 0.1 M cacodylate buffer (pH 7.4) at 4 °C for 2 h and washed thrice in cacodylate buffer. Subsequently, they were treated with 1% osmium tetroxide for 1 h at 4 °C and dehydrated by subsequent dilution series in ethanol and acetone finishing with 100% acetone before drying. The samples were dried in a EM CPD 300 (Leica Microsystem, Wetzlar, Germany) critical point drying device at 34.5 °C. Finally, samples were mounted on SEM stubs and sputter-coated with gold (5–10 nm).

Results

All the 11 studied vermiculations, developing on limestone substratum (except A1 and A3, in the Active branch, which were growing at the interface between limestone host rock and bat guano crusts), showed a considerable biological diversity.

Taxonomic Composition of Microbial Community

The preliminary qualitative analysis on the DNA extracted from vermiculations gave positive results for Prokaryotes and negative results for Eukaryotes. Online Resource 1 displays the archaeal (a) and bacterial (b) 16S rRNA gene-DGGE profiles of the sampled vermiculations. NGS analysis of 16S rRNA gene identified archaeal and bacterial taxa. *Archaea* were scarcely represented (Table 1). At the phylum level, *Thaumarchaeota* was characterized in all the vermiculations, with a relative abundance varying between 0.01 and 0.07%: *Woesearchaeota* was present in all the samples (0.01–0.04%), except for A2, P1, and T3, whereas *Euryarchaeota* was detected in F3 (0.01%) and P1 (0.03%). Moreover, unclassified *Archaea* were found in A3, F1, F2, F3, P1, T1, and T2 in percentages ranging from 0.01 and 0.09% (Table 1).

Table 1 Relative abundance (%) of *Archaea* at phylum level for each vermiculation sample

Phylum	A1	A2	A3	F1	F2	F3	F4	P1	T1	T2	T3
Unclassified	–	–	0.01	0.04	0.08	0.05	–	0.01	0.09	0.02	–
Euryarchaeota	–	–	–	–	–	0.01	–	0.03	–	–	–
Thaumarchaeota	0.01	0.06	0.06	0.05	0.07	0.05	0.05	0.03	0.07	0.05	0.06
Woesearchaeota	0.01	–	0.01	0.03	0.03	0.02	0.01	–	0.04	0.02	–

Bacteria composed almost the entire extracted DNA (Fig. 2). The major phylum in the total bacterial community was *Proteobacteria* (41.3–54.8%), followed by *Acidobacteria* (7.1–16.8%) > *Actinobacteria* (1.9–33.8%) > *Nitrospirae* (2.8–13.3%) > *Firmicutes* (1.5–6.6%) > *Planctomycetes* (2.0–4.2%) > *Chloroflexi* (0.9–2.7%) > *Gemmatimonadetes* (0.6–1.7%) > *Bacteroidetes* (0.04–1.7%) > *Latescibacteria* (0.2–1.3%). NGS analysis highlighted the presence of a very copious group of unclassified phyla with percentage ranging from 6.2 and 19.3%. Other 16 phyla were less represented (< 1%). The microbial abundances were very similar in all the vermiculations, except P1, dominated by *Actinobacteria* (33.8%) in addition to *Proteobacteria* (41.3%) (Fig. 2a). The most abundant classes within the *Proteobacteria* phylum were as follows: *Gamma-* (19.3–35.8%) > *Beta-* (6.3–17.4%) > *Alpha-* (4.6–7.2%) > *Delta-* (3.3–5.9%) (Fig. 2b). At the order level (Fig. 2c), *Gammaproteobacteria* was mainly represented by an ample unclassified group (17.7–33.1%) and by *Xanthomonadales* (< 2.3%), whereas *Alphaproteobacteria* included the *Rhizobiales* (1.7–5.1%) and *Rhodospirillales* (1.1–3.6%) orders. *Nitrospirales* > *Actinomycetales* > *Thermoanaerobacterales* > *Planctomycetales* > *Gemmatimonadales* > *Gaiellales* > *Anaerolineales* were also identified with an abundance below 5.9%. Numerous unclassified groups were present at the order level, increasing considerably in the subsequent taxonomic levels.

The dendrograms (Fig. 2), showing similarities and divergences between specimens based on taxon relative abundances, highlighted three groups, keeping enough in the graph representations of all three taxonomic levels. The clustering analysis showed a clear separation of P1, the only sample located in Paradise branch, from the other two groups, closer to each other (Fig. 2a–c). At the phylum level (Fig. 2a), A2, F1, F3, and T2 clustered together from the rest (A1, A3, F2, F4, T1, T3). At the class level (Fig. 2b), F2 grouped with A2, F1, F3, and T2, splitting up from A1, A3, F4, T1, and T3. Lastly, at the order level (Fig. 2c), F1, F3, F4, and T2 assembled a new cluster divided from the remaining samples. Figure 2 also shows the corresponding PCAs based on the total bacterial communities at the phylum (Fig. 2d), class (Fig. 2e), and order (Fig. 2f) levels. Analogous clusters of the dendrograms were also observed in PCA plots. The first (PC1) and the second (PC2) principal components accounted together for 86.04%, 83.81% and 84.73% of the data variance, respectively for phylum, class, and order taxonomic levels.

Microbial Community Richness and Diversity

The rarefaction curve plots, built based on the number of observed microbial groups vs. the number of sequences per sample, for both the four branches and the 11 individual samples, are reported in Online Resource 2 (a and b, respectively). Most curves tended to approach the saturation plateau, reinforcing the sufficiency of sequencing analysis, adequately representative of the investigated communities.

Alpha diversity estimation, using several metrics, is reported in Table 2. The total OTUs generated for each sample ranged from a maximum of 2127 to a minimum of 1323, whereas the average value of Good's Coverage was 99.78%, indicating that the analysis well covers the microbial diversity in vermiculation samples. Chao1 richness estimator resulted between 1444.8 and 2313.3. Shannon and Simpson diversity indices presented similar estimates among the samples (around 7 and close to 1, respectively), except for P1, which presented the lowest values (5.78 and 0.87, respectively).

Relationships Between Microbial Community and Geochemical Characteristics

Pearson's correlation coefficients between microbial phyla and geochemical and mineralogical characteristics [17] of each vermiculation are shown in Table 3a. *Deferribacteres*, *Latescibacteria*, and *Nitrospirae* displayed positive correlations ($0.74 < r < 0.77$; $p < 0.01$), with organic C, P, and Mo, respectively. Unclassified *Archaea*, *Armatimonadetes*, and *Ignavibacteriae* were negatively correlated ($0.61 < r < 0.66$; $p < 0.05$) with S. *Chloroflexi* were positively related with Ca, Mg, Sr, Ti, V, and Zn ($0.60 < r < 0.65$; $p < 0.05$), but negatively with C ($r =$ 0.66; $p < 0.05$). *Spirochaetes* were negatively correlated with Ca, Fe, Mg, Ti, Li, V, Cr, Zn, Cu, and quartz (with r values ranging from 0.61 to 0.67, and $p < 0.05$), and positively correlated with C and calcite (with correlation coefficients equal to 0.66 and 0.61, respectively and p values < 0.05). Furthermore, *N* showed a positive correlation with *Deferribacteres* phylum ($r = 0.70$; $p < 0.05$) and a negative relationship with *Elusimicrobia* phylum ($r =$

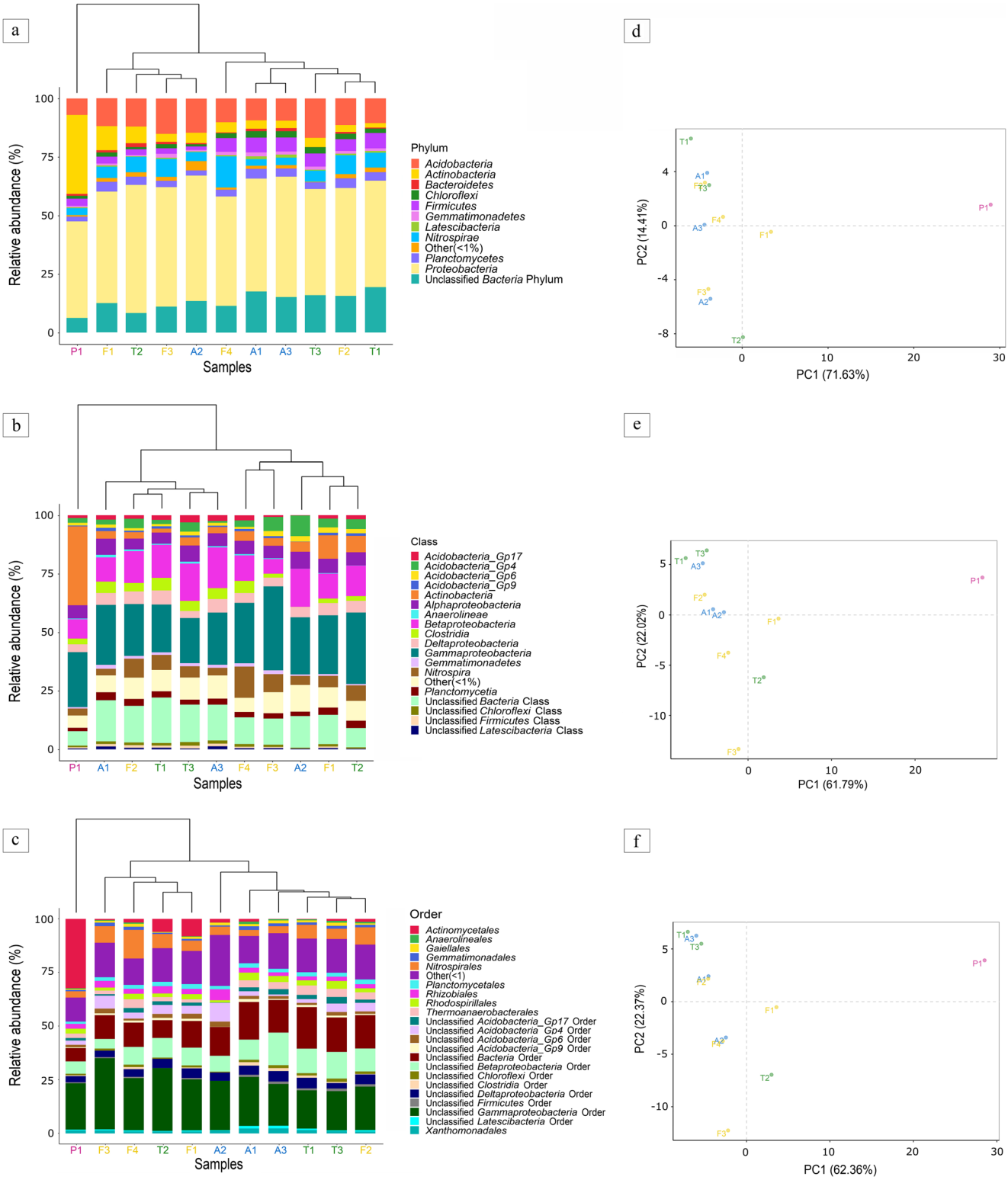

Fig. 2 Bacterial composition of vermiculations from Pertosa-Auletta Cave; the barplots show the relative abundances (%) at phylum (**a**), class (**b**), and order (**c**) levels of samples from the Active (A, blue), Fossil (F, yellow), Paradise (P, violet), and Tourist (T, green) branches, with corresponding dendrograms (**a**, **b**, **c**) and PCA analysis (**d**, **e**, **f**)

Table 2 Community richness and diversity estimated for each sample, using several alpha diversity metrics (Good's Coverage, Chao1, Shannon, Simpson)

Sample	Operational taxonomic units	Good's Coverage (%)	Chao1	Shannon	Simpson
A1	1431	99.88	1553.3	7.128	0.968
A2	1597	99.78	1780.1	7.265	0.978
A3	1712	99.81	1877.9	7.409	0.971
F1	2127	99.72	2313.3	7.739	0.977
F2	1963	99.60	2310.9	7.669	0.978
F3	1891	99.82	2009.6	7.228	0.952
F4	1730	99.73	1988.5	7.055	0.963
P1	1728	99.82	1909.3	5.784	0.874
T1	1929	99.80	2101.7	7.567	0.979
T2	1521	99.73	1705.6	7.149	0.969
T3	1323	99.88	1444.8	6.920	0.973

0.67; $p < 0.05$), whereas *Verrucomicrobia* revealed a negative correlation with Co, K, Mn, and N ($-0.63 < r < -0.65$; $p < 0.05$). Among the *Archaea* phyla, *Woesearchaeota* was positively correlated with organic C, showing a correlation coefficient of 0.64 (p value < 0.05).

The correlation analysis results between microbial groups identified in the 11 studied vermiculations are reported in Table 3b. Positive correlations ($p < 0.001$) among several groups were observed: unclassified *Archaea* phylum with *Woesearchaeota* ($r = 0.92$), *Euryarchaeota* with *Actinobacteria* ($r = 0.85$), *Lentisphaerae* with *Ignavibacteriae* ($r = 0.86$), and *Cyanobacteria*/Chloroplast with *Parcubacteria* ($r = 0.96$). *Spirochaetes* is the only one displayed highly negative correlation with *Firmicutes* ($r = -0.90$; $p < 0.001$). Moreover, *Chloroflexi* were positively correlated with *Gemmatimonadetes* ($r = 0.79$; $p < 0.01$), *Firmicutes* ($r = 0.83$; $p < 0.01$), and unclassified *Bacteria* phylum ($r = 0.65$; $p < 0.05$), but negatively with *Spirochaetes* ($r = -0.80$; $p < 0.01$) and *Cyanobacteria*/Chloroplast ($r = -0.65$; $p < 0.05$), whereas *Woesearchaeota* showed a positive correlation with *Verrucomicrobia* ($r = 0.83$; $p < 0.01$) and *Planctomycetes* ($r = 0.70$; $p < 0.05$). *Proteobacteria* displayed a positive correlation with *Candidatus* Saccharibacteria ($r = 0.77$; $p < 0.01$) and *Cyanobacteria*/Chloroplast ($r = 0.62$; $p < 0.05$); *candidate division WPS-1* was positively related with *Armatimonadetes* ($r = 0.79$; $p < 0.01$), *Cyanobacteria*/Chloroplast ($r = 0.74$; $p < 0.01$), *Parcubacteria* ($r = 0.81$; $p < 0.01$), and *Elusimicrobia* ($r = 0.68$; $p < 0.05$), but negatively correlated with *Firmicutes* ($r = -0.62$; $p < 0.05$). Unclassified *Bacteria* phylum showed a negative correlation with *Actinobacteria*, *Spirochaetes*, and *Euryarchaeota* ($-0.60 < r < -0.70$; $p < 0.05$), but it was positively correlated with *Firmicutes* ($r = 0.69$; $p < 0.05$). *Latescibacteria* showed a positive correlation with *Gemmatimonadetes* ($r = 0.61$; $p < 0.05$) and *Firmicutes* ($r = 0.68$; $p < 0.05$), whereas *Armatimonadetes* with *Elusimicrobia*, *Hydrogenedentes* and *candidate division WPS-2*, with correlation coefficients ranging from 0.62 to 0.71 and p value < 0.05. *Omnitrophica* were positively correlated ($p < 0.05$) with unclassified *Archaea* phylum ($r = 0.67$) and *Thaumarchaeota* ($r = 0.62$). Finally, *Verrucomicrobia* highlighted a positive correlation with unclassified *Archaea* phylum ($r = 0.73$; $p < 0.05$), *Gemmatimonadetes* with *Firmicutes* ($r = 0.62$; $p < 0.05$), and *Elusimicrobia* with *Parcubacteria* ($r = 0.68$; $p < 0.05$).

The NMDS biplot (Fig. 3), based on the microbiological and geochemical-mineralogical [17] characteristics of the analyzed vermicular deposits, showed a clear separation of the confidence ellipses grouping the Tourist and Fossil branches. The vermicular deposits from the active trail revealed intermediate characteristics, as highlighted by the partial overlapping of its confidence ellipse with the other two. Between the two most abundant minerals (calcite and quartz), calcite characterized the vermiculations from the four trails, whereas quartz mainly those of the Tourist and Active trails. Among the 24 elements (total Al, Ba, C, Ca, Co, Cr, Cu, Fe, K, Li, Mg, Mn, Mo, N, Na, Ni, P, S, Si, Sr, Ti, V, and Zn and organic C) analyzed, N, S, and organic C, mostly abundant in the vermiculations from the lightened trails (Paradise and Tourist), together with C, and to a lesser extent Mo, P, and Sr, showed a strong relationship with bacterial communities.

Confocal microscopic observations performed on samples A4 (Fig. 4a, b), F1 (Fig. 4c), and T1 (Fig. 4d) provided interesting information about the distribution and density of microbial communities (green-colored zones) on the mineral surface. As revealed by FESEM images (Online Resource 3), microbial structures were found mainly associated with clay minerals.

Discussion

Although vermiculations represent a perfect substratum suitable for microbes, probably participating also to their formation as mediators of geochemical processes [10, 20], very little is known about the microbiota of such enigmatic deposits. In this context, our study provides, for the first time, an overview

Table 3 Pearson correlation matrices between microbial phyla and geochemical characteristics of the studied vermiculations (a) and among their biological properties (b). Significant (***p < 0.001; **p < 0.01; *p < 0.05) correlation coefficients are also highlighted (positive in red, negative in blue)

a

	Si	Al	Ca	Na	F e	Mg	K	Ti	P	Mn	C	C org	S	Sr	Ba	Li	V	Cr	N	Ni	Zn	Cu	Co	Mo	Calcite	Quartz
Unclassified *Archaea*Phylum	-0.42	-0.39	-0.45	-0.39	-0.42	-0.41	-0.38	-0.45	-0.53	-0.33	0.43	0.53	-0.61*	-0.35	-0.39	-0.44	-0.47	-0.46	-0.23	-0.47	-0.52	-0.49	-0.39	-0.28	0.40	-0.40
Euryarchaeota	-0.15	-0.15	-0.16	-0.28	-0.16	-0.15	-0.07	-0.12	-0.22	-0.14	0.17	-0.16	-0.02	-0.20	-0.15	-0.17	-0.14	-0.02	0.01	-0.02	-0.20	-0.	21	-0.16	0.01	0.14	-0.14
Thaumarchaeota	-0.49	-0.54	-0.39	-0.50	-0.41	-0.30	-0.12	-0.35	-0.31	0.14	0.39	0.26	-0.27	-0.41	-0.57	-0.46	-0.41	-0.49	-0.31	-0.34	-0.40	-0.4	4	-0.07	-0.09	0.54	-0.54
Woesearchaeota	-0.27	-0.23	-0.34	-0.20	-0.30	-0.34	-0.38	-0.37	-0.38	-0.38	0.33	0.64*	-0.44	-0.23	-0.22	-0.30	-0.35	-0.35	-0.02	-0.41	-0.38	-0.33	-0.38	-0.29	0.25	-0.25
Unclassified *Bacteria* Phylum	0.45	0.44	0.45	0.45	0.44	0.44	0.36	0.42	0.29	0.29	-0.51	-0.10	-0.29	0.57	0.43	0.43	0.44	0.36	-0.50	0.32	0.40	0.39	0.37	-0.19	-0.43	0.43
Acidobacteria	0.07	0.03	0.18	0.08	0.17	0.29	0.37	0.21	-0.26	0.54	-0.14	-0.09	-0.03	0.09	-0.03	0.10	0.16	0.07	-0.09	0.21	0.13	0.13	0.43	-0.21	-0.01	0.01
Actinobacteria	-0.19	-0.18	-0.21	-0.27	-0.19	-0.21	-0.13	-0.17	-0.34	-0.15	0.25	0.03	0.17	-0.27	-0.19	-0.20	-0.19	-0.06	0.30	-0.05	-0.25	-0.22	-0.17	-0.04	0.18	-0.18
Armatimonadetes	-0.05	-0.05	-0.07	0.02	-0.09	-0.07	-0.20	-0.12	0.00	-0.20	0.00	-0.32	-0.62*	0.11	-0.04	-0.07	-0.09	-0.17	-0.55	-0.23	-0.12	-0.14	-0.17	-0.03	0.06	-0.06
Bacteroidetes	-0.14	-0.10	-0.25	-0.05	-0.22	-0.33	-0.43	-0.28	0.20	-0.50	0.25	0.25	0.29	-0.17	-0.05	-0.22	-0.21	-0.20	0.52	-0.29	-0.23	-0.17	-0.42	-0.37	0.12	-0.12
Chlamydiae	0.01	0.07	-0.10	0.06	-0.07	-0.17	-0.33	-0.16	-0.01	-0.46	0.10	0.48	0.02	0.01	0.11	-0.05	-0.10	-0.11	0.30	-0.22	-0.13	-0.05	-0.3	4	-0.34	-0.04	0.04
Chloroflexi	0.59	0.56	0.61*	0.59	0.59	0.60*	0.58	0.61*	0.57	0.46	-0.66*	-0.36	-0.03	0.65*	0.56	0.60	0.62*	0.57	-0.38	0.55	0.65*	0.59	0.55	0.12	-0.57	0.57
Deferribacteres	-0.37	-0.34	-0.41	-0.24	-0.36	-0.42	-0.41	-0.42	-0.24	-0.28	0.48	0.74**	0.33	-0.48	-0.33	-0.37	-0.41	-0.41	0.70*	-0.40	-0.34	-0.27	-0.34	-0.08	0.35	-0.35
Elusimicrobia	-0.35	-0.34	-0.35	-0.34	-0.39	-0.38	-0.46	-0.40	0.13	-0.41	0.26	-0.41	-0.59	-0.22	-0.32	-0.34	-0.36	-0.41	-0.67*	-0.48	-0.37	-0.42	-0.43	0.23	0.32	-0.32
Gemmatimonadetes	0.51	0.50	0.51	0.50	0.48	0.51	0.43	0.49	0.52	0.25	-0.58	-0.41	-0.21	0.56	0.53	0.53	0.50	0.45	-0.48	0.40	0.57	0.49	0.36	0.28	-0.	51	0.51
Lentisphaerae	-0.27	-0.24	-0.27	-0.23	-0.25	-0.25	-0.29	-0.29	-0.28	-0.20	0.23	-0.13	-0.57	-0.24	-0.24	-0.28	-0.29	-0.28	-0.37	-0.32	-0.36	-0	.34	-0.23	-0.21	0.22	-0.22
Planctomycetes	0.23	0.26	0.15	0.37	0.18	0.10	-0.03	0.10	0.17	-0.12	-0.17	0.31	-0.10	0.27	0.29	0.20	0.15	0.12	0.08	0.02	0.16	0.20	-0.01	-0.20	-	0.25	0.25
Proteobacteria	-0.14	-0.14	-0.17	-0.06	-0.18	-0.21	-0.30	-0.21	0.28	-0.25	0.17	0.02	0.20	-0.13	-0.11	-0.19	-0.16	-0.26	0.22	-0.28	-0.14	-0.12	-0.24	-0.18	0.15	-0.15
Spirochaetes	-0.60	-0.58	-0.63*	-0.54	-0.61*	-0.61*	-0.60	-0.63*	-0.46	-0.49	0.66*	0.26	-0.09	-0.60	-0.57	-0.64*	-0.62*	-0.62*	0.31	-0.60	-0.67*	-0.62*	-0.57	-0.30	0.61*	-0.61*
Verrucomicrobia	-0.42	-0.38	-0.51	-0.31	-0.49	-0.54	-0.63*	-0.55	-0.02	-0.65*	0.44	0.34	-0.52	-0.32	-0.33	-0.45	-0.50	-0.53	-0.21	-0.63*	-0.48	-0.48	-0.63*	-0.01	0.39	-0.39
BRC1	-0.20	-0.20	-0.19	-0.22	-0.20	-0.14	-0.13	-0.17	-0.11	-0.15	0.15	-0.19	-0.39	-0.13	-0.18	-0.22	-0.19	-0.21	-0.30	-0.20	-0.22	-0	.25	-0.18	-0.14	0.22	-0.22
***Candidatus* Saccharibacteria**	-0.54	-0.55	-0.55	-0 .51	-0.55	-0.57	-0.53	-0.55	0.07	-0.37	0.56	0.28	0.22	-0.54	-0.53	-0.59	-0.53	-0.59	0.27	-0.55	-0.52	-0.51	-0.47	-0.30	0.56	-0.56
***Cyanobacteria*/Chloroplast**	-0.19	-0.18	-0.19	-0.19	-0.20	-0.21	-0.27	-0.22	-0.09	-0.16	0.20	-0.10	0.04	-0.19	-0.19	-0.22	-0.20	-0.23	0.07	-0.24	-0.25	-0.2	1	-0.19	-0.17	0.19	-0.19
Firmicutes	0.45	0.44	0.46	0.44	0.44	0.43	0.42	0.45	0.48	0.30	-0.50	-0.02	0.04	0.48	0.45	0.48	0.45	0.42	-0.27	0.40	0.53	0.47	0.37	0.29	-0.4	6	0.46
Hydrogenedentes	-0.18	-0.18	-0.20	-0.08	-0.21	-0.20	-0.24	-0.23	-0.16	-0.23	0.19	0.02	-0.36	-0.10	-0.17	-0.17	-0.21	-0.24	-0.15	-0.27	-0.19	-0.	19	-0.24	0.19	0.19	-0.19
Ignavibacteriae	-0.47	-0.45	-0.49	-0.46	-0.49	-0.47	-0.49	-0.50	-0.21	-0.42	0.42	-0.24	-0.66*	-0.40	-0.44	-0.51	-0.49	-0.48	-0.46	-0.52	-0.56	-0.57	-0.47	-0.22	0.44	-0.44
Latescibacteria	0.43	0.44	0.36	0.45	0.34	0.27	0.12	0.32	0.77**	-0.10	-0.45	-0.34	-0.09	0.54	0.48	0.37	0.39	0.35	-0.35	0.22	0.39	0.35	0.08	-0.06	-0.44	0.44
Nitrospirae	-0.38	-0.37	-0.34	-0.32	-0.35	-0.31	-0.27	-0.35	-0.13	-0.19	0.35	0.19	-0.23	-0.43	-0.34	-0.28	-0.39	-0.41	-0.12	-0.39	-0.21	-0.	27	-0.28	0.76**	0.35	-0.35
Omnitrophica	-0.53	-0.50	-0.54	-0.54	-0.54	-0.54	-0.51	-0.55	-0.24	-0.42	0.50	0.44	-0.41	-0.46	-0.50	-0.53	-0.55	-0.56	-0.27	-0.57	-0.56	-0.	56	-0.50	-0.03	0.50	-0.50
Parcubacteria	-0.20	-0.20	-0.18	-0.21	-0.20	-0.19	-0.24	-0.21	-0.07	-0.13	0.16	-0.23	-0.14	-0.14	-0.21	-0.23	-0.19	-0.23	-0.18	-0.23	-0.27	-0	.25	-0.16	-0.23	0.20	-0.20
candidatedivisionWPS-1	-0.26	-0.25	-0.26	-0.22	-0.28	-0.26	-0.33	-0.29	-0.19	-0.25	0.22	-0.35	-0.43	-0.16	-0.26	-0.28	-0.27	-0.30	-0.32	-0.33	-0.35	-0	.33	-0.27	-0.13	0.26	-0.26
candidatedivisionWPS-2	0.13	0.16	0.06	0.13	0.05	0.01	-0.17	0.00	0.06	-0.28	-0.14	-0.15	-0.50	0.27	0.17	0.07	0.05	0.01	-0.46	-0.11	-0.04	-0.02	-0.17	-0.27	-0.14	0.14

Table 3 (continued)

b

	Unclassified *Archaea* Phylum	*Euryarchaeota*	*Thaumarchaeota*	*Woesearchaeota*	Unclassified *Bacteria* Phylum	*Acidobacteria*	*Actinobacteria*	*Armatimonadetes*	*Bacteroidetes*	*Chlamydiae*	*Chloroflexi*	*Deferribacteres*	*Elusimicrobia*	*Gemmatimonadetes*	*Lentisphaerae*	*Planctomycetes*	*Proteobacteria*	*Spirochaetes*	*Verrucomicrobia*	*BRC1*	*Candidatus* Saccharibacteria	*Cyanobacteria* Chloroplast	*Firmicutes*	*Hydrogenedentes*	*Ignavibacteriae*	*Latescibacteria*	*Nitrospirae*	*Omnitrophica*	*Parcubacteria*	*candidate division WPS-1*	*candidate division WPS-2*
Unclassified *Archaea* Phylum	1																														
Euryarchaeota	-0.14	1																													
Thaumarchaeota	0.52	-0.42	1																												
Woesearchaeota	0.92***	-0.33	0.33	1																											
Unclassified *Bacteria* Phylum	0.33	-0.61*	0.37	0.36	1																										
Acidobacteria	-0.01	-0.41	0.50	-0.10	0.17	1																									
Actinobacteria	-0.23	0.85***	-0.47	-0.32	-0.70*	-0.50	1																								
Armatimonadetes	0.16	-0.50	0.22	0.19	0.39	0.36	-0.46	1																							
Bacteroidetes	-0.02	0.05	-0.41	0.21	-0.36	-0.32	0.11	-0.21	1																						
Chlamydiae	0.29	-0.26	-0.16	0.50	0.13	-0.11	-0.27	0.09	0.56	1																					
Chloroflexi	0.00	-0.23	0.01	0.03	0.65*	-0.05	-0.41	-0.05	-0.24	-0.33	1																				
Deferribacteres	0.28	-0.38	0.13	0.47	-0.27	-0.06	-0.11	-0.22	0.56	0.37	-0.31	1																			
Elusimicrobia	0.06	-0.26	0.36	-0.06	0.25	0.00	-0.24	0.62*	-0.34	-0.10	-0.14	-0.26	1																		
Gemmatimonadetes	0.04	-0.11	-0.10	0.04	0.49	0.08	-0.51	0.04	-0.19	-0.06	0.79**	-0.41	-0.12	1																	
Lentisphaerae	0.45	-0.15	0.37	0.27	0.14	0.22	-0.23	0.20	-0.08	-0.10	-0.02	0.14	0.44	-0.02	1																
Planctomycetes	0.45	-0.58	-0.01	0.70*	0.51	-0.18	-0.46	0.20	0.33	0.33	0.47	0.47	-0.17	0.26	0.11	1															
Proteobacteria	-0.19	-0.49	0.08	-0.03	-0.08	0.37	-0.49	0.28	0.55	0.54	-0.34	0.39	0.15	-0.12	0.06	0.05	1														
Spirochaetes	0.12	0.12	0.00	0.15	-0.60*	0.21	0.23	0.25	0.52	0.32	-0.80**	0.39	-0.01	-0.58	0.06	-0.16	0.51	1													
Verrucomicrobia	0.73*	-0.32	0.23	0.83**	0.26	-0.31	-0.32	0.35	0.32	0.36	0.10	0.41	0.21	0.10	0.22	0.70*	0.09	0.19	1												
BRC1	0.25	0.31	0.04	0.12	-0.18	0.34	-0.11	0.13	0.18	0.13	-0.05	-0.23	-0.17	0.41	0.10	-0.19	0.21	0.41	0.13	1											
Candidatus Saccharibacteria	0.06	-0.18	0.34	0.08	-0.23	0.13	-0.19	-0.11	0.58	0.42	-0.44	0.49	0.11	-0.36	0.14	-0.10	0.77**	0.52	0.16	0.18	1										
Cyanobacteria/ Chloroplast	-0.29	-0.26	0.14	-0.30	-0.13	0.35	-0.10	0.36	0.03	0.26	-0.65*	0.07	0.53	-0.56	0.22	-0.40	0.62*	0.43	-0.30	-0.18	0.48	1									
Firmicutes	0.12	-0.26	0.09	0.18	0.69*	-0.31	-0.36	-0.18	-0.33	-0.12	0.83**	-0.19	-0.06	0.62*	-0.18	0.44	-0.43	-0.90***	0.19	-0.33	-0.41	-0.60	1								
Hydrogenedentes	0.17	-0.24	-0.01	0.29	0.01	-0.01	-0.03	0.67*	-0.07	-0.10	-0.06	0.06	0.18	-0.12	-0.18	0.36	-0.09	0.32	0.49	-0.01	-0.33	-0.12	-0.11	1							
Ignavibacteriae	0.45	0.15	0.27	0.23	-0.09	0.10	-0.05	0.17	0.13	-0.11	-0.08	0.02	0.38	0.04	0.86***	-0.02	0.10	0.29	0.33	0.47	0.28	0.08	-0.33	-0.11	1						
Latescibacteria	0.01	-0.13	-0.24	0.13	0.56	-0.46	-0.29	0.01	0.24	0.13	0.74	-0.25	0.02	0.61*	-0.12	0.52	-0.05	-0.53	0.36	-0.02	-0.11	-0.45	0.68*	-0.07	-0.01	1					
Nitrospirae	0.27	-0.20	0.31	0.22	-0.11	0.10	-0.32	0.05	-0.28	-0.12	0.00	0.27	0.18	0.27	0.19	0.02	-0.02	-0.05	0.31	0.15	-0.05	-0.18	0.14	0.19	0.14	-0.27	1				
Omnitrophica	0.67*	-0.19	0.62*	0.57	0.36	-0.24	-0.18	0.07	-0.18	0.27	-0.14	0.17	0.49	-0.21	0.31	0.12	-0.10	-0.10	0.51	-0.22	0.28	0.11	0.25	-0.08	0.22	0.03	0.22	1			
Parcubacteria	-0.21	-0.27	0.27	-0.28	0.04	0.36	-0.13	0.49	-0.12	0.14	-0.52	-0.11	0.68*	-0.50	0.30	-0.39	0.50	0.33	-0.25	-0.18	0.40	0.96***	-0.50	-0.07	0.17	-0.34	-0.25	0.20	1		
candidatedivision WPS-1	-0.10	-0.20	0.13	-0.15	-0.06	0.36	-0.05	0.79**	-0.13	-0.03	-0.49	-0.16	0.68*	-0.43	0.31	-0.23	0.35	0.52	-0.01	0.02	0.11	0.74**	-0.62*	0.44	0.29	-0.37	-0.13	-0.01	0.81**	1	
candidatedivision WPS-2	0.20	-0.36	0.08	0.25	0.56	0.05	-0.35	0.71*	-0.13	0.50	-0.12	-0.32	0.58	-0.01	0.10	0.14	0.23	0.04	0.24	-0.05	-0.01	0.47	0.00	0.21	0.01	0.21	-0.28	0.38	0.58	0.55	1

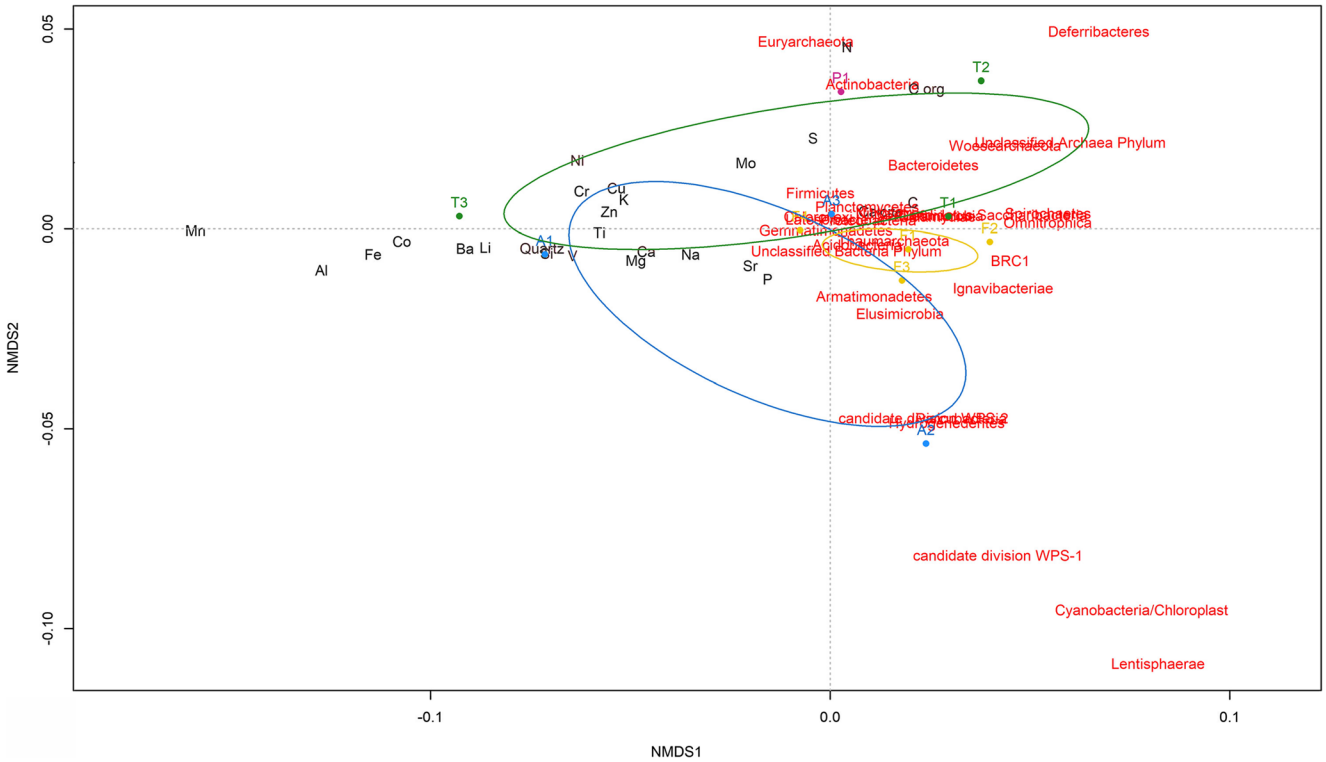

Fig. 3 NMDS analysis, with confidence ellipses ($\alpha = 0.05$) for the four branches [Active (A, blue), Fossil (F, yellow), Paradise (P, violet), and Tourist (T, green)], based on the total microbial community (red labels) and the geochemical characteristics (black labels) of the same vermiculations, as reported in Addesso et al. [17]

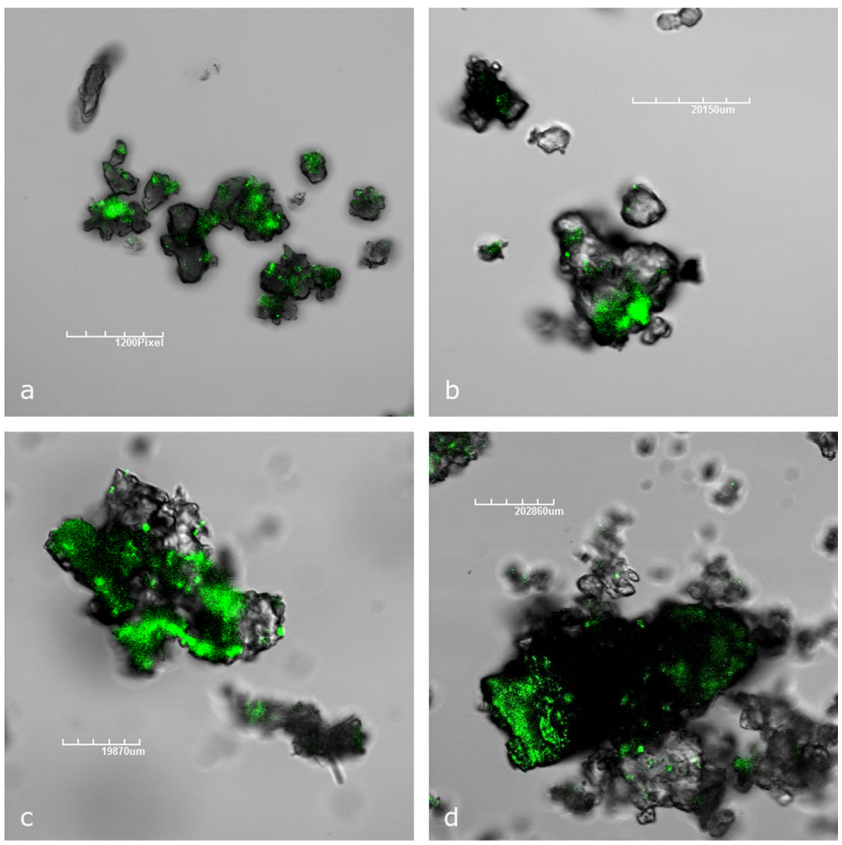

Fig. 4 CLSM images of A4 (**a**, **b**), F1 (**c**), and T1 (**d**) vermiculation samples, showing the presence of microbial clusters (green-colored zones) dyed with SYBR Green staining

on the microbial life associated with vermiculations from non-sulfidic karst systems.

The NGS approach revealed a biodiversity comparable to those observed in several matrices from different caves [10, 19, 20, 33–35]. *Proteobacteria* (41.3–54.8%), represented (in decreasing order) by *Gamma-*, *Beta-*, *Alpha-*, and *Deltaproteobacteria* classes, was the dominant phylum, likely in relation to the wide ranges in metabolism and phenotype, offering the capability to degrade a broad spectrum of organic substrates and to adapt to and thrive in the hostile cave environment [2]. The presence of *Proteobacteria* is often associated with Fe-Mn deposits [36, 37], both chemical elements were observed in vermiculations from Pertosa-Auletta Cave [17], and mainly related to the geochemical characteristics of the substratum, as highlighted by the NMDS. The carotenoid-producing gammaproteobacterial *Xanthomonadales* order was also detected, typical of yellow-colored colonies found in caves [38, 39]. Among *Alphaproteobacteria*, the *Rhizobiales* order, represented by members able to fix nitrogen and to oxidize iron and manganese, and the *Rhodospirillales* order, equally participating to the nitrogen cycle, were observed. They are typical surficial microorganisms [2], but, as suggested by Lavoie et al. [40], their presence in caves can be related to the migration of microorganisms from above lying soils, and once in the cave they start an adaptation process to the new surrounding environmental conditions. Similar to vermiculations from the Pertosa-Auletta Cave, those in the sulfuric acid Fetida Cave (Apulia, Italy) showed a great abundance of *Proteobacteria* (44-46%), but with copious microbial communities belonging to *Deltaproteobacteria* (25%) and *Epsilonproteobacteria* (16%), respectively, dominated by *Desulfobacterales* and *Campylobacterales*, involved in the sulfur cycle [19, 20].

Acidobacteria represented the second most abundant phylum, whose genetic and metabolic diversity is comparable to the highly diverse *Proteobacteria* [41–43]. *Acidobacteria* often occur together with chemolithoautotrophic *Gammaproteobacteria*, suggesting a mutualistic association between them: *Acidobacteria* gain energy oxidizing the reduced organic compounds (chemoorganotrophy) obtained from *Proteobacteria* autotrophic metabolism, an ecological advantage in cave oligotrophic environments [44]. Only in the green P1 vermiculation, in the lightened Paradise branch, the most represented phylum after *Proteobacteria* was *Actinobacteria* (33.8%), with *Actinomycetales* order, clearly different from the other vermiculations (1.9–10.3%), confirmed also by PCAs. The abundance of *Actinobacteria* in this vermiculation is justified by their association with *Cyanobacteria*, a well-known relationship in lightened subterranean environments [45].

Commonly found in soil systems, *Actinobacteria* may have an important ecological role in biogeochemical cycles of cave ecosystems, mediating mineralization processes [34] and producing bioactive compounds, such as antimicrobials that allow the biotic control on other populations [46]. Cuezva et al. [7] demonstrated they are able to capture CO_2 from the atmosphere and precipitate $CaCO_3$ polymorphs, as shown in FESEM images of the same samples reported in Addesso et al. [17]. In particular, *Actinomycetales* are able to degrade recalcitrant organic compounds [47]. The relative humidity and availability of endo- and exogenous organic matter in the Paradise branch can explain their colonization success. In fact, here, the moisture reaches approximately 100%, due to the presence of an underground river nearby, promoting the proliferation of *Actinomycetes* [48]. Moreover, the Paradise trail is lit and frequented by tourists who, together with photoautotrophic communities growing close to artificial light systems, bring an important input in terms of organic compounds, facilitating heterotrophic populations, including *Actinomycetales* [49].

The aerobic chemolithoautotrophic nitrite-oxidizing *Nitrospirae* and the anaerobic ammonium-oxidizing *Planctomycetes*, together with *Firmicutes*, able to reduce/oxidize sulfur, as well as chemo- or phototrophic *Chloroflexi*, were also found elsewhere in small amounts. Moreover, numerous less-represented taxonomic groups (with relative abundance < 1%) were observed in the 11 vermiculations investigated and their ecological role in this kind of ecosystem is still debated [2]. Among them, *Archaea* were also present, with the *Thaumarchaeota*, *Euryarchaeota*, and *Woesearchaeota* phyla, despite the archaeal DGGE profile highlighted a major number of bands in terms of core species richness. The same were found in considerable amount (< 4.3%) in Fetida Cave [20], where the relative abundances change (*Proteobacteria* > *Planctomycetes* > *Acidobacteria* > *Chloroflexi* > *Bacteroidetes* > *Actinobacteria* > *Nitrospirae*), likely due to the more extreme acidophilic environment, promoting the development of some bacterial groups rather than others. Despite the scarcity of knowledge about the archaeal group in cave ecosystems, it is well known that they give a relevant contribution to the global carbon nitrogen and sulfur cycles [22, 50, 51]. This may explain both the strong association between *Euryarchaeota* and N, and the relation of unclassified *Archaea* phylum groups, *Thaumarchaeota*, and *Woesearchaeota* with C and organic C highlighted by NMDS.

The Simpson index displays values close to 1 for all the samples, considering the dominant groups in the community and excluding the rare ones, indicating a low biodiversity and a high dominance. From the NGS results, it emerges that the dominant groups are unclassified already at the phylum level and this increases with the taxonomic level specificity. Values close to 7 were, instead, obtained for Shannon index, sensible also to the rare species, abundantly present in all the samples and certainly important from an ecological point of view.

Overall, geochemical and microbiological characteristics of the studied vermiculations differed among branches of the

Pertosa-Auletta Cave, with the greatest differences observed between those from tourist and unvisited branches. Anyway, macroelements (C, N, S, and P), as well as the organic matter, were mostly abundant in the vermiculations from the Paradise and Tourist branches, highlighting the presence of more abundant biomass in lightened trails, where the photoautotrophs proliferate. In these samples, also Mo and Sr were more abundant, indicating that a specialized microbial community could have resulted from some microbial lineages able to oxidize minerals containing such elements [52]. However, F4 sample showed a high abundance of *Nitrospirae* phylum compared to the other vermicular deposits that displayed also a high correlation with molybdenum, probably due to its content in the membrane-associated enzyme of the nitrite-oxidizing system [53]. Furthermore, the higher content of organic C in vermiculations from Fossil and Tourist trails [17] may explain the major abundance of *Nitrospirae* in such locations, where the availability of ammonia by ammonificators can increase the presence of nitrites, in turn usable by nitrite-oxidizing *Nitrospirae* group bacteria [33]. From Pearson correlation analysis, several associations emerge between biological and geochemical properties, as well as among the taxonomic groups, especially the rarest, but they are not at all easy to explain, due to the lack of information about their biogeochemical role in the cave ecosystem [33].

Confocal microscopy images showed a localization of DNA only in specific sites, recognizable in the green zones. This was confirmed also by FESEM images, as reported in Addesso et al. [17], showing the clayey deposits always associated with biogenic filamentous material, not ruling out the possibility that the microbes can interact or influence their behavior and evolution in the environment [54, 55].

The findings of the present study support the theory formulated by Jones et al. [10], suggesting that microorganisms play an active role in vermiculation genesis, producing organic matter and secondary minerals, enriching the calcite matrix, trapping and binding sediment particles and dissolving, through etching or pitting, the rock. This may happen in different environments, from sulfuric acid to normal karst caves. However, beyond the biological evidences, the possibility of coexistence of several processes remains. For example, decalcification of rock walls, due to the dissolution processes caused by the acidity of seeping or condensation waters, can contribute to create the primordial calcite matrix [56–59]; thereafter, neutralization of electrical charges in the small particles, associated to wet-dry phenomena, can determine the different morphologies [16, 60]. Nevertheless, further studies are required to clarify to what extent some processes prevail over others, determining the variety of vermiculations described.

The present study, describing the microbiota present in the vermicular deposits of the Pertosa-Auletta Cave and its relationships with geochemistry of vermiculations, fills the gap characterizing these topics in karst caves. The analyses carried out indicate a certain diversity of biological communities living in vermicular deposits, with a considerable percentage of unclassified lineages, already at the phylum level, demonstrating once more that the underground ecosystem hosts still a high number of unknown taxa. *Proteobacteria* and *Acidobacteria* were the predominant phyla, as generally observed in such environments, whereas *Actinobacteria* showed an increased growth due to the high humidity conditions and the input of organic matter from the considerable presence of tourists in the show cave. The involvement of such communities in the biogeochemical cycles is indisputable and the highlighted biological evidences confirm a tight interaction between biotic and abiotic factors in the formation of vermiculations. The obtained findings represent a crucial step for the protection and conservation of such unique ecological niches, making still more intriguing the knowledge and comprehension pathway of vermiculations.

Acknowledgments Great thanks go to the president, Dr. Francescantonio D'Orilia, and the scientific director, Prof. Mariana Amato, of MIdA Foundation for having believed in the project and to the skilled speleoguide, Mr. Vincenzo Manisera, for the precious support in the field (cave).

Funding Open access funding provided by Università degli Studi di Salerno within the CRUI-CARE Agreement. This work was supported by Musei Integrati dell'Ambiente Foundation, by the Spanish project MINECO [CGL2016-75590-P] with European Regional Development Fund and by University of Salerno [ORSA197159].

Compliance with Ethical Standards

Conflict of Interest The authors declare that they have no conflict of interest.

References

1. Lee NM, Meisinger DB, Aubrecht R, Kovacik L, Saiz-Jimenez C, Baskar S, Baskar R, Liebl W, Porter ML, Engel AS (2012) Caves and karst environments. In: Bell EM (ed) Life at extremes: environments, organisms and strategies for survival. CABI, Wallingford, pp 320–344

2. Tomczyk-Żak K, Zielenkiewicz U (2016) Microbial diversity in caves. Geomicrobiol J 33:20–38. https://doi.org/10.1080/01490451.2014.1003341
3. Kováč Ľ (2018) Caves as oligotrophic ecosystems. In: Moldovan OT, Kováč Ľ, Halse S (eds) Cave Ecology. Springer International Publishing, Cham, pp 297–307
4. Northup DE, Lavoie KH (2001) Geomicrobiology of caves: a review. Geomicrobiol J 18:199–222. https://doi.org/10.1080/01490450152467750
5. Galdenzi S, Maruoka T (2003) Gypsum deposits in the Frasassi caves, central Italy. J Cave Karst Stud 65(2):111–125
6. Engel AS, Stern LA, Bennett PC (2004) Microbial contributions to cave formation: new insights into sulfuric acid speleogenesis. Geol 32:369. https://doi.org/10.1130/G20288.1
7. Cuezva S, Fernandez-Cortes A, Porca E, Pašić L, Jurado V, Hernandez-Marine M, Serrano-Ortiz P, Hermosin B, Cañaveras JC, Sanchez-Moral S, Saiz-Jimenez C (2012) The biogeochemical role of Actinobacteria in Altamira Cave, Spain. FEMS Microbiol Ecol 81:281–290. https://doi.org/10.1111/j.1574-6941.2012.01391.x
8. Tisato N, Torriani SFF, Monteux S, Sauro F, de Waele J, Tavagna ML, D'Angeli IM, Chailloux D, Renda M, Eglinton TI, Bontognali TRR (2015) Microbial mediation of complex subterranean mineral structures. Sci Rep 5:15525. https://doi.org/10.1038/srep15525
9. Bontognali TRR, D'Angeli IM, Tisato N, et al (2016) Mushroom speleothems: stromatolites that formed in the absence of phototrophs. Front Earth Sci 4. https://doi.org/10.3389/feart.2016.00049
10. Jones DS, Lyon EH, Macalady JL (2008) Geomicrobiology of biovermiculations from the Frasassi cave system, Italy. J Cave Karst Stud 70(2):78–93
11. Miller AZ, Garcia-Sanchez AM, Martin-Sanchez PM, Costa Pereira MF, Spangenberg JE, Jurado V, Dionísio A, Afonso MJ, Iglé sias Chaminé HI, Hermosin B, Saiz-Jimenez C (2018) Origin of abundant moonmilk deposits in a subsurface granitic environment. Sedimentology 65:1482–1503. https://doi.org/10.1111/sed.12431
12. Jameson RA (1991) Management considerations for clay vermiculations. Proc of the Nat Cave Manag Symp Am Cave Conserv Assoc, Bowling Green, pp 39–144
13. Hedges J (1993) A review on vermiculations. Bol Soc Venez Espeleol 27:2–6
14. Hill CA, Forti P (1997) Cave minerals of the world. National Speleological Society, Huntsville
15. Parenzan P (1961) Sulle formazioni argillo-limose dette vermicolari. Atti Symp Int di Spel Varenna Mem 5:120–125
16. Bini A, Gori MC, Gori S (1978) A critical review of hypotheses on the origin of vermiculations. IJS 10:11–33. https://doi.org/10.5038/1827-806X.10.1.2
17. Addesso R, Bellino A, D'Angeli IM et al (2019) Vermiculations from karst caves: the case of Pertosa-Auletta system (Italy). CATENA 182:104178. https://doi.org/10.1016/j.catena.2019.104178
18. Camassa MM, Febbroriello P (2003) Le foval della Grotta Zinzulusa in Puglia (SE-Italia). Thalass Salentina 26(suppl):207–218
19. D'Angeli IM, Waele JD, Ieva MG, et al (2017) Next-generation sequencing for microbial characterization of biovermiculations from a sulfuric acid cave in Apulia (Italy). Proc of the 17th Int Congr of Speleol 1:377–380
20. D'Angeli IM, Ghezzi D, Leuko S, Firrincieli A, Parise M, Fiorucci A, Vigna B, Addesso R, Baldantoni D, Carbone C, Miller AZ, Jurado V, Saiz-Jimenez C, de Waele J, Cappelletti M (2019) Geomicrobiology of a seawater-influenced active sulfuric acid cave. PLoS One 14:e0220706. https://doi.org/10.1371/journal.pone.0220706
21. D'Angeli IM, Parise M, Vattano M et al (2019) Sulfuric acid caves of Italy: a review. Geomorphology 333:105–122. https://doi.org/10.1016/j.geomorph.2019.02.025
22. Parenzan P (1965) Le formazioni vermicolari della grotta di Sant'Angelo di Statte (Taranto). Atti IX Congr. Naz. di Speleol., Trieste. Memoria 7(2):101–104
23. Snaidr J, Amann R, Huber I, Ludwig W, Schleifer KH (1997) Phylogenetic analysis and in situ identification of bacteria in activated sludge. Appl Environ Microbiol 63:2884–2896
24. Lane DJ (1991) 16S/23S rRNA sequencing. In: Stackebrandt E, Goodfellow M (eds) Nucleic acid techniques in bacterial systematics. John Wiley & Sons, Inc., Chichester, pp 115–175
25. Großkopf R, Janssen PH, Liesack W (1998) Diversity and structure of the methanogenic community in anoxic rice paddy soil microcosms as examined by cultivation and direct 16S rRNA gene sequence retrieval. Appl Environ Microbiol 64:960–969. https://doi.org/10.1128/AEM.64.3.960-969.1998
26. Medlin L, Elwood HJ, Stickel S, Sogin ML (1988) The characterization of enzymatically amplified eukaryotic 16S-like rRNA-coding regions. Gene 71:491–499. https://doi.org/10.1016/0378-1119(88)90066-2
27. White TJ, Bruns T, Lee S, Taylor J (1990) Amplification and direct sequencing of fungal ribosomal RNA genes for phylogenetics. In: PCR Protocols. Elsevier, pp 315–322
28. Muyzer G, de Waal EC, Uitterlinden AG (1993) Profiling of complex microbial populations by denaturing gradient gel electrophoresis analysis of polymerase chain reaction-amplified genes coding for 16S rRNA. Appl Environ Microbiol 59:695–700
29. Edgar RC (2010) Search and clustering orders of magnitude faster than BLAST. Bioinformatics 26:2460–2461. https://doi.org/10.1093/bioinformatics/btq461
30. Caporaso JG, Kuczynski J, Stombaugh J, Bittinger K, Bushman FD, Costello EK, Fierer N, Peña AG, Goodrich JK, Gordon JI, Huttley GA, Kelley ST, Knights D, Koenig JE, Ley RE, Lozupone CA, McDonald D, Muegge BD, Pirrung M, Reeder J, Sevinsky JR, Turnbaugh PJ, Walters WA, Widmann J, Yatsunenko T, Zaneveld J, Knight R (2010) QIIME allows analysis of high-throughput community sequencing data. Nat Methods 7:335–336. https://doi.org/10.1038/nmeth.f.303
31. Magoč T, Salzberg SL (2011) FLASH: fast length adjustment of short reads to improve genome assemblies. Bioinformatics 27:2957–2963. https://doi.org/10.1093/bioinformatics/btr507
32. R Core Team (2019) R: A language and environment for statistical computing. R Foundation for Statistical Computing. R version 3.6.0
33. De Mandal S, Chatterjee R, Kumar NS (2017) Dominant bacterial phyla in caves and their predicted functional roles in C and N cycle. BMC Microbiol 17:90. https://doi.org/10.1186/s12866-017-1002-x
34. Gonzalez-Pimentel JL, Miller AZ, Jurado V, Laiz L, Pereira MFC, Saiz-Jimenez C (2018) Yellow coloured mats from lava tubes of La Palma (Canary Islands, Spain) are dominated by metabolically active Actinobacteria. Sci Rep 8:1944. https://doi.org/10.1038/s41598-018-20393-2
35. Hershey OS, Barton HA (2018) The microbial diversity of caves. In: Moldovan OT, Kováč Ľ, Halse S (eds) Cave Ecology. Springer International Publishing, Cham, pp 69–90
36. Northup DE, Barns SM, Yu LE, Spilde MN, Schelble RT, Dano KE, Crossey LJ, Connolly CA, Boston PJ, Natvig DO, Dahm CN (2003) Diverse microbial communities inhabiting ferromanganese deposits in Lechuguilla and Spider Caves. Environ Microbiol 5:1071–1086. https://doi.org/10.1046/j.1462-2920.2003.00500.x
37. Spilde MN, Northup DE, Boston PJ, Schelble RT, Dano KE, Crossey LJ, Dahm CN (2005) Geomicrobiology of cave ferromanganese deposits: a field and laboratory investigation. Geomicrobiol J 22:99–116. https://doi.org/10.1080/01490450590945889

38. Portillo MC, Gonzalez JM, Saiz-Jimenez C (2008) Metabolically active microbial communities of yellow and grey colonizations on the walls of Altamira Cave, Spain. J Appl Microbiol 104:681–691. https://doi.org/10.1111/j.1365-2672.2007.03594.x
39. Porca E, Jurado V, Žgur-Bertok D, Saiz-Jimenez C, Pašić L (2012) Comparative analysis of yellow microbial communities growing on the walls of geographically distinct caves indicates a common core of microorganisms involved in their formation. FEMS Microbiol Ecol 81:255–266. https://doi.org/10.1111/j.1574-6941.2012.01383.x
40. Lavoie KH, Winter AS, Read KJH, Hughes EM, Spilde MN, Northup DE (2017) Comparison of bacterial communities from lava cave microbial mats to overlying surface soils from Lava Beds National Monument, USA. PLoS One 12:e0169339. https://doi.org/10.1371/journal.pone.0169339
41. Hugenholtz P, Goebel BM, Pace NR (1998) Impact of culture-independent studies on the emerging phylogenetic view of bacterial diversity. J Bacteriol 180:4765–4774
42. Quaiser A, Ochsenreiter T, Lanz C, Schuster SC, Treusch AH, Eck J, Schleper C (2003) Acidobacteria form a coherent but highly diverse group within the bacterial domain: evidence from environmental genomics: Environmental genomics of Acidobacteria. Mol Microbiol 50:563–575. https://doi.org/10.1046/j.1365-2958.2003.03707.x
43. Barns SM, Cain EC, Sommerville L, Kuske CR (2007) Acidobacteria phylum sequences in uranium-contaminated subsurface sediments greatly expand the known diversity within the phylum. Appl Environ Microbiol 73:3113–3116. https://doi.org/10.1128/AEM.02012-06
44. Meisinger DB, Zimmermann J, Ludwig W, Schleifer KH, Wanner G, Schmid M, Bennett PC, Engel AS, Lee NM (2007) In situ detection of novel Acidobacteria in microbial mats from a chemolithoautotrophically based cave ecosystem (Lower Kane Cave, WY, USA). Environ Microbiol 9:1523–1534. https://doi.org/10.1111/j.1462-2920.2007.01271.x
45. Albertano P, Urzì C (1999) Structural interactions among epilithic cyanobacteria and heterotrophic microorganisms in Roman hypogea. Microb Ecol 38:244–252. https://doi.org/10.1007/s002489900174
46. Rangseekaew P, Pathom-aree W (2019) Cave Actinobacteria as producers of bioactive metabolites. Front Microbiol 10:387. https://doi.org/10.3389/fmicb.2019.00387
47. Sonia M-T, Hafedh B, Abdennaceur H, Ali G (2011) Studies on the ecology of actinomycetes in an agricultural soil amended with organic residues: II. Assessment of enzymatic activities of Actinomycetales isolates. World J Microbiol Biotechnol 27:2251–2259. https://doi.org/10.1007/s11274-011-0688-4
48. Zvyagintsev DG, Zenova GM, Doroshenko EA, Gryadunova AA, Gracheva TA, Sudnitsyn II (2007) Actinomycete growth in conditions of low moisture. Biol Bull Russ Acad Sci 34:242–247. https://doi.org/10.1134/S1062359007030053
49. Cañaveras JC, Sanchez-Moral S, Soler V, Saiz-Jimenez C (2001) Microorganisms and microbially induced fabrics in cave walls. Geomicrobiol J 18:223–240. https://doi.org/10.1080/01490450152467769
50. Cavicchioli R (2011) Archaea — timeline of the third domain. Nat Rev Microbiol 9:51–61. https://doi.org/10.1038/nrmicro2482
51. Offre P, Spang A, Schleper C (2013) Archaea in biogeochemical cycles. Annu Rev Microbiol 67:437–457. https://doi.org/10.1146/annurev-micro-092412-155614
52. Mann H (1990) Biosorption of heavy metals by bacterial biomass. In: Volesky B (ed) Biosorption of Heavy Metals. CRC Press, Boca Raton, pp 93–138
53. Spieck E, Ehrich S, Aamand J, Bock E (1998) Isolation and immunocytochemical location of the nitrite-oxidizing system in Nitrospira moscoviensis. Arch Microbiol 169:225–230. https://doi.org/10.1007/s002030050565
54. Dong H, Jaisi DP, Kim J, Zhang G (2009) Microbe-clay mineral interactions. Am Mineral 94:1505–1519. https://doi.org/10.2138/am.2009.3246
55. Cuadros J (2017) Clay minerals interaction with microorganisms: a review. Clay Miner 52:235–261. https://doi.org/10.1180/claymin.2017.052.2.05
56. De Joly R (1934) Ruissellement et percolations. Actes Congr D'Erfoud (Maroc), Com d'Etude des Eaux Souterr, pp 54-61
57. Waldner F (1936) Contributo alla morfologia del limo argilloso delle caverne. Osservazioni fatte nelle Grotte di Postumia. Grotte d'Italia 2:56–60
58. Renault P (1953a) Exploration du Grand Aven de Canjeurs. Bul du Com Na Spéléol 3:72–79
59. Renault P (1953b) Dépôts vermiculés d'argille de decalcification. 1° Congr Int de Spéléol, Paris
60. Montoriol-Pous J (1958) Sobre el origen de las vermiculationes arcillosas. Actes 2° Cong Int de Spéléol. Bari 1:389–395

CHAPTER 7

A multi-approach characterization of lampenflora in lit underground ecosystems

Rosangela Addesso, Daniela Baldantoni, Beatriz Cubero, Igor Tiago, Ana Teresa Caldeira, Jo De Waele, Ana Z. Miller*

Manuscript in preparation

**corresponding author*

The characterization of prokaryotic and eukaryotic communities composing lampenflora green biofilms from the Pertosa-Auletta Cave, as well as the study of their eco-physiology, contributed to the knowledge on lampenflora composition and behavior, above all in the interaction processes with the lithological substrates.

A multi-approach characterization of lampenflora in lit underground ecosystems

Rosangela Addesso [1], Daniela Baldantoni [1], Beatriz Cubero [2], Igor Tiago [3], Ana Teresa Caldeira [4], Jo De Waele [5], Ana Z. Miller [2,4]*

[1] Department of Chemistry and Biology "Adolfo Zambelli", University of Salerno, Via Giovanni Paolo II, 132, 84084 Fisciano (SA), Italy

[2] Instituto de Recursos Naturales y Agrobiología de Sevilla, IRNAS-CSIC, Av. Reina Mercedes, 10, 41012 Sevilla, Spain

[3] Department of Life Sciences, University of Coimbra, Rua da Matemática, 49, 3000-276 Coimbra, Portugal

[4] HERCULES Laboratory, University of Évora, Largo Marques de Marialva 8, 7000-809 Évora, Portugal

[5] Department of Biological, Geological and Environmental Sciences, University of Bologna, Via Zamboni, 67, 40126 Bologna, Italy

* Corresponding author: anamiller@irnas.csic.es

Abstract

Permanent artificial light systems in tourist underground environments promote the growth on rock surfaces of photoautotrophic biofilms, called lampenflora. They are responsible for the biological modification of the native community biodiversity and the irreversible destruction of the colonized substrates. However, until now not exhaustive chemico-physical techniques to remove and control lampenflora have been found. In this work, we investigated, using an integrated approach, the biodiversity and eco-physiology of lampenflora from the Pertosa-Auletta Cave (Italy), in order to give useful information in its sustainable controlling. Reflectance analysis showed that photoautotrophic biofilms are able to absorb the totality of the visible spectrum, reflecting only the near-infrared, due to the production of secondary pigments and the possess of several metabolic regimes. The biological matrix is mainly constituted by filamentous organisms knotted with the underlying mineral layer, made inconsistent by the biochemical attack of both prokariotes (mostly represented by *Brasilonema angustatum* sp.) and eukaryotes (*Ephemerum spinulosum* sp. and *Pseudostichococcus monallantoide*s sp.), composing the community. Besides the corrosion processes, $CaCO_3$ secondary minerals are also found in the matrix, whose precipitation may be biologically mediated.

Keywords: Photoautotrophic biofilms, Geo-biology, Biodeterioration, Show caves, Pertosa-Auletta Cave

1 Introduction

Since the 17th century, caves represented an important tourist attraction for their naturalistic and cultural value, swelling, in recent decades, to more than 250 million visitors per year worldwide (Cigna, 2016). However, human fruition of such charming environments affects their ecological equilibrium, introducing unnatural matter and energy inputs, such the release of CO_2 and heat, as result of tourists breathing, or the introduction of organic matter, including spores or plant seeds, attached on the clothing or the skin (de Freitas, 2010; Smith et al., 2013; Mulec, 2014). Nevertheless, the plague of the show caves is the development of lampenflora community, photoautotrophic biofilms growing on lit rock surfaces due to the presence of artificial light systems. Aerophytic cyanobacteria and algae generally compose the early stages of the community, creating the conditions for the successive colonization by bryophytes, ferns and vascular plants, as well as fungi (Pfendler et al., 2018; Mulec, 2019).

The lampenflora is now an urgent issue for the managers of show caves, due to the several changes implemented on the colonized surfaces, such as the aesthetical alteration caused by the green patinas, as well as the irreversible chemical corrosion of the substrates generated by the metabolic activities of the organisms composing the community, able to secrete organic acids promoting the surfaces dissolution (Baquedano Estévez et al., 2019). Moreover, it represents also an ecological problem, being a considerable organic input usable by the cave inhabitants in an ecosystem normally at oligotrophic regime, and affecting the autochthonous biodiversity, both qualitatively and quantitatively, for its opportunistic lifestyle (Mulec, 2019; Baquedano Estévez et al., 2019).

Given that currently there are no efficient and sustainable solutions to solve the lampenflora problem in show caves (both to clean the surfaces and to control its growth), a deep characterization of the green biofilm community from underground environments adapted to tourism, urges (Pfendler et al., 2018; Baquedano Estévez et al., 2019). To contribute to the knowledge of the show cave "alien" community (and to its control), this work aimed at providing a multi-approach (morphological, physiological and taxonomic) characterization of lampenflora from the Pertosa-Auletta Cave (Campania, Italy), growing on an unique calcareous substrate (Cafaro et al., 2016), but subjected to different lights. The understanding of lampenflora community composition and metabolism may be employed to propose focused effective and sustainable controlling actions, not only in show caves, but also in any artificially lit underground ecosystem.

2 Methods

2.1 Field activities

In the lit tourist trail of the Pertosa-Auletta Cave, largely described in Addesso et al. (2019), 4 areas spatially distributed, colonized by lampenflora and subjected to different lights, were chosen (Figure 1). *In situ*, non-destructive reflectance, using a Jaz System spectrometer (Ocean Optics), completed with a VIS-NIR module, and PAR (photosynthetically active radiation), through an irradiance quantum meter (LI-250 Light meter, Li-COR), were determined. In addition, measures of maximal photosystem II (PSII) photochemical efficiency, given by Fv/Fm (variable fluorescence/maximal fluorescence) were carried out on 30 minutes dark-adapted surfaces, using a portable photosynthesis yield analyzer (MINI-PAM, WALTZ, Germany), equipped with a

distance clip holder (Distance Clip 2010A, WALTZ, Germany), to assess the biofilms photosynthetic activity.

At the end, for each surface, a representative sample was collected, using disposable and sterile scalpel blades and Eppendorf tubes, and stored at -80 °C until processing.

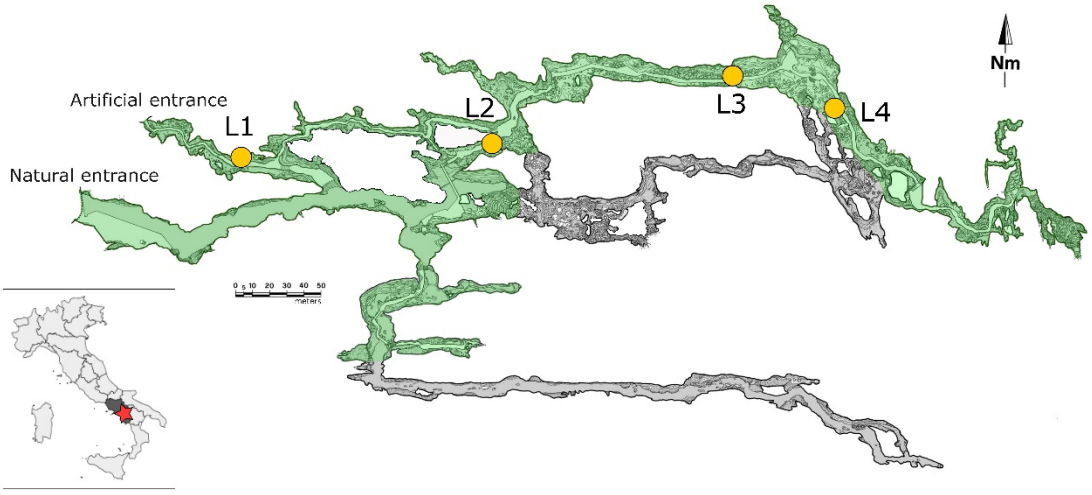

Figure 1 Pertosa-Auletta Cave map; the yellow circles indicate the studied lampenflora samples in the tourist trail (green)

2.2 Laboratory analyses

For microscopy surveys, oven-dried (50 °C) samples were analyzed by a FE-SEM - FEI Teneo (ThermoFisher, MA, USA) microscope, using the secondary electron detection mode, with an acceleration voltage of 5 kV for ultra-high resolution images.

For molecular analyses, FastDNA^{TM} Spin Kit for Soil was used to extract total DNA, according to the producer's protocol (MP Biomedical). The DNA amount was determined by a Qubit 2.0 Fluorometer (Invitrogen). The extracted DNA (with a minimum concentration of ~ 0.1 ng/μL), was analyzed via next-generation sequencing (NGS) targeting the V3–V4 hypervariable region of Prokaryotes 16S rRNA and V4 of Eukaryotes 18S rRNA, using Illumina MiSeq 2 × 250 paired end, according to Macrogen (Seoul, Korea) library preparation protocol. Chimeras were identified and

removed by means of USEARCH (Edgar, 2010). Resulting reads were processed in Qiime (Caporaso et al., 2010), whereas UCLUST (Edgar, 2010) was used for the similar sequences assignment to operational taxonomic units (OTUs) by clustering with a 97% similarity threshold. Paired-end reads were merged using FLASH (Magoč and Salzberg, 2011). RDP and NCBI were used, respectively, for Prokaryotes and Eukaryotes, as against reference database for taxonomic identification of query sequences.

2.3 Data analysis

Reflectance spectra were elaborated in the R 4.0.0 programming environment (R Core Team, 2020), with functions from the "photobiologylnOut" and "ggspectra" packages, and using the open-source vector graphics editor Inkscape 0.92. Alpha diversity analyses, including estimation of Chao1, Shannon, Simpson, and Good's Coverage indices, were performed through Qiime.

3 Results

3.1 Lampenflora physiological features

The lamps irradiating the sampled surfaces, located at diverse distances from them (from 1 to 4 m), exhibit different light fluxes, with PAR values ranging from 1.85 to 4.01 μmol m^{-2} sec^{-1}; moreover they have distinct colors, reflecting different wavelengths: green for L1 and L4 and white for L2 and L3 (Table 1). Reflectance spectra, reported in Figure 2, highlight that the 4 lampenflora samples absorb the totality of the visible light (~ 400-700 nm), reflecting the near-infrared radiation (~ 700-800 nm). The maximal PSII photochemical efficiency (Fv/Fm) shows values ranging between 0.698 and 0.720 (Table 1).

Table 1 Field measurements on the four lampenflora sampling sites, related to photosynthetic activity of their communities.

Sample	Fv/Fm	σ	PAR (µmol m^{-2} sec^{-1})	Distance light from wall (m)	Light color
L1	0.698	0.023	3.05	1.5	green
L2	0.720	0.114	4.01	3.5	white
L3	0.622	0.037	2.42	4	white
L4	0.704	0.018	1.85	2.5	green

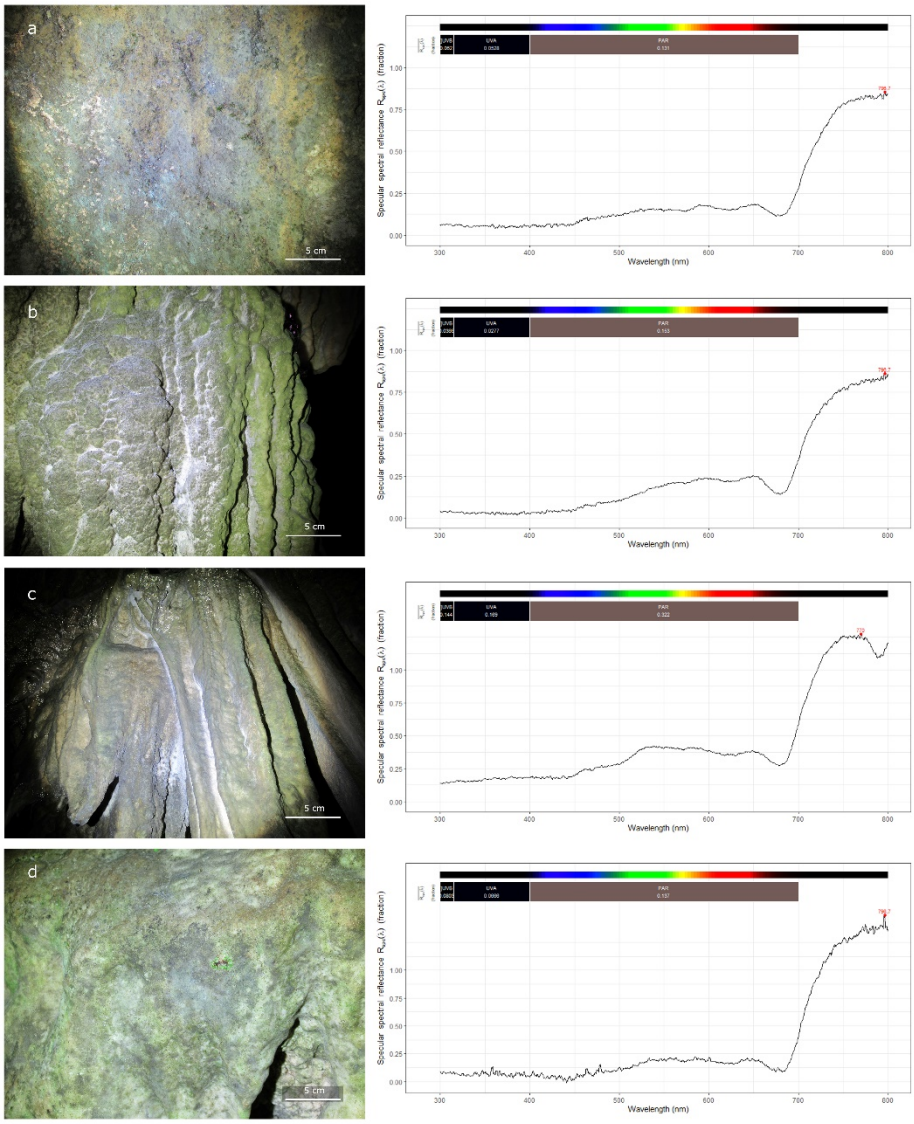

Figure 2 Picture of the 4 sampling sites, with the respective lampenflora reflectance spectra: (**a**) L1; (**b**) L2; (**c**) L3; (**d**) L4

3.2 Lampenflora morphological features

FE-SEM images (Figure 3) shed light on the organization of lampenflora community (Fig. S1). The organic matrix is mainly constituted by filamentous bacteria and algae, appearing to be strongly knotted between them and with the mineral substrate. In some

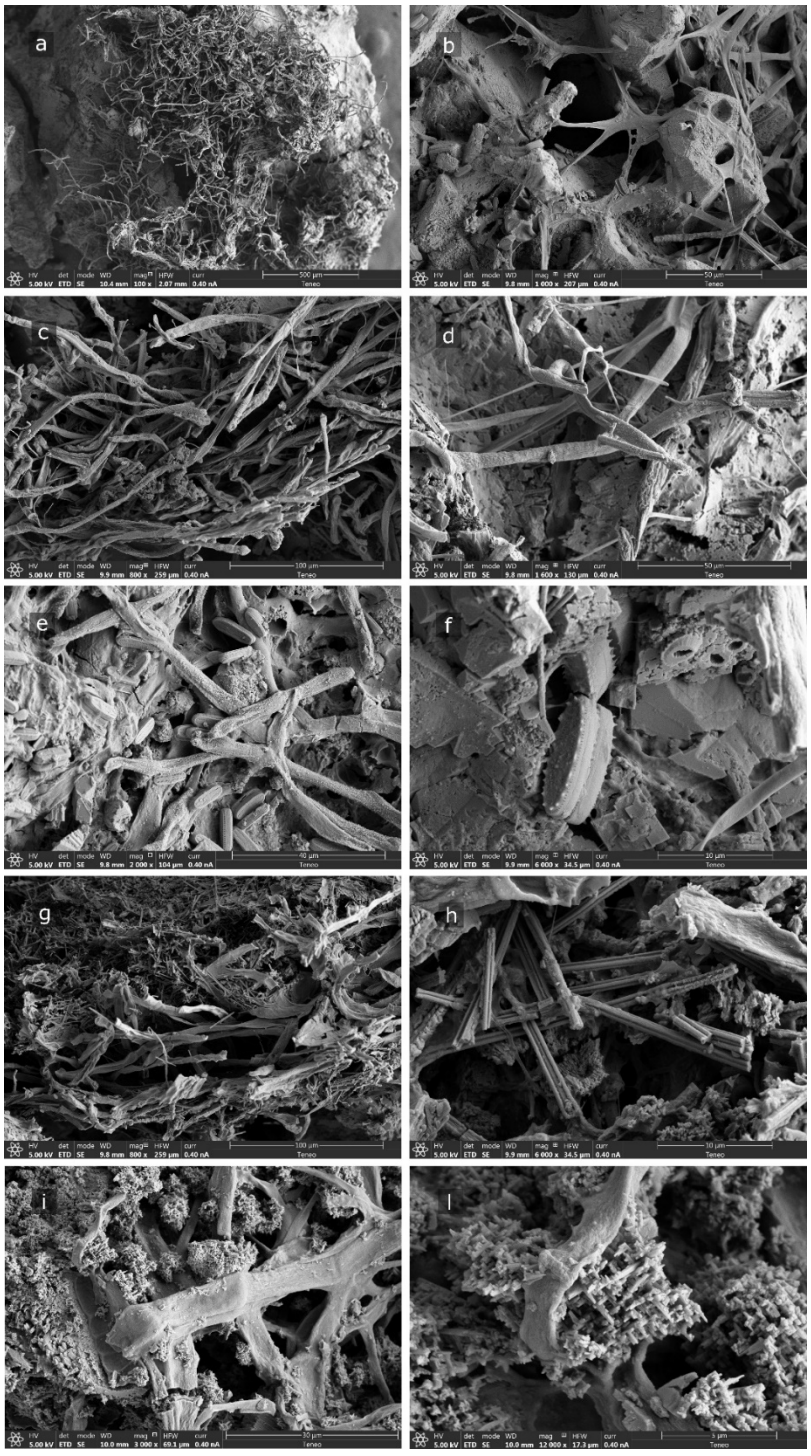

Figure 3 FE-SEM microscopy images of the biofilms. Filamentous organisms in L1 (**a**), L4 (**b**), L3 (**c**), L2 (**d**), diatoms in L4 (**e**) and L1 (**f**), biogenic calcite structures in L2 and L3 (**g** and **i**, respectively) with a focus on them (**h** and **l**, respectively) are shown

cases, it seems that the network of filamentous organisms traps minerals (Figures 3a, b, c and d), with evidences of substrates corrosion. Figures 3b, e and f show also the presence of diatoms, whereas Figure 3g, h, i and l reveal secondary minerals, in the various forms of calcite rods, spread in the matrix.

3.3 Lampenflora taxonomic features

DNA amounts extracted from lampenflora samples are reported in Table 2, presenting a minimum value equal to 11.8 ng/µL and a maximum value of 43.2 ng/µL. The 4 samples display similar bacterial composition (Figure 4I). The most abundant phylum is represented by *Cyanobacteria* (mean value: 66.50%) (Figure 4Ia), dominated by the *Brasilonema angustatum* sp., followed by *Proteobacteria* (mean value: 21.01%) > unclassified *Bacteria* (mean value: 3.64%) > *Actinobacteria* (mean value: 3.15%) > *Bacteroidetes* (mean value: 2.42%). Phyla less represented (< 1%) are also identified with a mean relative abundance equal to 3.28%. Among *Proteobacteria* classes (Figure 4Ib), the most represented are *Alpha-* (mean value: 17.74%), dominated, at the order level, by *Hyphomicrobiales* (mean value: 6.79%), *Caulobacterales* (mean value: 4.47%) and *Rhodospirillales* (mean value: 2.93%) (Figure 4Ic), *Gamma-* (mean value: 1.97%) and *Beta-proteobacteria* (mean value: 1.02%) classes.

Table 2 Amount of DNA extracted from ~ 0.250 g of lampenflora samples.

Sample	Amount (ng/µL)
L1	43.2
L2	27.4
L3	11.8
L4	20.8

Concerning the Eukaryotes identified, the 4 samples show a clear differentiation (Figure 4II). In L1, the major phylum is represented by *Streptophyta* (33.26%), followed by unclassified *Eucaryota* (24.05%), *Nematoda* (19.89%), dominated by *Plectus opisthocirculus* sp., *Bacillariophyta* (13.22%), represented by *Sellaphora bacillum* sp. and *Diadesmis gallica* sp., *Arthropoda* (3.34%), unclassified DNA sequences (1.77%) and *Cercozoa* (1.30%) phyla. Streptophyta (91.16%) constitute almost totally L2 sample. In L3, the most abundant phyla are: *Streptophyta* (63.85%) > *Cercozoa* (9.91%) > unclassified *Eucaryota* (7.82%) > *Imbricatea* (4.99%) > unclassified DNA sequences (3.87%) > *Chytridiomycota* (3.84%) > *Cryptomycota* (1.87%) > *Chlorophyta* (1.66%). L4 diverges from the other samples for the higher abundance of *Chlorophyta* (59.59%), represented by *Pseudostichococcus monallantoides* sp., followed by *Streptophyta* (15.87%) > unclassified *Eucaryota* (9.96%) > *Ascomycota* (6.21%) > *Nematoda* (3.58%) > *Bacillariophyta* (1.85%) > *Ciliophora* (1.13%). Moreover, all the samples display an amount of phyla less represented (< 1%), equal to 3.18, 4.57, 2.17 and 1.81%, respectively. *Strepthphyta* phylum, dominating the most samples, is totally represented by *Ephemerum spinulosum* sp.

Metrics employed for microbial community richness and diversity estimations are reported in Table 3. The analysis generated for each sample a range from 180 to 280 OTUs for Prokaryotes and a range from 80 to 193 OTUs for Eukaryotes. The analysis well covers the microbial diversity in lampenflora samples, given the average value of Good's Coverage equal to 1.0%. Chao1 richness estimator ranges between 207.5 and 345.0. Shannon diversity indices present estimates ranging from a minimum of 2.468 to a maximum of 3.830 for Prokaryotes and from 0.925 and 3.817 for Eukaryotes, whereas

Inverse Simpson diversity indices show values ranging from 0.480 to 0.729 for Prokaryotes and from 0.169 to 0.839 for Eukaryotes.

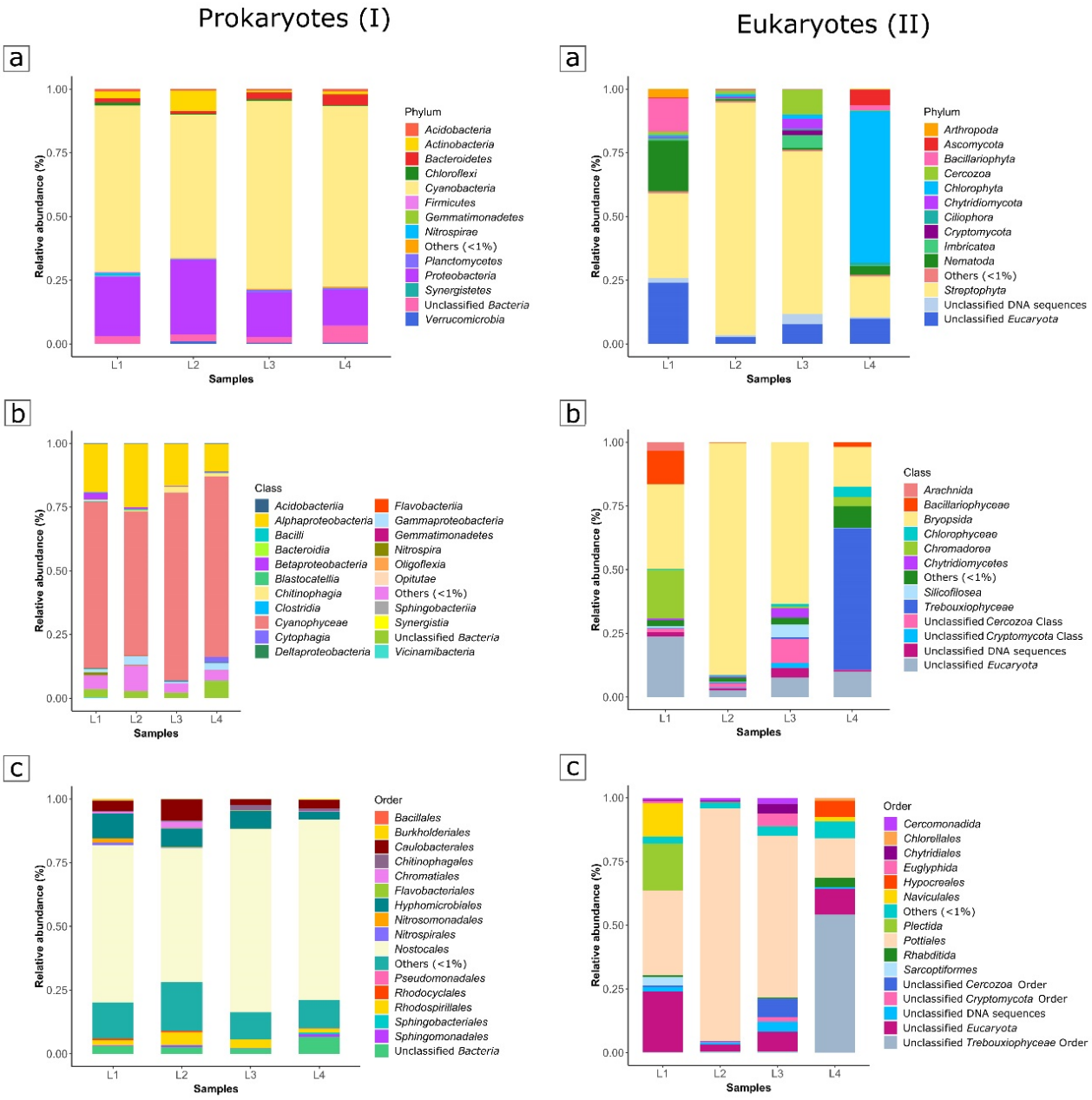

Figure 4 Prokaryotes (I) and Eukaryotes (II) composition of the lampenflora for each sample; the barplots show the relative abundances (%) at phylum (**a**), class (**b**), and order (**c**) levels

Table 3 Community richness and diversity of prokaryotes and eukaryotes estimated for each sample, using several alpha diversity metrics (Chao1, Shannon, Simpson, Good's Coverage).

	Sample	OTUs	Chao 1	Shannon	Inverse Simpson	Good's Coverage (%)
Prokaryotes(16S)	L1	277	310.2	3.830	0.729	1.0
	L2	280	345.0	3.740	0.717	1.0
	L3	253	287.2	2.468	0.480	1.0
	L4	180	207.5	2.510	0.499	1.0
Eukaryotes(18S)	L1	193	193.3	3.817	0.839	1.0
	L2	135	135.0	0.925	0.169	1.0
	L3	132	132.0	2.779	0.589	1.0
	L4	80	80.0	2.837	0.697	1.0

4 Discussion

The Pertosa-Auletta Cave is widely colonized by lampenflora, appearing it from a few tens of meters from the entrance up to the deeper zone. It is all over the surfaces interested by artificial light, located along the lit tourist trail, equipped with a LED lamps system, at adjustable spectrum. In addition to green biofilms, ferns and bryophytes are also present.

The maximal PSII photochemical efficiency, that represents an index of photosynthetic performance of photoautotrophs, denotes not ideal conditions if compared with the optimum value (0.83) for several photoautotrophic species and considering that lower values indicate stress conditions (Maxwell and Johnson, 2000). Despite the Fv/Fm of green biofilms analyzed in the Pertosa-Auletta Cave (0.62-0.72) highlights slightly lower values than the optimum, they are in accord with those reported by Grobbelaar (2000) and Pfendler et al. (2017), equal to 0.74 and 0.70 respectively, measured on

lampenflora from Cango Cave (South Africa) and La Glacière Cave (France), respectively. This proves an adequate physiological activity of lampenflora from the Pertosa-Auletta Cave, also where very low PAR was detected. In fact, as reported in Mulec (2019), lampenflora community can live in underground ecosystem also at very low photosynthetic photon flux density (PPFD), from 0.2 to several hundred μmol m^{-2} sec^{-1} photons, surviving in total darkness for a long time (Baquedano Estévez et al., 2019). Also at this very low PPFD, the light remains the main driver influencing the green biofilms growth in show caves, together with moisture and distance from the entrance (Piano et al., 2015).

In addition, lampenflora has a different behavior compared to the other photoautotrophs; indeed, as appears from the reflectance spectra, it reflects the green part of the spectrum, demonstrating to absorb the entire visible light (~ 400-700 nm) and to reflect only the near-infrared (~ 700-800 nm). Several species constituting lampenflora community, such as those belonging to *Cyanobacteria*, are capable to produce accessory pigments able to enlarge the absorption spectrum of visible radiation. Others, including algae, can have mixotrophic and heterotrophic regimes, using metabolic pathways different from photosynthesis (Roldan, 2006; Baquedano Estévez et al., 2019, Mulec, 2019). Therefore, lampenflora is able to adapt to different lighting conditions, so that intervening on light wavelengths to control its growth could be useless, notwithstanding the yellow light (~ 580 nm) seems to limit green biofilm developments on lit surfaces (Mulec, 2019). Also combining light wavelength with actions aimed to reduce the lamps switching times and their power, as well as to increase their distance from the surfaces, may result ineffective.

It has to be considered that lampenflora community acts with both destructive and constructive processes on colonized mineral matrices, as highlighted by FE-SEM microscopy. Being mainly constituted by epilithic organisms, it is in close relation with the colonized substrates, from which organisms can obtain nutrients secreting organic acids and others exopolymers able to dissolve the minerals, causing new structures from erosion processes, such as hole figures, and corroding surfaces (Northup and Lavoie, 2001; Mulec, 2009). Filamentous algae and cyanobacteria, in particular, can activate also a physical disruption of the substrates due to the penetration of their thready body carrying out a mechanical pressure with the consequent estrangement of mineral fragments and the increase of porosity of host rock (Caneva et al., 2008; Mulec, 2009; Baquedano Estévez et al., 2019). Moreover, *Cyanobacteria*, through the photosynthetic process, can promote the precipitation of $CaCO_3$ secondary minerals (Northup and Lavoie, 2001; Barton and Northup, 2007; Mulec, 2009; Krause et al., 2019; Baquedano Estévez et al., 2019; Popović et al., 2020), as shown by our findings, where sticks with smooth surfaces, probably calcite moonmilk (Miller et al., 2018), and also other calcitic secondary structures were found entangled to the biomass and on the underlying layer. Generally, moonmilk is presented as a white and very soft deposit, as well as the bed on which the lampenflora is commonly found, likely result of the substrate biogenic corrosion.

Regarding the diversity of the lampenflora community form the Pertosa-Auletta Cave, *Cyanobacteria* appear to be the most abundant among Prokaryotes, with the dominance of *Brasilonema angustatum* sp., nitrogen-fixer belonging to the large group of *Nostocales* order. With its heterocysts, this aerophytic filamentous cyanobaterial species actively participate to the biogeochemical cycles, promoting an important release of

bioavailable nitrogen (Vaccarino and Johansen, 2012) in a poor-nutrients ecosystem. Moreover, cyanobacterial species have a key role in the rooting of lampenflora community in lit underground environments, in fact, they represent the pioneering organisms, together with algae, that in the ecological succession prepare the substrate for the next colonization (Popović et al., 2017; Mulec, 2019; Baquedano Estévez et al., 2019; Havlena et al., 2021).

Concerning the *Eukariotes*, *Streptophyta* phylum is the most diffused, represented totally by the *Ephemerum spinulosum* sp., mosses member of the *Pottiaceae* family, preferring moist habitats (Ignatov et al., 2013). Only one sample (L4), located in the cave deepest section, is dominated by *Chlorophyta* phylum, exactly by the green-algae *Pseudostichococcus monallantoides* sp.

The Shannon and Simpson diversity indices highlight that lampenflora from the Pertosa-Auletta Cave is characterized by small biodiversity. However, the community close to the entrance displays a higher biodiversity than that in the deeper zone, probably due to the proximity to the outer surface. In fact, among the drivers influencing its characteristics, the natural transport route and the dissemination of propagules (surely more pronounced near the entry) represent important factors in the underground ecosystem colonization (Mulec, 2019).The lampenflora community organization is observable also in the optical microscopy images, where it is possible to highlight the presence of several tangled filamentous microorganisms and superior organisms (green algae, rotifer…) of the trophic chain that in lampenflora matrix can find a readily available food source. Although the taxa identified, at higher level, exhibited qualitatively and quantitatively similarities with lampenflora samples from several others cave environments (Pfendler et al., 2018; Jurado, et al., 2020; Burgoyne

et al., 2021), at species level, the detected groups are unique of the Pertosa-Auletta Cave, probably related to the surface autochthonous biodiversity, specific of the geographical area where the cave opens.

5 Conclusions

Our integrated study of lampenflora from the tourist Pertosa-Auletta Cave provides a comprehensive overview of this alien photoautotrophic community in lit underground environments, whose diversity and eco-physiology are still little known. Spectra reflectance survey reveals its capacity to absorb the entire visible radiation, reflecting only the near-infrared, thanks to several trophic pathways, that make this community resilient and darkness resistant. Among the deterioration processes highlighted by the microscopy analysis, there are evidences of precipitation of $CaCO_3$ secondary structures, such as rods, reminiscent of moonmilk, as well as destructive processes with the production of corrosion shapes, promoting an irreversible alteration of surfaces. Filamentous organisms, entangled to the minerals, mainly represented by the nitrogen-fixing *Brasilonema angustatum* cyanobacterial species, together with the eukaryotes *Ephemerum spinulosum* and *Pseudostichococcus monallantoides*, constitute the almost totality of the community. Our findings contribute to the comprehension of effective and sustainable controlling strategies of lampenfora in underground environments. Future investigations, focusing on the definition of lampenflora metagenomic profile, will try to clarify the specific functions of the community and the interactions among the organisms constituting it and with the environment.

Acknowledgments

Thanks to MIdA Foundation, manager of the Pertosa-Auletta Cave, and to the speleo-guide Vincenzo Manisera for the support.

Funding

This work was partly funded by University of Salerno (Italy) within the ORSA197159 and ORSA205530 projects. Grant PID2019-108672RJ-I00 funded by MCIN/AEI/ 10.13039/501100011033 and, as appropriate, by “ERDF A way of making Europe”, by the “European Union” or by the “European Union NextGenerationEU/PRTR”.

Conflict of Interest

The authors declare that they have no conflict of interest.

References

Addesso, R., Bellino, A., D’Angeli, I.M., De Waele, J., Miller, A.Z., Carbone, C., and Baldantoni, D. (2019) Vermiculations from karst caves: The case of Pertosa-Auletta system (Italy). CATENA 182, 104178.

Baquedano Estévez, C., Moreno Merino, L., de la Losa Román, A., Durán Valsero, J.J. (2019) The lampenflora in show caves and its treatment: an emerging ecological problem. International Journal of Speleology 48 (3), 249-277.

Barton, H.A., Northup, D.E. (2007) Geomicrobiology in cave environments: past, current and future perspectives. Journal of Cave and Karst Studies 69 (1), 163–178.

Burgoyne, J., Crepeau, R., Jensen, J., Smith, H., Baker, G., and Leavitt, S.D. (2021) Lampenflora in a Show Cave in the Great Basin Is Distinct from Communities on Naturally Lit Rock Surfaces in Nearby Wild Caves. Microorganisms 9, 1188.

Caneva G., Nugari, M.P., Salvadori, O. (2008) Plant biology for cultural heritage: biodeterioration and conservation. Getty Conservation Institute, Los Angeles, 408.

Cafaro, S., Gueguen, E., Parise, M., Schiattarella, M. (2016) Morphometric analysis of karst features of the Alburni Mts, Southern Apennines, Italy. Geografia Fisica e Dinamica Quaternaria 39, 121–128.

Caporaso, J.G., Kuczynski, J., Stombaugh, J., Bittinger, K., Bushman, F.D., Costello, E.K., Fierer, N., Peña, A.G., Goodrich, J.K., Gordon, J.I., Huttley, G.A., Kelley, S.T., Knights, D., Koenig, J.E., Ley, R.E., Lozupone, C.A., McDonald, D., Muegge, B.D., Pirrung, M., Reeder, J., Sevinsky, J.R., Turnbaugh, P.J., Walters, W.A., Widmann, J., Yatsunenko, T., Zaneveld, J., Knight, R. (2010) QIIME allows analysis of high-throughput community sequencing data. Nature Methods 7,335–336.

Cigna, A.A. (2016) Tourism and show caves. Z. Geomorphology 60 (Suppl. 2), 217–233.

de Freitas, C.R., 2010. The role and the importance of cave microclimate in the sustainable use and management of show caves. Acta Carsologica, 39, 477-489.

Edgar, R.C. (2010) Search and clustering orders of magnitude faster than BLAST. Bioinformatics 26:2460–2461.

Grobbelaar, J.U. (2000) Lithophytic algae: A major threat to the karst formation of show caves. Journal of Applied Phycology 12, 309–315.

Havlena, Z., Kieft, T.L., Veni, G., Horrocks, R.D., and Jones, D.S. (2021) Lighting effects on the development and diversity of photosynthetic biofilm communities in Carlsbad Cavern, New Mexico. Applied Environmental Microbiology 87,e02695-20.

Ignatov, M.S., Ignatova, E.A., Malashkina, E.V. (2013) *Ephemerum spinulosum* Bruch & Schimp. (BRYOPHYTA), a new species for Russia. Arctoa (2013) 22, 97-100.

Jurado, V., del Rosal, Y., Gonzalez-Pimentel, J., Hermosin, B., and Saiz-Jimenez, C. (2020) Biological control of phototrophic biofilms in a show cave: the case of Nerja Cave. Applied Sciences 10, 3448.

Krause, S., Liebetrau, V., Nehrke, G., Damm, T., Büsse, S., Leipe, T., et al. (2019) Endolithic Algae Affect Modern Coral Carbonate Morphology and Chemistry. Front Earth Sci 7, 304.

Magoč, T., Salzberg, S.L. (2011) FLASH: fast length adjustment of short reads to improve genome assemblies. Bioinformatics 27, 2957–2963.

Maxwell, K, Johonson, G.N. (2000) Chlorophyll fluorescence - a practical guide. Journal of Experimental Botany 51 (345), 659-68.

Miller, A.Z, Garcia-Sanchez, A.M., Martinsanchez, P.M., Costa Pereira, M.F., Spangenberg, J.E., Jurado, V., Dionísio, A., Afonso, M.J., Iglésias Chaminé, H.I., Hermosin, B., Saiz-Jimenez C. (2018) Origin of abundant moonmilk deposits in a subsurface granitic environment. Sedimentology 65, 1482–1503.

Miller, A.Z., Garcia-Sanchez, A.M., Martin-Sanchez, P.M., Costa Pereira, M.F., Spangenberg, J.E., Jurado, V., et al. (2018) Origin of abundant moonmilk deposits in a subsurface granitic environment. Sedimentology 65, 1482–1503.

Mulec, J. (2014) Human impact on underground cultural and natural heritage sites, biological parameters of monitoring and remediation actions for insensitive surfaces: Case of Slovenian show caves. Journal for Nature Conservation 10.

Mulec, J. (2019) Lampenflora. In Encyclopedia of Caves. Elsevier, pp. 635–641.

Mulec, J. and Kosi, G. Lampenflora algae and methods of growth control. Journal of Cave and Karst Studies 71(2), 109–115.

Northup DE, Lavoie KH (2001) Geomicrobiology of caves: a review. Geomicrobiology Journal 18,199–222

Pfendler, S., Einhorn, O., Karimi, B., Bousta, F., Cailhol, D., Alaoui-Sosse, L., et al. (2017) UV-C as an efficient means to combat biofilm formation in show caves: evidence from the La Glacière Cave (France) and laboratory experiments. Environ Sci Pollut Res 24, 24611–24623.

Pfendler, S., Karimi, B., Maron, P.-A., Ciadamidaro, L., Valot, B., Bousta, F., Alaoui-Sosse, L., Alaoui-Sosse, B., Aleya, L. (2018) Biofilm biodiversity in French and Swiss show caves using the metabarcoding approach: First data. Science of the Total Environment 615, 1207–1217.

Piano, E., Bona, F., Falasco, E., La Morgia, V., Badino, G., and Isaia, M. (2015) Environmental drivers of phototrophic biofilms in an Alpine show cave (SW-Italian Alps). Science of the Total Environment 536, 1007–1018.

Popović, S., Krizmanić, J., Vidaković, D., Karadžić, V., Milovanović, Ž., Pećić, M., and Subakov Simić, G. (2020) Biofilms in caves: easy method for the assessment of dominant phototrophic groups/taxa in situ. Environ Monit Assess 192, 720.

Popović, S., Simic, G.S., Stupar, M., Unkovic, N., Krunic, O., Savic, N., and Grbic, M.L. (2017) Cave biofilms: characterization of phototrophic cyanobacteria and algae and chemotrophic fungi from three caves in Serbia. Journal of Cave and Karst Studies 79, 10–23.

R Core Team (2020) R Core Team R: A Language and Environment for Statistical Computing.

Roldán, M., Oliva, F., Gónzalez del Valle, M.A., Saiz-Jimenez, C., and Hernández-Mariné, M. (2006) Does Green Light Influence the Fluorescence Properties and Structure of Phototrophic Biofilms? Appl Environ Microbiol 72, 3026–3031.

Smith, A., Wynn, P., and Barker, P. (2013) Natural and anthropogenic factors which influence aerosol distribution in Ingleborough Show Cave, UK. IJS 42, 49–56.

Vaccarino, M.A. and Johansen, J.R. (2012) *Brasilonema angustatum* sp. nov. (Nostocales), a new filamentous cyanobacterial species from the Hawaiian Islands. Journal of Phycology 48, 1178–1186.

Supplementary materials

Figure S1 Optical microscopy images of the biofilms. (**a**); (**b**); (**c**); (**d**). Lampenflora images was obtained on a transmitted light Nikon Eclipse E-100 Microscope, equipped with a digital Nikon DS-Fi1 camera and processed in the image analysis program NIS Elements F.

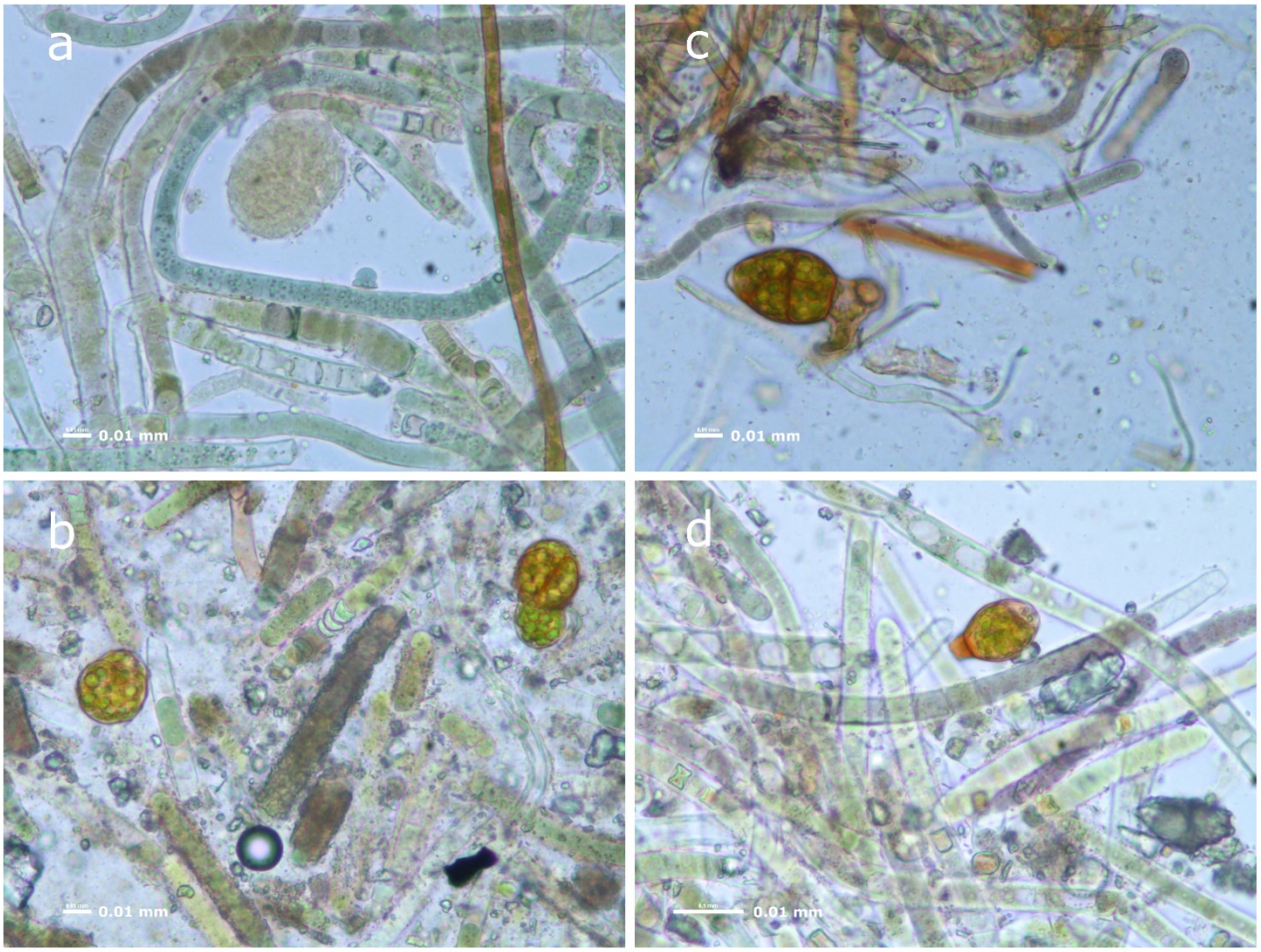

Section II

STRATEGIES FOR A SUSTAINABLE CAVE MANAGEMENT

The baseline study of Pertosa-Auletta cave ecology allowed defining several strategies for the sustainable management of speleological tourism, identifying the potential pressures due to the human presence in subterranean environment and providing new tools for damages mitigation.

In particular, an innovative high-resolution and low cost air monitoring system was proposed in Chapter 8, able to control the natural atmospheric dynamics as well as the tourist load of the Pertosa-Auletta Cave current management. Moreover, an explorative application of the cave airflow and particles scattering and deposition model, using COMSOL Multiphysics® software, for the first time in support of the tourism planning in vulnerable underground sites with a human fruition was also carried out (Chapter 9). Chapter 10 extended the study on the efficacy and sustainability, in terms of reduction and effects implemented on the rock surfaces, of the most used lampenflora removal and control methods (NaClO, H_2O_2 and UVC).

CHAPTER 8

Underground ecosystem conservation through high-resolution monitoring of show cave atmosphere

Rosangela Addesso, Alessandro Bellino*, Daniela Baldantoni

Submitted to Environmental Management (minor revisions)

**corresponding author*

A new tool to evaluate the tourism-induced alterations on the cave atmosphere has been proposed, through the development of novel low-cost and high-resolution monitoring stations and of useful methods to elaborate the obtained data.

Underground ecosystem conservation through high-resolution monitoring of show cave atmosphere

Rosangela Addesso, Alessandro Bellino* and Daniela Baldantoni

Department of Chemistry and Biology "Adolfo Zambelli", University of Salerno, Via Giovanni Paolo II, 132, 84084 Fisciano (SA), Italy

*Corresponding author: Alessandro Bellino, Tel.: +39 089 969542; Fax: +39 089 969603; email: abellino@unisa.it

Acknowledgments

Thanks to MIdA Foundation (SA, Italy), manager of the geosite Pertosa-Auletta Cave, for hosting the research activities and to Vincenzo Manisera, speleo-guide, for his untiring support. The research was carried out with funds from the ORSA197159 project, granted by the University of Salerno.

Abstract

The adoption of data-driven policies is increasingly recognized as the gold standard in managing and preserving ecosystems. The core strategy pivots on the role of monitoring in bridging policies and ecosystem dynamics, the scales of which dictate the necessary monitoring spatial and temporal resolution. In complex environments like cave ecosystems, where tourism fruition introduces moving sources of discontinuous disturbances, the adoption of high-resolution monitoring is crucial in assessing the system transient dynamics, a strategy hampered by the associated costs and workflow complexity.

With the aim of fostering the data-driven management of cave ecosystems, we provided a reference approach focused on the development of novel low-cost monitoring stations and their integration into a consistent analytical workflow aimed at evaluating the tourism-induced alterations of the natural dynamics and their scales.

The approach has been exemplified through its application in the Pertosa-Auletta Cave, one of the most important underground environments in Southern Italy, where it allowed analyzing the annual dynamics of temperature, relative humidity, CO_2, VOCs and particulate matter in terms of size and concentrations, understanding their coupling with the outer environment and assessing the alterations induced by tourism. On the one hand, findings shed novel light on the dynamics of this peculiar system, on the other hand, the simplicity, low-cost and effectiveness of the approach make it straightforwardly applicable to other underground ecosystems, where it can support the adoption of tailored management strategies.

Keywords: Atmospheric monitoring; Frequency spectra; Show caves; Tourist load; Time series.

Introduction

Caves are one of the most fragile ecosystems on Earth (White 2019). Being confined places, characterized by little spatial and temporal variability of several ecological factors, every anthropogenic disturbance can easily trigger alterations taking longer to settle, and possibly never returning to the initial states (Lobo et al. 2013). Unfortunately, the wonders of these peculiar ecosystems attract thousands of visitors every year (de Freitas 2010; Lobo et al. 2015; Danardono et al. 2018), that represent a serious threat for their preservation. The understanding of the nature and extent in space and time of the anthropogenic disturbances in caves is thus a priority for their sustainable management and long-term conservation (Cigna and Burri 2000; Korzystka et al. 2011; Lobo et al. 2013; Lobo et al. 2015).

Among the environmental compartments, the atmosphere inside caves is the most directly affected by tourism, and the one in which the effects of anthropogenic alterations reverberate at larger spatial scales due to mass flows. Although other forms of alterations may result in more visible injuries to the system, like the physical destruction of speleothems or the development of lampenflora, alterations of the atmosphere may have more subtle, but also more pervasive, effects on system dynamics. Notable examples are the heat from human body affecting cave temperature and relative humidity, the tourist breathing increasing the natural CO_2 concentration, and the introduction of alloctonous species (e.g. through spores) altering the endogenous communities (Chiesi 2002; Russell and MacLean 2008; Smith et al. 2013). All of these are able to affect the reactions at the interface between atmosphere, lithological substrate, water film and microbial community, that in turn controls most ecosystem processes like the formation/destruction of speleothems (Pulido-Bosch et al. 1997; Chiesi 2002; Calaforra et al. 2003; Milanolo and

Gabrovšek 2009; de Freitas 2010; Lang et al. 2015a; Lang et al. 2015b; Carrasco et al. 2016; De Vincenzi et al. 2016; Howarth 2019).

Obviously, not every cave responds to these alterations in the same manner. The degree of vulnerability can, in fact, depend upon the morphology of the cave, nature of the substrate, hydrological characteristics, age and, most importantly, tourist load in terms of number of tourists, temporal profile of visits (duration, frequency, breaks between and during tours) and extent of the cave visited. For example, morphological characteristics can produce internal climatic zonation, creating several spatial and temporal microclimatic niches that affect cave responses to changes (Russell and MacLean 2008).

Bringing all these aspects together in defining successful policies and management practices is a challenging task. In this context, the adaptive ecosystem management paradigm, considered the gold standard in addressing these challenges, pivots on environmental monitoring as the process allowing gathering information from the environment and assessing action outcomes, promoting their continuous adaptation. Although the natural dynamics, either spatial or temporal within the cave ecosystems usually occur at large scales (meters/hours and above), tourism-induced alterations can manifest themselves in transients at finer scales. This is especially true when considering the effects of tourism on the cave atmosphere, characterized by a naturally higher variability in space and time as compared to other environmental compartments. The understanding of the pressure exerted on the cave ecosystem by anthropogenic activities requires thus high resolution monitoring, in either space or time, that can be financially and technically challenging. Developing novel robust and low-cost means to continuously monitor the cave atmosphere can be thus crucial in empowering authorities with the right tools to apply the adaptive ecosystem

management to these systems. However, the monitoring itself proves pointless without the proper means of aggregating and analyzing the amount of data produced. In this context, the integration of advanced time-series analysis with high resolution monitoring has the potential to provide insightful results, through the extraction of ecologically meaningful information on small-scale transients within the system.

Moving from these considerations, the present research aimed at integrating high time resolution monitoring within a consistent analytical framework focused on evaluating the effects of anthropogenic alterations, their spatial behavior and their temporal scales. The implementation relied on the development of novel robust and low cost monitoring stations able to collect data on a large number of atmospheric parameters, and on the analysis of their temporal variations on sub-hourly to monthly scales. The approach has been exemplified through a field study in the Pertosa-Auletta Cave (Campania region, Italy), one of the largest underground systems of Southern Italy (Addesso et al. 2019; Addesso et al. 2021), hosting more than 60.000 visitors per year. The research was able to exploit also the unique scenario set up by the SARS-CoV-2 outbreak, creating an involuntary experimental setting, allowing evaluating the effects of different cave management policies over the time.

Materials and methods

The continuous monitoring of key atmospheric parameters (temperature, relative humidity, pressure, CO_2, VOC, particulate matter) was carried out through the development of two monitoring stations focused on providing good accuracy, robustness toward prolonged operation in saturating relative humidity and low cost. In particular, the stations were built around the popular ESP8266EX (Wemos D1 R2 development board, China) featuring a Tensilica L106 32-bit microprocessor with 80

MHz (160 MHz max) clock and a Wi-Fi module. Sensors for temperature, relative humidity, pressure, CO_2, VOC, typical particulate size (weighted average of the particle sizes in the analyzed air volume), PM0.5, PM1.0, PM2.5, PM4.0 and PM10, the details or which are reported in Table S1, were operated through a single I2C bus for the digital readout. Data retrieved were written at each cycle on a microSD card, by means of an I/O board operated through an SPI interface. A high accuracy (± 2 ppm) DS3231 real time clock (Maxim Integrated, USA) was included in the design and operated through the I2C bus. The entire system was powered through a switching power supply operated in SEPIC mode (Torpedo, Futura Elettronica, Italy), allowing the seamless switch between DC (5V) and a LiPo battery granting ~10 h of operation, recharged when DC was available. The entire electronics were enclosed in standard electrical cassettes and mounted upside-down (Fig. 1), with a fan continuously pulling air from below the stations and pushing it inside the cassette. Such a design allowed avoiding the occurrence of condensation upon the electronics and their long-term flawless operation. All the sensors were built inside the cassettes, with the exception of one of the temperature/relative humidity sensors (SH10/Adafruit 1298) enclosed in a sintered aluminum case, allowing its operation at ambient conditions and avoiding biased readings due to the heat from electronics. The presence of redundant sensors (3 for temperature and 2 for relative humidity) increased the robustness of the apparatus, allowing the crossed check of sensor functioning. Moreover, a push notification system was implemented within the board software through the Pushetta API (https://www.pushetta.com), allowing sending real-time notifications about possible malfunctioning of the stations on smart devices through the Wi-Fi module.

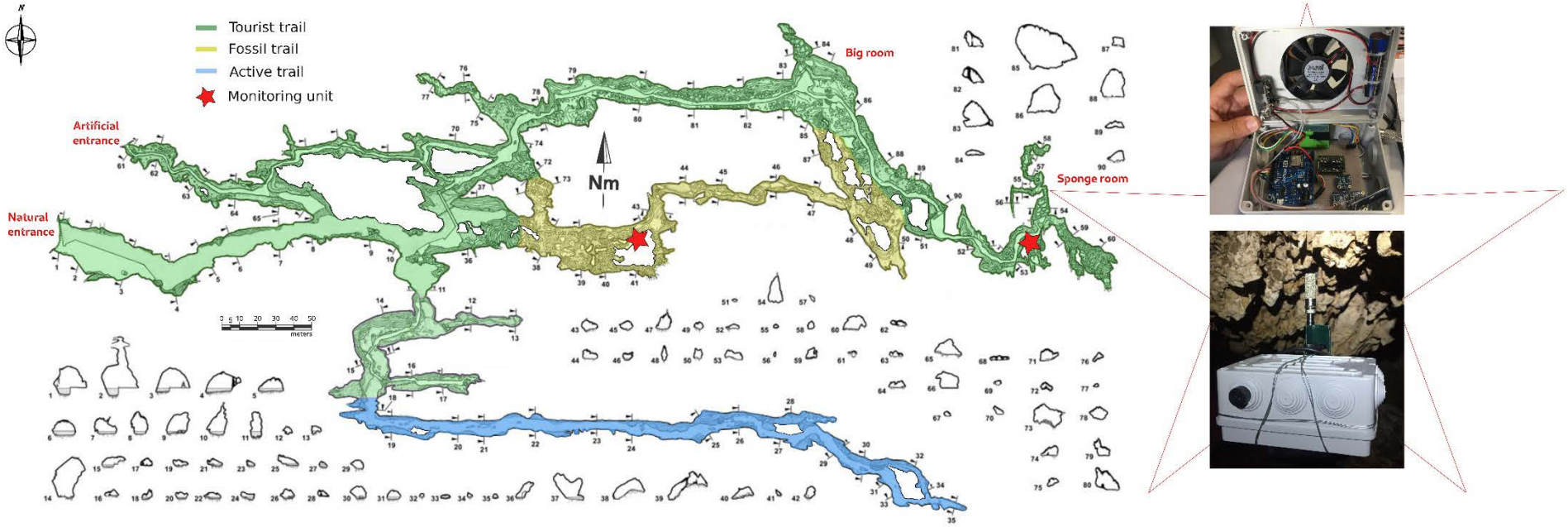

Fig. 1 The Pertosa-Auletta Cave system, with indication of the sectional profiles, the natural (always open, but inaccessible to tourists) and artificial (open on-purpose for tourist transit) entrances, the main trails (in different colors) and the locations of the monitoring stations (red stars). Images of the stations with the internal electronics and installed *in situ* are also shown

142 The two monitoring stations were located in two sections of the Pertosa-Auletta
143 Cave (Fig. 1), hereafter referred as “tourist trail” and “fossil trail” according to the
144 official denomination of the management authority, the description of which is
145 extensively reported in Addesso et al. (2019) and in Addesso et al. (2021). Station
146 positioning aimed at evaluating the relative amplitude and scales of the tourist-
147 induced contributions upon the natural fluctuations in atmospheric parameters,
148 allegedly mainly driven by the cave coupling with the external environment. As such,
149 the stations were set up in places subjected to different levels of tourism fruition and
150 at increasing distance from the cave natural entrance (Fig. 1). In particular, the first
151 one was installed in the final part of the tourist trail, lit, rich in speleothems due to the
152 intense dripping activity and habitually frequented by visitors. The second one was
153 installed in the middle of the fossil trail, which is closed to public to protect several
154 bats colonies, unlit, with few speleothems, numerous fractures and collapsing
155 deposits. In this way, the latter should be able to record the natural fluctuations in
156 atmospheric parameters with little contribution from tourists. Such contribution
157 should instead be recorded with high sensitivity by the former, due to the proximity of
158 tourist transit and the expected lower background fluctuations in the innermost part of
159 the cave.

160 Data were collected every minute from August 2019 to September 2020, with a
161 brief (2 weeks) interruption on January 2020 due to technical problems with the cave
162 power supply. All of the parameters were acquired during the entire period, with the
163 exception of CO_2, whose data were missed from November 2019 to January 2020 due
164 to an erroneous sensor recalibration that was later fixed. Overall, the monitoring
165 period consisted of 3 phases defined by the different tourism management: i)
166 unrestricted tourism (1st August 2019 - 9th March 2020), when an unlimited number of

167 tourists was allowed joining the tours and visiting the cave, ii) pandemic-related
168 lockdown (10th March 2020 – 10th June 2020), when the cave gates were closed and
169 nobody was allowed entering the cave, and iii) controlled tourism (11th June 2020 –
170 1st September 2020), when fewer and smaller tourist groups were allowed visiting the
171 cave at the same time, with shorter tours. Moreover, the path followed by tourists
172 during the 3rd phase ended in the "Big room" instead of the "Sponge room" (Fig. 1),
173 preventing tourists reaching the section monitored by the station in the tourist trail.
174 The monitoring station output consisted of a CSV file format, with data
175 organized in a matrix structure, and the (UTC) time-date field complying with the ISO
176 8601 format. Data were processed and analyzed within the R 4.10 programming
177 environment (R Core Team 2021), with functions of the "lubridate", "tsbox",
178 "tsibble", "fable", "feasts", "anomalize", and "WaveletComp". In particular, data
179 were imported and represented as multivariate time series using the *tsibble* object
180 representation. Data on the number of visitors within the cave, derived from the
181 authority registers, were expressed on the same time base of the monitoring data and
182 added to the latter, in order to evaluate possible relationships between tourist load and
183 atmospheric parameters. Time series were individually cleaned from outliers,
184 identified on the residuals of STL seasonal decomposition models through the
185 interquartile range (IQR) method, and substituted by values estimated from the STL
186 models. In order to estimate the multiple temporal scales subtending the fluctuations
187 in the monitored parameters and evaluate the possible co-variations between them and
188 the tourist load, wavelet periodograms and cross-periodograms were calculated. In
189 particular, the frequency spectrum of time series was analyzed through Morlet
190 wavelet transformation and the significance of the periods was evaluated through
191 simulations (n = 10) against white noise. The phase information derived from wavelet

192 analysis was employed instead in the analysis of the co-variations of bivariate time
193 series, through the calculation of wavelet cross-power spectra.
194
195 **Results**
196 The dynamics of all the analyzed parameters over the monitoring period are
197 shown in Fig. 2, with the monthly minima and maxima reported in Table S2.
198 Temperature, relative humidity and CO_2 are the only ones showing large scale
199 temporal dynamics, all the others appearing stationary over the year of monitoring,
200 with variations mostly occurring at small scales. These variations span several orders
201 of magnitude over the baseline in the case of VOCs and particulate concentrations or
202 are contained within 3 times the baseline in the case of the typical particulate size. In
203 the case of particulate concentrations, the widest fluctuations occur between
204 November and June, whereas the largest VOC fluctuations are evenly distributed
205 across the year of monitoring, with the exception of the period from March to July
206 (Fig. 2). The redundant temperature and humidity sensors provided the same trends of
207 the SHT10 sensor enclosed in the sintered aluminum case, with 0-lag cross-
208 correlations $r > 0.71$ ($P < 0.001$) in all the cases.
209 The lockdown phase spanned almost 4 months and allows evaluating the
210 background levels of the parameters with stationary fluctuations, by removing the
211 contribution of anthropogenic activities within the cave. An excerpt of the dynamics
212 recorded during this phase is shown in Fig. S1. Daily fluctuations are evident in most
213 of the traces, especially in VOCs, with comparable oscillations in both the trails, CO_2
214 monitored in the fossil trail and, to a lesser extent, relative humidity in the tourist trail.
215 Daily oscillations are recorded also in particulate matter concentrations, with the
216 different dimensional classes sharing the same trend, superimposed on faint weekly

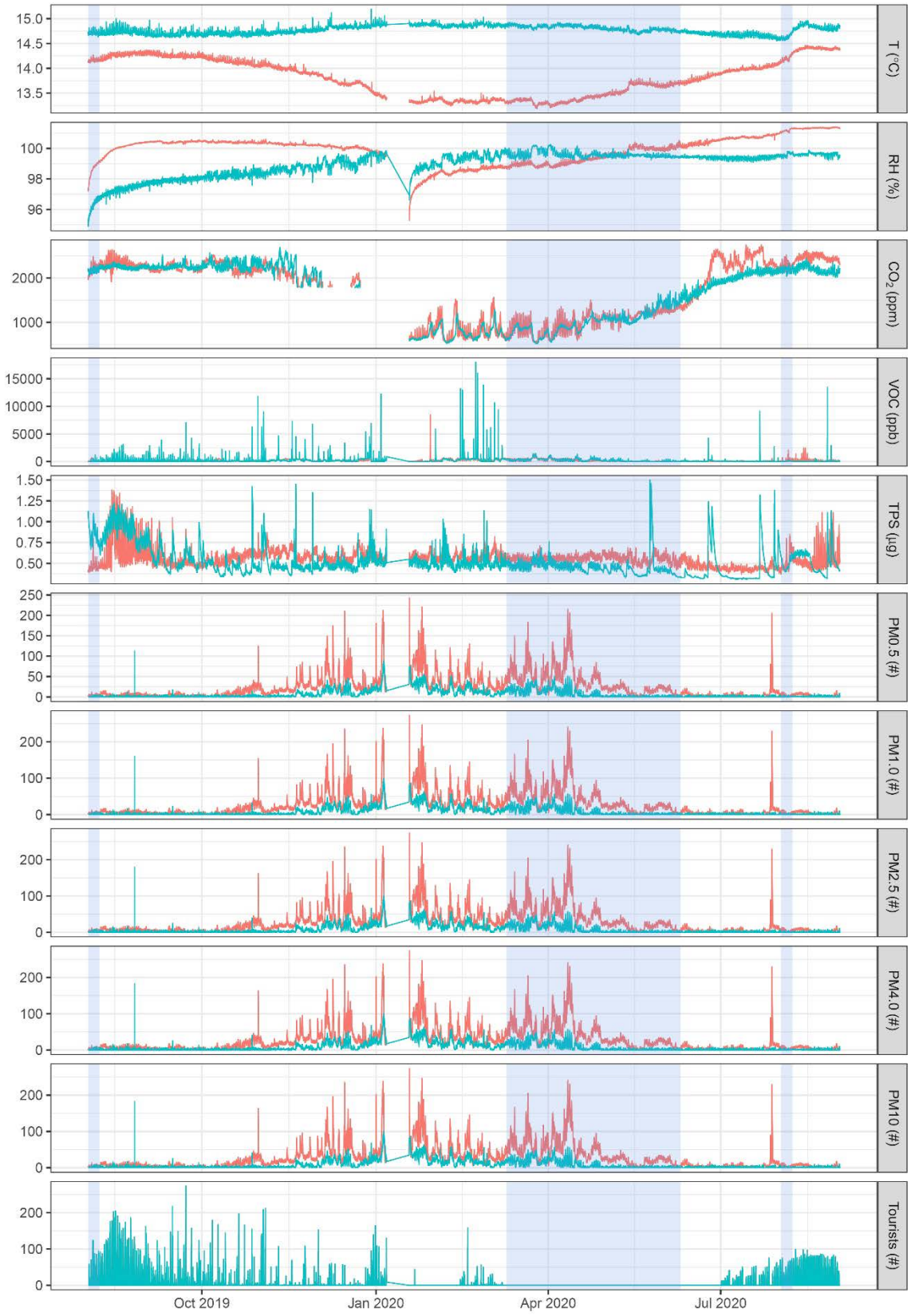

Fig. 2 Time series of all the parameters monitored (temperature: T, relative humidity: RH, CO_2, VOC, typical particulate size: TPS, PM0.5, PM1.0, PM2.5, PM4.0, PM10) in the tourist (green) and fossil (red) trails, as well as the number of tourists in the cave. Shaded areas indicate, in the order, the portion of time series detailed in Figs. S2 (extract from the phase of unrestricted tourism), S1 (pandemic-related lockdown) and S3 (extract from the phase of controlled tourism)

fluctuations in the case of the fossil trail. In all the traces, the amplitude of the variations reduces from the onset May. The typical particulate size is unique among the parameters investigated in showing approximately constant values over the entire period, which are comparable to the limit of detection of the sensor employed (~ 0.3 particles cm^{-3}). On the opposite, relative humidity is always close to the upper limits of sensor functioning, with a progressive increase in the fossil trail.

In terms of the dynamics during cave opening to the public, an excerpt from the first week of August in 2019 and 2020, under unrestricted and controlled tourism, respectively, is shown in Figs. S2 and S3. Daily oscillations are more evident in 2019 than in 2020, especially in CO_2, typical particulate size and temperature, as well as in the tourist trail in respect to the fossil trail. Superimposed on the daily oscillations, CO_2, temperature, VOCs and, to a lesser extent, relative humidity also show small scale variations that are concurrent with the passage of tourists. These variations were recorded in 2019 and in the tourist trail only, with the exception of CO_2, temperature and typical particulate size that show them also in the fossil trail or, in the case of the latter, exclusively in this trail. VOCs is the unique parameter showing small scale variations following the passage of tourists in 2020, which are evident in the fossil trail only.

Periodograms for the parameters analyzed in the tourist (Fig. 3) and the fossil (Fig. 4) trails highlight the presence of daily oscillations in most of the traces with harmonics at both higher and lower periods. In the tourist trail, CO_2, VOCs, temperature and, to a lesser extent, relative humidity show significant sub-day oscillation periods that are coherent with the passage of tourists in 2019, with the smallest ones in the order of a few minutes. Particulate matter also shows high frequency oscillations, but evenly distributed over the time-span of the analysis and

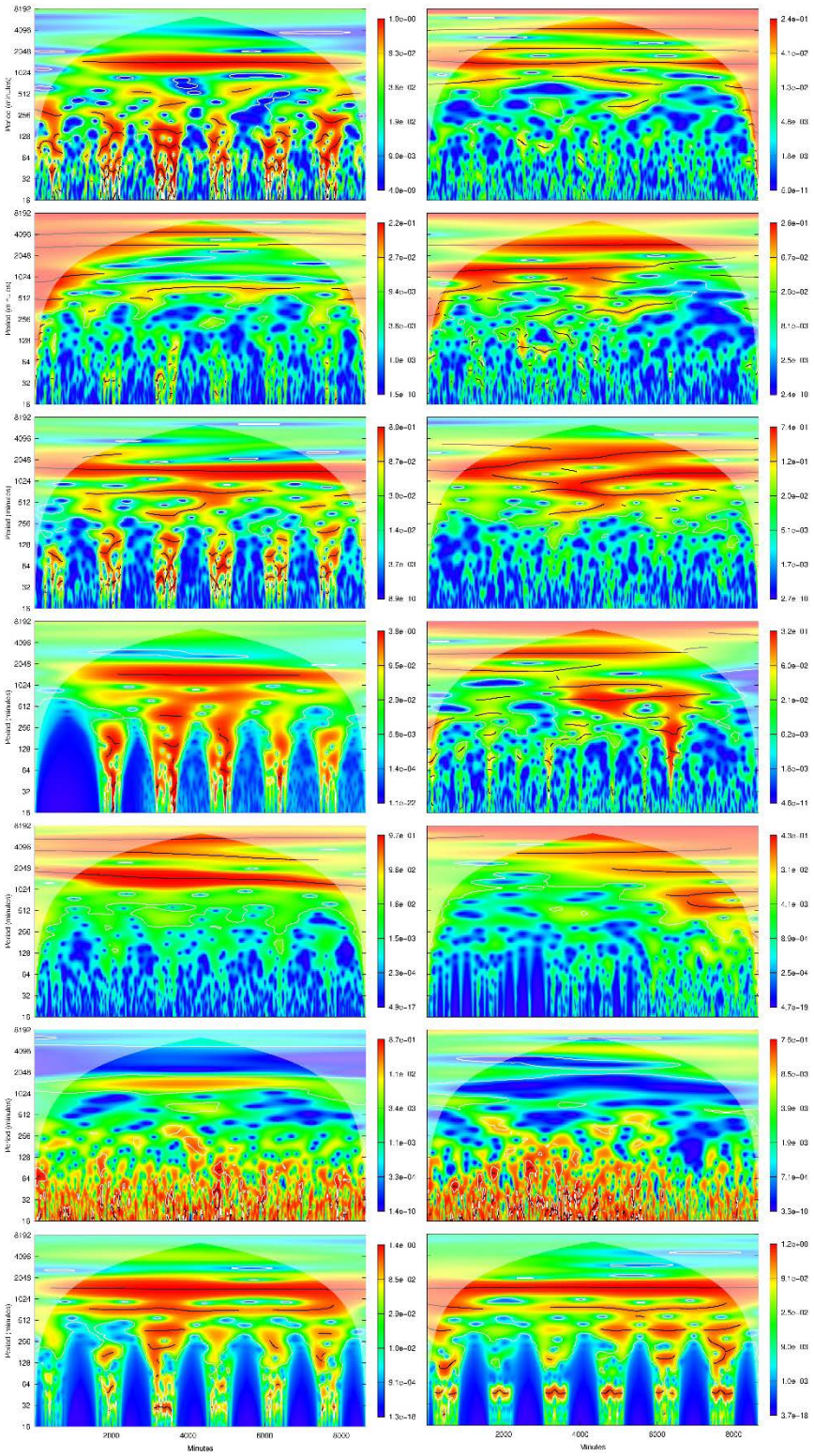

Fig. 3 Wavelet periodograms of the time series (from top to bottom: temperature, relative humidity, CO_2, VOCs, typical particulate size, PM10, number of tourists) during the first week of August 2019 (left column - from 2019-08-02 04:41:00 to 2019-08-08 04:41:00) and of August 2020 (right column - from 2020-08-02 04:41:00 to 2020-08-08 04:41:00) in the tourist trail. The x-axis indicates the minutes from the beginning of the time series, whereas the y-axis the wavelet periods (in minutes). Due to the similarity among the time series relative to the particulate matter classes, only the periodogram for PM10, as representative of the others, is shown. The wavelet power spectrum is represented on quantile scales, with white lines enclosing regions of significant (for $\alpha = 0.05$) periods and black lines indicating wavelet ridges

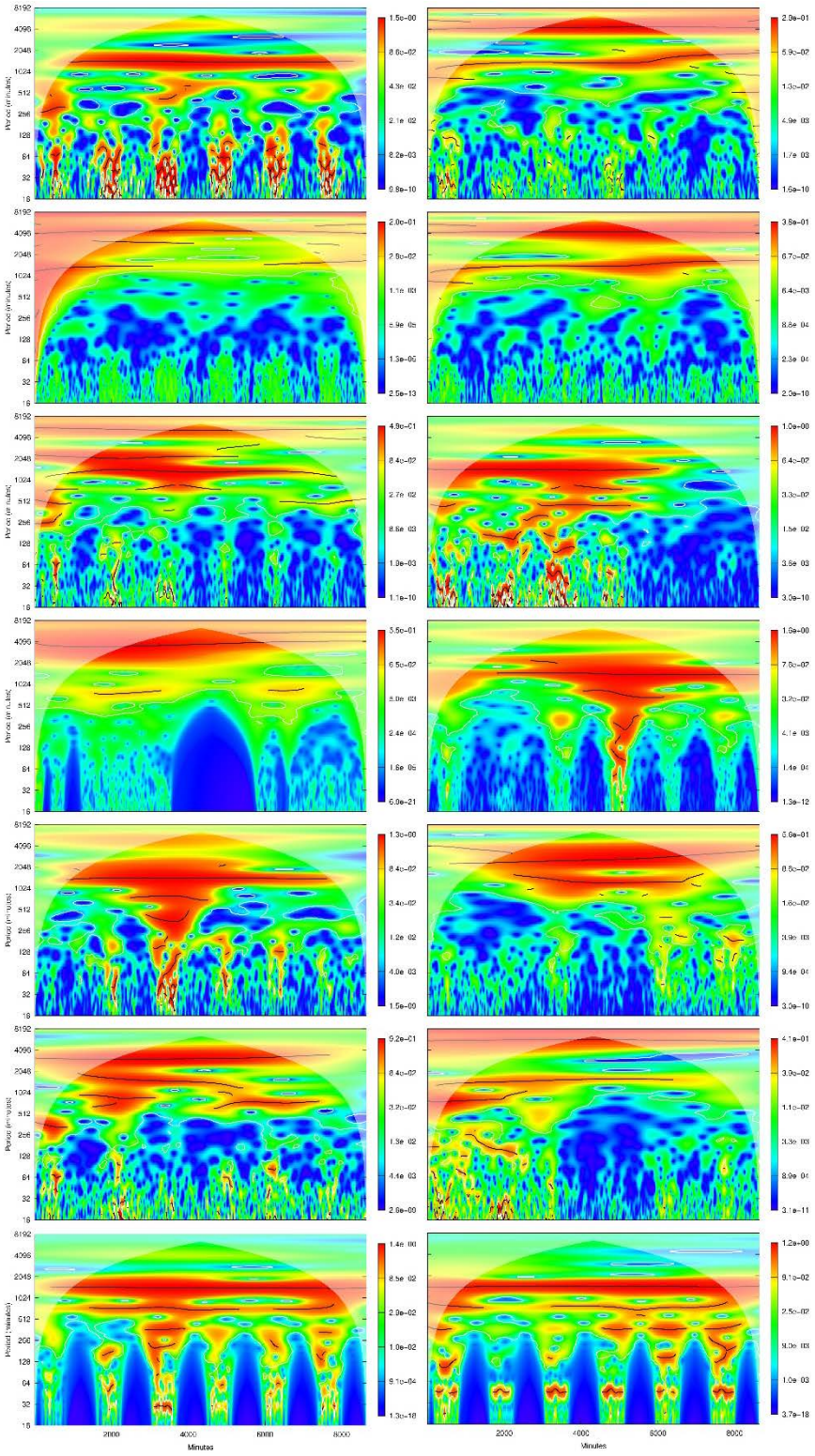

Fig. 4 Wavelet periodograms of the time series (from top to bottom: temperature, relative humidity, CO_2, VOCs, typical particulate size, PM10, number of tourists) during the first week of August 2019 (left column - from 2019-08-02 04:41:00 to 2019-08-08 04:41:00) and of August 2020 (right column - from 2020-08-02 04:41:00 to 2020-08-08 04:41:00) in the fossil trail. The x-axis indicates the minutes from the beginning of the time series, whereas the y-axis the wavelet periods (in minutes). Due to the similarity among the time series relative to the particulate matter classes, only the periodogram for PM10, as representative of the others, is shown. The wavelet power spectrum is represented on quantile scales, with white lines enclosing regions of significant (for $\alpha = 0.05$) periods and black lines indicating wavelet ridges

with a reduced contribution of daily fluctuations, that primarily determine, instead, the time series of the typical particulate size. The high frequency oscillations disappear in 2020 in the tourist trail from almost all the parameters but, where present, are either evenly distributed along the time series such as in particulate matter, or scattered throughout the time span of the analysis such as in relative humidity and VOCs, without clear patterns. With the exception of temperature, typical particulate size and CO_2, all the parameters recorded in the fossil trail in 2019 do not show high frequency variations coherent with the passage of tourists. However, even in the cases where the presence of fluctuations coherent with the passage of tourists were observed, the patterns are less clear than those observed in the tourist trail, especially for the typical particulate size and CO_2. The absence of frequency components attributable to the passage of tourists is common among the periodograms for the parameters recorded in the fossil trail in 2020, with the notable exception of VOCs.

The synchronicity between the time series of the monitored parameters and of the number of tourists was analyzed on the series showing the clearest coherency of the frequency patterns with the passage of tourists, *i.e.* CO_2, temperature and VOCs recorded in the tourist trail in 2019 (Fig. 5). The daily oscillations are in-phase in the case of temperature and VOCs and out-of-phase in the case of CO_2, with the number of tourists always representing the leading trace. The synchronicity in the harmonics at 12 hours is similar, instead, between CO_2 and VOCs, both in-phase and with the number of tourists as the leading trace, whereas it represents the lagging trace in the case of temperature. At periods lower than 12 hours all the cross-periodograms show wide phase variations, similar among the parameters, on time scales in the order of minutes/few hours, with the number of tourists shifting from the leading to the lagging trace.

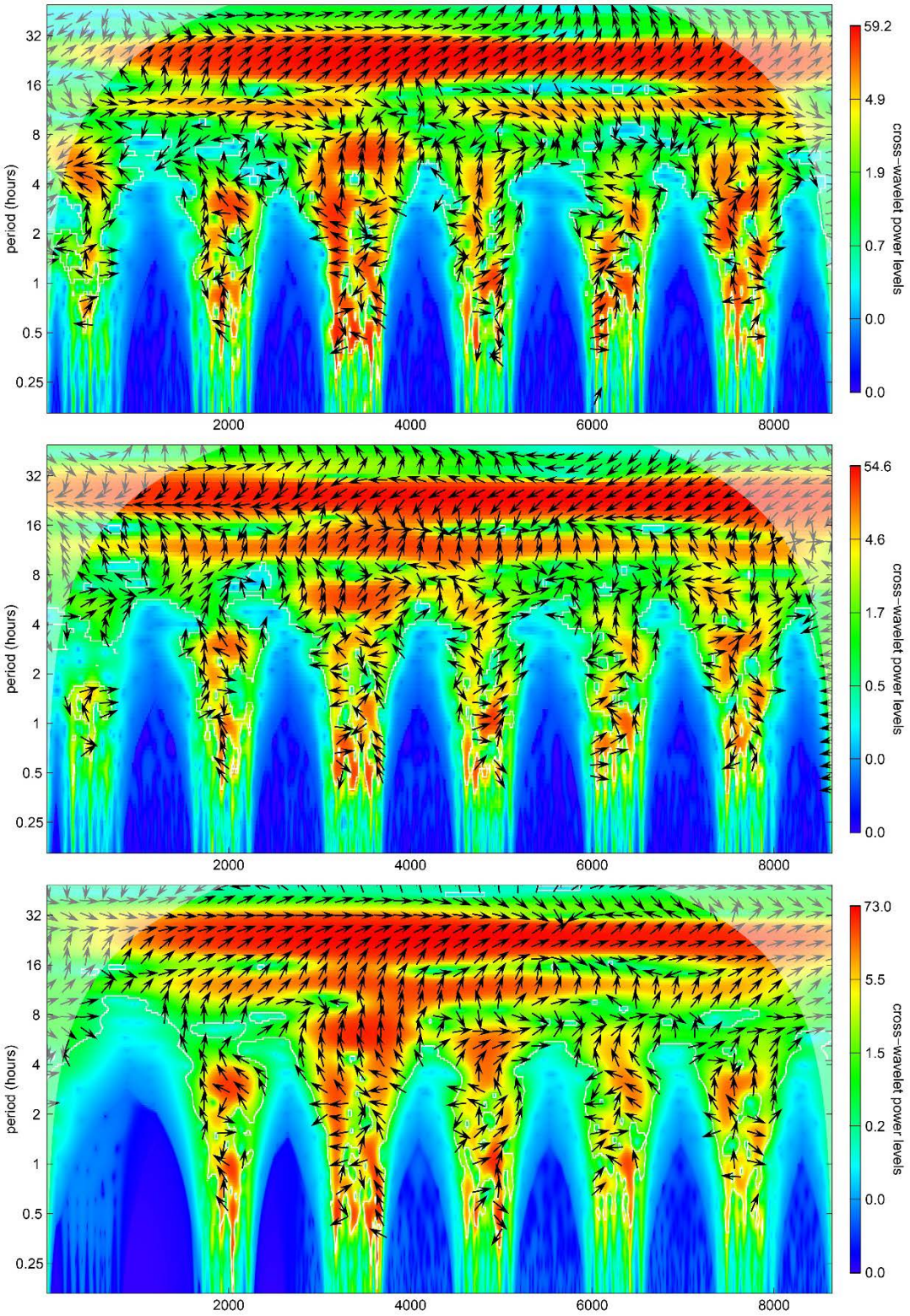

Fig. 5 Wavelet cross-periodograms between temperature (upper panel), CO_2 (middle panel), VOCs (bottom panel), and the number of tourists during the first week of August 2019 (from 2019-08-02 04:41:00 to 2019-08-08 04:41:00) in the tourist trail. The x-axis indicates the minutes from the beginning of the time series, whereas the y-axis the wavelet periods (in hours). The cross wavelet power spectrum is represented on quantile scales, with white lines enclosing regions of significant (for $\alpha = 0.05$) periods and black lines indicating wavelet ridges. Arrows represent the relative phase of the tourist and the parameter wavelets: wavelets are in-phase in I and IV quadrants and out-of-phase in II and III quadrants, with the tourist leading in the I and III quadrants and lagging in the II and IV. The arrow angle indicates the phase difference between the wavelets of the two series

Discussion

In terms of hardware, the monitoring stations proved effective and reliable over the entire experimental period, providing 1-minute resolution data for 13 months without clear evidences of long-term drifts or general electrical problems. The data from the redundant sensors further demonstrate the accuracy of the temperature and relative humidity recordings, a remarkable result considering the low cost of the stations, with raw prices in the order of one hundred euros. The unique fault observed during the experiment was on the software side, caused by a recalibration routine embedded within the CO_2 sensor that was later disabled. In spite of the lack of issues, however, two technical limitations are worth mentioning. The first lies in the inability of the particulate sensor to provide reliable size-partitioning of the particulate matter, an issue attributable to the low particulate concentration and its typical size, with values near the lowest limits of detection of the SCD30 sensor employed. The second limitation involves the long burn-in phase of the relative humidity sensor, attributable to its enclosing in a sintered aluminum case, needed to prevent condensation from harming the sensor. Overall, however, although they slightly limited the availability or quality of data, neither of these issues represented a critical drawback of the stations for the aims of the present research.

In terms of system dynamics, the positioning of the monitoring stations and the different cave management adopted over the time created spatial and temporal references allowing evaluating the natural dynamics of the cave, the effects of tourism, and how cave morphology shapes system responses. By all accounts, the effects of tourism appears negligible at large temporal and spatial scales, notwithstanding its intensity. Indeed, the strong seasonality in parameters like CO_2

292 and temperature, with contrasting trends between autumn-winter and spring-summer,
293 is coherent with the hypothesis of dynamics controlled by the annual variations in
294 solar irradiation in the Northern hemisphere. The tourism does not appear to affect
295 these trends, as demonstrated by the springtime increase in CO_2 concentrations pre-
296 dating the cave opening to the public and the lack of signal from the onset of tourism
297 on the trends. These considerations apply to both the trails that, however, show
298 interesting differences in their behavior regarding either the trends in the parameters
299 analyzed or the amplitude of daily oscillations.
300 The former scenario involves the temperature, whose annual trends between the
301 trails are in anti-phase, *i.e.* the fossil trail cools-down while the tourist trail warms-up.
302 To an extent, a similar contrasting behavior between trails is appreciable also in
303 relative humidity, although far less clearly due to the burn-in phase of the sensors and
304 the values always close to saturation. The morphology of the cave (Addesso et al.
305 2019; Addesso et al. 2021), with the fossil trail directly exposed to the inflow of
306 external air from the big natural entrance (30 m x 70 m) and the end of the tourist trail
307 constituting the recessed innermost part of the cave, may account for this behavior.
308 On the one hand, it is certainly responsible for the reduced amplitude of the annual
309 variations in the tourist trail but, on the other hand, may also explain its rise in
310 temperature when a decrease was actually expected. Indeed, the cooling of the cave,
311 beginning from the cave entrance, can force the water vapor in the innermost part of
312 the cave to progressively condense and release latent heat. Such a hypothesis is in line
313 with the described intertwined dynamics among external temperature, rock
314 cooling/warming and air drying/wetting (de Freitas and Littlejohn 1987; Forbes 1998;
315 de Freitas 2010) and can account for the rise in temperature during winter-spring.
316 Although the relative humidity trace in theory should provide insights on this process,

317 the values always close to saturation and the continuous inputs of vapor associated to
318 the water movements, especially intense in the tourist trail, actually hamper testing
319 such a hypothesis.

320 The dampening effect of cave morphology on the temperature changes in its
321 innermost part reverberates also on other parameters, especially particulate
322 concentrations. Indeed, they show wider daily oscillations in the fossil trail than in the
323 tourist trail, a behavior coherent with the influx of external air from the big entrance
324 conveying particulate matter (Badino 2010). In this context, it is interesting to note
325 hints of weekly fluctuations in particulate concentrations during the lockdown phase,
326 indicating the coupling of these concentrations with what happens in the outer
327 environment. Indeed, weekly signals in time series are signatures of anthropogenic
328 effects that, in the case of the Pertosa-Auletta Cave, could be exerted either directly,
329 e.g. through the influx of air affected by vehicular traffic, or indirectly through
330 possible alterations of bat activity. However, the occurrence of higher particulate
331 concentrations during winter-spring, a period of frequent poor weather in the area,
332 suggests that the influx of external air primarily controls particulate dynamics within
333 the cave. An important corollary result of these trends is the negligible effect exerted
334 by tourists on particulate concentrations, with the lowest values observed during the
335 highest tourist loads. This is obviously a result of the highly controlled behavior of
336 tourists enforced by guides, but nonetheless demonstrates that a correct management
337 of tourism can ensure its negligible impact on the particulate component of cave
338 atmosphere. This finding is further supported by the lack of high frequency signals
339 coherent with the passage of tourists in the periodograms of the particulate matter,
340 whereas they clearly indicate, instead, tourism-induced variations on other
341 parameters, most notably CO_2, temperature and VOC. In this context, the dynamics of

342 CO_2 are particularly interesting, since they are considered the most important proxy
343 for the effects of tourism on cave atmosphere (Lobo et al. 2013). Generally, caves
344 have a positive balance of CO_2, with source processes like decomposition of organic
345 matter, respiration by cave flora and fauna (including tourists), water degassing and
346 diffusion from the above soil largely exceeding the sinks, mainly restricted to water
347 dissolution and fixation by chemolithotrophs (Faimon 2006; de Freitas 2010;
348 Breecker et al. 2012; Mattey et al. 2016). The latter is fostered by geothermal activity
349 providing energy to the process (D'Angeli et al. 2019) that, however, lacks in the
350 Pertosa-Auletta Cave and contributes to CO_2 concentrations topping 2000 ppm in
351 summer-autumn. To a various degree, all the sources and sinks are controlled by
352 temperature and is thus unsurprising the close similarity between the annual dynamics
353 of CO_2 and temperature in the fossil trail. What is remarkable is the decoupling
354 between these traces in the tourist trail and the substantial overlapping of CO_2
355 dynamics between the tourist and the fossil trails, with the former constituting a sort
356 of average of the latter during winter-spring. Here, cave ventilation can play a key
357 role in CO_2 diffusion, especially in high-energy horizontal caves like the Pertosa-
358 Auletta Cave (Addesso et al. 2019; Addesso et al. 2021) facilitating airflow
359 exchanges, as do the inherent seasonality in several processes. Irrespective of the
360 processes involved in shaping the annual trends, however, tourism appears to control
361 CO_2 dynamics on scales in the order of minutes-few hours only and locally, in the
362 proximity of the visitors. In other words, the monitoring stations are able to record the
363 signals from tourists only when they pass in their proximity, and the signals decay
364 shortly after the passage. This finding holds true also for temperature and, especially,
365 VOCs, contributing to define a comprehensive scenario of tourism-induced alterations
366 to the system. Indeed, when tourists got to the end of the tourist trail, in 2019, the

high-frequency oscillations in CO_2, temperature and VOCs could be recorded by the station in the tourist trail only, with the exception of a faint signal on temperature in the fossil trail. In 2020, when tourists were allowed reaching the "Big room" only and stopping over at around one hundred meters away from the station in the fossil trail, the signals disappeared from the tourist trail and appeared in the fossil trail, albeit fainter and mostly on VOCs only.

The spatial decay of the tourism-induced signals appears thus to be faster for CO_2 and temperature than for VOCs, and it is likely controlled by the dilution of CO_2 and VOCs in the cave atmosphere and by the thermal energy absorption as latent heat. In this context, the naturally high CO_2 concentrations and large thermal capacity of saturated air make up for a quick disappearance of the contributions from tourist breathing and body heat exchanges. The usually low VOC concentrations, instead, allow the emissions from tourists, through exhalation or direct emission from skin and clothes (Fenske and Paulson 1999; Ziwei et al., 2020), to be recorded at larger distances. Interestingly, the absorption of thermal energy inputs as latent heat has been claimed to account for the similar quick decay of thermal signals from tourists also in the Eagle Cave (Domínguez-Villar et al. 2010). Remarkably, short-term tourism-induced variations in temperatures have been recorded in several caves, like the Candamo Cave (Hoyos et al. 1998), the Dechen Cave (Pflitsch et al. 2000), or the Santana Cave (Lobo et al. 2015), with variable recovery rates in the order of hours. This occurrence suggests that the induction of high-frequency temperature transients may be relatively common in show caves, with recoveries controlled by cave characteristics like morphology and hydrology. In this context, the present research introduces a novel dimension to the topic by demonstrating similar dynamics also for CO_2 and, especially, VOCs that, to our knowledge, has been never adopted in

392 monitoring tourism-induced alterations in underground ecosystems. Incidentally,
393 VOCs is also the parameter showing the clearest responses to tourist fruition,
394 accounting for promising developments in the search for effective proxies of
395 anthropogenic alterations. In terms of temporal scales, the large phase-shifts between
396 CO_2, temperature, VOCs and the tourist load trace support the hypothesis of
397 alterations dampening shortly after the passage of tourists. Indeed, the latter trace was
398 constructed from the logs of tourist entrances and exits, which made up for
399 unpredictable lags between the alleged and the true passage of visitors in the
400 proximity of the monitoring stations. The phase-shifts reflect both these lags and the
401 decay of signals from previously transiting groups, which result in rapid changes in
402 the relative phase of trace oscillations. The time span of these changes allows thus
403 grossly estimating the time scale of the tourism-induced alterations in the order of
404 minutes, which is coherent with spatial scales in the order of few meters. In this
405 context, the similarity in phase shifts among CO_2, temperature and VOCs is
406 remarkable and demonstrates the coherent temporal behavior of these proxies of
407 tourism-induced alterations.
408

409 **Conclusions**

410 From a conservation perspective, the high-resolution monitoring of the Pertosa-
411 Auletta Cave allowed fulfilling the main goal of the research, *i.e.* exemplifying a data-
412 driven evaluation of tourism sustainability, but the breadth and implications of the
413 findings are substantially wider. Indeed, they enhance our understanding of the cave
414 ecosystem by shedding light on its dynamics at multiple spatial and temporal scales,
415 on the coupling between the internal and external dynamics, and on the possible
416 drivers of several processes. On top of the relevance these topics bear for the

417 understanding of cave ecosystem ecology, they are crucial in setting references for the
418 evaluation of possible alterations and in defining appropriate conservation measures.
419 Overall, the tourism-induced alterations of the Pertosa-Auletta Cave integrate
420 within the natural fluctuations by contributing high-frequency signals that decay
421 quickly in space and time. In terms of cave conservation, such alterations are unable
422 to threaten the cave ecosystem functioning under the adopted tourism regimes and
423 demonstrate the sustainability of its management. Although such considerations apply
424 to the Pertosa-Auletta Cave only, due to their dependence upon factors like
425 morphology, climate or hydrogeology, the embraced approach can be
426 straightforwardly adopted into any show cave. Indeed, it is to be hoped that high-
427 resolution monitoring will meet increasingly high adoptions among cave
428 administrations, a process that could be only fostered by the low-cost of the stations,
429 their adaptability to different requirements through their modularity and the
430 exemplified analytical flow.
431

432 **Declarations**

433 *Funding*

434 The research was carried out with funds from the ORSA197159 project, granted
435 by the University of Salerno.

436 *Conflicts of interest/Competing interests*

437 None.

438 *Availability of data and material*

439 Data and materials are available upon request to the authors.

440 *Code availability*

441 The code developed for data analysis is available upon request to the authors.

References

Addesso R, Bellino A, D'Angeli IM, De Waele J, Miller AZ, Carbone C, Baldantoni D (2019) Vermiculations from karst caves: the case of Pertosa-Auletta system (Italy). Catena 182:104178.

Addesso R, Gonzalez-Pimentel JL, D'Angeli IM, De Waele J, Saiz-Jimenez C, Jurado V., Miller AZ, Cubero B, Vigliotta G, Baldantoni D (2021) Microbial community characterizing vermiculations from karst caves and its role in their formation. Microb Ecol 81:884-896.

Badino G (2010) Underground meteorology -"What's the weather underground?". Acta Carsologica 39(3): 427–448.

Breecker DO, Payne AE, Quade J, Banner JL, Ball CE, Meyer KW, Cowan BD (2012) The sources and sinks of CO2 in caves under mixed woodland and grassland vegetation. Geochim Cosmochim Ac 96:230-246.

Calaforra JM, Fernández-Cortés A, Sánchez-Martos F, Gisbert J, Pulido-Bosch A (2003) Environmental control for determining human impact and permanent visitor capacity in a potential show cave before tourist use. Envir Conserv 30:160–167.

Carrasco F, Vadillo I, Liñán C, Andreo B, Durán JJ (2016) Control of environmental parameters for management and conservation of Nerja Cave (Malaga, Spain). Acta Carsologica 31: 105-122.

Chiesi M (2002) La ricerca di requisiti di qualità nella fruizione e nell'adattamento turistico di una grotta (primo contributo). Le Grotte d'Italia. 5-13.

Cigna A, Burri E (2000). Development, management and economy of show caves. Int J Speleol 29.

Danardono D, Putra EBD, Haryono E, Nurjani E, Sunariya MIT (2018) Speleoclimate monitoring to assess cave tourism capacity in Gelatik Cave, Gunungsewu Geopark, Indonesia. For Geo 32:181–194.

D'Angeli IM, Ghezzi D, Leuko S, Firrincieli A, Parise M, Fiorucci A, Vigna B, Addesso R, Baldantoni D, Carbone C, Miller AZ, Jurado V, Saiz-Jimenez C, De Waele J, Cappelletti M (2019) Geomicrobiology of a seawater-influenced active sulfuric acid cave. PLOS ONE 14(8):e0220706.

De Freitas CR, Littlejohn RN (1987) Cave climate: assessment of heat and moisture exchange. J Climatol 7(6):553-569.

de Freitas CR (2010) The role and the importance of cave microclimate in the sustainable use and management of show caves. Acta Carsologica 39: 477-489.

De Vincenzi M, Fasano G, Materassi A (2016) Monitoraggio dei parametri fisici delle grotte costiere della Sardegna: l'esempio della Grotta Verde e del Bue Marino. Sixth International Symposium Monitoring of Mediterranean Coastal Areas. Problems and Measurement Techniques. Livorno (Italy).

Domínguez-Villar D, Fairchild IJ, Carrasco RM, Pedraza J, Baker A (2010) The effect of visitors in a touristic cave and the resulting constraints on natural thermal conditions for palaeoclimate studies (Eagle Cave, central Spain). Acta Carsologica/Karsoslovni Zbornik 39(3):491-502.

Faimon J, Štelcl J, Sas D (2006) Anthropogenic CO_2-flux into cave atmosphere and its environmental impact: A case study in the Císařská Cave (Moravian Karst, Czech Republic). Sci Total Environ 369:231–245.

Fenske JD, Paulson SE (1999) Human breath emissions of VOCs. J Air Waste Manag Assoc 49:594–598.

Forbes J (1998) Air temperature and relative humidity study: Torgac Cave, New Mexico. J Cave Karst Stud 60(1):27-32.

Howarth FG (2019) Chapter 7 - Adaptive shifts, in: White WB, Culver DC, Pipan T (Eds.), Encyclopedia of Caves (Third Edition). Academic Press, pp. 47–55.

Hoyos M, Soler V, Canãveras JC, Sánchez-Moral S, Sanz-Rubio E (1998) Microclimatic characterization of a karstic cave: human impact on microenvironmental parameters of a prehistoric rock art cave (Candamo Cave, northern Spain). Environ Geol 33(4):231-242.

Korzystka M, Piasecki J, Sawiński T and Zelinka J (2011) Climatic system of the Dobšinská Ice Cave. In: Bella P and Gažík P (Eds), 6th Congress International Show Caves Association Proceedings. Slovak Caves Administration, Liptovský Mikuláš, pp. 85-97.

Lang M, Faimon J, Ek C (2015a). The relationship between carbon dioxide concentration and visitor numbers in the homothermic zone of the Balcarka Cave (Moravian Karst) during a period of limited ventilation. Int J Speleol 44:167–176.

Lang M, Faimon J, Ek C (2015b) A case study of anthropogenic impact on the CO_2 levels in low-volume profile of the Balcarka Cave (Moravian Karst, Czech Republic). Acta Carsologica 44:71–80.

Lobo HAS, Boggiani PC, Perinotto JAJ (2015) Speleoclimate dynamics in Santana Cave (PETAR, São Paulo State, Brazil): general characterization and implications for tourist management. Int J Speleol 44:61–73.

Lobo HAS, Trajano E, de Alcântara Marinho M, Bichuette ME, Scaleante JAB, Scaleante OAF, Rocha BN, Laterza FV (2013) Projection of tourist scenarios onto fragility maps: Framework for determination of provisional tourist carrying capacity in a Brazilian show cave. Tour Manag 35:234–243.

514 Mattey DP, Atkinson TC, Barker JA, Fisher R, Latin J-P, Durrell R, Ainsworth
515 M (2016) Carbon dioxide, ground air and carbon cycling in Gibraltar karst. Geochim
516 Cosmochim Ac 184:88-113.
517 Milanolo S, Gabrovšek F (2009) Analysis of carbon dioxide variations in the
518 atmosphere of Srednja Bijambarska Cave, Bosnia and Herzegovina. Boundary-Layer
519 Meteorol 131:479–493.
520 Pflitsch A, Piasecki J, Niggemann S (2000) Untersuchungen zum Einfluss von
521 Touristen auf das Höhlenklima in der Dechenhöhle (Iserlohn, Deutschland).
522 Mitteilungen des Verbandes der Deutschen Höhlen- und Karstforscher 46(1/2):96-99.
523 Pulido-Bosch A, Martín-Rosales W, López-Chicano M, Rodríguez-Navarro
524 CM, Vallejos A (1997) Human impact in a tourist karstic cave (Aracena, Spain).
525 Environ Geol 31:142–149.
526 R Core Team (2021) R: A language and environment for statistical computing.
527 R Foundation for Statistical Computing, Vienna, Austria; https://www.R-project.org/
528 Russell MJ, MacLean VL (2008) Management issues in a Tasmanian tourist
529 cave: Potential microclimatic impacts of cave modifications. J Environ Manag
530 87:474–483.
531 Smith A, Wynn P, Barker P (2013) Natural and anthropogenic factors which
532 influence aerosol distribution in Ingleborough Show Cave, UK. Int J Speleol 42:49–
533 56.
534 White WB (2019) Chapter 47 - Exploration of caves—General, in: White,
535 W.B., Culver, D.C., Pipan, T. (Eds.), Encyclopedia of Caves (Third Edition).
536 Academic Press, pp. 407–413.

Ziwei Z, Junzhou H, Xudong Y (2020) An experimental method for measuring VOC emissions from individual human whole-body skin under controlled conditions. Build Environ 181:107137.

Supplementary materials

Table S1: Main sensors employed in the monitoring stations, with indication of the chip manufacturer and the commercial code.

Environmental parameter	**Manufacturer**	**Chip**	**Product code**
T, RH	Sensirion	SHT-10	Adafruit 1298
CO	Sensirion	SCD30	SCD30
VOC	Sensirion	SGP30	Adafruit 3709
TPS, PM0.5, PM1.0, PM2.5, PM4.0, PM10	Sensirion	SPS30	SPS30
Pressure*	NPX Semi	MPL3115A2	Adafruit 1893

*Atmospheric pressure was recorded, but not analysed in the present research

Table S2: Monthly maxima and minima of all the monitored parameters and the number of tourists.

Trail	Date	T (°C)	RH (%)	CO (ppm)	VOC (ppm)	TPS (m)	PM0.5 (#)	PM1.0 (#)	PM2.5 (#)	PM4 (#)	PM10 (#)	Tourists (#)
F	2019 Aug											
F	2019 Sep											
F	2019 Oct											
F	2019 Nov											
F	2019 Dec											
F	2020 Jan											
F	2020 Feb											
F	2020 Mar											
F	2020 Apr											
F	2020 May											
F	2020 Jun											
F	2020 Jul											
F	2020 Aug											
F	2020 Sep											
T	2019 Aug											
T	2019 Sep											
T	2019 Oct											
T	2019 Nov											
T	2019 Dec											
T	2020 Jan											
T	2020 Feb											
T	2020 Mar											
T	2020 Apr											
T	2020 May											
T	2020 Jun											
T	2020 Jul											
T	2020 Aug											
T	2020 Sep											

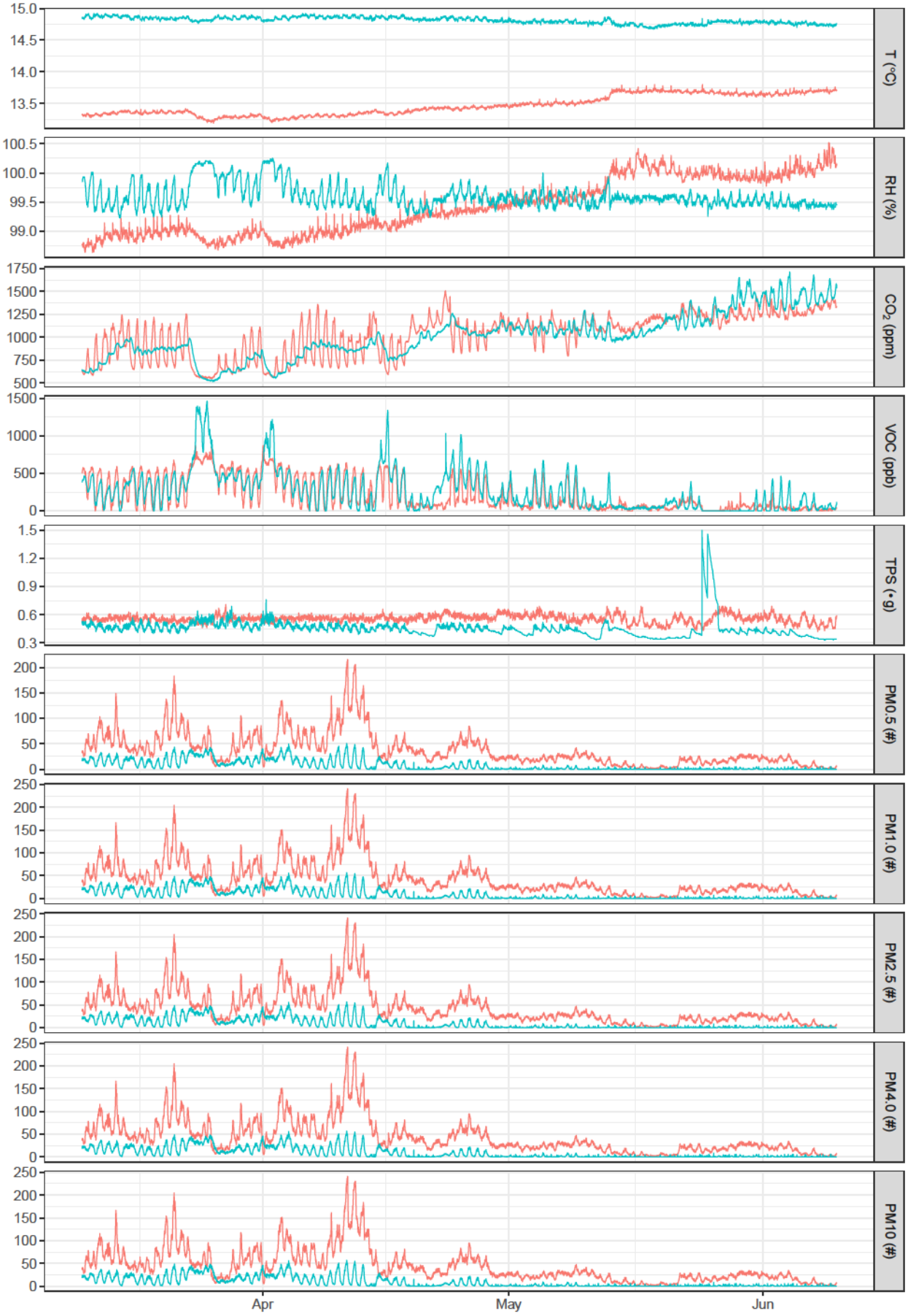

Fig. S1: Extract from the time series of all the parameters monitored (temperature: T, relative humidity: RH, CO_2, VOC, typical particulate size: TPS, PM0.5, PM1.0, PM2.5, PM4.0, PM10) during the lockdown phase (from 2020-03-10 00:00:00 to 2020-06-10 00:00:00) in the tourist (green) and fossil (red) trails.

Fig. S2: Extract from the time series of all the parameters monitored (temperature: T, relative humidity: RH, CO_2, VOC, typical particulate size: TPS, PM0.5, PM1.0, PM2.5, PM4.0, PM10) and of the number of tourists during the first week of August 2019 (from 2019-08-02 04:41:00 to 2019-08-08 04:41:00) in the tourist (green) and fossil (red) trails.

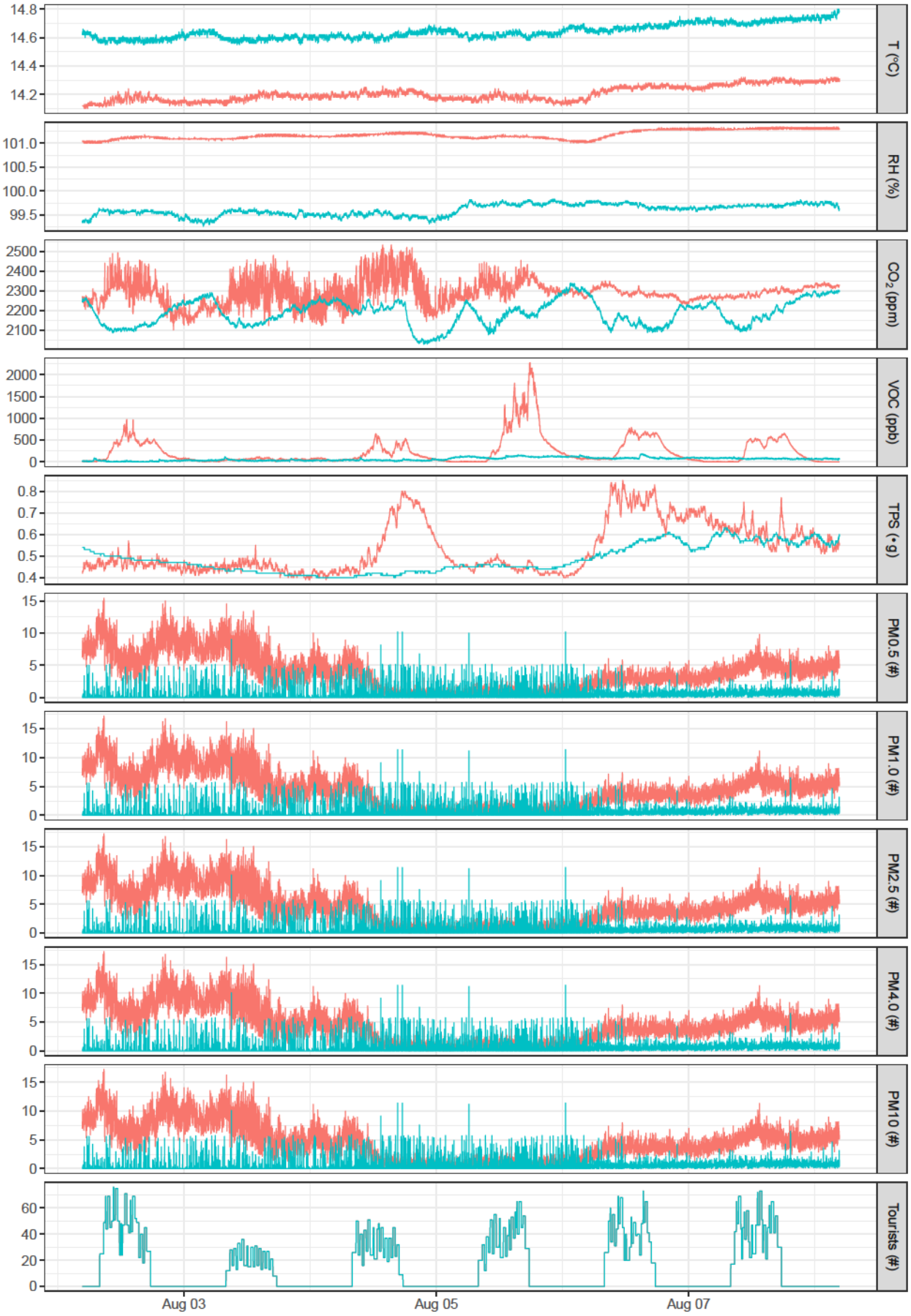

Fig. S3: Extract from the time series of all the parameters monitored (temperature: T, relative humidity: RH, CO_2, VOC, typical particulate size: TPS, PM0.5, PM1.0, PM2.5, PM4.0, PM10) and of the number of tourists during the first week of August 2020 (from 2020-08-02 04:41:00 to 2020-08-08 04:41:00) in the tourist (green) and fossil (red) trails.

CHAPTER 9

Sustainable tourist fruition of underground ecosystems: simulations of airflow and particle dispersions and depositions

Rosangela Addesso*, Stefano Pingaro, Bruno Bisceglia, Daniela Baldantoni

Manuscript in preparation

**corresponding author*

For the first time, COMSOL Multiphysics has been employed to simulate human impacts in cave environment, through fact-finding simulations using the physical model of the airflow and the scattering of particles transported by tourists, revealing a valid tool to suggest mitigation strategies and support the decision-making processes in tourism planning.

Sustainable tourist fruition of underground ecosystems: simulations of airflow and particle dispersions and depositions

Rosangela Addesso [1*], Stefano Pingaro [1], Bruno Bisceglia [2], Daniela Baldantoni [1]

[1] Department of Chemistry and Biology “Adolfo Zambelli”, University of Salerno, Via Giovanni Paolo II, 132, 84084 Fisciano (SA), Italy

[2] Department of Industrial Engineering, University of Salerno, Via Giovanni Paolo II, 132, 84084 Fisciano (SA), Italy

*: Corresponding author (Name: Rosangela Addesso; Address: Department of Chemistry and Biology “Adolfo Zambelli”, University of Salerno, Via Giovanni Paolo II, 132, 84084 Fisciano (SA), Italy; Tel.: +39 089 969542; Fax: +39 089 969603; email: raddesso@unisa.it)

Abstract

Underground ecosystems are often interested by massive tourist fruition for their naturalistic and cultural heritage. Being almost confined, human presence can affect their natural processes influencing, also irrevocably, their equilibrium, endangering the sites preservation. The most sensible managers of the subterranean accessible cultural sites are searching for methods controlling these dynamics and the modelling appears effective in preventing impacts scenarios, suggesting mitigation strategies. Employing COMSOL Multiphysic software and reproducing, in a simplified way, a section of Pertosa-Auletta Cave (Italy) tourist trail, for the first time, we provided a factfinding survey of the airflow and the scattering of particles transported by tourists. Considering pathway discontinuities, the simulations rebuilt the possible airflow, showing the particles movement and the deposition sites caused by different tourist loads, highlighting hotspots of damage. With suitable implementations, COMSOL can be an excellent tool for planning a sustainable management of these extraordinary ecosystems, supporting managers in decision-making processes.

Keywords: Atmosphere modelling, Anthropogenic impacts, Caves, Cultural heritage, COMSOL Multiphysics

1 Introduction

Cultural heritage sites interested by tourism represent an important opportunity to preserve the local historical identity as well as the naturalistic features of a focus area, diffusing their knowledge worldwide and promoting the economic development of the territory (Silva & Henriques 2021). Among them, a number of natural and artificial underground environments, including caves, catacombs, mines and hypogean holy places, hold high appeal of tourists for their cultural and environmental value (Jurado et al. 2008). However, thousands of visitors every year can arouse modifications in the environmental conditions, affecting (sometimes irreversibly) such confined ecosystems and compromising their integrity and conservation; therefore, probing the human impacts in such places became a need to safeguard the heritage sites and to manage their fruition properly (Cigna & Burri 2000; Mulec 2014; Lobo et al. 2015; Silva & Henriques 2021).

In addition to the indoor climatic changes caused by human breathing, with temperature, relative humidity and CO_2 concentrations increasing in atmosphere and often activating chemico-physical degradation processes of the lithic surfaces (Pulido-Bosch et al. 1997; Sánchez-Moral et al. 1999; Calaforra et al. 2003; de Freitas 2010; Smith et al. 2013), tourists are carrier of alloctonous particles, such as dust, fibers, hair, but also fungi, bacteria, spores and seeds. These constitute inorganic and organic inputs in the ecosystem, altering its natural ecological equilibrium (Chiesi 2002; Russell & MacLean 2008; Jurado et al. 2008; Smith et al. 2013; Mulec 2014; Bruno et al. 2014), as well as activating forms of walls biodeterioration, included mural paintings and speleothemes sufaces (Karbowska-Berent 2003; Jurado et al. 2008; Mulec 2019).

The degree of vulnerability can be variable among systems. It can depend on the type of the ecosystem (dimensions, opening, connection with external environments…) and of

tourist load and associated inputs, closely related to its fruition (visit duration, group size, breaks between and during tours…), but, especially in the case of natural caves, on their energy and mass flow (Calaforra et al. 2003; Russell & MacLean 2007; Lobo et al. 2013; Lobo, et al. 2015). For instance, underground systems with a high energetic level, and with recurring natural air or water supplies from external, are more resilient than those with a medium-low energy flow (Chiesi 2002; De Vincenzi et al. 2016). Moreover, morphological and structural characteristics produce an indoor spatial and temporal microclimatic zonation that can influence the system response to the changes (Russell & MacLean 2007).

Therefore, the complexity of underground ecosystems makes it hard the complete understanding of their ecological processes, as well as of the consequences activated by potential disturber factors. Models, representing in a simplified way the reality of these ecosystems, analyzing key factors and their behavior in different contexts (natural or artificial), predicting alternative scenarios of management, suggesting mitigation strategies of the anthropogenic impacts, supporting decision-makings and giving to the visitors an increasingly sustainable offer, may be an effective tool in managing natural resources (Bugmann et al. 2000; Schmolke et al. 2010). Using COMSOL Multiphysic software, we performed a first exploratory simulation application based on physical models of the underground airflow and particle dispersion and deposition processes carried out by tourists, with a view of proving its suitability to obtain exact and in-depth planning of tourism fruition of underground ecosystems.

2 Methods

To simulate and model the airflow and the particle dispersions and depositions, the application Cylinder flow in COMSOL Multiphysics® 4.3 software was employed, modelling tourist sections of the Pertosa-Auletta Cave (Addesso et al. 2019), in Southern Italy. This allowed examining the propagation of a variable and compressible flow within a 2D geometry. The program uses preset physical notions based on the drag and lift coefficients of the fluid (Schäfer et al. 1996; Application Library path: COMSOL_Multiphysics/Fluid_Dynamics/cylinder_flow):

$$C_D = \frac{2F_D}{\rho U_{mean}^2 \ A}$$

$$C_L = \frac{2F_L}{\rho U_{mean}^2 \ A}$$

where

- C_D: drag coefficient; it is a dimensionless coefficient used to quantify the drag of an object in a fluid environment, such as air or water. The lower coefficient, the lower aerodynamic or hydrodynamic resistance of the object
- C_L: lift coefficient; it is a dimensionless coefficient that relates the lift generated by a lifting body to the density of the fluid around the object, the fluid speed and an associated reference area
- ρ: fluid density
- U_{mean}: average fluid speed
- A: projected area

The model examines a flow in a cylinder, working in a two dimensional geometry, and results are reported in the longitudinal section. Simplified geometries of two cavity sections of the Pertosa-Auletta Cave (Figure 1), frequented by 60.000 tourists per year, were built. The first one consisted of a 2D cylinder, simulating a linear conduct of the cavity (blue line in Figure 1b), the second one was more articulated, trying to rebuild a

larger circular room, with tunnels for tourist entrance and exit (red line in Figure 1b). The values of the physical parameters characterizing the moving air mass simulations (Supplementary material) are derived by the real data recorded by two monitoring stations, installed in the cave to control key atmospheric factors (temperature, relative humidity, pressure, CO_2, VOC and particulate) (Unpublished results). The dimensional characteristics of the shapes are in scale with the real ones (Table S1). In addition, a

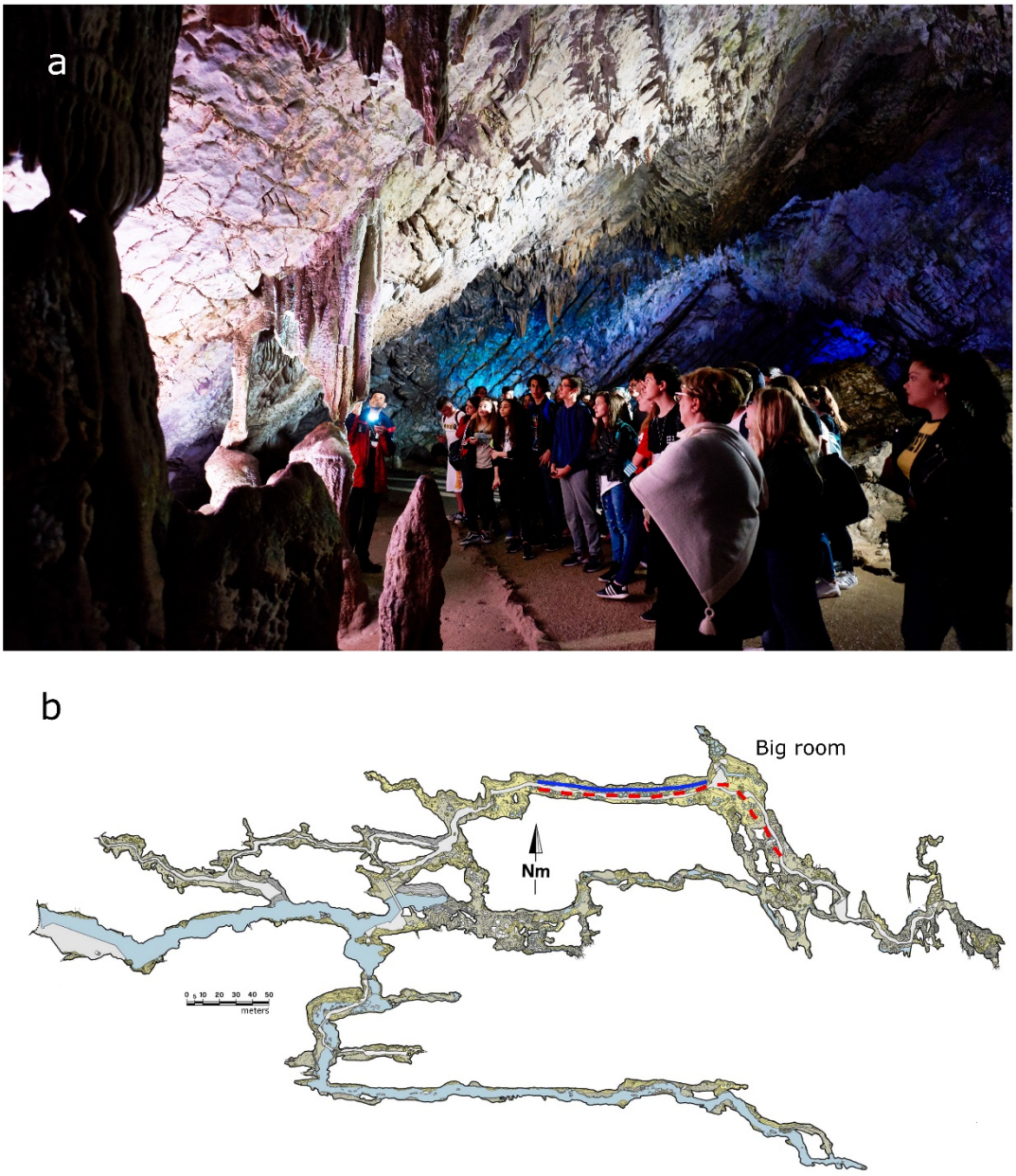

Fig. 1 a. Tourists in Pertosa-Auletta Cave (ph. Giuseppe Natalino) **b.** Pertosa-Auletta Cave map; blue line indicate the linear conduct considered for the first simulation; red line indicate the linear conduct and the big room considered for the second simulation.

discontinuity was added to the normal physical arrangement, representing a foreign body, which could be recognized as one person or a group of tourists visiting the trail, as well as a speleothem, such as a column, a stalactite or a stalagmite.

To follow the particulate matter movement dragged by the airflow, the Maximum particle tracking application provided by COMSOL Multiphysics® was also applied in both the sections analyzed. Not having data on the average wind speed inside the Pertosa-Auletta Cave, we based our study on literature information (Novas et al. 2017), reporting values around 1 m/s, which we set up at 3 m/s facilitating the vision of the processes.

In the outputs, the fluid speed is observable by a color palette (where red describes the most sudden air movement), whereas particulate matter (indicated by dots) is represented in not-real size. Being a time-dependent study, the final outputs of the simulations are released by the software in the form of short animations (only the frames considered most significant have been reported).

3 Results and discussion

Even if numerical modelling is a mature discipline and some procedures, such as the finite element method and others, are well known and documented in the literature, each application has its own specificities, from which can take advantage of, in order to simplify the problem and reduce the associated computational size. An easy application of classical methods often may lead to computation times that are much longer than required (Sirois & Grilli 2015). In this work, we simulated a simple model that involves the significant variables of the physical process. The 2D geometry allows an easy analysis of the results and permits a 3D study of the physical model. Starting from a simplified model to a gradually more complex one, COMSOL Multiphysics®, through the Cylinder flow and the Maximum particle tracking applications, allowed simulating

the airflow and the particle dispersions and depositions of tourist sections of the Pertosa-Auletta Cave, widely applicable in any subterranean system. It has to be considered that the system morphology can affect the cave microclimate and, consequently, the large part of the karst processes through several atmospheric variables, such as gas concentrations, temperature/relative humidity and the spread and deposition of particles (Wigley & Brown 1971; Faimon et al. 2011; Dredge et al. 2013). Figure 2a shows a simple 2D construction of the straight duct leading to the large room of the cave, revealing the basic level of the physical model behavior considering a

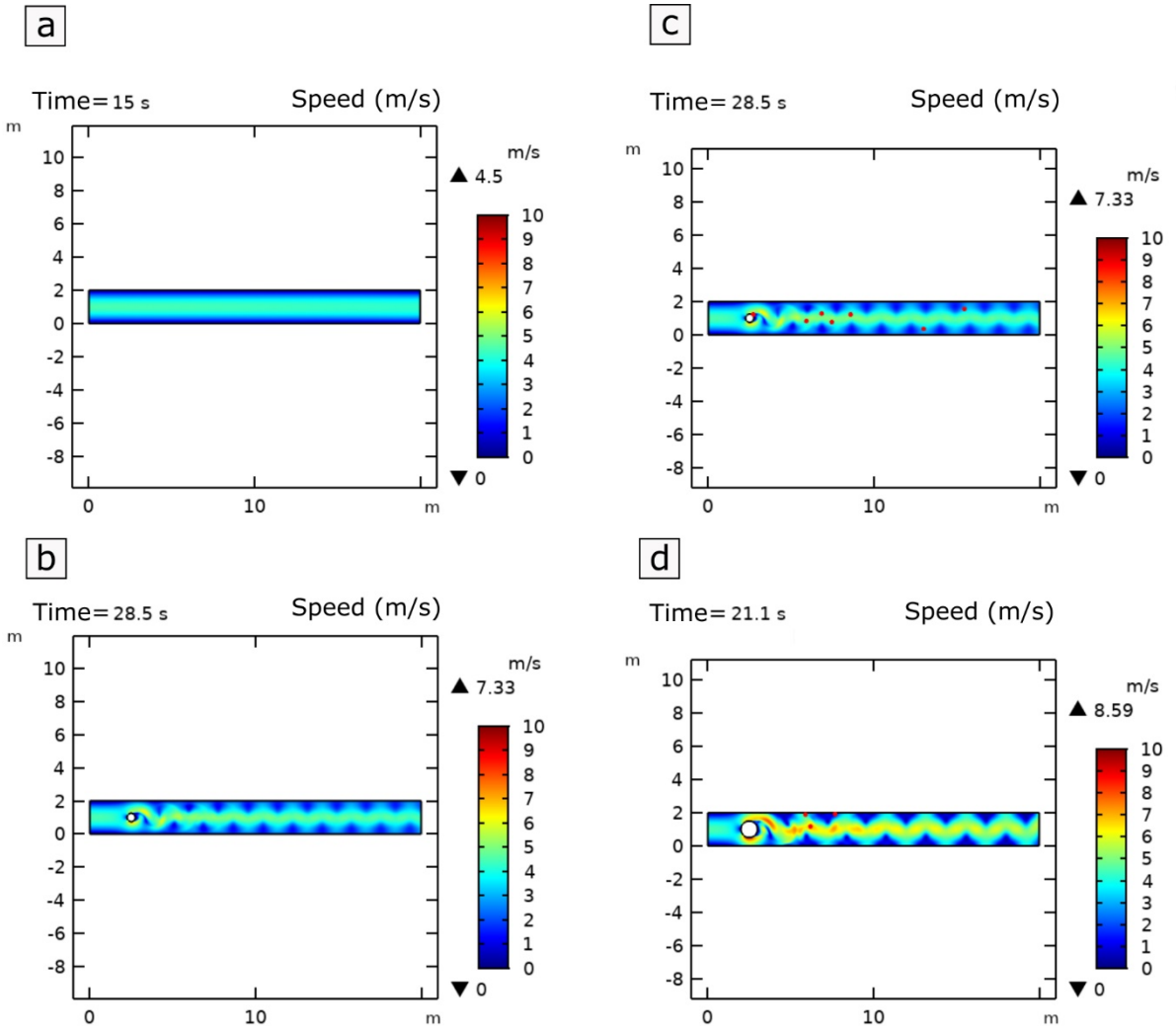

Fig. 2 Simulations based on a simplified geometry of a linear conduct of the Pertosa-Auletta Cave. **a.** Basic physical model behavior. **b.** Addition of a discontinuity, representing one person or a tourist group (white circle). **c.** Tracking of massive particles (red circles). **d.** Tracking of massive particles (red circles) with a larger discontinuity, representing one person or a tourist group (white circle).

compressible flow. The laminar fluid is arranged in a section without any kind of discontinuity, therefore, without any impediment to the fluid flow. In this case, the fluid is faster in the central part than in the areas into direct contact with the walls, where it proceeds slowly due to the friction. Adding a discontinuity (Figure 2b), representing for instance one person or a group of tourists, the initial laminar fluid course is modified, with interferences to the flow. The presence of an obstacle, characterized by Reynolds number equal to 100, causes an unstable wake, where the swirls alternately break away from the lateral regions forming a trail of laminar vortexes. It is interesting to note that, in the early phase of the simulation, the fluid impact with the obstacle produces strong turbulences traveling the cylinder. The maximum speed reached by the fluid is 6.72 ms^{-1}.

The tracking of massive particles is shown in the Figure 2c, where the origin of the release is located just close to the discontinuity. Analyzing the animation, it is observable that, at the beginning, the particles follow the flow line in all its directions, but, once picked up speed, they are no able to change direction quickly following the airflow, ending up to collide towards the domain walls. With a larger discontinuity (Figure 2d), due to an increased number of tourists, we can observe that the resulting air swirls are clearly larger than the previous simulation; this certainly causes a greater transport of particles by the fluid, because the speed reaches 9.06 ms^{-1}, as well as an evident greater deposition on the cave walls. On this natural scenario, the tourists, together with natural air movements, can give a significant contribution to the particulate matter scattering. They become vector of additional substances carried on their body and facilitating their arrival also in remote and deeper areas of the karst system, as well as they can re-suspend the deposited particles on the ground and the walls, going through the pathway (Smith et al. 2013; Dredge et al. 2013). The arrival of allochthonous natural/anthropogenic inorganic/organic aerosols causes several

consequent effects, such as the incorporation of dust or soot in speleothemes or the proliferation of seed and spores in tourist cavities due to the artificial light, placing at risk the preservation of the underground ecosystem (Mulec et al. 2019; Smith et al. 2013; Dredge et al. 2013). Moreover, high particulate concentrations can also affect air quality, causing problems for the human health, especially for the respiratory apparatus (Cetin et al. 2017). Nevertheless, in general, particulate matter is largely cut back in caves, due to the high air relative humidity, close to the saturation, reducing considerably the hanging particles by abatement (Cetin et al. 2017).

Adding further discontinuities (Figure 3a), such as speleothemes, the linear airflow is perturbed, influencing also the particle walks (Figure 3b and c), that follow the preferential flow lines. Introducing a number of tourists, 5 and 15, respectively in the Figures 3b and 3c, causes a more chaotic movement of air masses, with a consequent deposition of the particles in the low pressure zones. The animation of such simulation (Supplementary Content 1) was also reported. For a sustainable management of these ecosystems, managers can install active or passive particle trapping devices in such areas, in order to avoid damages on the structures.

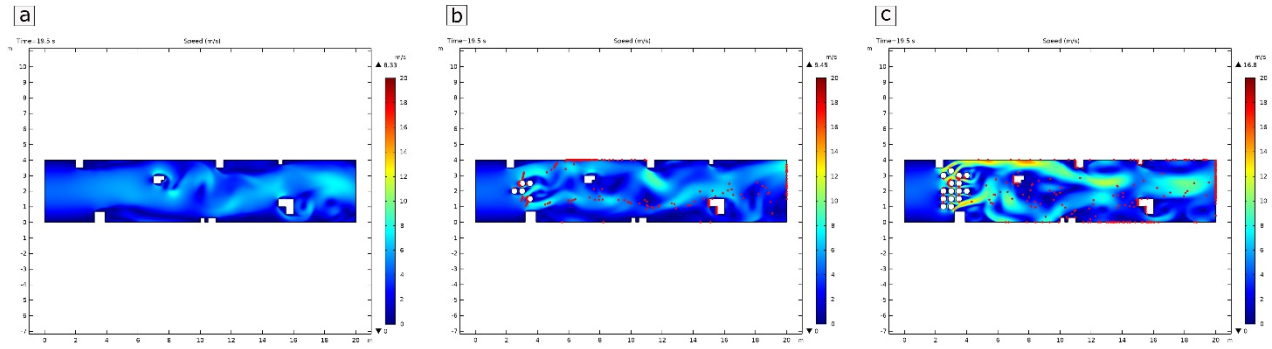

Fig. 3 Simulations based on a simplified geometry of a linear conduct of the Pertosa-Auletta Cave adding several discontinuities, such as speleothemes, representing typical obstacles in caves (white squares). **a.** Basic physical model behavior. **b.** Tracking of massive particles (red circles), considering a group of 5 visitors (white circles). **c.** Tracking of massive particles (red circles), considering a group of 15 visitors (white circles).

The simulation representing the path leading to the large room of the cave (Figure 4a) shows how the flow, coming from the initial straight section, before flowing into the

escape routes, especially in the wider one, bounces off hall wall. This produces another flow traveling along the entire curvilinear perimeter in a circular motion. The air speed quickly decreases in the straight section, remaining high in the center of the room, and then increasing again at the entrance of the flow escape routes. Particles do not deposit on the walls (Figure 4b), as in the first simulations, not following the entire path of the fluid, because the acquired speed determines an inertial force that pushes it towards the wall of the large room. This does not occur for the bigger particles, able to follow the sudden deviations of the wind, acquiring less velocity (Figure 4c).

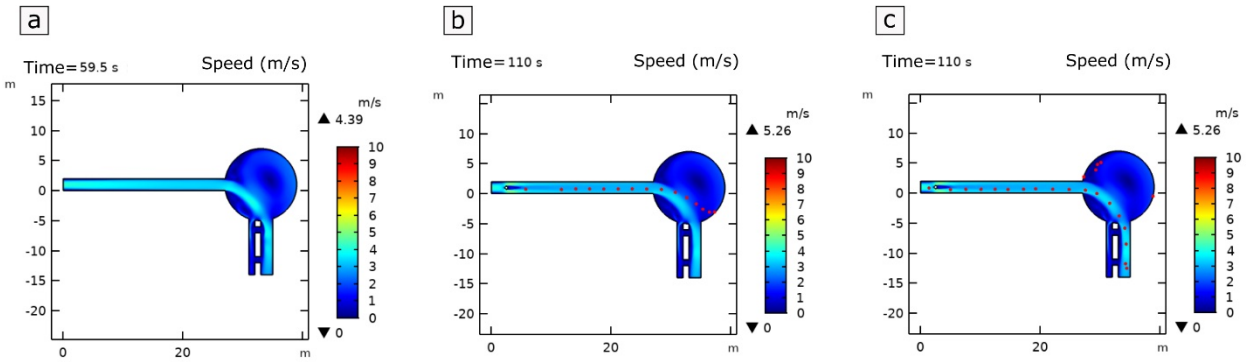

Fig. 4 Simulations based on an articulated geometry, trying to rebuild the large circular room of the Pertosa-Auletta Cave. **a.** Basic physical model behavior. **b.** Tracking of massive particles (red circles) from a discontinuity, representing one person or tourist group (white circle). **c.** Tracking of heavier massive particles (red circles) from a discontinuity, representing one person or tourist group (white circle).

Rendering the system more complex with several obstacles and tourist groups (Figure 5), such discontinuities act as deposition sites, representing high-risk areas of damages. Moreover, in the first case (Figures 5a and 5b), where 5 and 15 visitors are at the beginning of the conduct, the airflow pushes the most part of the particles on the walls due to the higher air speed developing along the extremities. The increase in the number of discontinuities in the conduct related to a major presence of tourists can cause the growth of the ventilation in the big room, which can promote the dispersion also beyond, in a deeper area of the cave. When 5 and 15 visitors (Figures 5c and 5d) arrive in the large room, the particles deposition become more intense. In addition, as showed

also in the Supplementary Content 2, the increase of the tourists in the big room distorts the airflow in a remarkable way stimulating the formation of further vortexes, generating other arms of the airflow, with an increasing scattering of the particles in the space.

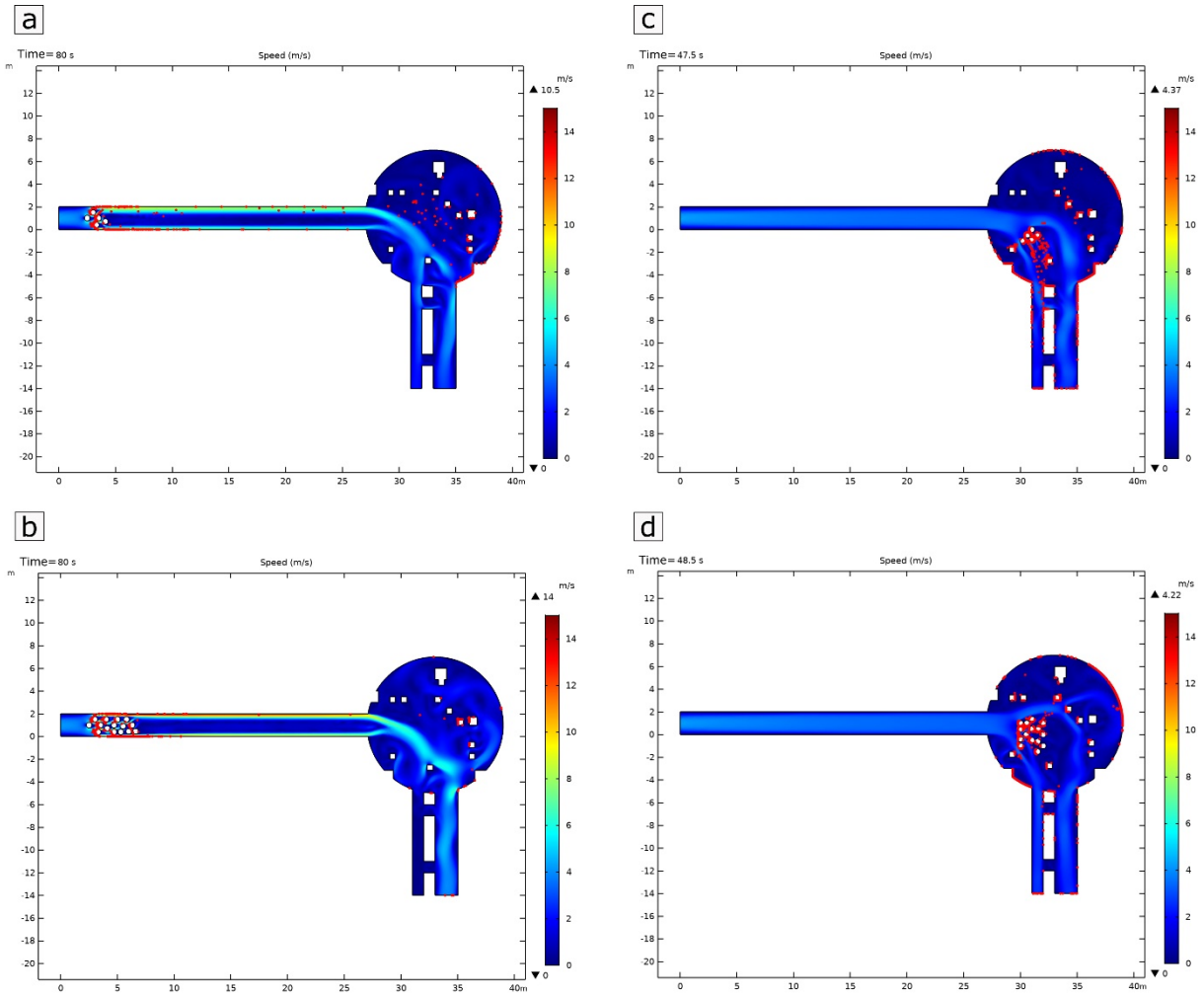

Fig. 5 Simulations based on a articulated geometry, trying to rebuild the large circular room of the Pertosa-Auletta Cave, adding several discontinuities, such as speleothemes, representing typical obstacles in caves (white squares). **a.** Tracking of massive particles (red circles), considering a group of 5 visitors (white circles), positioned at the beginning of the long conduct. **b.** Tracking of massive particles (red circles), considering a group of 15 visitors (white circles), positioned at the beginning of the long conduct. **c.** Tracking of massive particles (red circles), considering a group of 5 visitors (white circles), positioned in the large room. **d.** Tracking of massive particles (red circles), considering a group of 15 visitors (white circles), positioned in the large room.

Overall, the obtained results provided an exhaustive description of the physical processes related to the airflow and the particle dispersions and depositions in

underground ecosystems, but further implementations could take into account physical characteristics of the materials, as well as the exact shape of the study system. Moreover, the validation of coarse airborne particle simulations may be obtained by monitoring real cases (in terms of number of visitors per group, transit time, etc.) combined with a comprehensive and time-accurate monitoring of the key environmental parameters. Finally, it should be possible to create a graphic interface of the COMSOL Multiphysics® software, readily operable from managers of the sites to plan the tourist activities.

4 Conclusions

Although it is a first application, COMSOL Multiphysics® demonstrated to be a good device to support the sustainable management of underground ecosystems in relation to tourism planning, such as in the choice of visit-break locations and time during the tours, avoiding the most vulnerable sections or suggesting to install mitigation systems of the alterations, where anthropogenic impacts may be more intense. Indeed, this application is of general validity, being adaptable and implementable in relation to the different environments needing sustainable choices. In the case of the two simulated sections of the Pertosa-Auletta Cave, tourist load determines variations in both airflow and particle fates, influencing different areas, also deeper and far from the place of origin, to a different extent, according to the system morphology. Further implementations of such simulations in show caves (as well as in other underground ecosystems) may be obtained reproducing accurately the cave geometry (adding also the several discontinuities represented by speleothemes), and considering other physical features of the substrate. This goal may be easily achieved, in order to get the models as close as possible to the reality of the processes and help managers in oriented decisions to conserve these unique ecosystems.

Funding

The research was carried out with funds from the ORSA197159 and ORSA205530 projects, granted by the University of Salerno (Italy).

Conflicts of interest

None declared.

Acknowledgments

Thanks to MIdA Foundation (SA, Italy), manager of the Pertosa-Auletta Cave geosite.

References

Addesso, R., Bellino, A., D'Angeli, I. M., De Waele, J., Miller, A. Z., Carbone, C., & Baldantoni, D. (2019). Vermiculations from karst caves: The case of Pertosa-Auletta system (Italy). CATENA, 182, 104178. https://doi.org/10.1016/j.catena.2019.104178

Bruno, L., Belleza, S., Urzì, C., & De Leo, F. (2014). A study for monitoring and conservation in the Roman Catacombs of St. Callistus and Domitilla, Rome (Italy). In C. Saiz-Jimenez (A c. Di), The Conservation of Subterranean Cultural Heritage (pp. 37–44). CRC Press. https://doi.org/10.1201/b17570-6

Bugmann, H., Lindner, M., Lasch, P., Flechsig, M., Ebert, B., & Cramer, W. (2000). Scaling issues in forest succession modelling. Climatic Change, 44(3), 265–289. https://doi.org/10.1023/A:1005603011956

Calaforra, J. M., Fernández-Cortés, A., Sánchez-Martos, F., Gisbert, J., & Pulido-Bosch, A. (2003). Environmental control for determining human impact and permanent visitor capacity in a potential show cave before tourist use. Environmental Conservation, 30(2), 160–167. https://doi.org/10.1017/S0376892903000146

Cetin, M., Sevik, H., & Saat, A. (s.d.). Indoor air quality: the samples of Safranbolu Bulak Mencilis Cave. Fresenius Environmental Bulletin, 26(10), 7.

Chiesi, M. (2002). La ricerca di requisiti di qualità nella fruizione e nell'adattamento turistico di una grotta (primo contributo). Le Grotte d'Italia. 5-13.

Cigna, A., & Burri, E. (2000). Development, management and economy of show caves. International Journal of Speleology, 29. https://doi.org/10.5038/1827-806X.29.1.1

de Freitas, C.R. (2010). The role and the importance of cave microclimate in the sustainable use and management of show caves. Acta Carsologica, 39, 477-489.

De Vincenzi, M., Fasano, G., & Materassi, A. (2016). Monitoraggio dei parametri fisici delle grotte costiere della Sardegna: l'esempio della Grotta Verde e del Bue Marino. Sixth International Symposium Monitoring of Mediterranean Coastal Areas. Problems and Measurement Techniques. Livorno (Italy), September, 2016.

Dredge, J., Fairchild, I.J., Harrison, R.M., Fernandez-Cortes, A., Sanchez-Moral, S., Jurado, V., Gunn, J., Smith, A., Spötl, C., Mattey, D., Wynn, P.M., & Grassineau, N. (2013). Cave aerosols: distribution and contribution to speleothem geochemistry. Quaternary Science Reviews, 63, 23–41.

Faimon, J., Troppová, D., Baldík, V., & Novotný, R. (2012). Air circulation and its impact on microclimatic variables in the Císařská Cave (Moravian Karst, Czech Republic): air circulation and its impact on cave microclimate. International Journal of Climatology, 32, 599–623.

Jurado, V., Sanchez-Moral, S., & Saiz-Jimenez, C. (2008). Entomogenous fungi and the conservation of the cultural heritage: A review. International Biodeterioration & Biodegradation, 62(4), 325–330. https://doi.org/10.1016/j.ibiod.2008.05.002

Karbowska-Berent, J. (2003). Microbiodeterioration of mural paintings: A review. Art, Biology, and Conservation: Biodeterioration of Works of Art, 266–301.

Lobo, H. A. S., Trajano, E., Marinho, M. de A., Bichuette, M. E., Scaleante, J. A. B., Scaleante, O. A. F., Rocha, B. N., & Laterza, F. V. (2013). Projection of tourist scenarios onto fragility maps: Framework for determination of provisional tourist carrying capacity in a Brazilian show cave. Tourism Management, 35, 234–243. https://doi.org/10.1016/j.tourman.2012.07.008

Lobo, H., Boggiani, P., & Perinotto, J. (2015). Speleoclimate dynamics in Santana Cave (PETAR, São Paulo State, Brazil): General characterization and implications for tourist

management. International Journal of Speleology, 44(1), 61–73. https://doi.org/10.5038/1827-806X.44.1.6

Mulec, J. (2014). Human impact on underground cultural and natural heritage sites, biological parameters of monitoring and remediation actions for insensitive surfaces: Case of Slovenian show caves. Journal for Nature Conservation, 10.

Mulec, J. (2019). Lampenflora. In Encyclopedia of Caves (pp. 635–641). Elsevier. https://doi.org/10.1016/B978-0-12-814124-3.00075-3

Novas, N., Gázquez, J. A., MacLennan, J., García, R. M., Fernández-Ros, M., & Manzano-Agugliaro, F. (2017). A real-time underground environment monitoring system for sustainable tourism of caves. Journal of Cleaner Production, 142, 2707–2721. https://doi.org/10.1016/j.jclepro.2016.11.005

Pulido-Bosch, A., Martín-Rosales, W., López-Chicano, M., Rodríguez-Navarro, C.M., & Vallejos A. (1997). Human impact in a tourist karstic cave (Aracena, Spain). Environmental Geology, 31, 142–149.

Russell, M. J., & MacLean, V. L. (2008). Management issues in a Tasmanian tourist cave: Potential microclimatic impacts of cave modifications. Journal of Environmental Management, 87(3), 474–483. https://doi.org/10.1016/j.jenvman.2007.01.012

Sánchez-Moral, S., Soler, V., Cañaveras, J. C., Sanz-Rubio, E., Van Grieken, R., & Gysels, K. (1999). Inorganic deterioration affecting the Altamira Cave, N Spain: quantitative approach to wall-corrosion (solutional etching) processes induced by visitors. Science of The Total Environment, 243–244, 67–84. https://doi.org/10.1016/S0048-9697(99)00348-4

Schäfer, M., Turek, S., Durst, F., Krause, E., & Rannacher, R. (1996). Benchmark Computations of Laminar Flow Around a Cylinder. In E. H. Hirschel (A c. Di), Flow

Simulation with High-Performance Computers II (Vol. 48, pp. 547–566). Vieweg+Teubner Verlag. https://doi.org/10.1007/978-3-322-89849-4_39

Schmolke, A., Thorbek, P., DeAngelis, D. L., & Grimm, V. (2010). Ecological models supporting environmental decision making: A strategy for the future. Trends in Ecology & Evolution, 25(8), 479–486. https://doi.org/10.1016/j.tree.2010.05.001

Silva, H. E., & Henriques, F. M. A. (2021). The impact of tourism on the conservation and IAQ of cultural heritage: The case of the Monastery of Jerónimos (Portugal). Building and Environment, 190, 107536. https://doi.org/10.1016/j.buildenv.2020.107536

Sirois, F., & Grilli, F. (2015). Potential and limits of numerical modelling for supporting the development of HTS devices. Superconductor Science and Technology, 28(4), 043002. https://doi.org/10.1088/0953-2048/28/4/043002

Smith, A., Wynn, P., & Barker, P. (2013). Natural and anthropogenic factors which influence aerosol distribution in Ingleborough Show Cave, UK. International Journal of Speleology, 42(1), 49–56. https://doi.org/10.5038/1827-806X.42.1.6

Wigley, T.M.L., & Brown, C. (1971). Geophysical applications of heat and mass transfer in turbulent pipe flow. Boundary-Layer Meteorology, 1, 300–320.

Supplementary materials

Table S1 - Values (units of measurement in brackets) of physical parameters characterizing the two moving air mass simulations; **a.** Parameters of the first simulation, considering a linear cave conduct, reproduced by a 2D cylinder. **b.** Parameters of the second simulation, considering a big room of the cavity, with tunnels for tourist entrance and exit.

a.

Parameter	Value
Path length	20 [m]
Path width	2 [m] (Figure 2) and 4 [m] (Figure 3)
Average fluid velocity	3 [ms^{-1}]
Fluid density	1.218 [Kgm^{-3}]
Fluid temperature	286.15 [K]
Pressure	101325 [Pa]
Dynamic viscosity	$1.81x10^{-5}$ [Pa*s]
Discontinuity radius	0.25 – 0.50 [m]
Particulate radius	PM_{10}
Particulate mass	$4*\pi/3*1^{-9}$ [kg]

b.

Parameter	Value
Initial path length	27 [m]
Initial path width	2 [m]
Final path length	10 [m]
Final travel distance 1	1 [m]
Final path width	2 [m]
Large room radius	6 [m]
Average fluid velocity	3 [ms^{-1}]
Fluid density	1.218 [Kgm^{-3}]
Fluid temperature	286.15 [K]
Pressure	101325 [Pa]
Dynamic viscosity	$1.81x10^{-5}$ [Pa*s]
Discontinuity radius	0.25 – 0.50 [m]
Particulate radius	PM_{10}
Particulate mass	$4*\pi/3*1^{-9}$ [kg]

CHAPTER 10

Effects of the most commonly employed methods to control lampenflora community on its physiological activity and on the treated surfaces

Rosangela Addesso, Daniela Baldantoni, Beatriz Cubero, José Maria De La Rosa, José Antonio González Pérez, Igor Tiago, Ana Teresa Caldeira, Jo De Waele, Ana Z. Miller*

Manuscript in preparation

**corresponding author*

A study of the most employed chemico-physical control methods of lampenflora, applied in situ in the Pertosa-Auletta cave, has been conducted using an integrated approach to define their efficacy, and characterizing the effects on community biodiversity and physiology, as well as their potential damages implemented on treated surfaces.

Effects of the most commonly employed methods to control lampenflora community on its physiological activity and on the treated surfaces

Rosangela Addesso[1], Daniela Baldantoni[1], Beatriz Cubero[2], José Maria De La Rosa[2], José Antonio González Pérez[2], Igor Tiago[3], Ana Teresa Caldeira[4], Jo De Waele[5], Ana Z. Miller[2,4]*

[1] Department of Chemistry and Biology "Adolfo Zambelli", University of Salerno, Via Giovanni Paolo II, 132, 84084 Fisciano (SA), Italy

[2] Instituto de Recursos Naturales y Agrobiología de Sevilla, IRNAS-CSIC, Av. Reina Mercedes, 10, 41012 Sevilla, Spain

[3] Department of Life Sciences, University of Coimbra, Rua da Matemática, 49, 3000-276 Coimbra, Portugal

[4] HERCULES Laboratory, University of Évora, Largo Marques de Marialva 8, 7000-809 Évora, Portugal

[5] Department of Biological, Geological and Environmental Sciences, University of Bologna, Via Zamboni, 67, 40126 Bologna, Italy

* Corresponding author: anamiller@irnas.csic.es

Abstract

Removing and controlling lampenflora growth on rock surfaces in lit tourist underground environments is the challenge for their sustainable management. Such green biofilms, mainly constituted by cyanobacteria and algae, implement a biodeterioration of the substrates, as well as an ecological imbalance of the cave ecosystems. In this work, a thorough qualitative and quantitative investigation of the most employed methods (NaClO, H_2O_2 and UVC) of lampenflora elimination, considering its biological responses, as well as the alterations activated on the substrates, was provided, fine-tuned a replicable and complete method to assess their efficacy and functionality. NaClO showed great disinfection capacities for long time without altering surfaces. Conversely, H_2O_2 has proven to be very aggressive on the substrates, especially on vermiculation deposits, activating corrosion processes, due to the chemical alteration of the organic and inorganic compounds constituting the surfaces, without eliminating the death biomass, which promptly favors the biofilms recovery, already after three months from the treatment. Both the chemical treatments exhibited efficacy on photoautotrophs killing, with the resistance of *Proteobacteria* and *Bacteroidetes* bacterial phyla and, among the Eukaryotes, *Apicomplexa* and *Cercozoa*. UVC showed no effect with the protocols used in this work.

Keywords: Biofilms, Biodeterioration, Pertosa-Auletta Cave, Show caves, Cave management

1 Introduction

Artificial lighting in natural caves for tourism fruition causes the proliferation of lampenflora, green biofilms primarily constituted by photoautotrophic organisms (cyanobacteria, algae, ferns, mosses…), affecting lit surfaces, included speleothems and cave paintings, main tourist attractions of such environments (Mulec, 2019). Except for the entrance, photoautotroph organisms do not have reason to exist in underground ecosystems, where darkness prevails. Natural air and water flows, as well as animals and humans, contribute to the arrival of their cells, spores and seeds, that proliferate easily in the show caves, not only due to the artificial light systems, but also to the high relative humidity, the stable temperatures and several other drivers currently under study (Piano et al., 2015; Mulec, 2019; Baquedano Estévez et al., 2019).

Besides the aesthetical changes creating the unnatural soiled greenish coats, lampenflora implements the biodeterioration of cave surfaces. Several organisms secrete organic acids that chemically dissolute the rock, or mechanically damage it, when expanding anchor organs, like roots. Moreover, lampenflora causes an ecological imbalance in the oligotrophic subterranean ecosystems, representing a considerable “alien” organic supply available for the entire cave biota, and it can affect the autochthonous biodiversity, replacing it, being an invasive and opportunistic community (Olson, 2006; Mulec, 2019; Baquedano Estévez et al., 2019).

To nurse the “green disease” of the show caves, from the ‘70 up to today, the managers, supported also by research findings, intervened with several physical and chemical cleaning and growth control methods to remove the biomass from the substrates and to disinfect them preventing lampenflora development (Baquedano Estévez et al., 2019). The methods mostly employed are represented by mechanical removal with brush and

water or after liquid nitrogen application, new led lighting systems with emission spectra not coinciding with lampenflora absorption ones, or even several highly environmentally harmful chemicals, including herbicides (Mulec, 2019; Baquedano Estévez et al., 2019). Currently, the most commonly used in show caves is the low cost and efficient commercial bleach, but expensive in environmental terms, since it can release chlorinated organic compounds, potentially polluting for the cave water cycle and biota. Only recently, the hydrogen peroxide has been introduced as an eco-friendly remediation compound for cave surfaces from the green biofilms, thanks to the absence of reaction by-products (Faimon et al., 2003; Mulec, 2009; Trinh et al., 2018; Baquedano Estévez et al., 2019). Some managers adopted instead a germicidal lamp system with UVC irradiation, working outside the visiting hours. However, a perfect and definitive solution has not been found, and the combination of different methods remains the most useful way to lampenflora control (Grobbelaar, 2000; Olson, 2006; Mulec, 2009; Cigna, 2012; Mulec, 2019; Baquedano Estévez et al., 2019).

The actual efficacy and sustainability, in terms of lampenflora reduction and alterations activated on the surfaces by such methods, are still undefined. Our research provides an extensive study on the effectiveness of the most widely employed methods of lampenflora reduction and of the related substrate alterations, focusing on the taxonomic and functional biodiversity of prokaryotic and eukaryotic communities composing biofilms and on the modifications induced to their growing substrates. In particular, a section in the tourist trail of the Pertosa-Auletta Cave (South Italy), with the presence of either bare rock surfaces or vermiculations (peculiar sedimentary structures widely described in Addesso et al., 2019, 2020) was subjected to different treatments, shedding

light on the potential damages activated on the substrates and defining mitigation strategies supporting decision-making of the show cave managers.

2 Methods

2.1 Experimental plan and field activities

In order altering cave surface to the smallest extent and avoiding alterations by visitors, the experimental trial was set up in the final section of the Pertosa-Auletta Cave lit tourist trail (Supplementary material, Figure S1a). On walls covered by lampenflora, 4 areas (50 x 50 cm), divided each one in 4 different sub-areas to create treatment replicates (Supplementary material, Figure S1b), were delimited on both bare surfaces (Supplementary material, Figure S1c) and on surfaces covered by vermiculations (Supplementary material, Figure S1d). Once a month, we carried out chemical (15% H_2O_2 and commercial NaClO) or physical (8 hours during the night UVC irradiation; technical and installation characteristics in Supplementary material, Table S1) growth-control treatments on such surfaces, leaving untreated two controls for each typology of surface.

Before and after each treatment, we took pictures by a Canon SX620 Digital Camera, employed for the following image analyses. In the same occasions, we carried out *in situ* non-destructive maximal photosystem II (PSII) photochemical efficiency measurements, given by Fv/Fm (variable fluorescence/maximal fluorescence), on 30 minutes dark-adapted surfaces, using a portable photosynthesis yield analyzer (MINI-PAM, WALTZ, Germany), equipped with a distance clip holder (Distance Clip 2010A, WALTZ, Germany), to assess the biofilms photosynthetic activity.

The experiment lasted a total of eight months, from January to August 2020, with a break of three months, from March to May 2020, due to the Covid19 pandemic. At the end of the treatments, for each surface, a representative sample was collected, using disposable and sterile scalpel blades and Eppendorf tubes, and stored at -80 °C until processing.

2.2 Microscopy surveys

Lampenflora chlorophyll and its auto fluorescence was visualized through an epifluorescence microscope OLYMPUS BX 61, equipped with a digital camera (Olympus DP73) and a specific DAPI filter. Microphotographs were recorded at a 10X magnification and image captures were processed using Cell Sens software (OLYMPUS). Oven-dried (50 °C) samples were analyzed using a FE-SEM -FEI Teneo (Thermo Fisher, MA, USA) microscope using the secondary electron detection mode, with an acceleration voltage of 5 kV for ultra-high resolution images.

2.3 Molecular analysis

Fast DNA^{TM}Spin Kit for soil was used to extract total DNA, according to the producer's protocol (MP Biomedical). The DNA amount was determined by a Qubit 2.0 Fluorometer (Invitrogen).The extracted DNA (with a minimum concentration of ~ 0.1 ng/μL) was analyzed via next-generation sequencing (NGS) targeting the V3–V4 hypervariable region of Prokaryotes 16S rRNA and V4 of Eukaryotes 18S rRNA, using Illumina MiSeq 2 × 250 paired end, according to Macrogen (Seoul, Korea) library preparation protocol. Chimeras were identified and removed by means of USEARCH (Edgar, 2010). Resulting reads were processed in Qiime (Caporaso et al., 2010), whereas UCLUST (Edgar, 2010) was used for the similar sequences assignment to operational taxonomic units (OTUs) by clustering with a 97% similarity threshold.

Paired-end reads were merged using FLASH (Magočand Salzberg, 2011). RDP and NCBI were used, respectively, for Prokaryotes and Eukaryotes, as against reference database for taxonomic identification of query sequences.

2.4 Analytical pyrolysis

To evaluate the cleaning capacity of NaClO and H_2O_2, on the chemically treated surfaces and on the control surfaces sampled at the end of the field trial, direct pyrolysis-gas chromatography/mass spectrometry (Py-GC–MS) was performed using a double-shot pyrolyser (Frontier Laboratories, model 2020i) attached to a GC–MS Agilent 6890N sys-tem. Samples (10 mg) were placed in small crucible capsules and introduced into a preheated micro-furnace at 400 °C for 1 min. The pyrolysis volatile products were then directly injected into the gas chromatograph inlet line heated at 250 °C to prevent condensation. It was equipped with a HP-5ms-UI, low polar-fused silica (5%-Phenyl-methylpolysiloxane) (J&W Scientific) capillary column of 30 m × 250 μm × 0.25 μm film thickness (Ref. DB-5). The oven temperature was held at 50 °C for 1 min and then increased to 100 °C at 30 °C min^{-1}, from 100 °C to 300 °C at 10 °C min^{-1}, and stabilized at 300 °C for 10 min. The carrier gas was helium at a controlled flow of 1 mL min^{-1}. The detector consisted of an Agilent 5973 mass selective detector, and mass spectra were acquired at 70 eV ionizing energy. Compound assignment was achieved by considering diagnostic ions for the main homologous series, via low-resolution MS and via comparison with published and stored data in NIST and Wiley libraries. A semi-quantification of the products released by analytical pyrolysis was done for each sample by converting the peak areas to a percentage of the total chromatographic area. Minor compounds with 0.2% of the total chromatographic area were excluded.

2.5 Thermal analysis

Thermo-gravimetric and differential scanning calorimetric (TG-DSC) analyses of dried (40 ºC) samples were conducted using Discovery series SDT 650 simultaneous DSC/TGA instrument (T.A Instruments Inc. Delaware, USA) under a N_2 flow rate of 50 ml min^{-1}. The samples (5 mg) were placed in Alumina cups without cover and heated from 50 to 650 °C at a heating rate of 20 ºC min^{-1}. TG, dTG curves, mass loss and calorimetry were obtained via TRIOS software (T.A. Instruments, Delaware, USA). Experiments were performed twice with a reproducibility error of 1 %. The weight loss of the decomposed materials was divided into four groups in terms of the proportions of: W1 (moisture and very labile OM), W2 (labile OM), W3 (intermediate OM), W4 (recalcitrant OM) components.

2.6 Images and data analysis

To evaluate the visible lampenflora evolution during treatments, pictures were processed through ImageJ software to obtain a quantitative percentage value of photoautotrophic biofilms on surfaces.

Differences according to the single analyzed parameters based on the chlorophyll fluorescence and on the images analysis, were evaluated by three-way analyses of variance (three-way ANOVAs), followed by Tukey *post-hoc* tests, considering three fixed variables: the type of surface (bare and with vermiculation), the time and the type of treatments (control, NaClO, H_2O_2 and UVC irradiation).

All the statistical and graphical analysis was carried out in the R 4.0.0 programming environment (R Core Team, 2020), with functions from the “vegan”, “agricolae”, “ggplot2”, “dplyr”, “RColorBrewer” and “ggbreak” packages, and using theopen-source vector graphics editor Inkscape 0.92.

3 Results

3.1 Image analyses and maximal PSII photochemical efficiency

Figure 1 displays the visible lampenflora amount trends on the surfaces during the entire period of treatments. Both the types of surfaces, bare (Figure 1a) and with vermiculations (Figure 1b) showed a complete disappearance of green biofilms after NaClO treatment, whitening them, whereas the H_2O_2 aroused only a slight decrease of them. Control and UVC exhibited the same trend, indicating any effect due to the lamp. Moreover, all the area covered by lampenflora with vermiculations had gone through a gradual decline.

Figure 1 shows also the maximal PSII photochemical efficiency, measured before and after the several treatments on the two surface typologies, bare (Figure 1c) and with vermiculations (Figure 1d) covered by lampenflora. At time 0, they displayed Fv/Fm mean values, respectively for bare surface and with vermiculations, equal to 0.695 and 0.744. After the first chemical treatment, with H_2O_2 or NaClO, a decrease to 0 was observed, and it did not change for a month nor after the second treatment, indicating an almost complete reduction of biological activity. However, after three months break due to the Covid19 lockdown, there was a slight recovery of lampenflora, immediately stopped after the third treatment. No detectable effect occurred in relation to the biofilm photosynthetic activity on the surfaces interested by UVC treatments, exhibiting a trend similar to the control areas. The output parameters obtained by the three-way ANOVAs are reported in Table 1a and b, respectively for lampenflora amount trends and Fv/Fm.

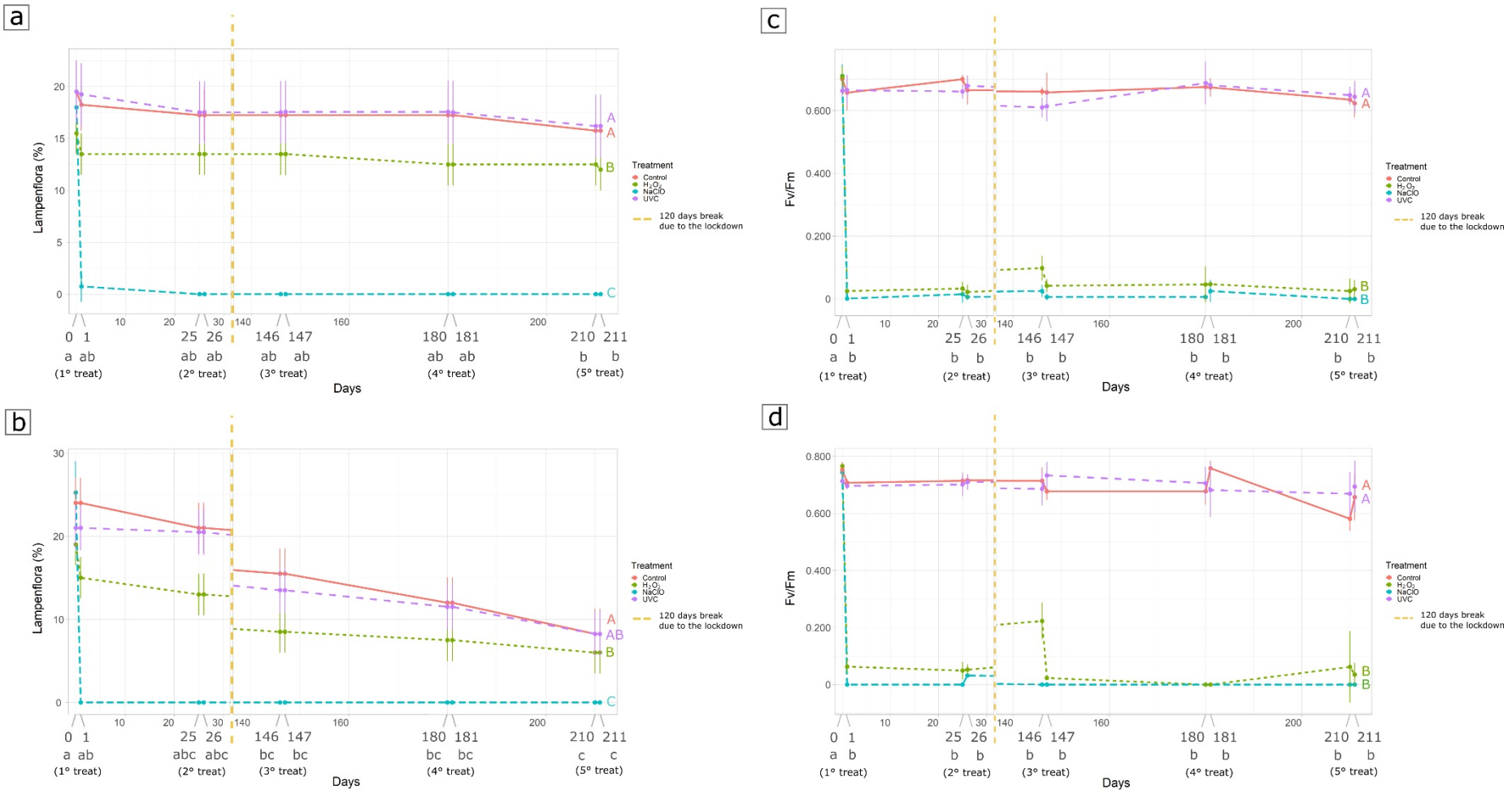

Fig. 1 Maximal PSII photochemical efficiency (Fv/Fm) and amount percentage value of biofilms on surfaces, measured before and after the several treatments (control, orange; H_2O_2, green; NaClO, light blue; UVC, violet) on bare (respectively, **a** and **c**) and with vermiculations (respectively, **b** and **d**) surfaces covered by lampenflora. Different letters indicate significant (for α=0.05) differences among treatments over time (small letters) and treatment typologies (capital letters), according to the Tukey *post-hoc* tests.

Table 1 Output parameters of the three-way ANOVAs using amount percentage values of biofilms on surfaces (**a**) and Fv/Fm data (**b**), considering the three fixed variables, the type of surface, the time and the treatments.

a.

	Df	F value	Pr(>F)
Surface type	1	3.214	0.0771
Time	1	46.056	2.45e-09
Treatment	3	64.747	< 2e-16
Residuals	74		

b.

	Df	F value	Pr(>F)
Surface type	1	0.826	0.367
Time	9	8.196	4.63e-08
Treatment	3	168.252	< 2e-16
Residuals	66		

3.2 Microscopy

In Figure 2I, the optical (a), epifluorescence (b) and FE-SEM (c) microscopy images from the treated bare surfaces covered by lampenflora are reported. This photoautotrophic community, apparently mainly constituted by filamentous bacteria and algae, appeared completely entangled to the mineral substrate. The UVC treatment did not show changes in their photosynthetic activity (red in b) nor in the microstructures (a, c), seeming to be intact like the control. The surface treated with NaClO looked to be free from any biomass, totally destroyed by such chemical solution, without significant damages to the substrate. H_2O_2 solution caused the community death, but not its removal, in fact, all the residual organic matter persisted on the substrates. The same behavior occurred for the treated lampenflora on surfaces with vermiculations (Figure

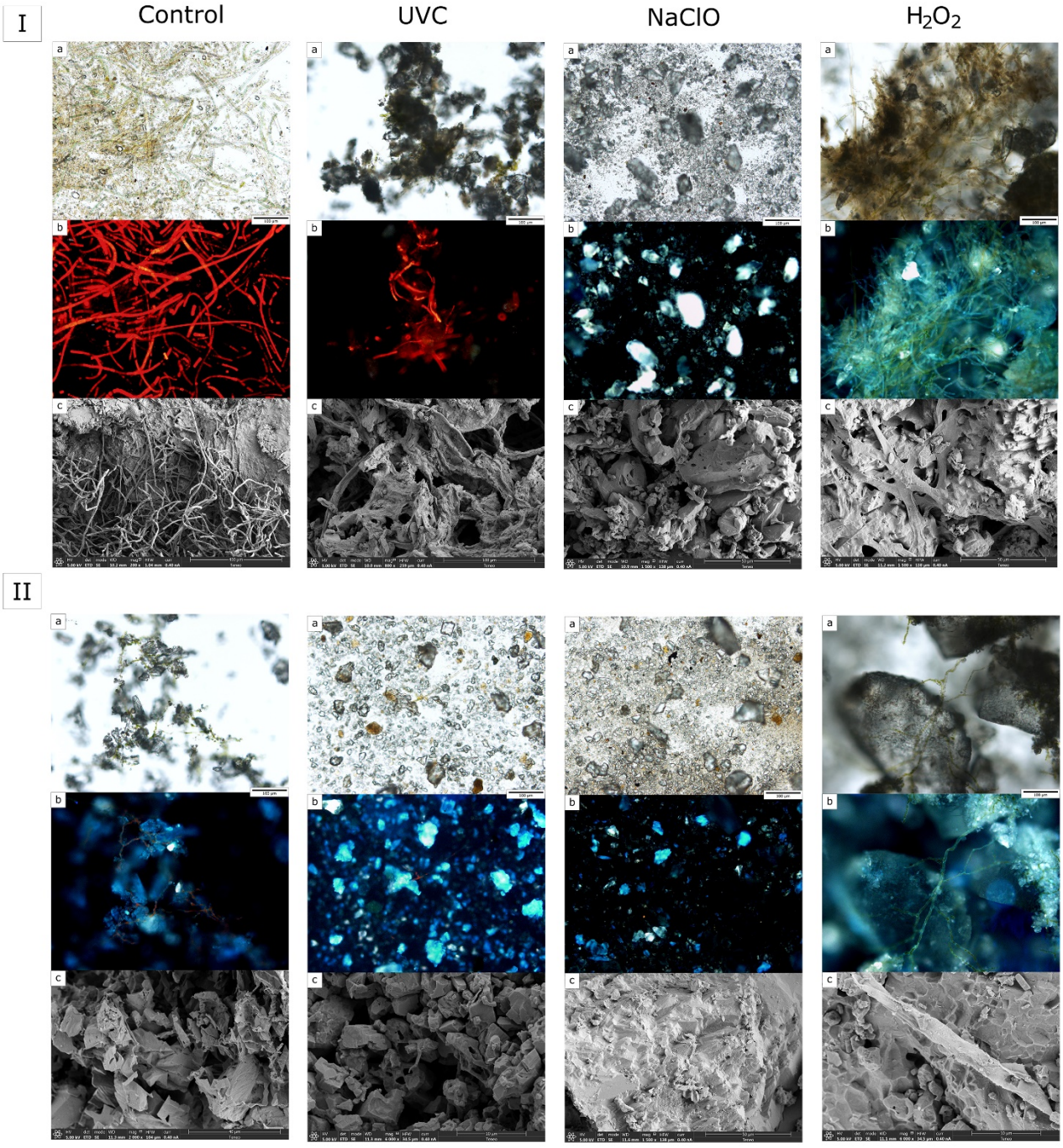

Fig. 2 Microscopy images of the biofilms on bare (**I**) and with vermiculations (**II**) surfaces for each treatment type (control, H_2O_2, NaClO, UVC): optical (**a**), epifluorescence (**b**) and FE-SEM (**c**).

2II), but, in this case, the communities are weakened, both in quantity and in the photosynthetic activity, evidenced by the poor state of the filamentous mass on substrates and by the feeble red showed in the epifluorescence microscopy images (b) from the control. Moreover, H_2O_2 treatment exhibited evidences of corrosion on these surfaces (c).

3.3 Taxonomic composition of lampenflora community

Table 2 reports the results about the preliminary quantitative analysis of the DNA extracted from lampenflora samples collected on bare surfaces and with vermiculations subjected to each treatments, at the end of the field trial. The two controls showed values, respectively for the two types of surfaces, equal to 11.7 and 0.6 ng/µL, the UVC treatments, equal to 10.5 and 8.6 ng/µL. The two chemical treatments, NaClO and H_2O_2, displayed values, respectively, equal to 0.3 and 5.0 ng/µL for bare surface and 0.1 and 2.7 ng/µL for vermiculated surfaces.

Table 2 Amount of DNA extracted from ~ 0.250 g of lampenflora samples.

Surface type	Treatment	Amount (ng/µL)
Bare surface	Control	11.7
	UVC	10.5
	NaClO	0.3
	H_2O_2	5.0
With vermiculations	Control	0.6
	UVC	8.6
	NaClO	0.1
	H_2O_2	2.7

Both Prokaryotes (Figure 3I) and Eukaryotes (Figure 3II) composed the extracted DNA. The major phylum in the total bacterial community of the control bare surface (Figure 3Ia) was represented by *Cyanobacteria* (41.2%), dominated, at class level, by

Cyanophyceae (41.2%) (Figure 3Ib) and, at order level, by *Nostocales* (39.3%) (Figure 3Ic). It is followed by *Proteobacteria* (36.0%), dominated by *Alpha-* (15.1%), *Beta-* (8.8%) and *Gamma-proteobacteria* (8.6%) classes (Figure 3Ib), followed by *Acidobacteria* (5.0%) > *Bacteroidetes* (3.3%) > *Actinobacteria* (2.4%) > *Firmicutes* (2.1%) > *Nitrospirae* (1.5%). Other less represented (<1%) taxa (2.5%) and a group of unclassified (6.0%) phyla were also detected. The control from surface with vermiculations (Figure 3Ia) exhibited a similar composition to the bare surface, with *Proteobacteria* (59.8%), dominated by *Gamma-* (24.7%), *Beta-* (24.7%) and *Alpha-proteobacteria* (7.1%) classes (Figure 3Ib), followed by Unclassified *Bacteria* (9.9%) > *Firmicutes* (9.0%) > *Nitrospirae* (5.4%) > *Bacteroidetes* (4.8%) > *Acidobacteria* (3.3%) > *Actinobacteria* (2.8%) > less represented (<1%) taxa (2.0%) > *Chloroflexi* (1.8%) > *Gemmatimonadetes* (1.2%), but with *Cyanobacteria* almost absent, showing a relative abundance equal to 0.4%.

The Prokaryotic DNA extracted by lampenflora from the bare surfaces treated with UVC displayed the most abundant phyla (Figure 3Ia) as follows: *Proteobacteria* (33.7%), dominated by *Alpha-* (14.4%), *Delta-* (7.7%), *Beta-* (6.4%) and *Gamma-proteobacteria* (5.5%) classes (Figure 3Ib) > *Cyanobacteria* (32.0%), dominated, at class level, by *Cyanophyceae* (32.0%) (Figure 3Ib) and, at order level, by *Nostocales* (31.26%) (Figure 3Ic) > *Bacteroidetes* (11.6%) >*Firmicutes* (6.5%) > Unclassified *Bacteria* (5.2%) > *Acidobacteria* (3.0%) > less represented (<1%) taxa (2.5%) > *Chloroflexi* (2.4%) > *Synergistetes* (2.0%) > *Actinobacteria* (1.1%). The surface with vermiculations treated with UVC, at phylum level (Figure 3Ia), was almost totally composed by *Proteobacteria*, with a percentage equal to 74.4%, represented by *Beta-* (38.9%), *Gamma-* (22.8%), *Alpha-* (9.56%) and *Delta-proteobacteria* (3.1%) classes

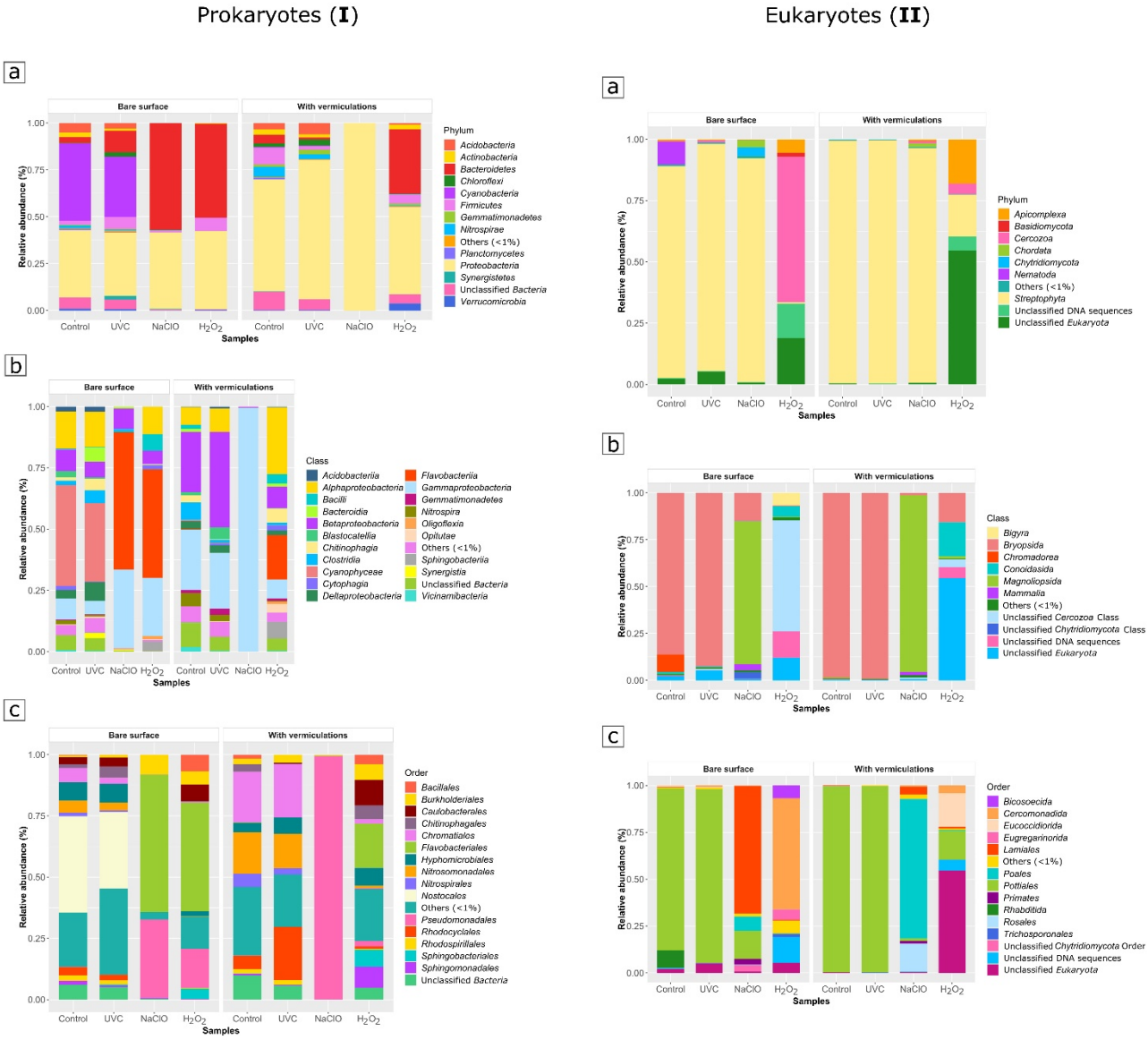

Fig. 3 Prokaryotes (**I**) and Eukaryotes (**II**) composition of the lampenflora from bare and with vermiculations surfaces for each treatment type (control, H_2O_2, NaClO, UVC); the barplots show the relative abundances (%) at phylum (**a**), class (**b**), and order (**c**) levels.

(Figure 3Ib), followed by *Acidobacteria* (6.1%) > Unclassified *Bacteria* (5.7%) > *Chloroflexi* (3.3%) > *Nitrospirae* (2.7%) > *Gemmatimonadetes* (2.5%) > *Firmicutes* (1.8%) > *Actinobacteria* (1.6%) > *Bacteroidetes* (1.0%) and less represented (<1%) taxa (1.0%).

Samples collected from the bare surfaces treated with NaClO and H_2O_2 exhibited similar microbial communities mainly constituted by *Bacteroidetes* (56.9% and 50.3%, respectively) phylum (Figure 3Ia), composed primarily by *Flavobacteriia* (55.9 and 44.2%, respectively) class (Figure 3Ib) and, at order level, by *Flavobacteriales* (55.9 and 44.2%, respectively) (Figure 3Ic), and *Proteobacteria* (40.8 and 41.8%, respectively, phylum (Figure 3Ia), dominated mainly by *Gamma-* (32.0 and 23.8%, respectively), *Alpha-* (0.2 and 11.2%, respectively) and *Beta-proteobacteria* (8.3 and 5.4%, respectively) classes (Figure 3Ib). The entire bacterial community of the sample from the vermiculated surfaces treated with NaClO is composed by *Proteobacteria* (100.0%) phylum (Figure 3Ia), primarily represented by *Gamma-proteobacteria* (99.4%) class (Figure 3Ib) and by *Pseudomonadales* (99.4%), at order level (Figure 3Ic). Community of the sample from the vermiculated surfaces treated with H_2O_2 turned up more biodiverse, composed primarily by *Proteobacteria* (46.5%) phylum (Figure 3Ia), represented by *Alpha-* (27.3%), *Beta-* (8.7%), *Gamma-* (7.7%) and *Delta-proteobacteria* (1.8%) classes (Figure 3Ib), and by *Bacteroidetes* (34.2%) phylum, dominated, at class level, by *Flavobacteriia* (18.1%) and *Sphingobacteriia* (6.9%) classes, followed by *Firmicutes* (5.1%) > Unclassified *Bacteria* (4.9%), *Verrucomicrobia* (3.8%) > *Actinobacteria* (2.5%) > G*emmatimonadetes* (1.1%) phyla. The almost entirety Eukaryotic DNA constituting the controls, as well as the UVC irradiated samples, from bare and vermiculated surfaces, was mostly represented by

Streptophyta (86.3 and 99.0% - 92.8 and 99.3%, respectively for control and UVC treatments) phylum (Figure 3IIa). This was dominated by *Bryopsida* (86.2 and 98.5% - 92.7 and 99.2%, respectively for control and UVC treatments) class (Figure 3IIb) and, at order level, by *Pottiales* (86.2 and 98.5% - 92.7 and 99.2%, respectively for control and UVC) order (Figure 3IIc). The bare surfaces and those with vermiculations treated with NaClO were mainly characterized by *Streptophyta* (91.4 and 95.8%, respectively) phylum (Figure 3IIa), dominated, at class level, by *Magnoliopsida* (76.2 and 94.2%, respectively) and *Bryopsida* (15.1 and 1.3%, respectively) (Figure 3IIb), and, at order level, by *Lamiales* (68.1 and 4.2%, respectively), *Pottiales* (15.1 and 1.3%, respectively) and *Poales* (7.6 and 74.3%, respectively) (Figure 3IIc). The major phyla composing eukaryotic community of the bare and vermiculated surfaces treated with H_2O_2 (Figure 3IIa) were represented by *Cercozoa* (59.3 and 4.3%, respectively), unclassified *Eucaryota* (19.0 and 54.6%, respectively), unclassified DNA sequences (13.9 and 5.7%, respectively), *Apicomplexa* (5.6 and 18.1%, respectively), and *Streptophyta* (0.6 and 17.11%, respectively) (Figure 3IIa).

3.4 Analytical pyrolysis

The compounds obtained by Py-GC/MS analysis (Figure 4, Table 3) were categorized into 5 families with known biogenic origin: n-alkane/alkene pairs (ALK); aromatic compounds (ARO), polysaccharide-derived (PS), nitrogen compounds (N), and contaminants (CONT). Differently from the vermiculated surfaces that presented no changes, neither qualitatively nor quantitatively, in chemical composition after both H_2O_2 and NaClO treatments, the bare surfaces showed differentiation. The first one exhibited many new chemical compounds peaks, mainly alkanes/alkenes, compared to the control; quite the opposite, the second one eliminated, almost totally, the existing

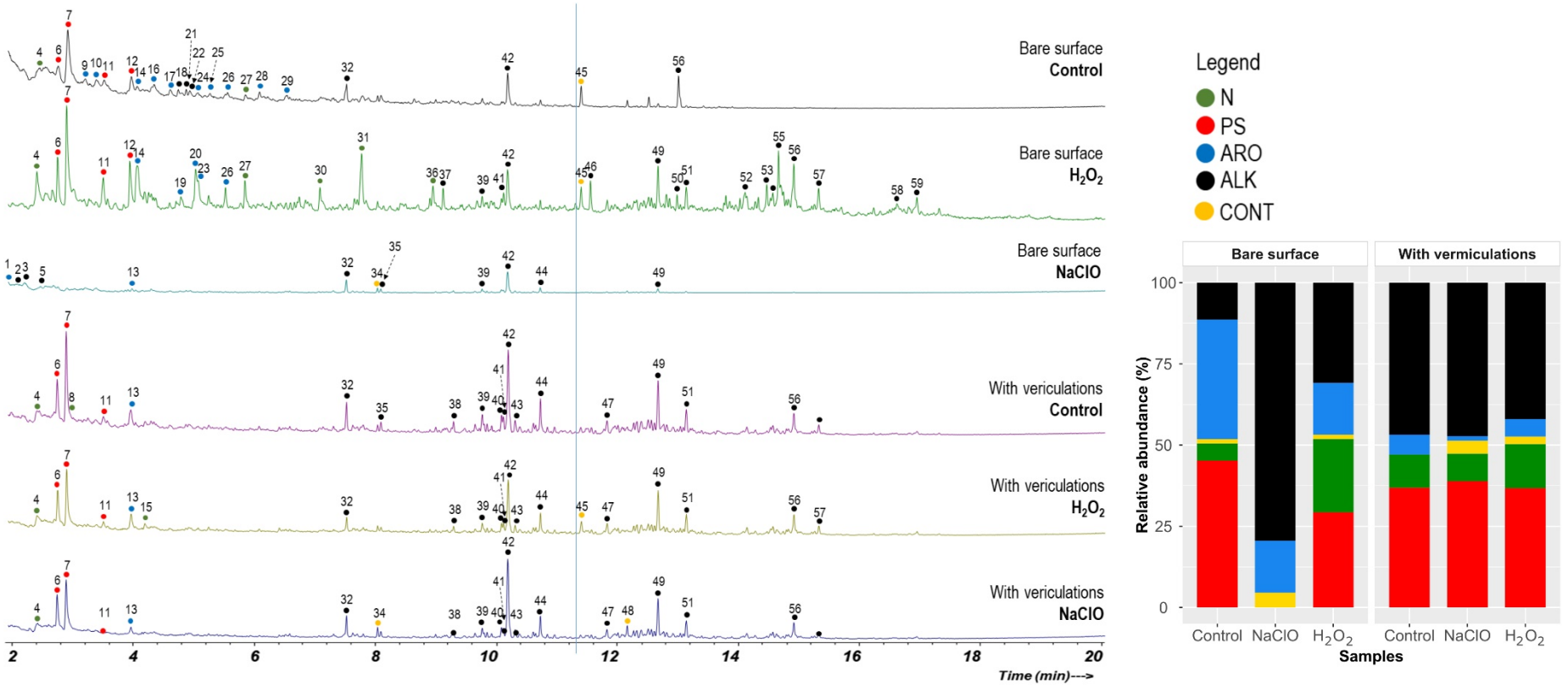

Fig. 4 Analytical pyrolysis (Py-GC–MS) with indication of the corresponding peak labels according to Table 3 and relative abundance (%) of the detected compounds in the biofilms from bare and with vermiculations surfaces for control, H_2O_2 and NaClO treatments.

Table 3 Products released by Py-GC–MS at 400 °C of the lampenflora from bare (BS) and with vermiculations (WV) surfaces for control, NaClO and H_2O_2 treatments with indication of the corresponding peak labels (Ref) according to Table 2. The peak label indicated in Fig. 8 (Ref), the retention time (RT), the relative abundance (%) of the total chromatographic area for each sample, the compounds (Library/ID) and component families (Origin) are specified.

Ref	RT	BS	BS	BS	WV	WV	WV	Library/ID	Origin
		Control	NaClO	H_2O_2	Control	NaClO	H_2O_2		
1	2.15	-	13.75	-	-	-	-	Benzene	ARO
2	2.27	-	20.22	-	-	-	-	2-Hexene, 2-methyl	ALK
3	2.53	-	6.34	-	-	-	-	3-Heptene, 4-methyl-	ALK
4	2.58	3.51	-	9.60	6.22	8.46	10.88	Pyridine	N
5	2.75	-	4.12	-	-	-	-	2-Hexene, 3,5-dimethyl-	ALK
6	2.83	9.77	-	6.73	12.68	15.91	12.85	2-Furfural	PS
7	2.98	20.77	-	12.68	20.02	21.30	20.69	3-Furfural	PS
8	3.07	-	-	-	3.98	-	-	1H-Pyrazole, 3,4-dimethyl-	N
9	3.27	5.24	-	-	-	-	-	Benzene dimethyl	ARO
10	3.45	6.23	-	-	-	-	-	Styrene	ARO
11	3.58	8.61	-	4.44	4.19	1.70	3.20	2,3,4-Trimethylfuran	PS
12	4.03	6.09	-	5.48	-	-	-	2-Furancarboxaldehyde, 5-methyl-	PS
13	4.04	-	2.26	-	6.11	1.48	5.41	Benzaldehyde	ARO
14	4.12	3.10	-	7.72	-	-	-	Phenol	ARO
15	4.25	-	-	-	-	-	2.70	Benzonitrile	N
16	4.40	7.12	-	-	-	-	-	Benzofuran	ARO
17	4.67	4.39	-	-	-	-	-	Benzene trimethyl	ARO
18	4.80	1.62	-	-	-	-	-	C11 Branched	ALK
19	4.84	-	-	1.32	-	-	-	Benzeneacetaldehyde	ARO
20	5.08	-	-	3.53	-	-	-	Methyl phenol	ARO
21	4.93	1.43	-	-	-	-	-	C11 Branched	ALK
22	4.99	2.14	-	-	-	-	-	Cycloheptane, 1,3,5-tris(methylene)-	ALK
23	5.12	-	-	2.09	-	-	-	3,5-Dihydroxytoluene	ARO
24	5.12	2.61	-	-	-	-	-	Benzene trimethyl	ARO
25	5.32	2.86	-	-	-	-	-	Benzene tetramethyl	ARO
26	5.61	2.67	-	1.33	-	-	-	Benzofuran, 2-methyl-	ARO
27	5.90	1.71	-	2.24	-	-	-	Benzyl nitrile	N
28	6.14	1.29	-	-	-	-	-	p-Cymene	ARO
29	6.59	1.24	-	--	-	-	-	Naphthalene	ARO
30	6.79	-	-	1.46	-	-	-	Benzenamine, 3-ethoxy-	N
31	7.13	-	-	2.37	-	-	-	Benzenepropanenitrile	N
32	7.56	1.33	10.48	-	3.78	3.86	2.73	C12 Branched	ALK
33	7.82	-	-	5.09	-	-	-	Indole	N
34	8.07	-	4.52	-	-	1.40	-	Column	CONT
35	8.13	-	3.41	-	1.41	-	-	Decane, 2,3,7-trimethyl-	ALK
36	8.99	-	-	1.73	-	-	-	Indole, 3-methyl-	N
37	9.15	-	-	1.40	-	-	-	Dodecanal	ALK
38	9.32	-	-	-	1.83	1.55	1.34	Decane, 2,3,6-trimethyl-	ALK
39	9.79	-	3.56	0.96	2.99	2.35	1.96	C13 Branched	ALK
40	10.11	-	-	-	1.89	1.54	1.31	Alk	ALK
41	10.15	-		1.02	1.76	1.63	1.35	1-Pentadecene	ALK
42	10.22	2.71	22.61	3.34	12.00	16.38	9.92	Pentadecane	ALK
43	10.34	-		-	1.82	1.61	1.23	C15 Branched	ALK
44	10.75	-	4.43	-	4.60	4.11	3.52	Alk	ALK
45	11.42	1.43	-	1.33	-	-	2.31	Diethyl Phthalate	CONT
46	11.58	-	-	1.53	-	-	-	Alk Branched	ALK
47	11.85	-		-	1.85	1.69	2.40	Alk Branched	ALK
48	12.18	-		-		2.55		Column	CONT
49	12.69	-	4.27	3.36	6.91	6.81	7.05	C19	ALK
50	13.03	2.10	-	0.98	-	-	-	Alk Branched	ALK
51	13.15	-	-	1.64	3.03	2.58	3.11	Alk Branched	ALK
52	14.12	-	-	1.73	-	-	-	2-Hexadecene, 2,6,10,14-tetramethyl-	ALK
53	14.48	-	-	1.78	-	-	-	Alk Branched	ALK
54	14.58	-	-	1.23	-	-	-	Alk Branched	ALK
55	14.67	-	-	4.01	-	-	-	2-Heptadecanone	ALK
56	14.93	-	-	4.04	2.92	3.08	4.20	Alk Branched	ALK
57	15.33	-	-	1.29	-	-	1.85	Alk Branched	ALK
58	16.62	-	-	0.93	-	-	-	Alk Branched	ALK
59	16.95	-	-	1.62	-	-	-	Alk C20	ALK

chemical species, with the persistence of few alkanes/alkenes and aromatic compounds peaks in little quantities.

3.5 Thermal analysis

Table 4 shows the total and relative weight loss of the biofilms from bare and with vermiculation surfaces for the different treatments. All the treated samples (bare and with vermiculation) are characterized by a lower weight loss (2-to-4 times lower) than the control samples, which are characterized by a high abundance of very labile OM and recalcitrant OM (W1 and W4 respectively).

Table 4 Comparative thermogravimetry (TG) and differential scanning calorimetry (DSC) parameters in samples of the biofilms from bare and with vermiculations surfaces for control. UVC. NaClO and H_2O_2 treatments summarizing: Total weight loss for the temperature interval 50–650 ºC (% ± 1%). weight losses and relative weight losses for the temperature intervals. 50–120 ºC.120–200 ºC. 200–400 ºC. 400–600 °C. and temperature of the main exothermic peaks.

		Bare surface				With vermiculations			
TG		**Control**	**UVC**	**NaClO**	**H_2O_2**	**Control**	**UVC**	**NaClO**	**H_2O_2**
Moisture and very labile OM-W1	**50–120 ºC**	2.1	0.4	0.3	0.3	2.8	0.9	0.4	0.4
Labile OM-W2	**120–200 ºC**	0.7	0.2	0.2	0.1	0.9	0.4	0.1	0.2
Int OM-W3	**200–400 ºC**	2.1	0.8	0.7	0.6	2.2	1.3	0.5	0.7
Recalcitrant OM-W4	**400–600 ºC**	3.1	1.0	1.1	0.7	3.6	1.4	1.5	0.8
Total weight loss	**50–650 ºC**	8.0	2.4	2.3	1.7	9.5	3.9	2.5	2.1
Relative Weight Loss (%)									
Moisture and very labile OM-W1	**50–120 ºC**	26	16	13	18	29	22	16	21
Labile OM-W2	**120–200 ºC**	9	8	8	6	9	9	4	9
Int OM-W3	**200–400 ºC**	27	35	31	34	24	33	20	32
Recalcitrant OM-W4	**400–600 ºC**	39	41	48	42	38	36	60	38
DSC									
Max of main Exo peak (ºC)		356	405	404	425	445	421	430	425
Q released (Exo)	**[J g-1]**	1790	1260	960	1410	1320	1160	1180	1190
Q' (labile to recalcitrant OM)	**[J g-1 OM]**	26	18	15	23	20	17	14	19

The differential scanning calorimetry (DSC) data shows an increase of the thermal resistance of the treated bare biofilms, which is evidenced by the rise of the maxima of the exothermic peaks. Biofilms with vermiculation showed a greater relative abundance of the most thermally labile fraction (W1) than the corresponding bare sample, which agree with a decrease of the released heat per unit of organic matter (Q´ released).

4 Discussion

To solve the problem of lampenflora in show caves, fine-tuning surfaces cleaning methods to remove it and to prevent its growth, without compromising the wall integrities and the underground habitat, now accounts a challenge and a priority for the most sensible managers who have the will to realize a sustainable management of these fragile ecosystems. However, little is known about the effects of the most used lampenflora removing physical (UVC) and chemical (NaClO, H_2O_2) methods, both on lampenflora metabolism and treated surface compositions. Furthermore, there is not a standardized action to quantitatively and qualitatively monitor the treatment efficacies over time (Baquedano Estévez et al., 2019). Thanks to the results of our study, a useful overview of the processes activated on surfaces by the commonly employed methods of lampenflora control was provided, shedding light on both the community evolution following the treatments and their potential alterations on the substrates.

The maximal PSII photochemical efficiency measures (quantum yield), proved to be a valid *in situ* and not-destructive way, to follow the metabolic dynamics of the lampenflora in caves, representing a proxy of the physiological status of the community related to the photosynthetic activity (Figueroa et al., 2017). The Fv/Fm values, before any treatment, recorded on the green biofilms from the Pertosa-Auletta Cave were in

accord with those of the lampenflora growing in Cango Cave (South Africa) (mean value 0.74; Grobbelaar, 2000) and in La Glacière Cave (France) (mean value 0.70; Pfendler et al., 2017). The chemical treatments (NaClO and H_2O_2) zeroed completely the quantum yields already after the first application, due to the oxidation reactions of the organic substrates (Faimon et al., 2003), totally destroyed, in the first case, and damaged, in the second one, as shown also by microscopy images, whom, after three months without treatments, showed signs of recovery. The visible colonization resulted also different between the two chemical treatments: NaClO acted without damaging neither bare nor vermiculated surfaces, whereas H_2O_2 produced a slight brightening, but all the death organic matter remains on surfaces, representing an energy source for the cave biota (Mulec, 2019). Moreover, H_2O_2 treatment appeared visibly corrosive for vermiculations, mainly constituted by calcite (Addesso et al, 2019), producing an effervescent reaction, indicator of dissolution phenomenon activation, being hydrogen peroxide more aggressive than karst water (Faimon, 2003; Trinh et al., 2018). Therefore, if, on the one hand, a higher concentration might need to eliminate the organic matter, on the other, its corrosive power increases, requiring a chemical riequilibration of the solution (Faimon, 2003). As suggested by Trinh et al. (2018), it may be appropriate a controlled water-jet washing or surfaces brushing to remove completely the biomass, taking care to bring the residues out of the cave, maintaining the lower concentration. Anyway, in this case, an accurate analysis of typology of surfaces needs. Indeed, it can be recommended on hard surfaces but not on soft, like vermiculations.

The gradual decrease in lampenflora colonization of surfaces with vermiculations, also supported by the amount of DNA extracted from this sample, can be explained by the

switching off of one of the three lamps installed in this section of the cave for tourism fruition, confirming that the light represents the main driver determining the green biofilm growth (Piano et al., 2015).

In relation to the taxonomic community composition, the most abundant photosynthetic taxon in the Pertosa-Auletta Cave lampenflora biofilms, considering the untreated bare surface, was represented by *Cyanobacteria*, exactly by the aerophytic filamentous cyanobacterial species *Brasilonema angustatum* (39.3%), belonging to the *Scytonemataceae* family, isolated from the island of Oahu, Hawaii (Vaccarino and Johansen, 2012), and by *Aerosakkonema funiforme* (1.8%), gas-vacuolated oscillatorioid cyanobacterium, isolated from freshwater (Thu et al., 2012). In is known (Popović et al., 2017; Mulec, 2019; Baquedano Estévez et al., 2019; Havlena et al., 2021) that *Cyanobacteria* are among the pioneering organisms that in the lampenflora ecological succession give rise to the phenomenon. The vermiculated untreated surface revealed an almost absence of photoautotrophic organisms (< 1%), whereas constituting by several other phyla, commonly found in cave environment (Tomczyk-Żak and Zielenkiewicz, 2016). Almost the entire Eukaryotic DNA extracted from both the untreated surface types was composed by *Ephemerum spinulosum*, plants belonging to the *Pottiaceae* family, typically found in dampest environments (Ignatov et al., 2013). After both chemical treatments on bare surfaces, the photoautotrophs passed away from the community, with the persistence mainly of *Proteobacteria* and *Bacteroidetes*, which went also on vermiculated surfaces treated with H_2O_2, whereas those treated with the commercial bleach presented only *Proteobacteria*. Concerning the Eukaryotes, H_2O_2 treatment has proven more successful on *Streptophyta* phylum than NaClO (having no

effect), with a residual presence of *Apicomplexa*, a group of unicellular protists, and *Cercozoa* phyla, with the resistance also of unclassified groups.

UVC lamps did not produce alterations, neither in the community nor in the substrate structure, likely in relation to a too mild treatment. An increase of time exposition of surfaces from one to four times a month probably would have determined appreciable effects, but unfortunately, for logistic reasons related also to the Covid19 pandemic, further methods improvements had not been possible. According to these findings, the Py-GC/MS analyses were performed only on the chemically treated and untreated surfaces, highlighting different macromolecular compositions of the samples. The untreated surfaces, mainly composed by nitrogen compounds (pyridine), were rich in protein constituents (Saiz-Jimenez et al., 2021), associated with polysaccharide products, represented by furan compounds and their derivatives. Alkanes/alkenes were also relatively abundant, possibly related to bacterial activity (Kaal et al., 2020); among the pyrolyzates, members of the aromatic compound family, commonly observed in natural biomolecules (Miller et al., 2016), there were also various products, even if in little amount. The analysis of the chemically treated surfaces provided interesting information about the not relevant effects of NaClO on surface compositions, and the changes implemented on bare surfaces after H_2O_2 treatment, which promoted the dissolution of substrates, producing alkanes/alkenes compounds with high chemical diversity.

Concerning thermal analyses, due to the estimated 1% reproducibility error, no significant distinctions can be made between treatments, but some differences and interesting information were found. The sharp reduction of the total weight loss of the treated biofilms and the transfer of the relative weight loss from W1 (labile OM) to W3

and W4 for the treated biofilms compared with the control ones is indicative of the elimination of labile organic remains by the treatments, which also caused an alteration of the composition of the remaining organic materials. The thermal degradation of control samples is characterized by the high relative abundance of very labile OM, typically composed by polysaccharides (the main constituent of EPS), whereas the thermograms of treated biofilms showed a great relative abundance of recalcitrant OM, typically composed by lignin moieties. In contrast, the TG curves of NaClO treated biofilms were characterized by the lowest relative abundance of very labile and labile OM, suggesting an effective removal of fresh biofilms. The dTg and DSC of showed peaks with maxima at 356 ºC for the control at bare surface, corresponding to cellulose decomposition (Pappa et al., 2003), whereas the treated biofilms showed maxima ranging 404 to 425 ºC, which correspond to the thermal degradation of lignin.

5 Conclusions

Our results provide relevant and useful information concerning the efficacy of the most employed lampenflora control and removal physical (UVC) and chemical (NaClO, H_2O_2) methods in show caves, offering a comprehensive evaluation of biofilm physiology and composition, as well as of the potential deterioration processes of substrates in response to their applications. Commercial bleach treatment seems to be the most efficient method in relation to both surface sterilization and visible cleaning over long time, with unaltered substrates; however, its toxicity is known. Considered the "greenest" method, H_2O_2 treated surfaces showed a recovery of lampenflora after three months without applications, with evident dissolution processes, activated on surfaces. Indeed, hydrogen peroxide promotes the presence of novel chemical species and the visible deterioration of vermiculations deposits. In addition, the organic matter was not

completely eliminated, and the death matrix needs to be removed through brushing or water jet. UVC did not show evidence of problem solving with the method used in such research.

Acknowledgments

We thank the following institutions and people: MIdA Foundation, manager of the Pertosa-Auletta Cave, the speleo-guide Vincenzo Manisera and all the MIdA staff, Melandro Caving Group, Castel di Lepre Caving Group, CAI Napoli, Vespertilio Caving Group, Sa.Gest. srl, for having facilitated all the field activities with their technical and logistical support.

Funding

This work was partly funded by University of Salerno (Italy) within the ORSA197159 and ORSA205530 projects. Grant PID2019-108672RJ-I00 funded by MCIN/AEI/10.13039/501100011033 and, as appropriate, by “ERDF A way of making Europe”, by the “European Union” or by the “European Union Next Generation EU/PRTR”.

Conflict of Interest

The authors declare that they have no conflict of interest.

References

Addesso, R., Gonzalez-Pimentel, J.L., D'Angeli, I.M., De Waele, J., Saiz-Jimenez, C., Jurado, V., Miller, A.Z., Cubero, B., Vigliotta, G., Baldantoni, D. (2020) Microbial Community Characterizing Vermiculations from Karst Caves and Its Role in Their Formation. Microbial Ecology 81:884–896.

Addesso, R., Bellino, A., D'Angeli, I.M., De Waele, J., Miller, A.Z., Carbone, C., and Baldantoni, D. (2019) Vermiculations from karst caves: The case of Pertosa-Auletta system (Italy). CATENA 182: 104178.

Baquedano Estévez, C., Moreno Merino, L., de la LosaRomán, A., DuránValsero, J.J. (2019) The lampenflora in show caves and its treatment: an emerging ecological problem. International Journal of Speleology, 48 (3), 249-277.

Caporaso, J.G., Kuczynski, J., Stombaugh, J., Bittinger, K., Bushman, F.D., Costello, E.K., Fierer, N., Peña, A.G., Goodrich, J.K., Gordon, J.I., Huttley, G.A., Kelley, S.T., Knights, D., Koenig, J.E., Ley, R.E., Lozupone, C.A., McDonald, D., Muegge, B.D., Pirrung, M., Reeder, J., Sevinsky, J.R., Turnbaugh, P.J., Walters, W.A., Widmann, J., Yatsunenko, T., Zaneveld, J., Knight, R. (2010) QIIME allows analysis of high-throughput community sequencing data. Nature Methods 7:335–336.

Cigna, A., (2012) The problem of lampenflora in show caves. Slovenský Kras Acta Carsologica Slovaca, 50 (1), 5-10.

Edgar, R.C. (2010) Search and clustering orders of magnitude faster than BLAST. Bioinformatics 26:2460–2461.

Faimon, J., Štelcl, J., Kubešová, S., and Zimák, J. (2003) Environmentally acceptable effect of hydrogen peroxide on cave "lamp-flora", calcite speleothems and limestones. Environmental Pollution 122: 417–422.

Figueroa, F.L., Álvarez-Gómez, F., delRosal, Y., Celis-Plá, P.S.M., González, G., Hernández, M., and Korbee, N. (2017) In situ photosynthetic yields of cave photoautotrophic biofilms using two different Pulse Amplitude Modulated fluorometers. Algal Research 22: 104–115.

Grobbelaar, J.U. (2000) Lithophytic algae: A major threat to the karst formation of show caves. Journal of Applied Phycology 12: 309–315.

Havlena, Z., Kieft, T.L., Veni, G., Horrocks, R.D., and Jones, D.S. (2021) Lighting effects on the development and diversity of photosynthetic biofilm communities in Carlsbad Cavern, New Mexico. Applied Environmental Microbiology 87:e02695-20.

Hebelka, J. (2014) Methodology of lampenflora removal in caves accessible for tourists. The cave administration of the Czech Republic, Průhonice, 15 p.

Ignatov, M.S., Ignatova, E.A., Malashkina, E.V. (2013) *Ephemerum spinulosum* Bruch &Schimp. (BRYOPHYTA), a new species for Russia. Arctoa (2013) 22: 97-100.

Kaal, J., Plaza, C., Rodríguez, M.P., and Biester, H. (2020) Towards understanding ecological disaster in the Harz Mountains (Central Germany) by carbon tracing: pyrolysis-GC-MS of biological tissues and their water-extractable organic matter (WEOM). 8: 18.

Magoč, T., Salzberg, S.L. (2011) FLASH: fast length adjustment of short reads to improve genome assemblies. Bioinformatics 27: 2957–2963.

Miller, A.Z., De la Rosa, J.M., Jiménez-Morillo, N.T., Pereira, M.F.C., González-Pérez, J.A., Calaforra, J.M., and Saiz-Jimenez, C. (2016) Analytical pyrolysis and stable

isotope analyses reveal past environmental changes in coralloid speleothems from Easter Island (Chile). Journal of Chromatography A 1461: 144–152.

Mulec, J. (2019) Lampenflora. In Encyclopedia of Caves. Elsevier, pp. 635–641.

Olson, R. (2006) Control of lamp flora in developed caves. In: Hildreth-Werker V. &Werker J.C. (Eds.), Cave conservation and restoration. National Speleological Society, Huntsville, p. 343-348.

Pappa, A., Mikedi, K., Tzamtzis, N., Statheropoulos, M. (2003) Chemometric methods for studying the effects of chemicals on cellulose pyrolysis by thermogravimetry–mass spectrometry. Journal of Analytical and Applied Pyrolysis 67: 221–235.

Pfendler, S., Einhorn, O., Karimi, B., Bousta, F., Cailhol, D., Alaoui-Sosse, L., et al. (2017) UVC as an efficient means to combat biofilm formation in show caves: evidence from the La Glacière Cave (France) and laboratory experiments. Environmental Science and Pollution Research 24: 24611–24623.

Piano, E., Bona, F., Falasco, E., La Morgia, V., Badino, G., and Isaia, M. (2015) Environmental drivers of phototrophic biofilms in an Alpine show cave (SW-Italian Alps). Science of the Total Environment 536: 1007–1018.

Popović, S., Simic, G.S., Stupar, M., Unkovic, N., Krunic, O., Savic, N., and Grbic, M.L. (2017) Cave biofilms: characterization of phototrophic cyanobacteria and algae and chemotrophic fungi from three caves in Serbia. JCKS 79: 10–23.

R Core Team (2020) R Core Team R: A Language and Environment for Statistical Computing.

Saiz-Jimenez, C., Martin-Sanchez, P.M., Gonzalez-Perez, J.A., and Hermosin, B. (2021) Analytical pyrolysis of the fungal melanins from *Ochroconis* spp. isolated from Lascaux Cave, France. Applied Sciences 11: 1198.

Thu, N.K., Tanabe, Y., Yoshida, M., Matsuura, H., and Watanabe, M.M. (2012) *Aerosakkonema funiforme* gen. et sp. nov. (Oscillatoriales), a new gas-vacuolated oscillatorioid cyanobacterium isolated from a mesotrophic reservoir. Phycologia 51: 672–683.

Tomczyk-Żak, K. and Zielenkiewicz, U. (2016) Microbial Diversity in Caves. Geomicrobiology Journal 33: 20–38.

Trinh, D.A., Trinh, Q.H., Tran, N., Guinea, J.G., and Mattey, D. (2018) Eco-friendly Remediation of Lampenflora on Speleothems in Tropical Karst Caves. JCKS 80: 1–12.

Vaccarino, M.A. and Johansen, J.R. (2012) *Brasilonema angustatum* sp. nov. (Nostocales), a new filamentous cyanobacterial species from the Hawaiian Islands. Journal of Phycology 48: 1178–1186.

Supplementary material

Figure S1. Pertosa-Auletta Cave map, showing in green the tourist trail. Red circle indicates the chosen section for treatments. **b**. Schematic experimental plan. **c**. Delimited area of a bare surface covered by lampenflora. **d**. Delimited area of a surface with vermiculations covered by lampenflora.

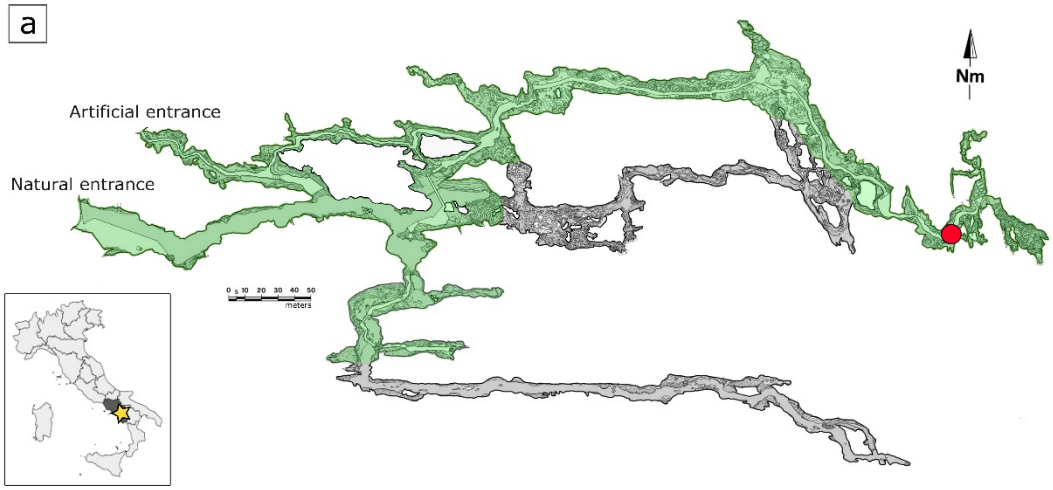

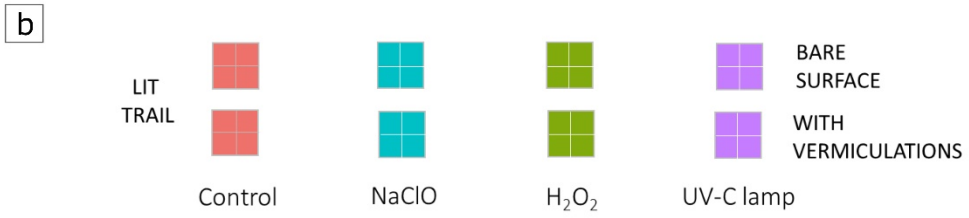

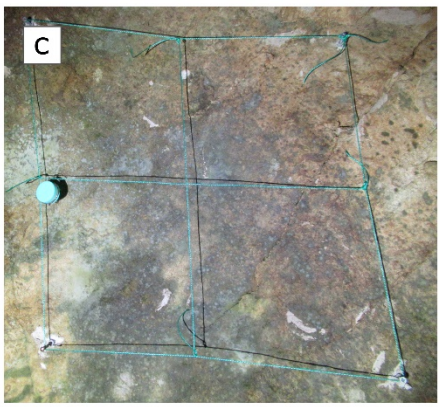

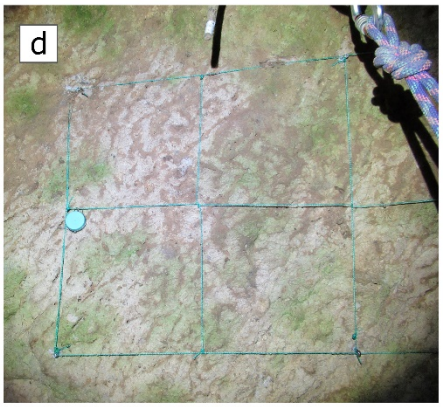

Table S1 Technical and installation features of UVC lamps

Led type	INOLUX IN-C33DTDU13535 UVC LED
Power LED MAX	4 mW
Power module LED MAX	12 mV
Spectrum wavelengths	265-285nm
Viewing angle	130°
Distance from surface	40-50 cm

Overall conclusions

The characterization of abiotic and biotic compartments of the model underground ecosystem, the Pertosa-Auletta cave, allowed evaluating its natural dynamics and ecological state. In particular, the substrates, including vermiculations sedimentary structures, the water and the atmosphere compartments, as well as the alien lampenflora biofilms, generated by permanent artificial lights, were deeply investigated. Moreover, the developed methods for a high-resolution monitoring of the atmosphere, of the airflow dynamics, and particle dispersions and depositions processes, as well as the techniques tested to remove and control lampenflora minimizing the damages on the surfaces, allowed proposing new strategies toward a sustainable management of the underground ecosystems.

The main outcomes deriving from the two main sections of the PhD project are reported below.

I. After investigating three different peculiar morphologies, water filaments, vermiculations and moonmilk deposits, from sulfuric acid karst system, we chose the Pertosa-Auletta cave, a normal karst environment, as a model. Firstly, we characterized the vermiculations, adopting an integrated approach, which allowed obtaining a comprehensive knowledge of their chemical and microbiological composition. The study highlights their calcitic mineralogical nature and the domination in the microbial community of *Proteobacteria, Acidobacteria* and, in higher humidity conditions, of *Actinobateria*, with several unknown groups. Moreover, traces of microbial activity were highlighted, with evidences of dissolution morphologies and organic matter, as well as secondary minerals precipitation biologically mediated, supporting the hypothesis of an involvement in their formation processes.

Clastic sediments from the Pertosa-Auletta Cave showed variable compositions, except for one sample, which exhibited the highest amount of organic matter and of C, Cu, Mo, N, P, Pb, S and Zn concentrations, clearly contaminated by guano. This demonstrates the important organic supply that the bat colonies provide in cave environments, as well as the potential bioindication role of such organic matter. Carbonate and dolomitic minerals, reflecting the calcareous and dolomitic original substrate in which the cave opens, mainly constitute them. This is also true for water, where drip and river waters do not exhibit relevant differences, showing high concentration of Ca, for the contact of the same limestone substrates, constituting the entire Alburni Massif system, of which the cave is part, characterized by a high hydrogeological heterogeneity and anisotropy. Moreover, chemical analysis of the Pertosa-Auletta cave waters highlighted differences among the three investigated trails: in particular, in the fossil trail, water appeared to be contaminated by P and N compounds due to the bats guano, without excluding a pollution from the surface due to the farm fields above. Organic C, transported by water through leaching from the top soil, constitutes almost the entire C. The seasonal dynamics exhibited highest amount of several elements (Cd, Co, Cu, Mn, Mo, Ni, Pb, Ti and Zn) in summer sampling, probably due to the dry weather reducing the dilution effect. The investigation on lampenflora biofilms showed their diverse behavior from the normal phototrophs: the spectra reflectance survey displayed lampenflora capacity to absorb the entire visible radiation, reflecting only the near-infrared, thanks to its capability to produce accessory pigments and its various metabolic pathways. Microscopy highlighted precipitation of $CaCO_3$ secondary minerals, like moonmilk, and corrosion shapes, demonstrating the irreversible damages of

colonized substrates. The community is mainly composed by filamentous organisms, in interaction with the minerals, dominated by *Brasilonema angustatum* cyanobacterial species, and, among the *Eukaryotes*, by *Ephemerum spinulosum* and *Pseudostichococcus monallantoides*.

II. From the high-resolution air monitoring emerged that the Pertosa-Auletta Cave appears to be able to reconquer the stationary state in few time after tourist visits, likely being a high energy system with a very big entrance, promoting airflows. It was also possible highlighting large-scale seasonal trends of temperature, relative humidity and CO_2 parameters, mainly related to the external air influences. Moreover, the isolation of the developed monitoring station in the tourist trail, due to the closure of that section for Covi19 pandemic, allowed demonstrating that there is a cave microclimatic zonation depending on morphology and energy regime of the system, given that there are not recorder alterations in that period. Conversely, in the fossil trail, not frequented by visitors, a propagation of the alterations related to the tourist presence in cave occurs.

COMSOL Multiphysics® demonstrated to be a good tool supporting the tourism planning in underground environments, such as in the choice of visit-break locations and time during the tours, avoiding the most exposed sections to the deposition particles and suggesting to install mitigation systems where anthropogenic impacts are more relevant.

Finally, the experimental trial on the most employed chemical (NaClO, H_2O_2) and physical (UVC) methods for lampenflora removal revealed the good efficacy of NaClO, both in terms of biomass elimination, sterilization and integrity of surfaces. H_2O_2 showed to be very corrosive on the substrates, with

the release of other chemical species, especially on the vermiculated ones, without removing the death biomass. The most resistant groups after such treatments were *Proteobacteria* and *Bacteroidetes* for *Prokaryotes*, and *Apicomplexa* and *Cercozoa* for the *Eukaryotes*, with the complete elimination of phototrophs. UVC showed no effect with the protocols used.

Overall, the research highlights that tourism and its associated activities trigger various knock-on effects with irreversible repercussions in all the system. Anyway, only an accurate and integrated characterization of the cave environment, providing interesting information about the fundamental natural processes characterizing the system, allows proposing sustainable management strategies. Indeed, a multidisciplinary investigation can reveal the ecological quality state of the cave environment, as well as helping in the identification of potential disturbance drivers of the ecosystem equilibrium, in order to take effective prevention measures, with a limitation of harmful consequences jeopardizing the integrity and the safeguard of such extraordinary natural heritage. Future efforts will try to clarify the endokarst and top soil properties, contributing to the comprehension of the past and current cave fluviokarst activity, and understanding the genesis processes of cave sediments, as well as the chemical features of the cave waters. Moreover, further studies about the biochemical/metabolic processes involved in the interaction dynamics of the microbiota and lampenflora biofilm with mineralogical substrates will also implement, clarifying the specific functions of the community and their ecological role in the cave ecosystem, searching for innovative and integrated approaches to control the lampenflora growth through new and sustainable strategies.

List of scientific publications and meeting communications during the PhD project

(*: corresponding author)

Publications on indexed journals

Addesso, R.*, De Waele, J., Cafaro S., Baldantoni, D. (2022) Geochemical characterization of clastic sediments sheds light on energy sources and on alleged anthropogenic impacts in cave ecosystems. International Journal of Earth Sciences. doi: 10.1007/s00531-021-02158-x

Addesso, R.*, Gonzalez-Pimentel, J.L., D'Angeli, I.M., De Waele, J., Saiz-Jimenez, C., Jurado, V., Miller, A.Z., Cubero, B., Vigliotta, G., Baldantoni, D. (**2020**) Microbial community characterizing vermiculations from karst caves and its role in their formation. Microbial Ecology 81: 884–896 doi: 10.1007/s00248-020-01623-5

D'Angeli I.M., Ghezzi D., Leuko S., Firrincieli A., Parise M., Fiorucci A., Vigna B., **Addesso, R.**, Baldantoni, D., Carbone, C., Miller, A.Z., Jurado, V., Saiz-Jimenez, C., De Waele, J., Cappelletti, M.* (**2019**) Geomicrobiology of a seawater-influenced active sulfuric acid cave. PLoSONE 14(8): e0220706doi: 10.1371/journal.pone.0220706

Addesso, R., Bellino, A.*, D'Angeli, I.M., De Waele, J., Miller, A.Z., Carbone, C., Baldantoni, D. (**2019**) Vermiculations from karst caves: The case of Pertosa-Auletta system (Italy). Catena. 182:104178 doi:10.1016/j.catena.2019.104178

Addesso, R., Bellino, A.*, Baldantoni, D. (**submitted to Environmental Management, minor revisions**) Underground ecosystem conservation through high-resolution monitoring of show cave atmosphere.

Book chapters

Fiorillo, F., Pagnozzi, M., **Addesso, R.**, Cafaro, S., D'Angeli, I.M., Esposito, L., Leone, G., Liso, I.S., Parise, M.* (**2021**) Uncertainties in understanding groundwater flow and spring functioning in karst. In: AGU Books. Wiley Black Well doi: 10.1002/essoar.10508452.1

Publications in preparation

Addesso, R.*, Pingaro, S., Bisceglia, B., Baldantoni, B. Sustainable tourist fruition of underground ecosystems: simulations of airflow and particle dispersions and depositions.

Addesso, R.*, Morozzi, P., Tositti, L., De Waele, J., Baldantoni, B. Dripping and river waters shed light on cave ecohydrology

Addesso, R., Baldantoni, D., Cubero, B., Tiago, I., Caldeira, A.T., De Waele, J., Miller, A.Z.* A multi-approach characterization of lampenflora in lit underground ecosystems.

Addesso, R., Baldantoni, D., Cubero, B., De La Rosa, J.M., González Pérez, J.A., Tiago, I., Caldeira, A.T., De Waele, J., Miller, A.Z.* Effects of the most commonly employed methods to control lampenflora community on its physiological activity and on the treated surfaces.

Meeting Communications

Bellino, A., **Addesso, R.**, Baldantoni, D. (**2021**) High-resolution atmospheric monitoring in cave ecosystems: dynamics, impacts and implications for management and conservation. Environmental Research 2021 – IOP Publishing, 15th-19thNovember 2021(virtual meeting)

Addesso, R., Baldantoni, D. (**2021**) Lampenflora growth-control treatments, the challenge of the show caves. Congresso Nazionale S.It.E - Società Italiana di Ecologia., online, 25-27 Ottobre 2021 (virtual meeting)

Addesso, R., Miller, A.Z., De Waele, J., Baldantoni, D. (**2021**) Cave vermiculations, life hotspots for studies of hypogean microbiology. EANA 2021 Conference, 7th-10th September 2021. (virtual meeting)

Addesso, R., Cafaro, S., Papaleo, F., Alaggio, R., D'Orilia, F., Amato M. (**2021**) The geosite of Pertosa-Auletta cave: an educational journey into the underworld. EGU General Assembly 2021, 19th–30thApril 2021(virtual meeting)

Addesso, R., Baldantoni, D. (**2021**) Shedding light on vermiculations: a key step towards their conservation. Incontro Dottorandi in Ecologia e Scienze dei Sistemi Acquatici, Stazione Zoologica Anton Dohrn, Napoli, 13-15 aprile 2021 (virtual meeting)

Addesso, R., De Waele, J., Baldantoni, D. (**2020**) Lampenflora, the alien of show caves: monitoring and treatments. Conservation of Fragile Karst Resources Proceedings, 18th-20th August 2020, 16.

Addesso, R., Bellino, A., D'Angeli, I.M., De Waele, J., Miller, A.Z., Carbone, C., Baldantoni, D. (**2019**) Integrated approach for the geochemical characterization of vermiculations from Pertosa-Auletta Cave (southern Italy). 27th International Karstological School "Classical karst", Karst Hydrogeology - Research Trends and Applications. Postojna (Slovenia), 17th - 21stJune 2019, 81.

Addesso, R., Baldantoni, D., Bellino, A. (**2019**) Cave vermiculations and microbiota, an ecological journey. Capitale Naturale: la Gestione per la Conservazione - XXIX

Congresso Nazionale S.It.E - Società Italiana di Ecologia. Ferrara (Italia), 10 - 12 Settembre 2019, 50.

Addesso, R., Baldantoni, D., Bellino, A., Vigliotta, G., De Waele, J., D'Angeli, I.M., Saiz-Jimenez, C., Miller, A.Z., Gonzalez-Pimentel, J.L., Jurado, V., Cubero, B., Carbone, C., Amato, M. (**2018**) Bio- and geodiversity of vermiculations from Pertosa-Auletta Cave (southern Italy). 113th Congress of the Italian Botanical Society (5th International Plant Science Conference). Fisciano (SA, Italia), 12th – 15th September 2018; 59**.**

Popular publications

Addesso, R. (**2021**) I macroinvertebrati bentonici, bioindicatori dello stato di salute dei fiumi. Collana MIdA A Agricoltura e Ambiente. Pertosa, 2021.

Nicolosi, G., **Addesso, R.** (**2021**) Vivere al buio, la fauna invertebrata della grotta di Pertosa Auletta. Collana MIdA A Agricoltura e Ambiente. Pertosa, 2021.

Addesso, R., Torre, R., Pellegrino, A., Franciolini, R. (**2020**) Grani del futuro. Il valore della biodiversità cerealicola come cibo e futuro. Collana MIdA A Agricoltura e Ambiente. Pertosa, 2020.

Addesso, R. (2019) Vermicolazioni delle Grotte di Pertosa-Auletta. Un brulicare di vita microbica estrema. Collana MIdA A Agricoltura e Ambiente. Pertosa, 2019.